DEVELOPING AN INJECTABLE IN-SITU-FORMING CALCIUM POLYPHOSPHATE SYSTEM AS A HEMOSTATIC AGENT

by

Arash Momeni Boroujeni

Submitted in partial fulfilment of the requirements
for the degree of Doctor of Philosophy

at

Dalhousie University
Halifax, Nova Scotia
March 2015

To my wonderful wife, Bahar,
and my parents
for their patience, support and encouragements

Table of Contents

List of Tables

List of Figures

Abstract

Sodium Polyphosphate (NaPP) is a linear inorganic polymer formed from PO_4 structural units. NaPP glass is soluble in water, but addition of multivalent cations to its solutions results in a precipitate and formation of a polyphosphate coacervate. These coacervates are comprised of hydrated chains of polyphosphates that are immiscible with water. It has been shown that polyphosphate chains released from platelets after activation may play a significant role in the coagulation cascade. This observation alludes to the great potential especially for these polyphosphate coacervates in hemostasis applications. In this thesis, detailed studies of a polyphosphate coacervate system derived from NaPP and divalent cations, namely calcium, strontium and barium, are described together with the potential of an *in situ* forming coacervate as an embolic agent.

NaPPs with degrees of polymerization (D_p)<500 were successfully achieved by fractionation of NaPP glass that was prepared from $NaH_2PO_4.H_2O$. NaPPs with D_p>500 were produced successfully by ion-exchange of potassium Kurrol salt that was prepared from KH_2PO_4. The effects of divalent cation (Ca, Sr and Ba) addition to NaPP solutions were comprehensively studied, and it is shown that the number of divalent cations required for coacervation depends on different variables such as the NaPP concentration, the D_p, and the type of divalent cation. Polyphosphate coacervates prepared from different NaPPs and cations were found to degrade at a fast rate, limiting them to short-term bio-applications. Additional rheological studies revealed that viscoelastic properties of these coacervates depend profoundly on the cation type and NaPP D_p, allowing one to tweak their composition to achieve a desired physical property. Polyphosphate coacervates were found to be an excellent candidate for hemostasis applications, decreasing clotting time significantly especially when very long chain polyphosphates were used. Lastly a polyphosphate liquid embolic system with optimum radiopacity, injectability and cyto-compatibility was developed and tested *in vivo* with promising results. The ability of a polyphosphate coacervate to be loaded with an anticancer drug, with a subsequent slow rate of release, was also demonstrated. Overall this thesis establishes the potential of a polyphosphate *in situ* forming system and polyphosphate coacervates in general as a unique platform for bio-applications.

List of Abbreviations Used

^{31}P-NMR	Phosphorus^{31} Nuclear Magnetic Resonance
3D	Three dimensional
AAS	Atomic Absorption Spectroscopy
ACS	American Chemical Society
ADP	Adenosine diphosphate
alpha2-AP	alpha2-antiplasmin
ANOVA	Analysis of variance
aPTT	Activated partial thromboplastin time
ATP	Adenosine triphosphate
AVM	arteriovenous malformations
COO	Carboxylic group
CPP	Calcium polyphosphate
DMEM	Dulbecco's Modified Eagle's Medium
DMSO	Dimethyl sulfoxide
DNA	Deoxyribonucleic acid
Dox	Doxorubicin
$\overline{D_p}$	Average degree of polymerization
D_p	Degree of polymerization
DTA	Differential thermal analysis
EDAC	1-ethyl-3-[3-(dimethylamino)propyl]carbodiimide
EDS	Energy-Dispersive X-ray Spectroscopy
EDTA	Ethylene-di-amine-tetra-acetate
ERD	Elastic recoil detection
EXAFS	Extended X-ray absorption fine structure
FBS	Fetal bovine serum
FTIR	Fourier transformed infrared
G'	elastic (storage) modulus
G"	viscous (loss) modulus
HAP	Hydroxyapatite
HEPES	(4-(2-hydroxyethyl)-1-piperazineethanesulfonic acid)

ICP	Inductive coupled plasma emission spectroscopy
ISO	International Organization for Standardization
$(K/P)_{KH_2PO_4}$	Potassium to phosphorus molar ratio of KH_2PO_4
$(K/P)_{IE}$	Potassium to phosphorus molar ratio in the ion-exchanged sodium polyphosphate
LDH	Lactate dehydrogenase enzyme
MAS-NMR	Magic angle spinning nuclear magnetic resonance
Me	Metal cation
Me*	Divalent cation to phosphorus molar ratio at the cloudy point
Me^{I}	Monovalent metal cation
Me^{II}	Divalent metal cation
MES	2-(N-morpholino)ethanesulfonic acid
$\overline{M_n}$	Number average molecular weight
M_{TO}	Total number of terminal oxygen atoms per cation in a phosphate glass
MTT	3-(4,5-dimethylthiazol-2-yl)-2,5-diphenyltetrazolium bromide
$\overline{M_w}$	Weight average molecular weight
N/A	Not applicable
NaPP	Sodium polyphosphate
N_{MeO}	Coordination number of a cation Me in phosphate glasses
NMR	Nuclear Magnetic Resonance
NS	Not significant
O_b	Bridging oxygen
p	p-value in statistics
P2Y receptor	a family of purinergic G protein-coupled receptors
PAA	Poly acrylic acid
PBS	Phosphate buffer saline
pH	Potential hydrogen
pK	Dissociation constants
pKa	Acid dissociation constant
PPP	Platelet poor plasma
PT	Prothrombin time
PVA	Poly vinyl alcohol

PVSF	Poly(vinyl sulfonate)
Q^0	Phosphorus in orthophosphate
Q^1	Phosphorus in the end of the chain phosphate groups
$Q^{2\text{-meta}}$	Phosphorus in the phosphate rings
$Q^{2\text{-middle}}$	Phosphorus in the middle of the chain phosphate groups
Q^3	Phosphorus in the branching point of phosphate groups
R^+	Alkali cation
SEM	Scanning electron microscopy
STD	Standard deviation
TACE	Trans-arterial chemoembolization
TBS	Tris buffer saline
TF	Tissue factor
TFPI	Tissue factor pathway inhibitor
TGA	Thermogravimetric analysis
tPA	Tissue-type plasminogen activator
Tris	Tris(hydroxymethyl)aminomethane
uPA	Urokinase-type plasminogen activator (uPA).
w/v	Weight/volume (gram/milliLiter)
wt%	Weight percentage
XPS	x-ray photoelectron spectroscopy
XRD	x-ray diffraction
Å	angstrom
γ	Shear strain
δ	Phase angle
η	Viscosity
$[\eta]$	Intrinsic viscosity
η^*	Complex viscosity
η_{sp}	Specific viscosity
θ	Fraction of condensed counterions
λ_B	Bjerrum length
ξ	Charge density parameter
τ	Shear stress
ω	Frequency

Acknowledgments

I gratefully acknowledge funding from the Natural Sciences and Engineering Research Council of Canada CREATE BioMedic program. I would also like to acknowledge the contribution of my supervisory committee members, Dr. Daniel Boyd, Dr. Robert J. Abraham and Dr. Josef Zwanziger and most especially my supervisor, Dr. Mark J. Filiaggi. I would also like to acknowledge Gordon Hall for his support in the lab, and Dr. Ellen Brennan and Sean Curley, who carried out cell viability assay and drug release studies, respectively.

Chapter 1 Introduction

1.1 Preface

For several years the research focus of our group has been calcium polyphosphate (CPP) glasses and their potential as a biomaterial. When I commenced my doctoral program with Dr. Filiaggi, I was challenged to develop an injectable system based on polyphosphates. I began by experimenting on CPP-poly acrylic acid and CPP-alginate systems. While both systems showed potential, I was not convinced that they were unique and novel enough to warrant developing further as the basis for my thesis.

One day in the lab I dissolved CPP glass using ethylene-di-amine-tetra-acetate (EDTA) to obtain a clear solution, and promptly refrigerated the solution. The following day I realized that a very thin "oily", highly viscous transparent material[1] had formed at the bottom of the solution. I was intrigued by this observation; this coacervate layer subsequently dissolved away when the solution reached the room temperature but should have never formed, remaining as a sodium polyphosphate (NaPP) phase, given EDTA's role in sequestering calcium ions. This observation prompted me to wonder what would happen if I added calcium ions to a NaPP solution obtained from EDTA dissolved CPP; preliminary studies quickly revealed that adding excess calcium chloride solution to the solution led to the formation of an opaque coacervate layer that did not dissolve away. I subsequently commenced preparing NaPP glass in the lab for the first time, followed by its dissolution and addition of calcium solution to again form this coacervate layer, which I hypothesized to be hydrated form of CPP. A review of the literature subsequently

[1] From now on, this material is called coacervate. The term coacervate will be defined later. Here, it is sufficient to think of it as a mixture of hydrated chains.

uncovered a few references on this subject, but overall I was surprised by the apparent lack of research concerning this phenomenon and especially its potential as a biomaterial. Consequently, I decided to focus on the formation of CPP using NaPP solutions as a novel and unique injectable biomaterial, with an emphasis in particular on the hemostasis potential of this system owing to the significant body of literature suggesting polyphosphates play a major role in the blood coagulation cascade.

I carried out my doctoral studies with two distinct but related goals in mind: to answer a series of basic scientific questions about this system, and to understand how we could control and further utilize this system for bio-applications. The first aim was to synthesize and thoroughly characterize different molecular weights of NaPPs. Detailed in Chapter 2, these NaPPs were subsequently used throughout this thesis project. In Chapter 3, I explore this coacervation phenomenon, determining in particular the amount of divalent cations (including calcium) required for phase separation in NaPP solutions. I also evaluate the pH, viscosity and chain structure of these NaPP solutions in the presence of divalent cations, and examine as well the composition of the coacervate and the process of Ca substitution for sodium in the system; the comprehensive studies described here contribute greatly to our basic understanding of this system and our subsequent capacity to control its behavior.

In Chapter 4, the physical properties of the coacervate and its dependence on processing variables including NaPP molecular weight and divalent cation type are provided. This chapter also includes studies on the *in vitro* degradation of these polyphosphate coacervates under different conditions.

Chapter 5 focuses specifically on those properties of the coacervate that affect its application as a hemostatic agent. Here, a whole blood clotting test and measures such as prothrombin time, partial thromboplastin time and platelet adhesion are used to assess the effect of the coacervate on the coagulation cascade and its ability to form a clot.

While progressing through my doctoral studies, I together with Dr. Filiaggi and Dr. Abraham, an interventional radiologist, successfully applied for an early stage commercialization grant specifically to evaluate the potential of this injectable system as a liquid embolic agent. Chapter 6 summarizes the results of my studies on the radiopacity, injectability and cytocompatibility of this polyphosphate embolic system. Included here as well is an investigation of drug loading and release from these polyphosphate coacervates, a requirement for a liquid embolic agent intended to be used in treating liver cancer.

Chapter 7 provides an overall summary and requisite conclusions to this thesis project, while also containing suggestions for future studies.

To start things off, the remainder of this Chapter provides a comprehensive background and literature review on polyphosphates, their interactions with water, and their role in the coagulation cascade.

1.2 Background and Historical Context

In 1816 Berzelius wrote about amorphous phosphoric acids ranging from viscous liquids to materials classified as either glasses or unusually rigid liquids at room temperature [1]. Seventeen years later, Thomas Graham prepared vitreous sodium phosphate exhibiting the metaphosphate composition (Na_2O/P_2O_5 = 1) by heating sodium dihydrogen

phosphate to high temperature followed by chilling the melt suddenly [2]. This compound, Graham salt, was referred to erroneously as sodium *hexametaphosphate* for over 100 years until 1954, when Van Wazer concluded, based on evidence from several studies of Graham salt solutions, that it was indeed a mixture of linear polymers, polyphosphates, and a few ring phosphates [3].

In fact, most common glasses can be considered inorganic polymers of oxygen bonding elements (Si, P, B) that are forming 3D networks in the presence of cations such as sodium, calcium, and aluminum. In most cases, these inorganic polymers cannot be dissolved in any solvent without complete destruction of the compound; the three-dimensional network of most silicate glasses, for instance, can only be dissolved in extremely basic or acidic solutions where the Si-O-Si bond breaks down. In contrast, some exceptions such as sodium silicate form a hydrated 3D polymer of extremely high molecular weight in contact with water. The orthosilicates (SiO_4^{-4} monomeric anions) in this network polymerize upon addition of acid and depolymerize at a moderate rate back to the orthosilicate upon addition of base [3]. In practice, this is the basis of the sol-gel method for the preparation of silicate glasses that now competes against melting methods especially in the processing of bioglasses. Another interesting glass that also dissolves in water is sodium polyborate, but B-O-B bonds are not stable and immediately degrade into their monomers upon dissolution in water [4]. In contact with water, the situation for all phosphate-based glasses is quite different; most dissolve and degrade in the presence of water but the rates of these two reactions are highly dependent on the composition of the glass [5]. In the case of Graham salt, chains of polyphosphates are released in the solution at a very high dissolution rate. Dilute solutions of these chains never polymerize but only

slowly undergo degradation by hydrolysis toward the monomer (orthophosphate) at rates that are comparable to the hydrolytic degradation of many organic polymers [3]. In addition, although branched points where PO_4 groups share oxygen atoms with three neighboring groups are present in a classification of phosphate based glasses known as ultraphosphates, these three-way bonds are not stable and immediately cleave upon contact with water. This means that only orthophosphates, simple rings, or unbranched chains (linear polymers) are present in aqueous solutions of phosphate based glasses [3, 5].

Shortly after the discovery of Graham salt, it was found that its solutions had the ability to prevent precipitation or re-dissolve precipitates of the alkaline earth metals [6]. This chelating ability of Graham salt solutions was an obscure piece of information of little interest to either science or applied technology until 1933, when Hall [7] applied this effect to the removal of calcium, magnesium, and certain other metal cations from water [6], opening up a significant market for Graham salt as a water-softening agent. This application subsequently sparked a considerable emphasize on this compound within the academic community during the 1950's. Indeed, most of the current knowledge on the polyphosphates and more specifically Graham salt is from this era. *For this thesis project, we aim to utilize the exceptionally high solubility of Graham salt in water and the subsequent potential to precipitate polyphosphates under certain conditions as the basis for an in-situ-forming system for biomedical applications, with a focus on hemostasis*.

In this chapter, glasses as biomaterials are introduced initially, with a focus in particular on the central theme of our research group. Then a brief description of different

classifications and structures in phosphate glasses is provided. Subsequently, glasses and crystalline phases in the systems Na_2O-P_2O_5 and Na_2O-CaO-P_2O_5 are introduced, followed by a summary of the current body of knowledge regarding interactions between water and phosphate chains. Finally, recent publications on the role phosphate chains play in the blood coagulation cascade are reviewed.

1.3 Glasses as biomaterials, the focus of our research group and an injectable approach

The application of glass as a biomedical device goes back to the 13^{th} century, when convex and concave lenses were utilized for the first time in eyeglasses [8]; however as a biomaterial, the potential of glasses has only been recently appreciated. Interestingly, glasses valued as a biomaterial lack the chemical durability that is considered the strength of other common glasses. Two of the most famous applications of glasses as biomaterials are in glass-ionomers cements for dental applications [9] and Bio-glasses for use in orthopaedics [10], where their mechanisms are directly related to their weak chemical durability and subsequent ion release.

Glass-Ionomer cements are two phase systems: aluminosilicate glass powder phase and polyalkenoate liquid phase. Aluminosilicate glasses in the system of (SiO_2-Al_2O_3-CaO) are susceptible to degradation at low pH, so addition of polyalkenoate solutions (usually poly acrylic acid) provide hydrogen ions that replace calcium and aluminum within the glass networks and consequently release them into the solution; these released ions subsequently precipitate out the polymer phase by cross-linking its carboxylic (COO^-) groups [9]. In short, mixing of the two phases triggers a series of reactions that ultimately

leads to a cement in which the remaining glass powders are entrapped within a 3D cross-linked network of polymers.

Bio-glasses are also dependent on their poor chemical durability. First reported by Larry Hench [10], these glasses were originally in the system of (SiO_2-CaO-Na_2O-P_2O_5), with the most famous compositional designation known as *45S5*®. The unique property of Bio-glass is its ability to form a hydroxyapatite (HAP) layer on its surface when in contact with water. HAP is the main inorganic component of the bone, so these glasses are considered bioactive because of their ability to bond with the bone. The mechanism of HAP formation on the glass surface has been fully described by Hench [11].

For these glasses, silicon plays the main role as network former and not phosphorus, in sharp contrast to CPP glass that is central to our research group's efforts. CPP glass is in the system CaO-P_2O_5, where the molar ratio of [CaO]/[P_2O_5] is exactly 1 (or [Ca]/[P] = 0.5). In our lab this glass is prepared by calcining calcium phosphate monobasic monohydrate ($Ca(H_2PO_4)_2.H_2O$) overnight at 500°C to yield calcium phosphate monobasic dehydrate ($Ca(H_2PO_4)_2$) that is then melted at 1100°C for 2 hr [12]; at this high temperature, a series of condensation reactions occurs in which a molecule of water is lost and a P-O-P bond is formed (Figure 1.1).

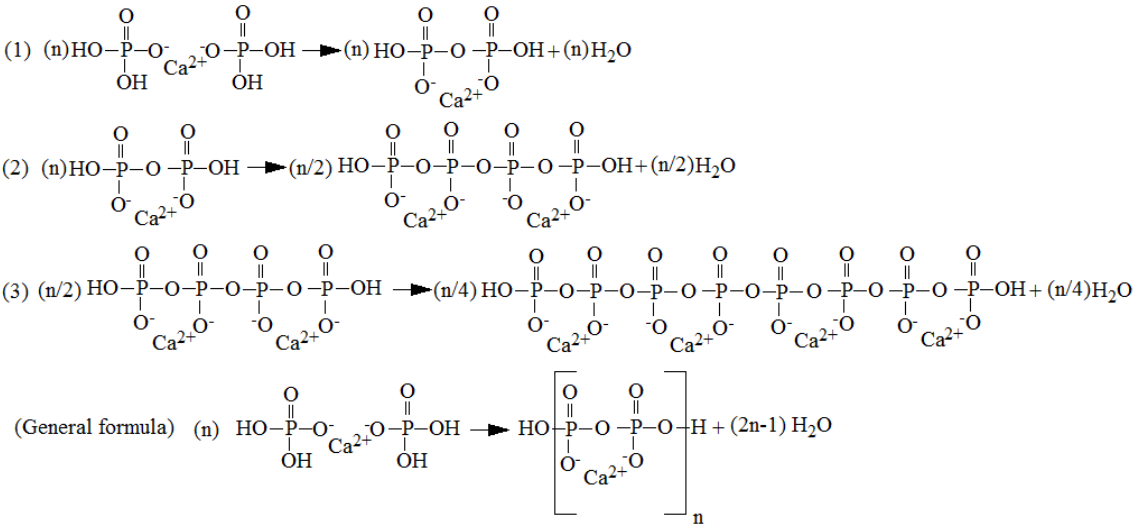

Figure 1.1 Schematic of some of the condensation reactions that form CPP chains.

With a [Ca]/[P] molar ratio of 0.5, one should theoretically end up with only calcium metaphosphate *rings*, or a series of chains with *infinite lengths* (Figure 1.1) if this reaction continues to the point where all water molecules are lost. In practice, however, as is seen with ^{31}P-NMR [13, 14] and similar to what has been reported for Graham salt ([Na]/[P] = 1) [3], it is very difficult to remove the last trace of water from the melt; no matter how long or to what temperature one heats the melt, the chain length will not grow beyond a certain length. In the case of Graham salt, average degrees of polymerization ($\overline{D_p}$) greater than 250 are rarely achieved [3]. In addition, because phosphate rings are considerably less stable than phosphate chains [5, 15], the CPP glass obtained upon quenching the melt consists mostly of phosphate chains with an $\overline{D_p}$ of 67, with few traceable phosphate rings [13, 14]. Heating our melts for longer times may yield slightly higher $\overline{D_p}$; however, the trade off is an increase in the proportion of ring phosphates. It is known that the proportion of rings in Graham salt increases as the $\overline{D_p}$ becomes larger; about 9 percent of the total phosphorous is present as rings in a glass having a $\overline{D_p}$ of 200

[3]. In fact, nature abhors infinity, and the formation of rings despite their instability appears to be a mechanism to avoid infinite or extremely long chains at high temperatures [3]. Intramolecular termination (backbiting) or formation of branches might also limit the growth in $\overline{D_p}$, but formation of branching point is not favored in polyphosphates due to steric limitation.

Until now, our group has been focused on CPP, calcium phosphate glass made up of these polyphosphates chains. Similar to many phosphate-based glasses, CPP powder in presence of water will gel, dissolve and degrade ultimately into calcium and orthophosphate ions. These are the main constituents of the inorganic component of bone, HAP, and *neutral* solutions that are saturated with these ions mainly precipitate out HAP [16]. This is the reason why CPP is a great candidate as a bone interfacing material because it is believed that, in contact with body fluid, it will degrade and in the process be replaced by HAP [17, 18]. However, it is the unique ability of CPP to act as a drug delivery agent that has truly garnered the attention of our group [12-14, 19-22].

Drug delivery is an interdisciplinary field of science in which different delivery formats, from nanospheres to *in situ* forming depots, are used to either target drugs at their site of action or to control their release. A long sustained release within the therapeutic window would prevent, for example, the need for multiple administrations of the drug while minimizing the chance of reaching toxic levels after each dosing. If administered locally, one can also reduce the side effects of chemotherapeutics significantly [23]. The ability of CPP to act as a drug delivery agent is directly related to its hygroscopic nature [21]; CPP powders that are exposed to an aqueous environment will form a coacervated layer

on their surfaces, but transformation of the whole glass particle needs time and depends on water diffusion [24] . Indeed, if one uses very fine glass powder and prolonged water contact, the whole glass powders will transform to an “oily”, highly viscous transparent material. The transformation of CPP from a glassy to a coacervate-like state is reversible; by drying, a coacervate sample transforms back to a glass (albeit with lower polyphosphate $\overline{D_p}$ [13]). In several reported studies by our group, CPP powders have been mixed with a small volume of water and drug to form a paste that is then transferred to a disc-shape mould and allowed to gel in a nearly 100% humid environment at 37°C. Following gelling (coacervation), the discs are dried for a minimum of 24 hr at 37°C in atmospheric air [14, 19-21]. These disks, referred to as G1 disks, have demonstrated a sustained release of vancomycin on the order of a week [21], but they also show a significant burst release near 40% [14]. We believe that during gelling, some of the drug diffuses into the coacervated surface of the CPP powders and some remains free on the surface of glass particles. Then during drying, the coacervated particle surfaces revert back to the glass, entrapping the portion of drug that has diffused in; also in this process, glass powders are fused together [25], forming the G1 disks. The drug burst release is probably due to the free drug that has not diffused into the coacervated layer and, indeed, subsequent studies have shown that multiple gelling steps in combination with G1 particle compaction (G2 disks) minimize the burst release, likely by increasing the portion of the entrapped drug to that of free drug [21].

Despite its perceived advantages, this approach has inherent constraints, yielding a drug delivery format with poor mechanical properties and disks that were not particulary useful shape-wise which could be only applied in open surgeries. These limitations have

prompted our group to look for alternative approaches such as injectable *in situ* forming CPP systems. Mixing of CPP powder with conventional calcium phosphate cements is one method to achieve such a system. However, this approach was found to significantly delay the setting time of these cements, supposedly by preventing HAP nucleation and/or growth due to the chelating of calcium ions by polyphosphates or by simply making the solution more acidic [26]. Another method to achieve an injectable, CPP-containing *in situ* forming system is to utilize its calcium ion release properties to crosslink anionic polymers such as poly acrylic acid (PAA) or alginate. This mechanism is similar to that seen with Glass-ionomer cements, with the exception that aluminosilicate glass is replaced by CPP. Indeed, early preliminary experiments involving mixing of CPP with PAA solution resulted in the formation of a hard cement, albeit with a long setting time (about an hour) that could be adjusted. Addition of PAA may be a means of controlling the degradation rate of the CPP and enhancing drug delivery; it may also improve the mechanical properties of CPP discs. Nevertheless, it is possible that addition of non-degradable PAA to CPP may obstruct the unique ability of CPP to gel and consequently interfere with its full drug delivery capability. Cements similar to this formulation have previously been developed by mixing other calcium phosphate salts with PAA [27, 28]; however, none have evolved into a practical product probably because they are non-degradable, mechanically weaker than traditional Glass-ionomers – likely due to the absence of tri-valent Al ions (Al^{3+}), and prone to erosion [9].

Compared to these two mechanisms, another novel mechanism to achieve an injectable *in situ* forming system of CPP involves direct precipitation (coacervation) of CPP from polyphosphate solutions. It has been known for quite some time that when excess amount

of multivalent ions are added to a solution of Graham salt, the solution becomes cloudy [29], and flocculants [5], or gummy, highly viscous materials (coacervate) [5, 30] start to form. There has been few researches on potential of such coacervates as glass precursor [31-38], but based on current available evidence, there are no reported studies of corresponding injectable systems for biomedical applications. The overall aim of this thesis project, then, is to better understand this system and its application as a biomaterial in hemostasis, as will be discussed comprehensively in the following chapters. Essential to this chapter, though, is some relevant background on polyphosphates as both a glass and in solution.

1.4 Phosphate glasses: Building blocks and Classification

The basic building block of crystalline and amorphous phosphates is the most stable form of phosphorus compounds [5], P-tetrahedra, which result from the formation of sp^3 hybrid orbitals by the P outer electrons ($3s^2 3p^3$). Here, four electrons of P are covalently shared with the four O^- atoms, and the fifth electron is promoted to a 3d orbital where strong π-bonding molecular orbitals are formed with an oxygen 2p electron [39]. In fact, in the PO_4^{3-} structure, the π-bond and negative charges are in resonance between all four oxygen atoms, so there is no difference between any of these bonds [5] (Q^0 in Figure 1.2). These tetrahedra molecules can link through covalent bridging oxygens to form various phosphate anions by condensation reactions. For instance, at high concentration, phosphoric acids start to react with each other forming P-O-P bonds and releasing a water molecule:

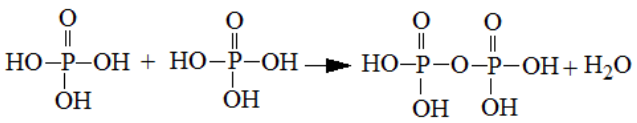

The extent of these reactions and the $\overline{D_p}$ of the polyphosphate anions that are formed is directly related to the concentration of phosphoric acid; in highly concentrated solutions (P_2O_5 > 89.4 wt%), more than 86 % of phosphates have degree of polymerization higher than 14 [40].

The formation of P-O-P bridges between phosphates is not necessarily linear (polyphosphate). In fact, when the number of P per chain (n_P) exceeds 3, metaphosphates can also be formed:

Tri-metaphosphate: 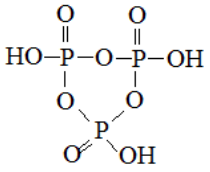 , or tetra-metaphosphate: 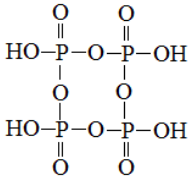

At an n_P of 4 or higher, a new class of phosphates referred to as ultraphosphates can form through branching:

Tetra-ultraphosphate: 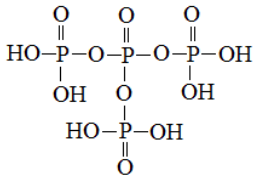

Given the number of structures possible, phosphate tetrahedra are classified based on the number of bridging oxygens per tetrahedron (i) using the Q^i terminology that is shown in Figure 1.2.

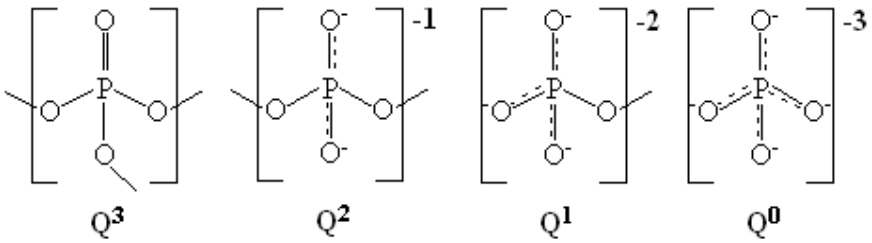

Figure 1.2 Phosphate tetrahedral sites that exist in phosphate glasses (Adapted from [39]).

Q^3 sites are the least stable sites in polyphosphate anions and they are rapidly hydrolyzed when introduced to water, forming much more stable Q^2 sites [3]. In sodium phosphate glasses, the rate constant (k) for this reaction at 25°C was found by Strauss [41, 42] to be $8(\pm4)\times10^{-3}$ min^{-1}, based on the following equation:

$$\frac{b_r}{b_{r0}} = 10^{-0.434\times k\times t} \qquad \text{Equation 1.1}$$

where b_r is the number of branches per mg of polymer, t is the time in min. and k is the rate constant in min^{-1}. The symbol b_{r0} refers to b_r at $t = 0$. At this rate, after almost 12 hours in solution, all Q^3 sites are replaced by Q^2 sites.

The addition of metallic cations to chains of polyphosphate anions results in phosphate based glasses. Binary phosphate glasses are described stoichiometrically as $x Me^{I}_2O$ (or $Me^{II}O$) - $(1-x)P_2O_5$, where Me^{I} represents a monovalent cation such as Na^+, and Me^{II} represents a divalent cation such as Ca^{2+} [39]. With CPP, for example, x is equal to 0.5 and its general formula is 0.5 CaO – 0.5 P_2O_5. In fact, the value of x determines the classification of these glasses as ultraphosphates, metaphosphates or polyphosphates (Table 1.1).

Table 1.1 Classification of binary phosphate glasses based on the *x* value and the theoretical fraction of phosphorus sites exists in them [5, 39].

Classification of binary phosphate glass (xMe^{I}_2O (or $Me^{II}O$) - $(1-x)P_2O_5$)	*x* value	[O]/[P] ratio	Fraction of different phosphorus sites (%)			
			Q^0	Q^1	Q^2	Q^3
Vitreous P_2O_5	x=0	2.5	0	0	0	100
Ultraphosphate	0<x<0.5	2.5 to 3	0	0	$x/(1-x)\times100$	$(1-2x)/(1-x)\times100$
Metaphosphate	x=0.5	3	0	0	100	0
Polyphosphate	0.5<x<0.67	3 to 3.5	0	$(2x-1)/(1-x)\times100$	$(2-3x)/(1-x)\times100$	0

1.5 Structure of phosphate glasses

Phosphate glass structure, especially in the ultraphosphate region, is more complicated than silicate glasses due to the presence of double-bond oxygen atoms [43]. Structural

studies of crystalline ultraphosphates indicate that the local coordination environment of the modifying cations includes terminal oxygens from both Q^2 and Q^3 [39]. Where Q^3 sites are included in the coordination environment, double-bond oxygen atoms are also bound to the cations (Figure 1.3-left).

The coordination number (N_{MeO}) values at different glass compositions have been reported by XRD and EXAFS studies, and have been found to be highly dependent on metal oxide (MeO) content (Figure 1.3) [43]. For instance, the N_{MeO} of calcium in 0.25 CaO – 0.75 P_2O_5 (x = 0.25) is 8, with N_{MeO} decreasing with increasing CaO until, at 0.33 CaO – 0.67 P_2O_5 (x = 0.33), it reaches 6 – assumed to be the lowest coordination possible. After this value of x, calcium atoms must share double-bound and non-bridging oxygen atoms (Figure 1.3), leading to a drastic change in glass properties such as density [43]. Thus, calcium atoms within CPP (x = 0.5) are forced to share some of their coordinated oxygen atoms with each other. To be precise, the coordination number of calcium atoms in CPP glass is reported to be 7 [44, 45], and because the total number of terminal oxygen atoms per cation (M_{TO}) (including double-bound and non-bridging oxygen atoms) is 4, 3 out of 4 terminal oxygen atoms are bound to two calcium atoms. This sharing of oxygen atoms is likely one of the main reasons for the highly hygroscopic nature of CPP glass and of polyphosphate glasses overall.

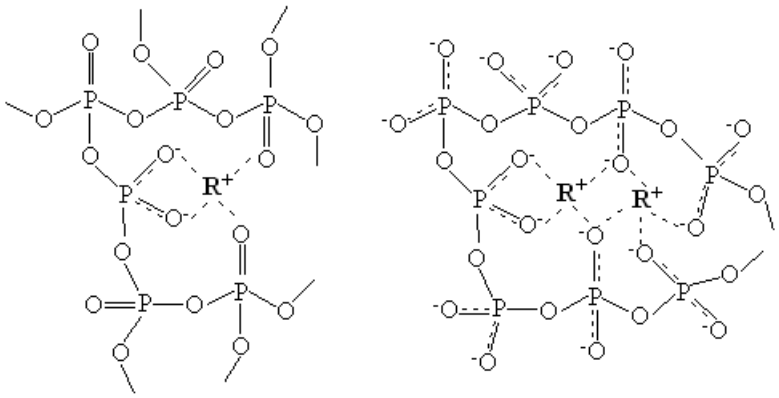

Figure 1.3 Schematic representations of alkali (R^+) bonding in phosphate glasses when $M_{TO}>N_{MeO}$ (left) and $M_{TO}<N_{MeO}$ (right) (Adapted from [39]).

In general for any phosphate-based glass, the value of M_{TO} and N_{MeO} determine two structurally different compositional ranges: when $M_{TO} > N_{\mathrm{MeO}}$, sufficient individual terminal oxygen atoms are available for coordination with each cation and so these cations can exist in an isolated state. In contrast, when $M_{TO} < N_{\mathrm{MeO}}$, there are not enough terminal oxygen atoms to satisfy the coordination environment of every cation, so cations must share the available terminal oxygen atoms [39]. Some of the N_{MeO} values for metaphosphate glasses are reported in Table 1.2 and the value of M_{TO} can be determined by

$$M_{TO} = v(\frac{1}{x}) \quad \text{Equation 1.2}$$

where v is the cation valence in the x $(Me_{2/v}O)$ - $(1\text{-}x)$ P_2O_5 glass system.

Table 1.2 Cation coordination number (N_{MeO}) reported for metaphosphate glasses [39].

Cation	Li^+	Na^+	K^+	Mg^{2+}	Ca^{2+}	Sr^{2+}	Zn^{2+}
Coordination number (N_{MeO})	4±0.4	5±0.4	6.7	4	7±0.4	5.1	4

1.6 Sodium polyphosphate glasses and its crystalline forms

Unlike our research group's prior focus on CPP glass, this thesis will target NaPP glass which, similar to CPP, is in the metaphosphate region where $x = 0.5$. In contrast to CPP glass, alkali polyphosphate glasses including NaPP glass are highly soluble in water,

which allows studying them using conventional polymer characterization methods [3]. The phase diagram of sodium phosphate is represented in Figure 1.4 from x of 0.5 ($Na_2O.P_2O_5$) to 0.67 ($2Na_2O.P_2O_5$) [5]. In the metaphosphate region, one resides exactly on the left axis, and rapid quenching of the melts with [Na]/[P] ratio of one at the temperatures above 627.6°C results in NaPP glass, also known as Graham salt. Crystalline forms of NaPP exist as well. Overall, there are six different crystalline forms of NaPP, where $NaPO_3$-I, I' and I" are crystalline trimetaphosphate rings, while $NaPO_3$-II, III (Maddrell salts) and IV (Kurrol salt) are extremely long chains of polyphosphates. A helical chain where the chains repeat themselves every four phosphorus atoms is reported for sodium Kurrol salts [46-48]. However, in Maddrell salts the chains repeat themselves every three units and they do not spiral, instead forming zigzag shapes [5, 49, 50]. This variety in crystalline structures is partly due to the high elasticity of the polyphosphate chain. The typical P-O_b-P angle is ~135° [51], but could go as high as 173.2°, demonstrating how elastic these chains really are [52]. These periodic chains continue beyond a crystal unit and ultimately break down at certain chain length with an OH terminal group without affecting the overall crystalline phase. It is known that the length of these chains in crystalline sodium and rubidium polyphosphates is extremely long (over a thousand), similar to that of crystalline potassium polyphosphate, Kurrol salt [5].

NaPP glass consists of a wide range of chains that are rarely exceeding 200 phosphorus atoms per chain. Strauss et al. [41, 42] have shown that for long chains of NaPP glass ($\overline{D_p}$ ~200), approximately one out of every thousand phosphorus atoms is a branching unit (0.1%) that disappears completely within about 12 hr after the sample is dissolved. In

NaPP glass, both experiments and models [53, 54] have shown that the average Na-O distance is ~2.38 Å, with a coordination number of 5±0.4 for sodium that is in good agreement with its coordination number of 6 in the crystalline form. In contrast to NaPP glass, it is extremely difficult to get potassium metaphosphate glass to form because the rate of dehydration of potassium dihydrogen orthophosphate becomes appreciably fast around 205-208°C and the chains grow extremely fast, resulting in a mixture of extremely long chains that are crystalized easily into potassium Kurrol salt.

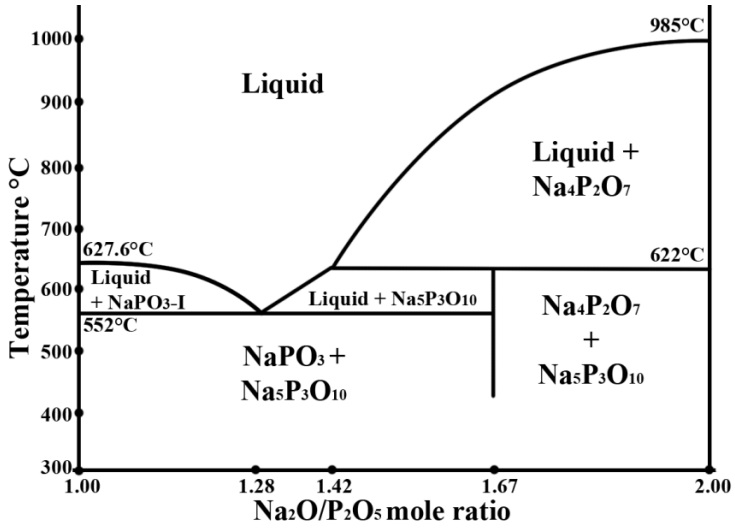

Figure 1.4 The sodium phosphate phase diagram between $Na_2O.P_2O_5$ and $2Na_2O.P_2O_5$ (Adapted from [5]).

1.7 Sodium calcium polyphosphate glasses and its crystalline forms

Glasses in the system Na_2O-CaO-P_2O_5 have also been the center of attention as a tissue engineering scaffold due to the potential to control their dissolution rates based on the Na/Ca ratio [55-60]. Figure 1.5 shows the region where these glasses can be achieved [55]. Similar to binary glasses, in the polyphosphate region where the values of x are approaching the pyrophosphate value of 0.67, the system does not form a glass and instead rapidly crystalizes. In the metaphosphate region (x=0.5), it is possible to have a

glass at all different Na/Ca ratios (Figure 1.5). Glasses in the metaphosphate region are related to the calcium-sodium polyphosphate coacervates that are the focus of this thesis, and their general formulation is yNa$_2$O - (1-y)CaO - P$_2$O$_5$, where $0 \leq y \leq 1$. At one extreme we have CPP glass (y=0) and at the other end, NaPP glass (y=1). As expected, Q^2 sites are dominant in the ^{31}P-NMR analysis of these glasses, which is the signature of long chains of polyphosphates [56]. In the metaphosphate region of these complex glasses, crystalline phases also exist as shown in the phase diagram in Figure 1.6 [5].

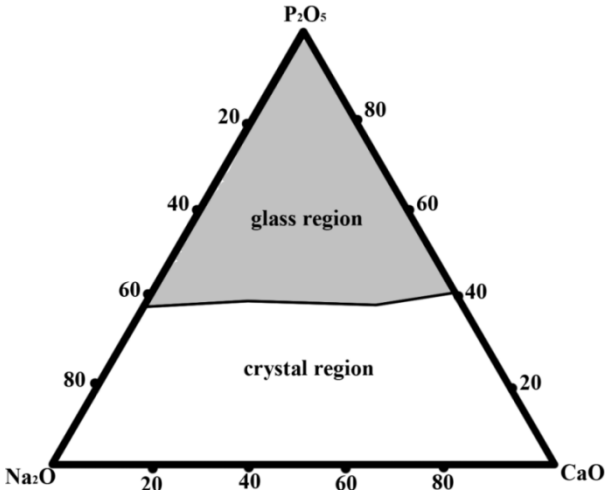

Figure 1.5 Composition of sodium-calcium-phosphate glass forming region (mol%) (Adapted from [55]).

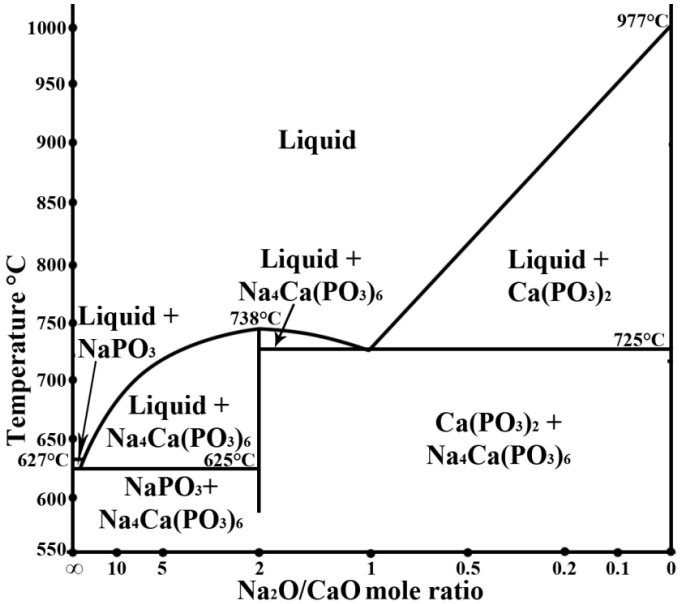

Figure 1.6 The sodium calcium metaphosphate phase diagram between Na$_2$O.P$_2$O$_5$ and CaO.P$_2$O$_5$ (Adapted from [5]).

In general, crystalline complex polyphosphate compounds containing alkali metals (Me^{I} = Li, Na or K) and divalent cations (Me^{II}) may be found in these stoichiometries, i.e. $Me^{I}Me^{II}(PO_3)_3$, $Me^{I}_4Me^{II}(PO_3)_6$, $Me^{I}_2Me^{II}(PO_3)_4$ or $Me^{I}Me^{II}_2(PO_3)_5$ [61]. Currently, only the first two stoichiometries have been identified for the $y$$Na_2O$ - (1-y)CaO - P_2O_5 system. $Na_4Ca(PO_3)_6$ is constituted of two tri-metaphosphate rings, where one calcium is shared between two tri-metaphosphate anions [57, 58]; in contrast, $NaCa(PO_3)_3$ is a long zigzag chain of polyphosphate that repeats itself every three phosphorus atoms [59]. Other crystalline polymorphs of the $y$$Na_2O$ - (1-y)CaO - P_2O_5 system may also exist, including structures similar to the benitoite-type structure of calcium potassium tri-metaphosphate ($KCa(PO_3)_3$) [62] or cobalt potassium polyphosphate ($KCo(PO_3)_3$), where helix chains of polyphosphates entrap cobalt atoms within their spiral confinement [63].

1.8 Polyphosphates and water

It is well known that phosphate glasses are vulnerable to water and this has limited their applications in industry. In contrast, as a biomaterial for drug delivery and tissue engineering applications, this limitation is considered the greatest advantage of these glasses; therefore it is essential to understand the reactions between phosphate glasses and water. In phosphate glasses, the vulnerability to water is a result of a series of complicated reactions, and the rate of each of these reactions is directly related to the modifying cation. In general, these series of reactions can be categorized into three sequential steps: coacervation, dissolution and degradation.

1.8.1 Coacervation of polyphosphates

Upon contact with water the surface of phosphate glasses transforms into a highly viscous water immiscible liquid or coacervate[1] [64]. The transformation involves several steps and its rate depends on the glass composition. The initial, almost instantaneous step is the hydration of cations on the surface of the glass with molecular water. This behavior is common in many salts where cations have irregular coordination environments due to the low stoichiometric ratio of O atoms/cations (e.g. $Na_2CO_3.H_2O$, NaH_2PO_4 and $Na_2HPO_4.2H_2O$) [65]. In CPP glass, there are four oxygen atoms for each calcium atom, insufficient to satisfy the calcium coordination number of 7. Consequently, calcium cations share the available oxygen atoms and in this process their coordination environment becomes distorted; in CPP glass, 5 oxygen atoms are at the distance of 2.36 Å and the other 2 are at the 2.86 Å [44]. As a result of this distortion, and upon contact with water or moisture in the air, a competition occurs between polyphosphate terminal oxygen and water oxygen to bond with calcium. In this process, the molecular water adsorbs to the CPP glass in a reaction similar to the hydration of its precursor, $Ca(H_2PO_4)_2.H_2O$. This phenomenon is common in every metaphosphate glass including NaPP glass.

[1] Bungenberg De Jong and Kruit used the term 'coacervate' for the first time in 1929 to describe polymer particles coming together in a heap. In this work, the term is used to describe a highly viscous liquid that is immiscible with water. The coacervate is constituted of a highly concentrated mixture of polymer chains that are hold together by a combination of electrostatic and hydrophobic forces. There is *no cross-linking between polymer chains in the coacervate* and therefore, there is no significant elastic behavior. So a coacervate should be considered just as an extremely viscous liquid and it should not be confused with the term hydrogel. Hydrogels are also constituted of a series of polymer chains but they are held together due to the chemical or physical *cross-linking* of the chains. Because of this cross-linking, hydrogels show an elastic behavior and they usually do not flow, though some flow may be possible if these crosslinks are sufficiently weak.

SAXS [66], FTIR [32, 67-69] and DTA/TGA [36, 67, 69-71] have all shown that, after drying, this molecular water remains in the glass that has been in contact with water or humidity. The exact stoichiometric amount of this molecular water is unknown ($[Me^{I}PO_3]_n$ or $[Me^{II}(PO_3)_2]_n$. x H_2O) but depends on the relative humidity and the contact time [68]. In magnesium polyphosphate [72] and calcium polyphosphate [73], 31.7% (wt%) and 18% of the air-dried glass films are water, respectively. This molecular water does not leave the system by washing with ethanol or long drying using drying agents (e.g. $CaSO_4$), and can only be removed by heating. This dehydration process has been studied by a combination of XRD, NMR, FTIR and DTA/TGA in CPP [67], and magnesium polyphosphate [71]. It has been shown that most of this water leaves the glass below 200°C but only a part of it vaporizes, with the remainder reacting with polyphosphates to form mono- and di-phosphates. As the heating continues these mono- and di-phosphates may condense again to form pyrophosphates, other polyphosphates as well as different crystalline structures [67, 71].

Molecular water bonding is just the first step of the hydration process in polyphosphate glasses. It is known that when particles of NaPP glass are added to water, their surfaces immediately become gelatinous (coacervate) and then they congeal together to form a sticky transparent mass that disappears into the solution after 1-2 hr [5]. The same coacervate mass has been reported for CPP [73-75], magnesium polyphosphate [75], and sodium-calcium polyphosphate [76, 77] glasses in contact with water. When fine particles (< 20 μm) of CPP glass are kept in contact with water for 2-3 days, water diffuses into them, they congeal and transform to a coacervate [73-75]. SEM has shown that when larger glass particles are introduced to water, only the surface (thickness of ~10

μm) transforms to this coacervate state [76]. While water penetrates the surface, the coacervated surface dissolves and degrades into the solution; therefore, it is believed that the thickness of this coacervated layer should remain constant [76, 77]. Understanding the properties of this coacervate is essential to my project, as the *in situ*-forming depot created with addition of divalent cations to NaPP solutions is indeed a coacervate. In the glass, cations crosslink a number of different chains based on their coordination number, but in the coacervate the chains are not crosslinked, at least in calcium and magnesium polyphosphates [72, 78]. Viscosity measurements of magnesium and calcium polyphosphate coacervates have shown that these coacervates are highly viscous Newtonian solutions with no elastic network structure [78]. In contrast, the presence of trivalent cations such as aluminum in the polyphosphate glass results in a hydrogel instead of a coacervate [72, 79]. Presumably, one polyphosphate chain could chelate a small divalent cation, but in presence of a trivalent cation the third valence crosslinks two polyphosphate chains and forms a hydrogel.

XPS [76] and inductive coupled plasma emission spectroscopy (ICP) [77] have shown that the molar ratio of cation to phosphorus in a coacervate formed from a polyphosphate glass is the same as that of the original glass (e.g. 0.5 for CPP and 1 for NaPP); in the transformation from a glass to a coacervate, then, no ion is leached from the glass into the solution. By means of elastic recoil detection analysis (ERD), Bunker et al. [77] showed that the amount of hydrogen in the coacervate is significantly high and they concluded that it is in the form of H_2O. This high amount of water in the coacervate is very well documented; for a CPP coacervate, the amount of entrapped water is reported to be ~52% (wt%) [73], while values around 60% are reported for magnesium polyphosphate

coacervate [71, 72]. Water is the only solvent for soluble polyphosphate glasses such as NaPP [5], and in a similar pattern, it is a good plasticizer for the less soluble polyphosphate glasses such as CPP. Presumably, the entrapped water forms the hydrated shell of cations and phosphates in the coacervate, allowing the polyphosphate chains with their counter-ions to pass along each other. This plasticizer effect of water has been shown by viscosity measurements of coacervates at different volumes of water, with a higher volume of water corresponding to a lower viscosity for the coacervate [78]. So overall, a coacervated polyphosphate is a hydrated polyphosphate glass in which cations are no longer crosslinking the chains and water is acting as the plasticizer between the chains. The question remains as to how these chains are held together, and why they do not go into the solution if they are completely hydrated and not bound together. This is a result of a combination of electrostatic, hydrophobic and entropic forces that originates from the highly charged nature of the polyphosphate chain and its reactions with its counterions. To better understand this behavior, it is essential to understand the properties of polyelectrolytes in their counterion environment as well as the active precipitation mechanisms in the presence of multivalent ions.

1.8.2 Polyelectrolytes

Polyelectrolytes, or polymers bearing dissociated ionic groups (Figure 1.7), are a fascinating class of macromolecules that exhibit a number of interesting phenomena due to their dual character of highly charged electrolytes and macromolecular chain structure [80]. A polyphosphate chain is composed of a series of charged phosphate groups, and since there is no organic backbone, this polymer is regarded as one of the most hydrophilic polyelectrolytes [81]. Immediately after the findings of Van Wazer that

confirmed Graham salt as a long chain polyphosphate, Strauss focused on studying the properties of polyelectrolytes using polyphosphate chains as the model [82-87].

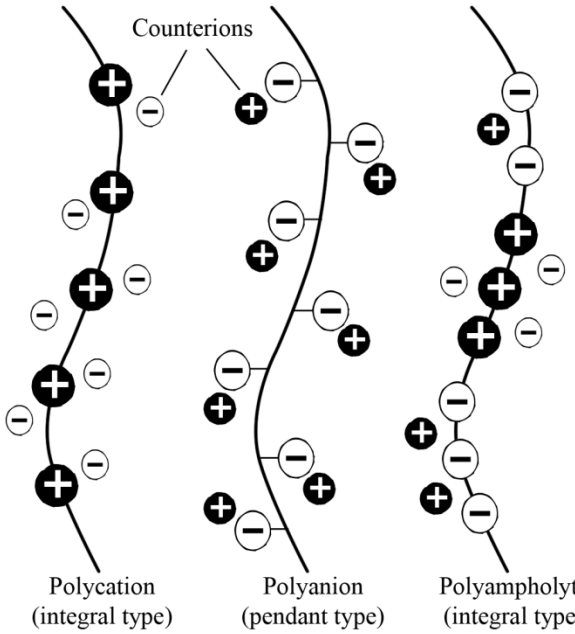

Figure 1.7 Classification of polyelectrolytes into polycations, polyanions and polyampholytes (Adapted from [80]).

Unlike low molecular weight electrolytes, which are dispersed evenly in a solution, polyelectrolytes cause a high concentration of charge in their vicinity that consequently attracts most of the counterions to their environment. The dimensionless charge density parameter (ξ) introduced by Lifson and Katchalsky [88] is defined as follows:

$$\xi = \frac{e^2}{\varepsilon k_B T b} = \frac{\lambda_B}{b} \qquad \text{Equation 1.3}$$

where b is the distance between two charged groups on the polyion, ε the dielectric constant, T the Kelvin temperature, k_B the Boltzmann constant, and λ_B is the Bjerrum length, defined as the distance at which the Coulomb interaction between two unscreened elementary charges is equal to the thermal energy. The charge density determines the interactions of the polyion with counterions, and most of the properties of a

polyelectrolyte can be described by this parameter using different theoretical approaches [89-92]. According to the Manning theory [89-91], counterions exist in three different states in a polyelectrolyte solution. The first group includes counterions that are chemically site bonded to the polymer chain; this group is referred to as *condensed* counterions. In the second group, the counterions are still in close proximity to the polymer chain but they are *not* condensed. These counterions, known as the *diffused layer*, are able to move along the axis of the polymer chain and are entrapped in the vicinity of the polyion due to electrostatic forces. Finally, the last group consists of counterions that are freely scattered in the solution.

The fraction of condensed counterions is directly related to the charge density of the polyelectrolyte. In a highly charged polyelectrolyte ($\xi > 1$), the distance between charged groups is smaller than the Bjerrum length ($\lambda_B < b$), and as a result the system is unstable and counterions condense on the polymer to decrease the effective charge density to the value of one ($\xi = 1$). In the limit of infinite dilution, the fraction of condensed counterions (θ) is then given by [89]:

$$\theta = \frac{1}{Z}\left(1 - \frac{1}{Z\xi}\right) \qquad (\text{for } Z\xi > 1) \text{ Equation 1.4}$$

where Z is the valence of the counterion. Manning theory, and the description of counterion positions based on this theory, can be used to explain some of the reported results of polyphosphates in solution, and to give an overall picture of the interactions between polyphosphate and its counterions in solution, in the coacervate and in our system. It could also be related to the two kinds of sites that have been reported for

calcium in polyphosphate solutions. These two kinds of sites will be explained later in this background.

1.8.3 Complexing and precipitation of polyelectrolytes in the presence of counterions

A number of important industrial applications for linear polyphosphates are based upon their ability to form soluble complexes with metal ions. The term *sequestration* is also used to describe this complexing process whereby ions such as Ca^{2+} could remain *in solution* and yet essentially act as if they were not there [7]. Even monovalent ions are chelated by polyphosphate chains, and this complexing ability is a general phenomenon found for all polyelectrolytes with high charge density. In polyphosphates, the percentage of dissociated monovalent ions (free ions) decreases rapidly with increasing degree of polymerization until it reaches 33% at a $\overline{D_p}$ of approximately 100 (Figure 1.8) [5, 93]. Monovalent ions do not dissociate completely because of the high charge density of the chain.

The stability of the counterion-polyphosphate-complexes has been the subject of several studies [6, 84-86, 94-96]. These studies have measured the dissociation constants (pK) of different counterion-polyphosphate-complexes and have reported values such as $pK_{Na}=3$ for the sodium-polyphosphate-complex [5]. The ability of polyphosphate to complex alkaline earth metal ions is much greater than its ability to complex alkali metal ions. The dissociation constants for the alkaline earth metals are from 10^2 to 10^7 times larger than the dissociation constants for the alkali metals [5, 6]. These pK values are directly related to the $\overline{D_p}$ of condensed polyphosphates; as the $\overline{D_p}$ increases, the dissociation constant

of the complex increases, tending to plateau at a $\overline{D_p}$ of ~10; as a result, the $\overline{D_p}$ of commercial Graham salts for water softening is higher than 10, usually 14 [6]. Because of these high pKs, addition of Graham salt to most multivalent salts results in their dissolution. In fact, EDTA is the only salt that has a pK value higher than a polyphosphate chain and this is why it is used for dissolving polyphosphate glasses.

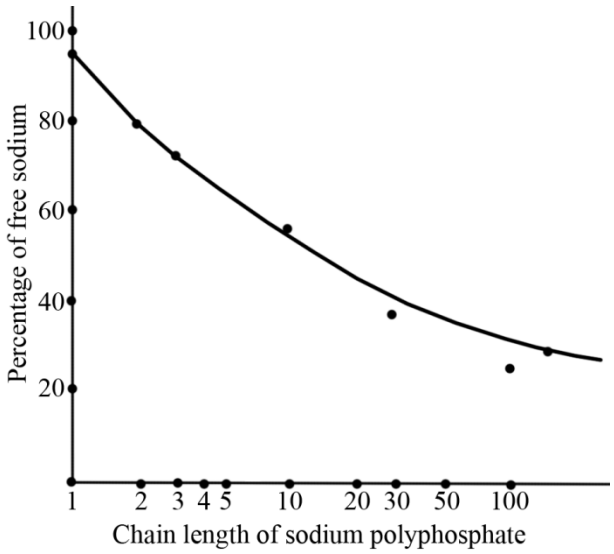

Figure 1.8 Degree of dissociation of sodium salts of chain phosphates in solution (Adapted from [5]).

The amount of divalent ions, especially calcium and magnesium, that can be sequestered by polyphosphate chains has been extensively studied due to its relevance for industrial applications. With softening of hard water, for example, a precipitate forms in the NaPP solution when the molar ratio of calcium to phosphorus exceeds 10% (Note that this precipitate forms between calcium and the precipitating anion and not polyphosphate; therefore, it is not a coacervate) [6]. The presence and amount of precipitating anions affect significantly the Ca/P molar ratio where precipitation occurs. Most of the studies on polyphosphate complexing of calcium have been conducted in the presence of these precipitating anions [6, 96]. In these studies the amount of calcium to form a barely discernible precipitate is dependent upon two competing equilibria [6]:

Ca^{2+} + polyphosphate-anion ↔ Calcium-polyphosphate complex

Ca^{2+} + precipitating-anion ↔ Calcium precipitate

If the precipitating anion is in excess and it is an anion of a highly insoluble calcium salt (e.g. CaF_2), then the second reaction is favored and the complexing ability of the polyphosphate drops significantly. In these cases, precipitation happens between Ca^{2+} and that precipitating anion at very low Ca/P molar ratios (Table 1.3). This means that we should avoid adding high concentrations of precipitating anions to our system because they bond to calcium ions, and the precipitate that is formed is a salt of that precipitating anion and calcium rather than a coacervate.

Table 1.3 Complexing of Ca^{2+} by different polyphosphates in presence of large amount of precipitating anions [6].

Polyphosphate $\overline{D_p}$	Concentration of polyphosphate solution (M in phosphorus)	Precipitating anion added to polyphosphate solution	Concentration of precipitating anion (M)	Controlled value of pH	Assumed composition of precipitate	Ca/P molar ratio where precipitate forms (%)
5	0.015	Fluoride	0.1	10	CaF_2	1
5	0.015	Oxalate	0.1	10	CaC_2O_4	4
5	0.015	Carbonate	0.1	12	$CaCO_3$	25
5	0.015	Sulfate	0.1	10	$CaSO_4$	42
5	0.015	Orthophosphate	0.1	11.5	HAP	3
5	0.01-0.05	Orthophosphate	0.1	8	$CaHPO_4$	16±1
14	0.01-0.05	Orthophosphate	0.1-0.15	8	$CaHPO_4$	13±1
75	0.01-0.05	Orthophosphate	0.1-0.15	8	$CaHPO_4$	11±3

In contrast, in the absence of precipitating anions, only polyphosphate chains bond with calcium ions that are added to the solution in their highly soluble salt forms such as $CaCl_2$ or $Ca(NO_3)_2$. Here, precipitation in the form of a coacervate happens at much higher Ca/P molar ratios compared to the situations where there is a precipitating anion. For instance, in a polyphosphate with an $\overline{D_p}$ of 75 and concentration of 0.01-0.05 M, the precipitation happens at a Ca/P molar ratio of 11±3% in presence of 0.1 M orthophosphate (*here, the precipitate is a salt of calcium and orthophosphate*), and at a Ca/P ratio of 33±4% in its absence (*here, the precipitate is a coacervate of CPP*) [6]; the precipitated coacervate so-

formed in the absence of precipitating anions converts to a polyphosphate glass when it is dried. The making of this coacervated precipitate is the focal point of this thesis.

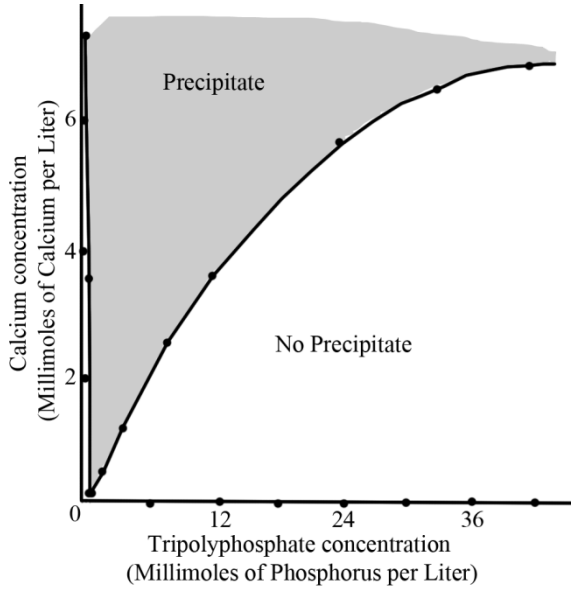

Figure 1.9 Precipitation phase diagram of calcium-tri-polyphosphate system at 60°C (Adapted from [6]).

Figure 1.9 shows the precipitation phase diagram of a calcium-tripolyphosphate system in the absence of precipitating anions, and the line determines the boundary between precipitating and non-precipitating regions at 60°C. The precipitating region is very wide and comes close to the calcium axis, so close in fact that this narrow area of clear solution is generally overlooked. The Ca/P molar ratios corresponding to the right boundary of the precipitating region range from 33% near the origin, to 16% at the highest concentrations studied [6]. Of course this phase diagram is for a very short chain tripolyphosphate and, to our knowledge, there are no reports of phase diagrams for higher $\overline{D_p}$ polyphosphates. However, there are similar precipitation phase diagrams of other high chain length polyelectrolyte-calcium systems, such as the polyacrylic acid (PAA)-calcium system [97, 98].

Figure 1.10 shows the precipitation phase diagram of a PAA-calcium system at three different PAA degrees of polymerization. At low PAA concentrations, precipitation appears first for the largest molecular weight, while at high concentrations the demixion line (i.e. the boundary line between precipitating and non-precipitating regions) is nearly independent of the degree of polymerization. Delsanti has attempted to explain these phase diagrams by comparing different multivalent-polyelectrolyte systems [97-99]. He realized that the nature of condensation phenomenon described in the Manning theory should be differentiated based on the functional group of the polyelectrolyte. For polyelectrolytes containing anionic functional groups that have high dissociation constant with divalent cations, such as sulfonate on poly(vinyl sulfonate) (PVSF), the condensation reaction is basically *electrostatic in nature*. In contrast, if the polyelectrolyte functional group is an anion that has a low dissociation constant with a divalent cation, such as carboxylate on PAA or phosphate on polyphosphate, then the condensation reaction is *chemical*. The presence of *chemical condensation* is necessary for precipitation of polyelectrolytes by divalent counterions. As a result, divalent cations do not precipitate PVSF solutions but they precipitate PAA solutions. Interestingly, the only divalent cation that precipitates PVSF is Ba^{2+}, which is known for its highly insoluble sulfate salts [97, 98].

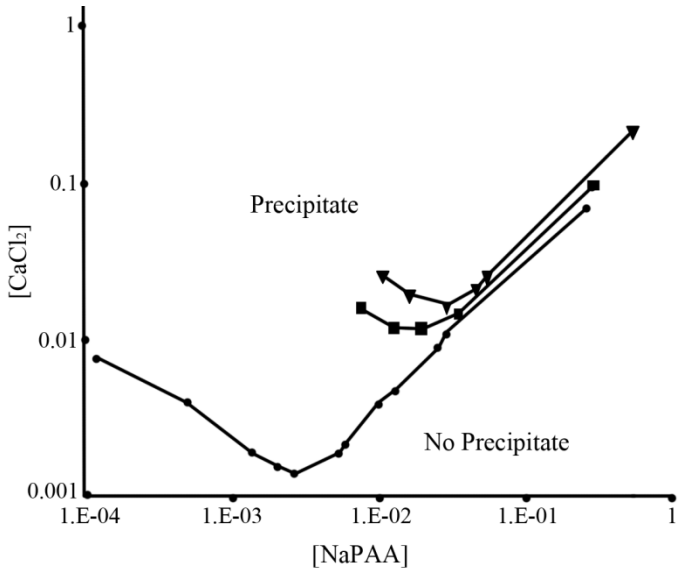

Figure 1.10 Experimental NaPA/$CaCl_2$ precipitation phase diagrams; Degree of polymerization: 40 (triangles), 70 (squares), 8300 (circles) (Adapted from [97, 98]).

Delsanti showed that chemically condensed divalent cations exist both in mono-complex ($[AMe^{II}]^+$; A is a functional group on a polyelectrolyte and Me^{II} is a divalent cation) and di-complex (A_2Me^{II}) states. He proposed the following equation to semi-quantitatively describe the experimental precipitation phase diagram of Me^IPAA (Me^I is a monovalent cation such as sodium poly acrylic acid) or other similar polyelectrolytes in presence of divalent cations [97, 98]:

$$\frac{1}{D_p C_m} + \frac{\sigma^3}{1-\varphi} + \frac{Z_{eff}^2}{2I} - 2(1 - f' - f - f_m - f_d)(f_m + f')|V_{12}| - 2\sigma^3 X_d f_d = 0$$

Equation 1.5

where D_p is the degree of polymerization, C_m is the number of monomers (functional groups) per unit volume, σ^3 is the volume of the monomer, $\varphi = C_m\sigma^3$ is the volume fraction occupied by the polymer, $Z_{eff} = (f + 2f' + 2f_m + f_d - 1)$, I is the ionic strength of the solution, and X_d is the parameter related to the interaction between water and the di-complex (A_2Me^{II}). The water is assumed to be a good solvent ($X_d = 0$) for negatively

charged free functional groups (A^-) and positively charged mono-complexes ($[AMe^{II}]^+$). The local attraction V_{12} has the following form:

$$V_{12} = -\frac{\pi\lambda_B^2}{\sqrt{8\pi\lambda_B I}}B \qquad \text{Equation 1.6}$$

where λ_B is the Bjerrum length as described in Equation 1.3 and B is a numerical factor of the order of 1. Parameters f_m and f_d represent the *chemically condensed* mono-complex ($[AMe^{II}]^+$)), and di-complex (A_2Me^{II}) fraction of monomers, respectively, and parameters f and f' are the monomer fractions carrying *electrostatically condensed* counterions Me^I and Me^{II}, respectively.

The first three positive terms in Equation 1.5 are the forces acting against precipitation, and the last two negative terms are in favor of precipitation. The first term comes from the entropy of the polymer, the second term represents the steric excluded volume and the third term corresponds to the electrostatic repulsion between negatively charged monomers having an effective charge Z_{eff}. The fourth term arises from interaction between negatively charged free functional groups (A^-) and those possessing an effective positive charge. The last term comes from the hydrophobic force that is caused by chemically condensed di-complexes [97, 98].

Figure 1.11 shows the relative interaction of these terms at constant PAA concentration of 0.01 M at different [Ca]/[COO] ratios. The effect of entropy and steric-excluded volume is negligible at this polymer concentration, and the main force responsible for polyelectrolyte stability is the electrostatic repulsion. As the amount of calcium in the system increases, the electrostatic repulsive force decreases while electrostatic attractive and hydrophobic forces increase. Precipitation occurs when the hydrophobic term is

equal to the repulsive term in absolute value, which corresponds to the crossing point of the two upper curves in Figure 1.11 [97]. One should note that the attractive force alone is not enough for precipitation to occur and, as a result, cations that do not chemically condense (e.g. monovalent cations) are not able to cause a precipitate. Therefore, we could say that the *NaPP coacervate dissolves rapidly because* Na^{+} *do not chemically condense on polyphosphate chains, but CPP coacervate does not dissolve because* Ca^{2+} *chemically condense on polyphosphate chains and make them hydrophobic.*

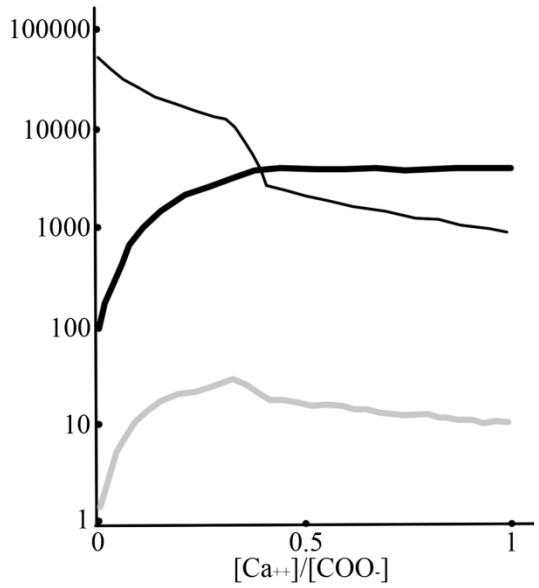

Figure 1.11 Variation of interaction terms of the equation 1.5 as a function of the added calcium (the monomer concentration is fixed to 0.01 M): (thin black line) repulsive electrostatic term, (thick black line) attractive term due to the dicomplexation in absolute value, (thick gray line) attractive electrostatic term in absolute value (Adapted from [97, 98]).

1.8.4 Analytical studies of coacervation between polyphosphate and different cations

It has been known for some time that adding excess amounts of different divalent cations to NaPP solution causes precipitates similar to the PAA-divalent cation system. Large cations (Ba^{2+}, Sr^{2+}, Pb^{2+}, Ag^{+}, Bi^{2+}, ZrO^{2+}, $UO_2{}^{2+}$, and $Hg_2{}^{2+}$) in excess give flocculent, solid precipitates, whereas smaller cations (Ca^{2+}, Mg^{2+}, Zn^{2+}, Mn^{2+}, Ni^{2+}, Co^{2+}, Fe^{2+},

Fe^{3+}, Cr^{3+}, Hg^{2+}, and Cu^{2+}) yield coacervates [5]. Monovalent cation additions do not result in a precipitate unless they are at high concentrations (e.g. NaBr 0.47 M solution [87]). Recently, coacervate precipitates have become the center of attention of some research groups mainly as a precursor for preparation of different complex polyphosphate glasses in low temperature. There are reports of polyphosphate coacervates with cations such as Mn^{2+} [36], Ni^{2+} [69, 100], Co^{2+} [69, 100], Fe^{3+} [31, 32, 35, 68], Mg^{2+} [37, 71, 72, 78, 101-103], Ca^{2+} [31, 33, 34, 37, 67, 70, 78, 102-105], Al^{3+} [35, 79, 102], and Zn^{2+} [38, 106]. In all of these reports, soluble salts of these cations (chloride or nitrate) are added to NaPP solutions and a coacervate is formed. Polyphosphate glasses are obtained by drying this coacervate in a desiccator or by addition of ethanol.

Raman studies of coacervates have provided some interesting results. The main bands of the Raman spectra of polyphosphates are at ~690 and ~1180 cm^{-1}, corresponding to P-$O_{bridged}$ and P-$O_{terminal}$ symmetric stretching modes, respectively [33, 39, 69, 100]. Raman band broadening, a frequency shift and a decrease in the ratio of the amplitudes of these two bands are reported depending on the cation that is bonded to the P-$O_{terminal}$ group [39]. In NaPP coacervates, these bands are reported at 684 and 1164 cm^{-1} [69], in CPP coacervate at 698 and 1168 cm^{-1} [33], in Ni^{2+}coacervate at 694 and 1164 cm^{-1}, and in Co^{2+} coacervate at 694 and 1162 cm^{-1} [69, 100]. It is interesting that at low Co/P molar ratios (<12-17%), the P-$O_{bridged}$ band suddenly increases from 684 cm^{-1} at NaPP to 694 cm^{-1}, while simultaneously the P-$O_{terminal}$ band decreases from 1164 to 1159 cm^{-1}. Then, as the Co/P molar ratio increases, the P-$O_{bridged}$ band is maintained around 694 cm^{-1} while the P-$O_{terminal}$ band goes back up to 1162 cm^{-1} [100]. These observations and their dependence on the Co/P molar ratio is explained based on the assumption that

complexing between metal ions and polyphosphate chains occurs in two different kinds of sites depending on the Co/P molar ratio; at low Co/P ratios, cobalt ions are chelated at *cage-like* sites on the chain where they cannot interact with water. At these sites, bonding of cobalt ion to the terminal oxygen atoms decreases the electronic density of the P-$O_{terminal}$ bond but increases the electronic density of the P-$O_{bridged}$ bond, causing vibrational modes to behave opposite each other. At higher Co/P molar ratios, cobalt ions are chelated at a second, more exposed site where they can interact with water molecules, which increases the electronic density of the P-$O_{terminal}$ bond and its Raman band [69, 100].

The presence of these two kinds of sites is also suggested based on the EXAFS [100], and europium luminescence spectroscopy [104]. Filho, et. al utilized the possibility of substituting spectroscopically active trivalent Eu^{3+} for divalent Ca^{2+} to understand the interaction between these ions and polyphosphates [104]. Based on this study, they concluded that for low Ca/P molar ratios, Ca^{2+} would locate in cage-like sites with a coordination number of 6 provided by phosphate units of the polyphosphate chain. However, when Ca/P molar ratio passes ~17%, Ca^{2+} is expected to occupy a second family of sites where they could interact with water molecules. These cage-like sites also exist in the europium-polyphosphate system but their saturation happens at a lower Eu/P molar ratio of ~10% [104]. EXAFS studies by Silva et. al also confirmed the presence of these two kinds of sites in cobalt and nickel polyphosphate systems [100]. They concluded that, similar to the calcium-polyphosphate system [104], in cobalt and nickel polyphosphate systems, the cage-like sites are saturated at the M/P molar ratio of ~17%;

further addition of these cations results in occupation of a second site where cations interact with water molecules [100].

P-NMR [67, 71, 76, 81, 93, 104, 106-109] is the other method that have been utilized to study the coacervation of polyphosphates by divalent cations. Van Wazer showed that in liquid ^{31}P-NMR spectra of condensed phosphates, isolated (Q^0), end (Q^1), middle (Q^2) and branching-point (Q^3) PO_4 groups give separate resonance peaks [107, 108]. When a chain of atoms is attached to a phosphorus atom, the neighboring atom has the greatest effect on the chemical shift (e.g. oxygen atoms in orthophosphate), with the atom next in line (e.g. next phosphorus atom in condensed phosphates) having the next most important effect, and so forth [108]. In polyphosphates, upfield shifts[1] of ~-10 and -18 to -20 ppm are found, respectively, for end and middle groups [93, 107, 108]. Measuring the ratio of areas under the peaks of middle and end phosphate groups is a method for determining the $\overline{D_p}$ of polyphosphates. Using this method, Sinyaev et. al [67] and Umegaki et. al [71] showed that the molecular composition and $\overline{D_p}$ of the precipitated coacervate of calcium and magnesium polyphosphates is not different from the starting NaPP. More interesting are liquid ^{31}P-NMR studies of metal ion complexing by polyphosphate solutions and its effects on phosphorus resonance. Crutchfield et. al [109] studied the complex formation between tri-polyphosphate and calcium or magnesium. They showed that complexing affects the chemical shift of the middle P nucleus much more strongly than that for the end P nucleus. The complexing caused downfield shifts for the middle P atoms of chain phosphates in agreement with the results of Miyajima et. al on zinc-polyphosphate

[1] The chemical shifts in ppm are defined as 10^6 $(H_r - H_s)/H_r$ where H_s and H_r are the magnetic fields required for resonance in the sample and in a reference, respectively. Reference here is 85% H_3PO_4 solution.

system [81] and Filho et. al on calcium-polyphosphate system [104], but in contrast to results reported by Palavit et. al [106].

The downfield deshielding effect of complexing can be explained by considering the distortion of the electronic environment around P arising from the proximity of a metal ion that causes a shift in the center of anionic electron density toward the cation with respect to the P nucleus; this constant outward polarization of electronic charge tends to deshield the P nuclei and shift their peak downfield [109]. Another interesting result reported by Crutchfield [109] and Miyajima [81] is the change in the rate of chemical shift at 1 : 1 metal ion to tripolyphosphate ion molar ratio (Me/P molar ratio~33%), implying the change in behavior of the system at this stoichiometry and the desire for formation of 1 : 1 complexes.

1.8.5 Dissolution and degradation of polyphosphates

During or after the transformation of polyphosphate glasses into the coacervates, two other phenomena that may occur are *chain hydrolysis* and *dissolution*. It is generally accepted that the dissolution of polyphosphate glasses is congruent [5, 76, 77, 110, 111], i.e. the dissolved products in the solution have identical composition (same molar ratios) with that of the bulk glass at all times. This kind of dissolution requires no ion to be leached preferentially, in agreement with the concept that these glasses transform to a coacervated layer where highly charged polyphosphates keep the counterions within their vicinity. However, it has also been suggested that chains are released into the solution *without any hydrolysis* and, once in solution, degradation begins [76, 77, 102]. This statement is probably true for highly soluble forms of polyphosphate glasses such as NaPP or polyphosphates where the multivalent ion to phosphorus molar ratio is lower

than the value that causes precipitation (~30%). In these glasses, chains at the hydrated coacervate layer are released into the solution at much higher rates than their degradation rate. For instance, Delahaye et. al [76] showed that for a glass with the composition of $0.68Na_2O – 0.32CaO - P_2O_5$ (y=0.68; Ca/P molar ratio = 16%), the MAS-NMR spectrum of the pristine glass and the hydrated glass are similar. In contrast, in CPP or other polyphosphate glasses where dissolution rates are lower than degradation rates, chain hydrolysis should be expected to start at the coacervated layer.

Although there remains some debate as to where and when chain hydrolysis starts, the fact that chain hydrolysis happens is undisputed. A superficial perusal of the literature gives the impression that the condensed phosphates are quite unstable; however, the half-life of P-O-P linkages with respect to hydrolysis *at neutral pH and room temperature* is of the order of magnitude of years [5]. Still, a number of factors can accelerate the rate at which chain phosphates undergo hydrolytic degradation in aqueous solution. The major factors and their approximate effect on degradation rate are listed in Table 1.4.

Table 1.4 The effect of different factors on the rate of P-O-P bond hydrolysis [5].

Factor	Approximate effect on rate
Temperature	10^5-10^6 faster from freezing to boiling
pH	10^3-10^4 slower from strong acid to base
Enzymes	As much as 10^5-10^6 faster
Colloidal gels	As much as 10^4-10^5 faster
Complexing cations	Very many-fold faster in most cases
Concentration	Roughly proportional
Ionic environment in the solution	Several-fold change

The degradation rate constant (k) defined by Equation 1.7 has been calculated for different polyphosphate systems and its variation with temperature can be denoted by the Arrhenius equation:

$$k = A_f e^{-E_a/RT} \qquad \text{Equation 1.7}$$

where the temperature independent term, A_f, is called frequency factor, E_a is called the activation energy, and R and T are the gas constant and the absolute temperature, respectively. The activation energy of a P-O-P bond is 25 kcal/mole [5, 110], which is equivalent to doubling the degradation rate every 5°C; this explains why temperature has the greatest effect on polyphosphate chain hydrolysis (Table 1.4). Acidic environments and complexing cations also reduce the activation energy, and as a result the degradation rate increases. The activation energy of polyphosphate in the presence of calcium (CPP) is 19 kcal/mole, significantly lower than the value of 25 kcal/mole for the Graham salt [110]. Therefore, CPP degrades 5 to 10 times faster than NaPP under comparable conditions (but, notably, it *dissolves* more slowly) [110]. At neutral pH and low temperatures, *dissolved* CPP degrades slowly. For instance, at a pH of 6 and temperature of 25°C the half-life of *dissolved* CPP is more than 180 days, but at a pH of 1 and temperature of 50°C, it is less than a day! [110]

Hydrolysis of polyphosphate chains proceeds via four major routes: (1) hydrolytic scission in the interior of the chain to produce two shorter chains; (2) hydrolytic scission of the chain at an end group with the production of orthophosphates; (3) splitting off of tri-metaphosphates from an end of the chain; and (4) splitting out of tri-metaphosphate from the interior of the chain [112-114]. It has been shown that splitting off of small rings, mostly tri-metaphosphates, from an end of the chain is the main route of degradation of polyphosphates in neutral and alkaline solution [5, 40, 113, 114]. Later, these rings degrade into their corresponding polyphosphate such as tri-polyphosphate, which itself slowly degrades into pyro- and orthophosphate. In acidic solution there is also some random scission along the chain [5, 40]. Figure 1.12 shows the distribution of

species in the hydrolytic degradation of dissolved CPP chains ($\overline{D_p}$ of 23) at pH of 1 and 6 [110]. In agreement with the mechanism discussed above, at pH of 6, the formation of ring phosphates is the main route for degradation process, but at pH of 1, random scission and formation of orthophosphates dominate. As CPP degradation continues, the solution becomes saturated by calcium and phosphate ions and, depending on the pH, precipitates such as HAP [77], $Ca_3(HP_2O_7)_2.4H_2O$ and $Ca(H_2PO_4)_2.H_2O$ [103] start to form.

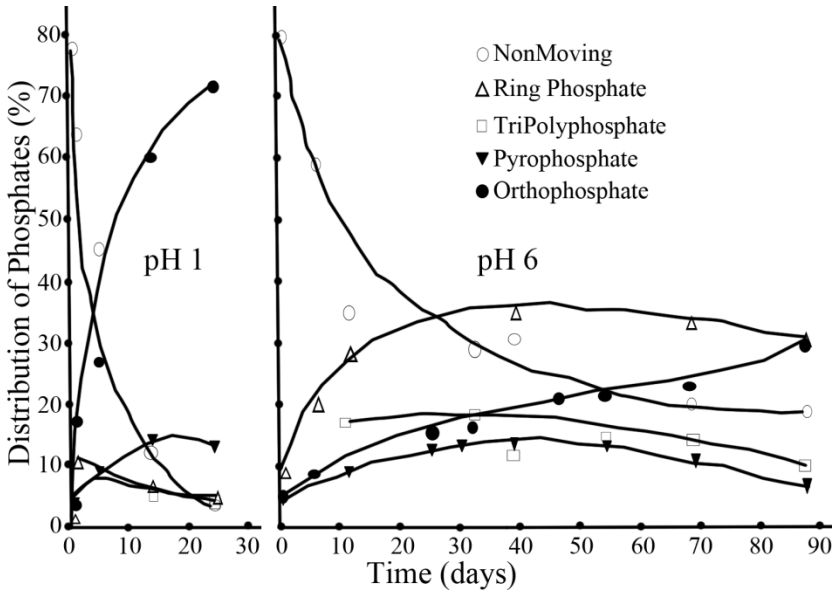

Figure 1.12 Distribution of species in hydrolytic degradation of dissolved CPP glass at 25°C (Polyphosphate designated here as Non-moving is constituted of chains with the $\overline{D_p}$ of 23) (Adapted from [110]).

The overall weight loss of polyphosphate glasses in the system of yNa$_2$O - (1-y)CaO - P_2O_5 in water is reported in Table 1.5 [55, 56, 76, 77]. The reported weight loss rates (dissolution rates) in these studies are not exactly the same because of variables such as temperature, pH, available surface area, and method of studying the solubility (static vs. cumulative), but the overall results follow a similar pattern. In general, higher calcium content increases the durability of the glass (Table 1.5).

Table 1.5 Dissolution rate of different calcium-sodium-polyphosphate (metaphosphate) glasses based on the overall weight loss of the sample.

Glass composition yNa$_2$O-(1-y)CaO-P$_2$O$_5$	Ca/P molar ratio (%)	Dissolution rates reported at different studies (g/cm^2.min)			
		Delahaye [76]	Bunker [77]	Uo [55]	Ahmed [56]
0.8Na$_2$O-0.2CaO-P$_2$O$_5$	10	69×10^{-5}	5×10^{-5}	2.8×10^{-8}	-
0.7Na$_2$O-0.3CaO-P$_2$O$_5$	15	11×10^{-5}	-	-	-
0.6Na$_2$O-0.4CaO-P$_2$O$_5$	20	4.5×10^{-5}	3×10^{-6}	2×10^{-8}	-
0.4Na$_2$O-0.6CaO-P$_2$O$_5$	30	1.4×10^{-6}	-	-	3×10^{-6}
0.3Na$_2$O-0.7CaO-P$_2$O$_5$	35	-	-	-	2×10^{-6}
0.2Na$_2$O-0.8CaO-P$_2$O$_5$	40	6×10^{-7}	-	-	1×10^{-7}
0Na$_2$O-CaO-P$_2$O$_5$	50	3×10^{-7}	-	-	-

Delahaye [76] and Ahmed [56] reported that in acidic conditions, the dissolution rate of polyphosphate glasses is fast at the beginning but it slows down over time. They concluded that this is caused by the increase in the ionic strength of the leaching solution. Interestingly, however, the increase in the ionic strength is not the only cause of this decrease in dissolution rate. Delayahe showed that pristine glasses dissolve at a higher rate than aged ones (ones that have been in highly ionized solutions for a period of time), when both corroded at the *same* ionic strength. Hence, he concluded that ionic strength induces a modification of the hydrated surface [76]. This result is interesting because it proposes that keeping polyphosphate glasses in a highly ionized solution for a period of time makes their surface more durable against water corrosion.

1.9 Polyphosphates and hemostasis

Inorganic polyphosphate is found in every cell in nature but it has not been investigated thoroughly [115-117]. One of the reasons for this is the lack of evidence for any essential metabolic role. Another reason has been the inadequacy of methods to establish the authenticity and size of polyphosphate and its abundance at very low concentrations [118]. In eukaryotes, polyphosphates are found in large amounts and at different $\overline{D_p}$ in subcellular organelles and in yeast vacuoles at levels as high as 20% of the cell dry weight [116]. Due to the abundance of polyphosphates in eukaryotes, its function has

been extensively studied in these microorganisms [115-120]. Many distinctive functions appear likely for polyphosphates, depending on its abundance, $\overline{D_p}$, biologic source, and subcellular location. These include serving as an energy supply and ATP substitute, an osmotic inert reservoir for phosphate, a chelator of metals, a buffer against alkali, a channel for DNA entry, a cell capsule and a regulator of responses to stresses and adjustments for survival in the stationary phase of culture growth and development [118, 119]. In higher animals, polyphosphates having apparent chain lengths ranging from less than 10 to over 5000 orthophosphate units have been found in rat brain and liver as well as in a number of other mammalian tissues [121]. In mammalian cells, they are found in nuclei, mitochondria, lysosomes, and plasma membranes; however, their functions are not yet well-understood [122]. Significant polyphosphate amounts have been found in human mandibular-derived osteoblast-like cells, postulating its role in bone formation and calcification in presence of calcium ions [123]. Because of this, much research has focused on the role of polyphosphates as an osteoblast stimulant [122-124], and in its ability to act as a bone precursor [125, 126].

However, there is another cell population in the human body that has polyphosphates in concentrations higher than any other, and that is platelets. In bacteria as well as in several unicellular eukaryotes, polyphosphate accumulates in acidic granules known as *acidocalcisomes* where it can reach millimolar or molar levels. Acidocalcisomes have been shown to possess calcium- and proton-accumulating activities in their limiting membranes, have very high density (both in weight and by electron microscopy), and are also rich in pyrophosphate, calcium, and other cations. Human platelets possess an organelle, the dense granule, with morphological and biochemical similarities to

acidocalcisomes. Platelet dense granules store extremely high concentrations of calcium together with ATP, ADP, serotonin, and pyrophosphate. The internal matrix pH of the dense granules is 5.4 [127]. Ruiz et. al [127] showed that similar to eukaryotes' acidocalcisomes, dense granules from human platelets are also rich in polyphosphate, which is secreted upon thrombin stimulation.

Transmission electron microscopic imaging of dense granules within a platelet was obtained along with elemental analysis showing that these electron dense granules are rich in calcium and phosphorus atoms, with the P/Ca molar ratio of 1.76 [127]. The concentration of polyphosphate within these dense granules was found to be around 130 mM, making the overall polyphosphate concentration within platelets to be around 1.1 mM; this is 10-20 times higher than that measured in rodent tissues such as brain, heart, kidney, lung and liver [127]. However, in contrast to other cells, all of the polyphosphate detected in platelets are smaller than 100 phosphorus atoms per chain, with the $\overline{D_p}$ estimated to be between 70 to 75 phosphorus atoms per chain [127]. As shown in Figure 1.13, platelets that are treated with thrombin release their intragranular components, including polyphosphates, in less than a minute. Different components that are secreted by platelets from their dense granules are ATP, ADP, pyrophosphate, calcium and serotonin. ATP could act on P2Y receptors on endothelial cells to release prostacyclin and nitric oxide, which in turn cause vasodilation. ADP acts as a platelet agonist and is important for the activation of additional platelets and their recruitment to the site of injury. Similarly, serotonin serves to activate additional platelets while additionally having a vasoconstrictive action that reduces flow at the site of injury, thereby limiting blood loss. Calcium could be important for the binding of adhesive proteins to their

platelet receptors [127]. All of these observations suggest that there has to be a function for pyrophosphate and polyphosphate in the blood clotting cascade as well.

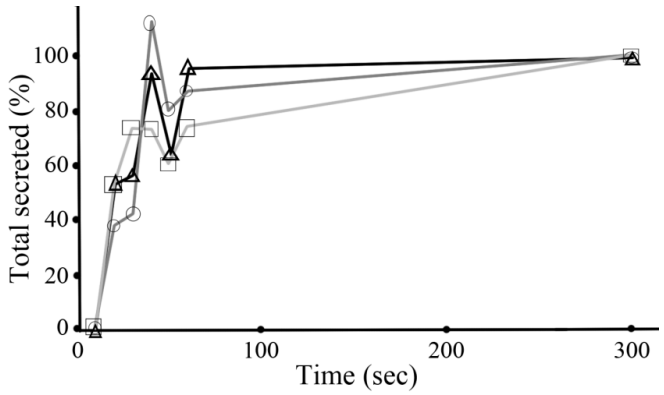

Figure 1.13 Time course of thrombin-induced serotonin (triangles) release compared with pyrophosphate (squares) and polyphosphate (circles) (Adapted from [127]).

Following these initial reports, Smith and Morrissey published several other articles [128-130] and a patent [131] explaining the function of polyphosphate in blood coagulation and the possibility of targeting polyphosphates to modulate the coagulation cascade. To understand the effects of polyphosphate on this cascade, it is necessary to understand the mechanism of blood coagulation and clot lysing. A schematic of the clotting cascade is shown in Figure 1.14. Here, various clotting factors are indicated by their Roman numerals. The intrinsic cascade, also known as the contact pathway, is initiated when contact is made between blood and certain artificial surfaces. The extrinsic pathway, also known as the tissue factor pathway, is initiated upon vascular injury that leads to exposure of tissue factor. The two paths converge at the activation of factor X to Xa. Factor Xa has a role in the further activation of factor VII to VIIa. Active factor Xa hydrolyzes and activates prothrombin to thrombin. Thrombin can then activate factor XI, VIII and V, furthering the cascade. Ultimately, the role of thrombin is to convert fibrinogen to fibrin, which forms clots [131].

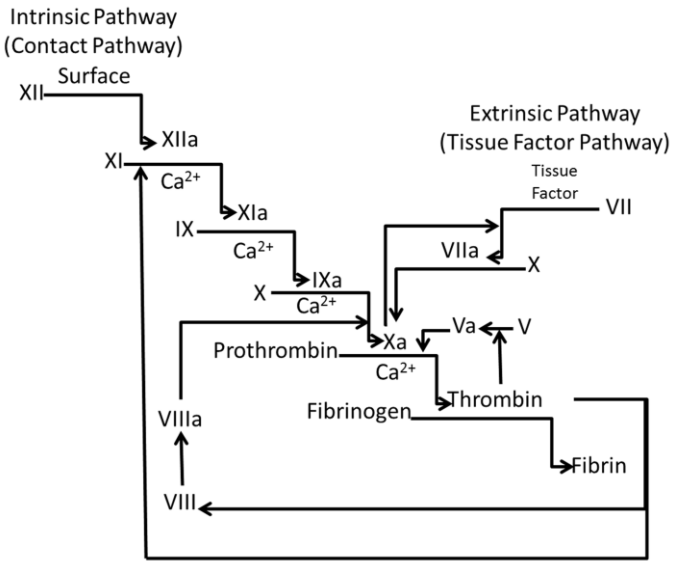

Figure 1.14 The blood clotting cascade and its two pathways (Adapted from [131]).

Following initiation of this coagulation cascade, several mechanisms activate to control its rate. Most important is tissue factor pathway inhibitor (TFPI) that binds very tightly to the active site of coagulation factor Xa and inhibits its enzymatic activity. The inhibited TFPI:Xa complex can then bind to the complex of factor VIIa and tissue factor (TF), resulting in a fully inhibited tetramolecular complex (TF:VIIa:TFPI:Xa). This effectively shuts down further growth of the blood clot [131]. The fibrinolytic system is then responsible for the breakdown of fibrin clot. Plasminogen activates by tissue-type plasminogen activator (tPA) or urokinase-type plasminogen activator (uPA). The product of plasminogen activation is plasmin, whose activity is regulated by alpha2-antiplasmin (alpha2-AP). Plasmin proteolytically degrades fibrin into soluble fibrin degradation products [131].

Polyphosphate acts at 3 different points in the blood coagulation cascade: (1) triggering the contact pathway by activating factor XII; (2) accelerating the activation of factor V by thrombin and factor Xa; and (3) increasing the stability of fibrin [132]. The ability of polyphosphate to trigger the contact pathway is highly dependent on its $\overline{D_p}$ [130, 132].

Using polyphosphate preparations of narrowly defined polymer size, Smith et. al found that the capacity for polyphosphates to activate the contact pathway increased as polymer length increased. Thus, polyphosphates purified from human platelets (size range, 60-100mers) had a specific activity in this clotting assay that was, on a mass basis, 4.9±0.9-fold higher than kaolin[1]. Bacterial polyphosphate had a very high specific activity, while the strongest procoagulant activity in this assay was exhibited by polyphosphates having $\overline{D_p}$ higher than 1000 phosphorus atoms per chain, which had a specific activity 3000-fold higher than that of kaolin [130]. The procoagulant activity of polyphosphate in this clotting assay was dependent on the contact pathway, as XII-deficient plasma did not clot [130].

The ability of polyphosphates to activate factor V is also dependent on their $\overline{D_p}$ [130, 131]. The maximum factor V activation is achieved with polyphosphates that are approximately 125-200 phosphates long, while progressively longer polymers (especially >400mers, including bacterial polyphosphates) still have high specific activities though somewhat reduced compared with 125mers [130]. Polyphosphates shortened factor Xa-initiated clotting times equally well in normal and factor XII-deficient plasma, indicating that this effect of polyphosphate is independent of the contact pathway of blood clotting [130].

Lastly, it has been shown that fibrin clots that have been formed in presence of polyphosphates are much more stable against fibrinolysis [129, 130, 133]. Mutch et. al

[1] To understand the relative potencies of these different polyphosphates, they converted their clotting times into specific activities, based on kaolin equivalents. This was accomplished by determining the concentration, on a mass basis, of kaolin, a procoagulant agent, that would yield the same clotting time observed with a given concentration of polyphosphate.

showed that polyphosphates bind with fibrinogen likely at or near a calcium binding site of fibrinogen in presence of Ca. This binding does not affect the polymerization process or crosslinking of fibrin but does result in a heterogeneous network of fibrin filaments compared to the homogenous network of fibrin filaments in polyphosphate's absence [133]. This ability of polyphosphate to down-regulate fibrinolysis occurred only when clots were formed in the presence of the polymer and not when polyphosphate was added after clot formation [129, 130, 133]. According to Mutch et. al [133], plasmin is less efficient at cleaving fibrin formed in the presence of polyphosphate due to the fibrin heterogeneity. This heterogeneity also decreases the capacity of fibrin to act as a cofactor in tPA-mediated plasminogen activation, thereby reducing plasmin generation and further delaying fibrinolysis [133]. It has also been reported that fibrin filaments formed in the presence of polyphosphates have higher turbidity and mass-length ratio [129].

1.10 Summary

Phosphate glasses are classified into different groups depending on the cation to phosphorus molar ratio. The focus of this thesis is on the metaphosphate glasses and specifically NaPP glass having a sodium to phosphorus molar ratio of 1. This glass and some of its crystalline derivatives are comprised of long chain polyphosphates. Interactions between phosphate glasses and water are complicated and highly depend on the modifying cations. In this case, NaPP glass is soluble in water but addition of multivalent cations to its solutions results in a precipitate and formation of a coacervate. This type of precipitation is a common phenomenon with polyelectrolytes, and it is governed principally by hydrophobic and electrostatic forces. Polyphosphate coacervate, considered here to have great potential as a biomaterial, is comprised of hydrated chains

of polyphosphates that are immiscible with water. It has been shown that polyphosphate chains are released from platelets after activation and may play significant role in the coagulation cascade. This observation alludes to the great potential especially for these polyphosphate coacervates in hemostasis applications.

The overall objective of this thesis was *developing and characterizing polyphosphate coacervates as a novel biomaterial and more specifically focusing on the in situ forming calcium polyphosphate system for hemostasis applications*. In the following chapters, detailed studies of a polyphosphate coacervate system derived from NaPP precursor solutions are described together with the potential of an *in situ* forming coacervate in hemostasis and as a liquid embolic agent.

Chapter 2 Sodium Polyphosphate Synthesis[1]

2.1 Objective

The main objective of this chapter is *synthesis and characterization of NaPPs with different degrees of polymerization*.

2.2 Introduction

The *in situ* forming polyphosphate system is comprised of sodium polyphosphate (NaPP) and divalent cation solutions that, on contact, form a coacervate that is immiscible with water. The average degree of polymerization ($\overline{D_p}$) (i.e. average number of phosphates per chain) of these NaPPs is an important factor in determining the physical and biological properties of this *in situ* forming system. NaPP with different $\overline{D_p}$ are not available for purchase; therefore, preparing different molecular weights of polyphosphates was the first goal of my thesis. The aim of this chapter is to describe the approaches taken to producing, and subsequently characterizing, NaPP polymers with a broad range of reproducible $\overline{D_p}$ values.

Thomas Graham prepared vitreous sodium phosphate exhibiting the metaphosphate composition (Na_2O/P_2O_5 = 1) by heating sodium dihydrogen phosphate to high temperature, followed by chilling the melt suddenly [2]. This compound is generally known as Graham salt and was erroneously labeled a sodium hexametaphosphate (a ringed structure) for over 100 years until work by Van Wazer [3] concluded that Graham

[1] Significant elements of the methodology and results presented in this chapter form the basis for the following publication: "*A. Momeni, M.J. Filiaggi, Synthesis and characterization of different chain length sodium polyphosphates, J. Non-Cryst. Solids, 382 (2013) 11-17*". See Appendix A.

salt solutions consisted, instead, of a mixture of linear polymers (i.e. polyphosphates) with the following general chemical formula:

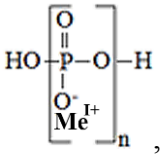

, where Me^{I+} is a monovalent cation in this case Na^{+} and n is the degree of polymerization (D_p).

NaPP glass is a distribution of polyphosphate chains; by its fractionation, polyphosphates having low $\overline{D_p}$ can be obtained. However, synthesis of longer polyphosphates is more complicated as it requires dissolution of a crystalline polyphosphate phase. Here we comprehensively describe synthesis and characterization of NaPP with average degree of polymerization ($\overline{D_p}$) from 50 up to 25,000.

2.3 Materials & Method

2.3.1 Preparation of NaPP

2.3.1.1 Preparation of NaPP with D_p < 500

Sodium phosphate monobasic monohydrate ($NaH_2PO_4.H_2O$; Sigma-Aldrich; ACS grade) was used to prepare NaPP with $\overline{D_p}$ lower than ~500. This method was adapted from Van Wazer [134]. $NaH_2PO_4.H_2O$ was heated in a Thermolyne Type 46200 High Temperature Furnace in a platinum-5% gold crucible from 25°C to 700°C over a 90 min period, keeping the melt at 700°C for 1, 3 or 9 hr followed by quenching on a copper plate at room temperature. These glasses were made in triplicate. The oxide and hydroxide layers on the copper plate were removed prior to quenching using acetic acid and sodium

chloride solution together and a brush. In order to confirm the absence of any copper residue in the NaPP glass, the glass surface was assessed by Energy-Dispersive X-ray Spectroscopy (EDS) (Hitachi S-4700 FEG Scanning Electron Microscope equipped with Inca EDS system, Japan). Water was not used as the quenching medium because NaPP is soluble in water. In addition, copper was selected over stainless steel as the quenching plate after blackening of glass surface was noted with the latter, suggesting a reaction had taken place.

The NaPP glass is a mixture of polyphosphates with different $\overline{D_p}$ and ring phosphates. The solubility of these compounds is different depending on the solvent's dielectric constant. Therefore, they can be separated by serial addition of acetone to water. In order to fraction the NaPP glass, the frit was ground to facilitate dissolution in deionized water; here, 52 g of NaPP glass was added to 500 mL of deionized water and the volume later adjusted to yield a 10% (w/v) NaPP solution. The solution was stirred using a magnetic stirrer for 12 hr; a 12 hr mixing time is required for removal of unstable phosphate branching points (Q^3) [42]. This solution was paper filtered in order to remove any possible insoluble parts and the volume adjusted to 520 mL. 1 mL of this solution was collected for phosphorus concentration analysis and the remainder divided into 13 Falcon® 50 mL tubes (40 mL per tube) to be fractioned by serial addition of acetone. Acetone (Fisher; ACS) was added to each tube until a stable cloudy solution was obtained (~ 4 mL of acetone). This stable cloudy solution was vortexed for 20 second, mixed for 15 min on an orbital shaker, then centrifuged at 4,400 rpm for 5 min to obtain an oily precipitate and a clear supernatant. This precipitate, designated the first fraction, is the longest chain polyphosphate fraction; this was subsequently frozen at -20°C. The

remainder of the supernatant solution was collected, added to a fresh tube and fractioned again with acetone addition; this process was repeated 6 to 7 times overall. Each of the remaining fractionation steps required less acetone (the solution already has acetone from the previous fraction collection) , with the subsequent volumes (in order) of 0.5 mL, 0.5 mL, 0.5 mL, 1 mL, 2 mL and 6 mL. After obtaining the last fraction, the volume of the remaining solution was measured and a 1 mL sample collected for phosphorus concentration analysis. The frozen oily precipitates contain water and acetone, so in order to obtain NaPP powder, these frozen samples were freeze-dried using a FreeZone® 1 Liter Benchtop Freeze Dry System (Labconco Corp., USA) for at least 24 hr at -43°C at pressures lower than 133×10^{-3} mBar, resulting in a lyophilized product that was labeled and kept in a freezer until use.

2.3.1.2 Preparation of NaPP with D_p > 500

To prepare NaPP with $\overline{D_p}$ higher than ~500, the method of Pfanstiel was adapted [135]. Potassium phosphate monobasic (KH_2PO_4; Sigma-Aldrich; ACS) was heated in the furnace in a platinum-5% gold crucible from 25°C to 775°C over a 90 min period, then held at 775°C for 30 min, 2 or 50 hr prior to cooling the crucible bottom in water. The resulting product is a water insoluble crystalline phase of KPO_3 known as the potassium Kurrol salt. The Kurrol salt was grounded and then washed by preparing a 20% (w/v) aqueous suspension of its powder that was magnetically stirred at 4°C for 20min. The Kurrol salt was then paper-filtered, washed with ethanol and dried in a desiccator for 24 hr. This washing procedure was carried out to remove any water-soluble potassium tripolyaphosphate ($K_5P_3O_{10}$) contamination from the Kurrol salt. Water soluble NaPP was obtained from Kurrol salt by an ion exchange process in which potassium cations

were replaced by sodium cations. A slurry of Kurrol salt was prepared in previously boiled deionized water followed by dry Amberlite™ IRP69 sodium sulfonate resin addition and rigorous mixing using a mechanical stirrer (2000 rpm) at 30°C in a pH range of 8-8.5, continually adjusted by dropwise addition of 0.1 M tetramethylammonium hydroxide solution. These alkaline conditions were maintained in order to minimize polyphosphate hydrolysis; the base was chosen specifically because tetramethylammonium cation has minimum affinity to phosphate groups [135]. During mixing the solution becomes viscous implying the polymeric nature of the solution. After mixing, all of the Kurrol salt powder was dissolved and the solution paper-filtered to remove the resin. The solution was frozen and subsequently freeze-dried for 72 hr at -43°C in pressures lower than 133×10^{-3} mBar to remove the water and obtain NaPP with $\overline{D_p}$ higher than ~500. The Kurrol salt/resin weight ratio, mixing time and concentration of the Kurrol salt in the slurry were varied in order to determine the optimum conditions under which a maximum amount of potassium could be replaced by sodium while minimizing resin waste.

2.3.2 NaPP Characterization

2.3.2.1 Compositional analysis

Small variations from unity in the K/P molar ratio of the KH_2PO_4 ($(K/P)_{KH_2PO_4}$) are reported to significantly affect the $\overline{D_p}$ of NaPP that is obtained through potassium Kurrol salt [135]. The $(K/P)_{KH_2PO_4}$ of our stock KH_2PO_4 was determined by EDS, Inductively Coupled Plasma Optical Emission Spectroscopy (ICP) (Optima™ 7300 V ICP-OES, Perkin Elmer Instruments, USA) and a pH measurement method to confirm the K/P

molar ratio of 1. For the pH measurement method, the pH of 0.1 M KH_2PO_4 in CO_2-free water under nitrogen gas at 25°C was measured and its variation from the theoretical pH of KH_2PO_4 under similar conditions was used to determine the $(K/P)_{KH_2PO_4}$ [135].

The amount of phosphate in all NaPP samples was assessed either by ICP or by titration. For the latter, 50 mg of each sample was dissolved in 10 mL 6 N HCl, maintaining in boiling water for 4 hr, followed by a ~20 hr cool down period. The solution was then titrated with 1 M NaOH, with the moles of 1 M NaOH required between two inflection points, pH 3.5 and 8, equal to the moles of phosphate in 50 mg of a sample.

The efficiency of the ion exchange process was also evaluated by measuring the remaining potassium to phosphorus molar ratio in the ion-exchanged NaPP ($(K/P)_{IE}$). Here, the amounts of potassium and phosphorus in ion-exchanged samples were measured by Perkin Elmer 2380 Atomic Absorption Spectroscopy (AAS) and titration, respectively. The $(K/P)_{IE}$ was also verified by ICP for select samples.

2.3.2.2 Thermal analysis

Thermal behavior and amount of residual water in all NaPP samples after lyophilization was determined by Differential Scanning Calorimetry and Thermal Gravity Analysis (DSC/TGA) using a STA 409 PC LUXX® thermal analyzer (Netzsch, Germany). A baseline was obtained using an empty platinum crucible and the instrument calibrated using calibration standard powders (biphenyl, $RbNO_3$, $KClO_4$, Ag_2SO_4, CsCl, K_2CrO_4, $BaCO_3$ covering the range 69°C to 806°C). Approximately 20 mg of each sample was added to the platinum crucible and the DSC/TGA data was collected from 25°C to 1000°C at the heating rate of 10°C/min. DSC/TGA data of $NaH_2PO_4.H_2O$, KH_2PO_4 and

Kurrol salt were also obtained. All DSC/TGA data were analyzed using Proteus® Software.

2.3.2.3 D_p Analysis

Liquid ^{31}P Nuclear Magnetic Resonance (NMR), titration and viscosity studies were carried out to determine the $\overline{D_p}$ of NaPP. Approximately 100 mg of NaPP was dissolved in ~1 mL D_2O (or 10% D_2O in H_2O) to be analyzed by a Bruker AV300MHz NMR spectrometer at 101.26 MHz, using a 15° pulse, 65536 (64 k) data points giving a 0.8 s acquisition time, a 7.0 s repetition rate and greater than 100 scans. This 7.0 s relaxation time has previously been shown to be suitable for polyphosphate analysis [19, 136-138]. Spectra were analyzed by Bruker TopSpin 1.3 software and reported using the d scale, with positive values downfield, and were referenced to an 85% solution of H_3PO_4 in H_2O. The peaks around 0, -9, -21, -23 and -35 ppm represent the Q^0 (^{31}P in orthophosphate), Q^1 (^{31}P in the end of the chain phosphate groups), $Q^{2\text{-middle}}$ (^{31}P in the middle of the chain phosphate groups), $Q^{2\text{-meta}}$ (^{31}P in the phosphate rings) and Q^3 (^{31}P in the branching point of phosphate groups), respectively [108]. The $\overline{D_p}$ of NaPP was determined by the following equation based on the area under the peaks [19]:

$$\overline{D_p} = \frac{2 \times (Q^1 + Q^{2-middle} + Q^3)}{Q^1} \qquad \text{Equation 2.1}$$

To determine the $\overline{D_p}$ by titration, 100 mg of NaPP was dissolved in 10 mL of cooled down deionized boiled water, yielding a solution pH of around 5-6. This pH was brought down below 4.5 using 0.1 M HCl and then titrated by addition of 1 M and 0.1 M NaOH solutions using a micropipette. The moles of NaOH used to titrate the NaPP solution

between two inflection points, pH 4.5 and 9, reflects the number phosphate groups at the end of the chains [3]. This value was used to determine the $\overline{D_p}$ based on the following equation [93]:

$$\overline{D_p} = \frac{20 \times \text{weight (g) of NaPP dissolved in solution}}{\left(\begin{array}{l}\text{mL of 1 M NaOH required between two inflection points-} \\ \text{mL of 1 M NaOH required for water titration between two inflection points}\end{array}\right)} \qquad \text{Equation 2.2}$$

Both NMR and titration give number average D_p and therefore, the number average molecular weight ($\overline{M_n}$) is equal to $102 \times \overline{D_p}$, where the value of 102 represents the molecular weight of the $NaPO_3$ monomer. In contrast, viscosity measurements provide the weight average molecular weight ($\overline{M_w}$). NaPP with $\overline{D_p}$ lower than 500 and those with $\overline{D_p}$ higher than 500 were dissolved in 0.035 N and 0.35 N NaBr solutions, respectively, at concentrations lower than 0.015 g/mL. The viscosity of these solutions was measured using a DV3^{TM} cone-plate rheometer (Brookfield, USA) at 25°C. A linear graph of [specific viscosity/concentration] was plotted against concentration and an extrapolation of this graph to zero concentration carried out to yield intrinsic viscosity ($[\eta]$); this value was used to calculate the $\overline{M_w}$ based on the following equations [82, 87]:

$$[\eta](\text{in 0.035 N NaBr}) = (10^{-5} \times \overline{M_w}) + 0.025 \qquad \text{Equation 2.3 for NaPP with } \overline{D_p} < 500 \text{ at 25°C.}$$

$$[\eta](\text{in 0.35 N NaBr}) = 0.65 \times 10^{-4} \times \overline{M_w}^{0.69} \qquad \text{Equation 2.4 for NaPP with } \overline{D_p} > 500 \text{ at 25°C.}$$

2.4 Results

2.4.1 NaPP with D_p < 500

Figure 2.1 shows the DSC/TGA graph of $NaH_2PO_4.H_2O$. From ~70°C to 150°C, the compound loses ~13% of its weight, implying the loss of one molecule of water per phosphate unit and formation of NaH_2PO_4. Around 220°C, there is a further ~6.5% mass loss suggesting the release of one water molecule per two phosphate units and formation of $Na_2H_2P_2O_7$, with a subsequent ~6.5% mass loss again at approximately 350°C, implying the loss of another molecule of water per two phosphate units and formation of trimetaphosphate rings (i.e. $Na_3P_3O_9$). Finally, the compound melts around 640°C and NaPP glass is obtained by quenching this melt. Quenching on a stainless steel oxide plate formed a black layer on the surface of the glass that was in contact with the plate, suggesting a reaction between the melt and the stainless steel oxide layer. In contrast, glasses quenched on the copper plate were visually clear, with EDS analysis showing no sign of copper contamination in the glass (Figure 2.2).

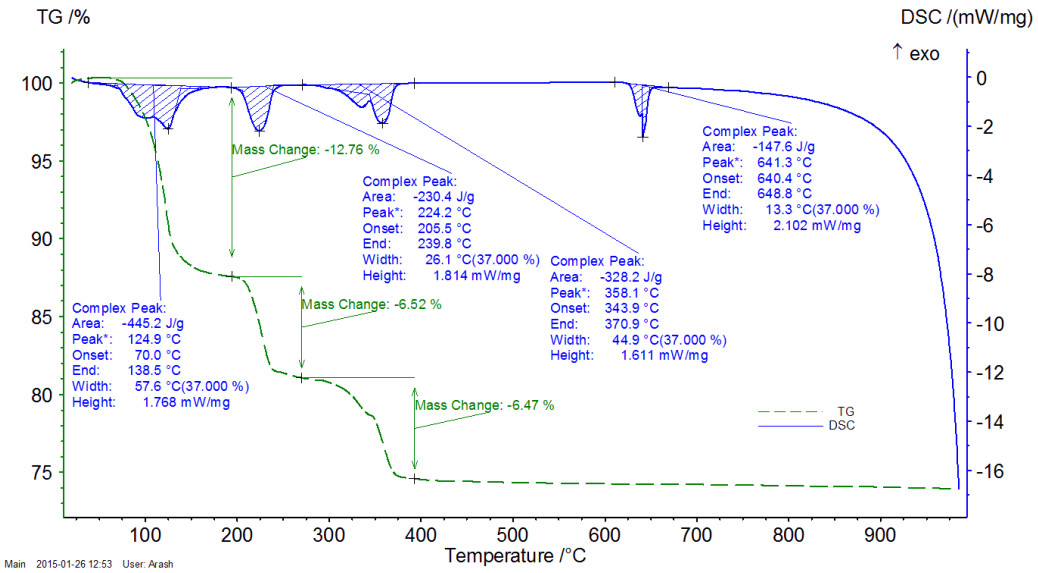

Figure 2.1 DSC/TGA graph of $NaH_2PO_4.H_2O$

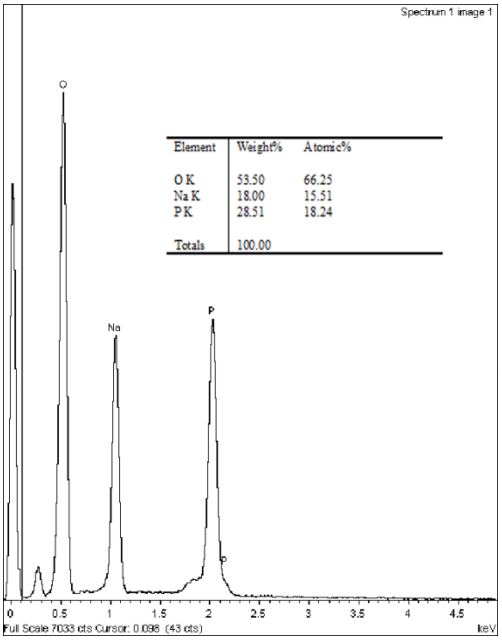

Figure 2.2 EDS graph of NaPP glass quenched on copper plate.

Representative liquid ^{31}P NMR spectra of NaPP glasses kept at 700°C for 1, 3 or 9 hr, corresponding to a $\overline{D_p}$ of 186±17, 131±12 or 174±15 (n=3), respectively are shown in Figure 2.3. Based on a two-tailed student's t-test, no significant difference was found between the $\overline{D_p}$ of 1 and 9 hr samples, but both groups were significantly ($p < 0.05$) longer than the 3 hr samples. A NaPP glass was also prepared by keeping the melt at the higher temperature of 970°C for 1 hr, yielding a $\overline{D_p}$ of 183±10 (n=3) that was not significantly different from glass prepared by keeping the melt at 700°C for 1 hr. Based on the NMR results, the fraction of ring metaphosphates ($Q^{2\text{-meta}}$) was consistently 4.5-5% of the total phosphorus atoms in all of the NaPP glasses. A very small peak representing Q^3 sites was also detected in dissolved NaPP glasses, with its area implying less than one phosphate branching point for every 1000 phosphate units.

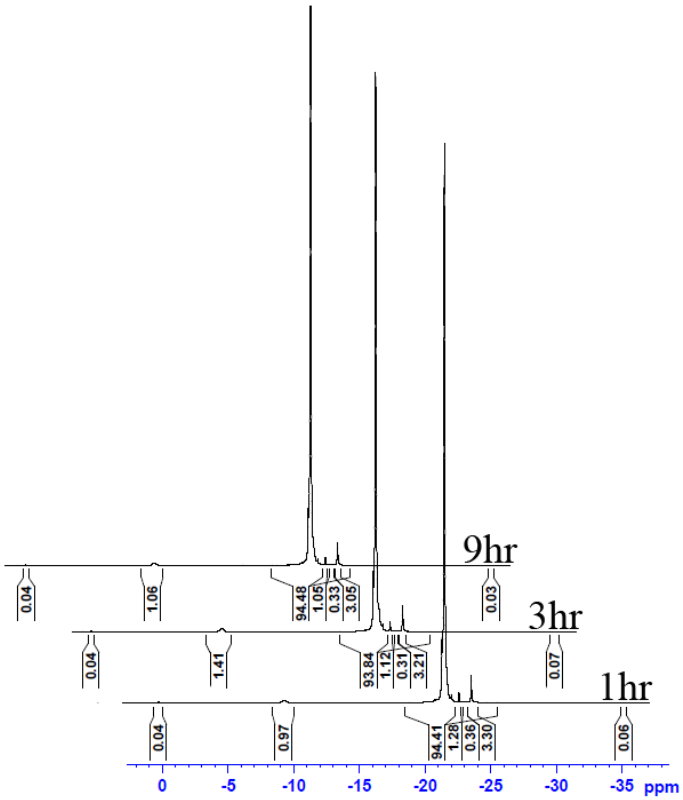

Figure 2.3 Liquid ^{31}P NMR spectra of NaPP glasses prepared by keeping the melt at 700°C for 1, 3 and 9 hr. With the exception of lowest spectrum, all other NMR spectra are shifted downfield for clarity.

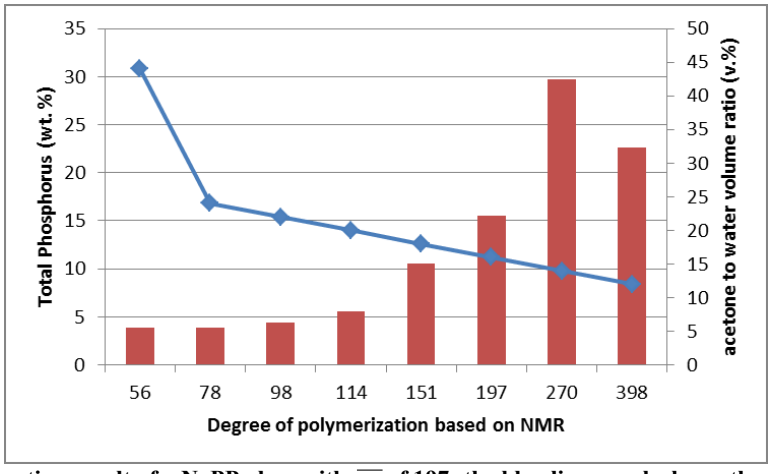

Figure 2.4 Fractionation result of a NaPP glass with $\overline{D_p}$ of 197: the blue line graph shows the amount of acetone required for precipitation of each fraction (y-axis on the right); red columns show the percentage weight of each fraction (y-axis on the left).

NaPP glasses that were maintained at 700°C for 1 or 3 hr were fractioned by serial acetone addition to their solutions. As shown in Figure 2.4, long chains precipitated early with a small amount of acetone, but precipitation of shorter chains required much more

acetone. Figure 2.4 also shows the $\overline{D_p}$ of each of the fractions. The original NaPP glass prior to fractioning had a $\overline{D_p}$ of 197; more accurately, it can be described as having a wide distribution of different polyphosphate chains with $\overline{D_p}$ starting from 56 up to 398, with the $\overline{D_p}$ fraction of 270 contributing almost 30% to the original NaPP glass mass. Figure 2.5 shows the corresponding liquid ^{31}P NMR spectra for these eight fractions. As the chains get longer the area under the Q^1 peak becomes smaller while the area under the $Q^{2\text{-middle}}$ peak becomes larger. Figure 2.6 shows the titration of the same fractioned NaPPs; the required volume of NaOH increases as the chains become shorter. Good correlation was obtained between $\overline{D_p}$ values determined by NMR and titration (Figure 2.7). This was especially true for short chains, where a slope of 1.04 was obtained. However, as the chains get longer, the accuracy and precision of the titration method decreases and these two methods do give comparable, if not the same, results. Also, as the chains get longer more NMR scans are required to achieve an accurate result.

Theoretically, the distribution of chains in a NaPP glass with an original $\overline{D_p}$ of $\overline{n}$ can be determined using the random distribution equation [134, 139]:

$$f_x = \frac{x}{\overline{n}(\overline{n}-2)}\left(\frac{\overline{n}-2}{\overline{n}-1}\right)^{x-1} \qquad \text{Equation 2.5 for } x>2;\ \overline{n}>2.$$

where f_x is the fraction of total number of phosphorus atoms having the $\overline{D_p}$ of x.

Using this equation, a comparison between theoretical and experimental distribution of our polyphosphates was carried out in two NaPP glasses prepared by keeping the melt at

700°C for 1 and 3 hr. As shown in Figure 2.8, the experimental distribution fit the theoretical distribution perfectly at low $\overline{D_p}$, but as chains get longer the theoretical curve overestimates the percentage of total number of phosphorus atoms in polyphosphates with large $\overline{D_p}$.

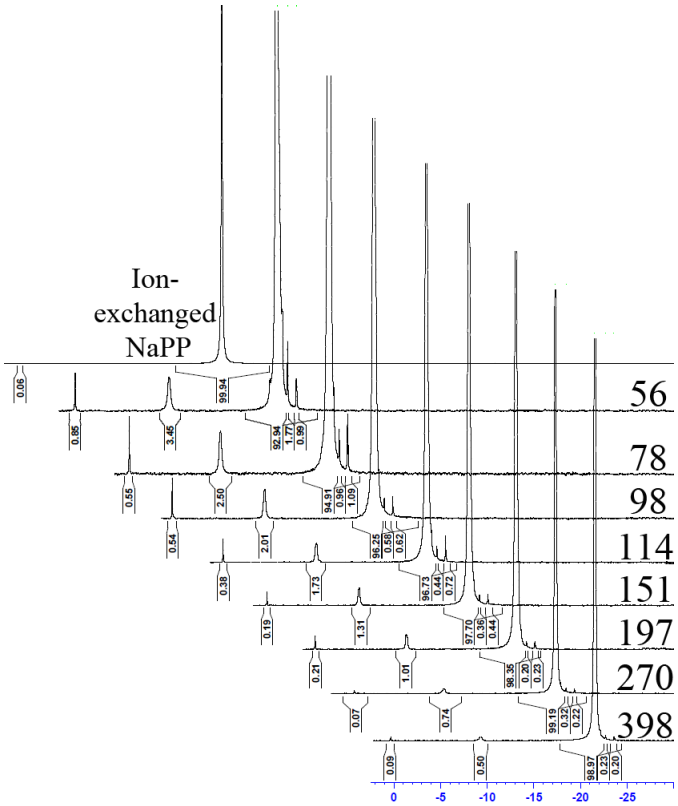

Figure 2.5 Liquid ^{31}P NMR spectra of NaPP fractions obtained from a NaPP glass with $\overline{D_p}$ of 197: numbers show the measured $\overline{D_p}$ for each fraction. Spectrum of an ion-exchanged NaPP is also shown. With the exception of the lowest spectrum, all other NMR spectra are shifted downfield for clarity.

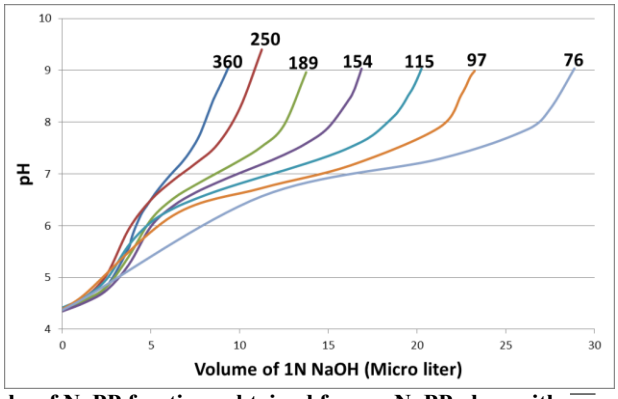

Figure 2.6 Titration graphs of NaPP fractions obtained from a NaPP glass with $\overline{D_p}$ of 197: numbers show the measured $\overline{D_p}$ for each fraction.

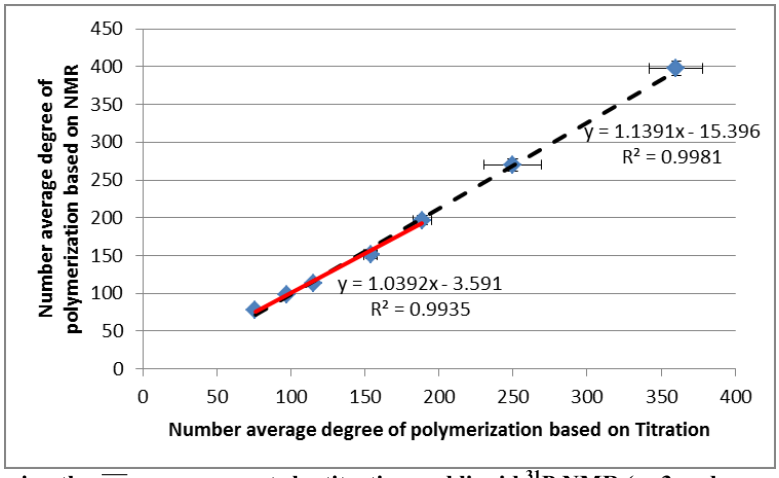

Figure 2.7 Comparing the $\overline{D_p}$ measurements by titration and liquid ^{31}P NMR (n=3 and error bars show STD). The solid line is a trend line passing the first five points while the dashed line passes all seven data points.

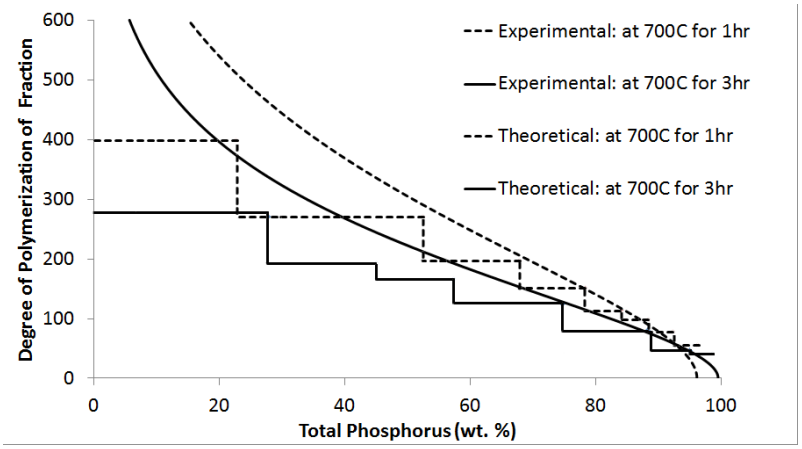

Figure 2.8 Comparing the theoretical and experimental distribution of polyphosphate in NaPP glasses prepared by keeping the melt at 700°C for 1 and 3 hr with original $\overline{D_p}$ of 197 and 135, respectively. Stepwise curves show experimental $\overline{D_p}$ of fractions plotted against cumulative percentage of phosphorus and solid line curves show theoretical plots of $\overline{D_p}$ against cumulative percentage of phosphorus calculated from equation 2.5

Table 2.1 summarizes the fractionation results of two NaPP glasses. The $\overline{M_n}$ value measured by NMR for the original glasses correlates with the $\overline{M_n}$ value calculated using the following equation based on the fractionation results.

$$\overline{M_n} = \frac{\sum N_i M_i}{\sum N_i} \qquad \text{Equation 2.6}$$

The $\overline{M_w}$ of NaPPs as determined using viscosity measurements is also displayed in Table 2.1 along with $\overline{M_w}$ and dispersity values calculated using the following equations based on the fractionation results:

$$\overline{M_w} = \frac{\sum N_i M_i^{\,2}}{\sum N_i M_i} \qquad \text{Equation 2.7}$$

$$\text{dispersity} = \frac{\overline{M_w}}{\overline{M_n}} \qquad \text{Equation 2.8}$$

Here, M_w measured by these two methods did not correlate.

Table 2.1 Summary of fractionation results for two NaPP glasses prepared by keeping the melt at 700°C for either 1 or 3 hr.

Fractions of 700°C for 1hr	[a] $\overline{M_n}$ (g/mol) × 10^4	Milli Moles in 52g glass	[b] $\overline{M_w}$ (g/mol) × 10^4	[c]Residual water (wt.%)	[d]Weight loss (wt.%)	Fractions of 700°C for 3hr	[a] $\overline{M_n}$ (g/mol) × 10^4	Milli Moles in 52g glass	[b] $\overline{M_w}$ (g/mol) × 10^4	[c]Residual water (wt.%)	[d]Weight loss (wt.%)
Fraction1	4.6	1.5	7.1	3.5	11.1	Fraction1	2.8	5.2	3.9	10.6	10.2
Fraction2	3.8	3.4	5.0	4.1	10.3	Fraction2	2.0	4.6	2.5	9	10.9
Fraction3	2.8	2.7	2.6	7.4	10.7	Fraction3	1.7	3.8	1.8	8.6	10.4
Fraction4	1.9	5.5	2.2	7.0	10.1	Fraction4	1.3	7.1	1.3	5.8	14.1
Fraction5	1.2	6.8	1.3	5.3	9.6	Fraction5	0.8	8.6	1.0	10.6	10.2
Fraction6	0.6	6.5	0.7	3.7	13.5	Fraction6	0.5	7.3	0.6	5.8	12.0
Fraction7	N/A	N/A	N/A	N/A	N/A	Fraction7	0.4	4.5	0.4	8.6	9.0
$\overline{M_n}$ of original NaPP glass based on the fractionation result (g/mol) × 10^4					1.9	$\overline{M_n}$ of original NaPP glass based on the fractionation result (g/mol) × 10^4					1.2
$\overline{M_n}$ of original NaPP glass based on its NMR measurement (g/mol) × 10^4					2.0	$\overline{M_n}$ of original NaPP glass based on its NMR measurement (g/mol) × 10^4					1.4
$\overline{M_w}$ of original NaPP glass based on the fractionation result (g/mol) × 10^4					2.7	$\overline{M_w}$ of original NaPP glass based on the fractionation result (g/mol) × 10^4					1.7
$\overline{M_w}$ of original NaPP glass based on its viscosity measurement (g/mol) × 10^4					3.4	$\overline{M_w}$ of original NaPP glass based on its viscosity measurement (g/mol) × 10^4					2.5
Dispersity of original NaPP glass based on the fractionation result					1.41	Dispersity of original NaPP glass based on the fractionation result					1.38

[a] $\overline{M_n}$ is determined based on liquid ^{31}P-NMR.

[b] M_w is determined based on viscosity measurements.

[c] Residual water is determined based on phosphate concentration analysis.

[d] Weight loss is determined based on TGA analysis between 25-500°C.

One should note that fractioned NaPPs contain residual water after freeze-drying. Figure 2.9 compares the DSC/TGA graph of un-fractioned NaPP glass with that of fractioned NaPP. Since the un-fractioned NaPP has no residual water, there is no weight loss in the

TGA graph. There is, however, an exothermic peak around 350°C in the DSC graph representing transformation into sodium trimetaphosphate ring or long chain NaPO3-II [5]. This is followed by melting around 630°C. In contrast, the DSC/TGA graph of fractioned NaPP glass is more complex due to the residual water. There is a ~2.7% weight loss between 80-135°C, followed by a slow weight loss of ~1.2% until 350°C, whereby a sharp weight loss of ~6.9% occurs. There is a reaction occurring between residual water and NaPP glass between 80-135°C because the weight loss is accompanied by an exothermic rather than an endothermic peak. Presumably, polyphosphate chains are being degraded into sodium pyrophosphate, which then transform into sodium trimetaphosphate rings at 350°C. The percentage of weight loss upon heating is reported in Table 2.1 for all fractioned NaPP fractions.

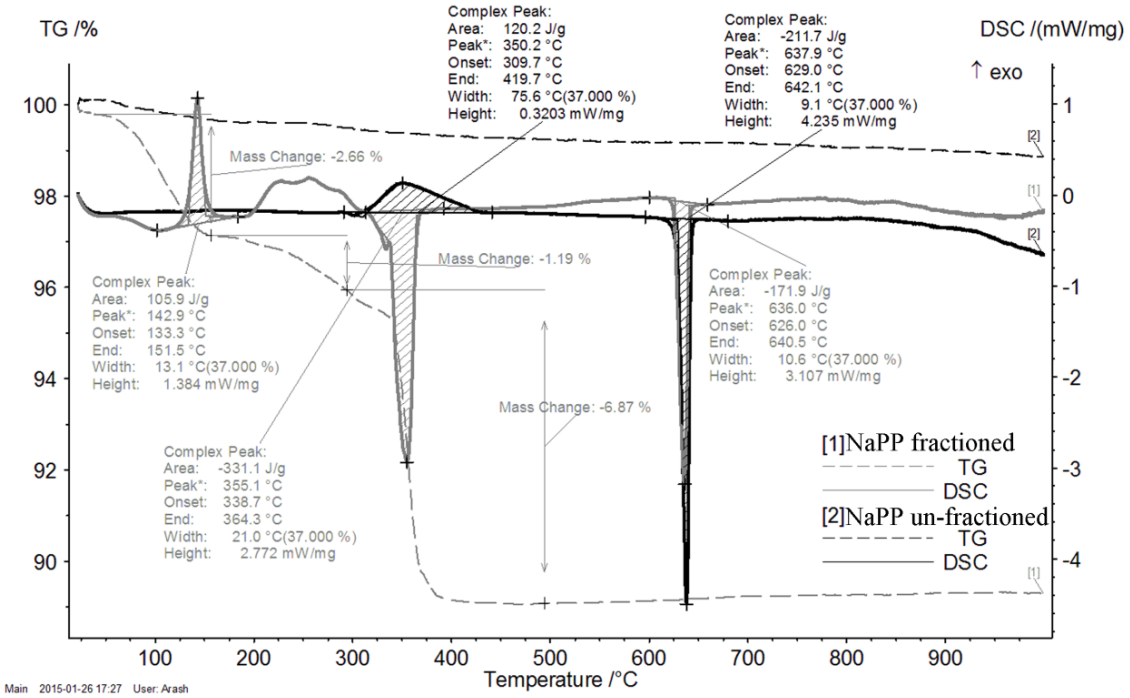

Figure 2.9 DSC/TGA graphs of an un-fractioned NaPP glass and a fractioned NaPP glass.

Since water is reacting with the NaPP glass, TGA is not an accurate method for determining the percentage of residual water in the fractioned samples. Instead, the

amount of sodium phosphate in each sample was determined by titration and subtracted from the original weight of the sample to determine the weight percentage of residual water. As reported in Table 2.1, fractioned NaPP glasses contained between 3 to 11% residual water by weight.

To confirm that sodium phosphate concentration measurements by titration were accurate, a known weight of $NaH_2PO_4.H_2O$ was dissolved in water and titrated as a control along with samples. Based on these controls, the sodium phosphate concentration as determined by titration had an accuracy error of only 2.3% (n=5). Figure 2.10 shows a typical titration plot of sodium phosphate solution starting from pH as low as 2 up to pH as high as 12. In later studies, phosphate concentrations were determined easily using an ICP unit purchased for the biomaterials lab.

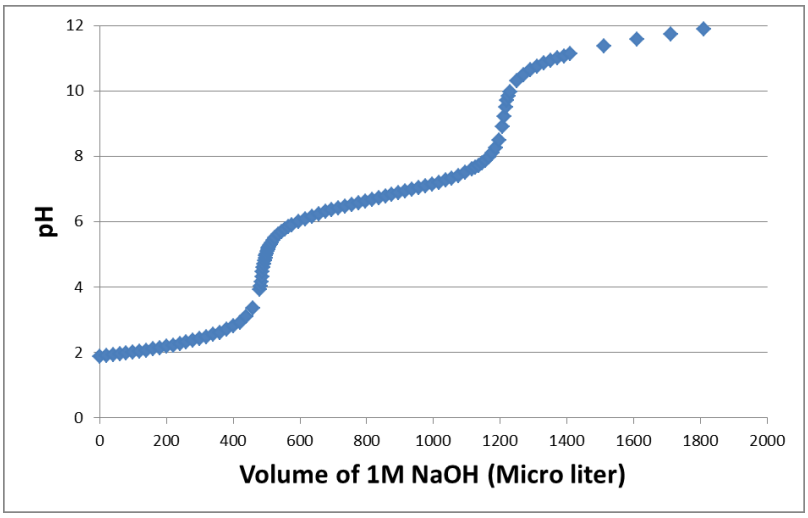

Figure 2.10 Titration graph of NaH_2PO_4 solution.

2.4.2 NaPP with D_p > 500

Small variations of $(K/P)_{KH_2PO_4}$ from unity is reported to significantly affect the $\overline{D_p}$ of NaPP that is obtained through potassium Kurrol salt [135]. The $(K/P)_{KH_2PO_4}$ of our stock material was 0.92±0.02 based on EDS, while ICP gave a value of 1.05±0.01. However,

neither of these methods is sensitive enough to confirm the exact value of $(K/P)_{KH_2PO_4}$. Instead, the pH of 0.1 M KH_2PO_4 in CO_2-free water under nitrogen gas at 25°C was measured and its variation from the theoretical pH of KH_2PO_4 under similar conditions, reported in [135], was used to determine the $(K/P)_{KH_2PO_4}$. Based on this method, $(K/P)_{KH_2PO_4}$ was found to be 1.000±0.001, essentially equal to one, and therefore no $(K/P)_{KH_2PO_4}$ adjustment of the stock material was performed.

DSC/TGA evaluation of KH_2PO_4 (Figure 2.11) revealed a sudden weight loss of ~13% between 182-358°C, implying the loss of one water molecule per phosphate unit and formation of long chain crystalline KPO_3, also known as potassium Kurrol salt [135]. Subsequently an ion exchange resin was used to dissolve the Kurrol salt, replacing potassium with sodium in order to release the polyphosphate chains into the solution. The challenge was to replace the maximum amount of potassium with sodium in these long chain polyphosphate solutions. Figure 2.12 shows the dependence of $(K/P)_{IE}$ on the amount of resin that was used during the ion exchange process. The higher the amount of resin, the more potassium is replaced by sodium. However, $(K/P)_{IE}$ values lower than 10% could only be achieved with a Kurrol salt to resin weight ratio of 1 to 10. Diluting the solution or increasing the mixing time did not decrease the $(K/P)_{IE}$. In contrast, using the same amount of resin (1 to 6 weight ratio) but doing so in 3 steps (1 to 3:1.5:1.5) rather than one (1:6) decreased the $(K/P)_{IE}$ to values lower than 5%. Based on these observations, the final procedure for obtaining NaPP with $\overline{D_p}$ higher than ~500 and $(K/P)_{IE}$ lower than 5% was as follows: first, 4.5 g of dried Kurrol salt was added to 13.5 g of dry Amberlite^{TM} IRP69 sodium resin in 100 mL water. The solution was

rigorously mixed for 90 min at 2000 rpm at 30°C in pH range of 8-8.5, continually adjusted by addition of 0.1 M tetramethylammonium hydroxide solution. After mixing, the solution was paper-filtered to remove the resin and, subsequently, 6.75 g of fresh resin was added to the filtered solution and mixed under similar conditions for 30 min. This step was repeated, and the final solution paper-filtered and freeze-dried. Using this method the weight of NaPP obtained after freeze drying was always higher than 3.3 g, or effectively a yield of higher than 80%.

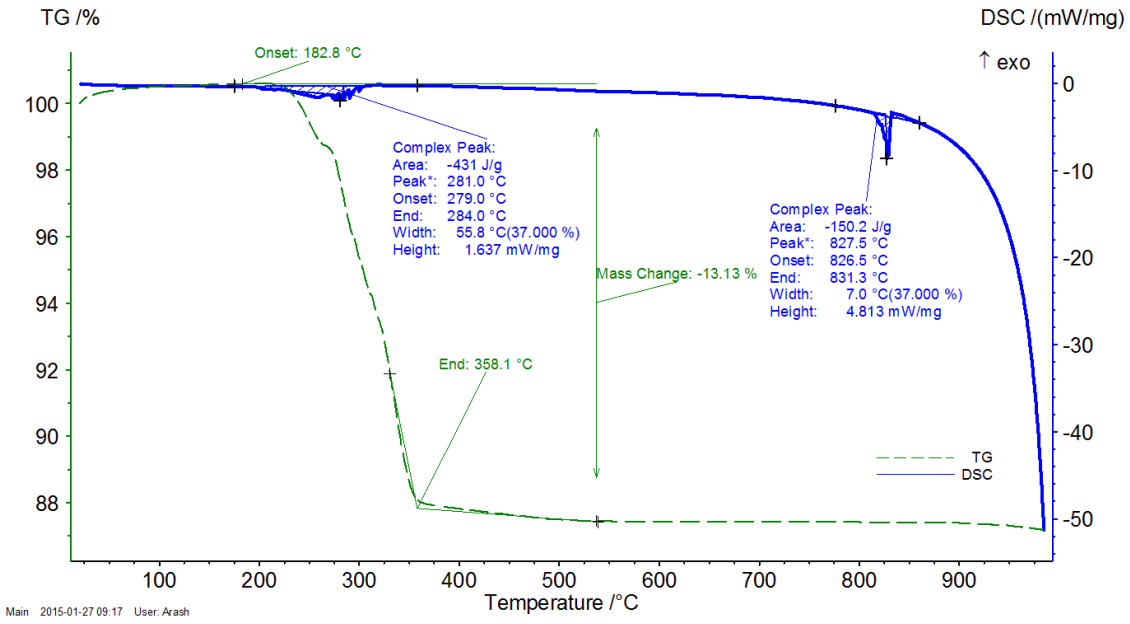

Figure 2.11 DSC/TGA graph of KH_2PO_4

Even dilute solutions of these polyphosphates are viscous, a characteristic feature of long chain polymers. Both liquid P-NMR and titration failed to determine the $\overline{D_p}$ of these long chain polyphosphates because both methods rely on their ability to detect the number of end group phosphates (Q^1). Even after 2300 scans, no Q^1 peak was detected (Figure 2.5; ion-exchanged NaPP), suggesting that $\overline{D_p}$ was at least higher than 3000 ($\overline{M_n}$ ~ 30E+04 g/mol) based on the signal to noise ratio.

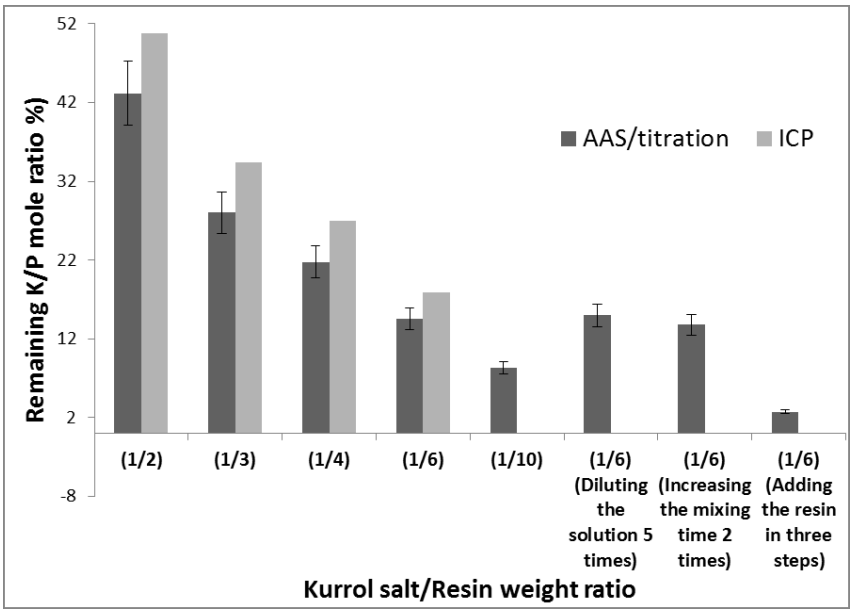

Figure 2.12 Dependence of the K/P ratio of ion-exchanged NaPPs on the experimental conditions.

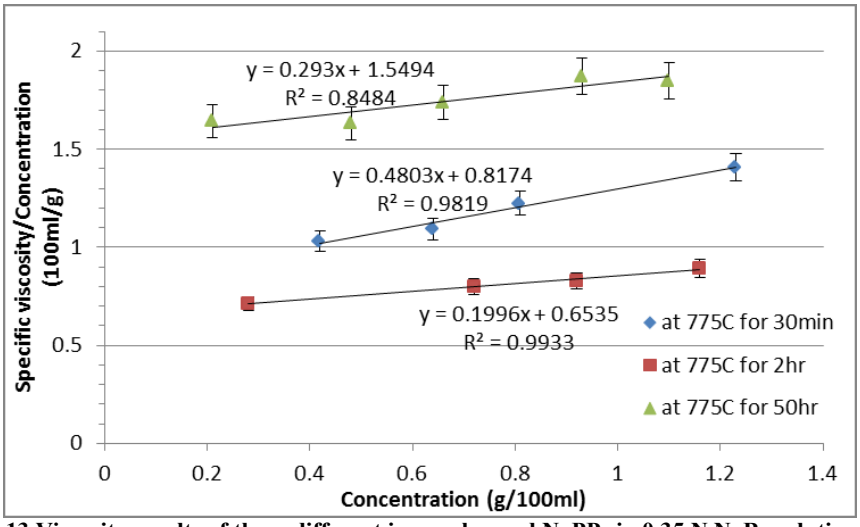

Figure 2.13 Viscosity results of three different ion-exchanged NaPPs in 0.35 N NaBr solution at 25°C.

The only feasible way to determine the $\overline{D_p}$ was found to be by viscosity measurements. Figure 2.13 shows the viscosity results of these long chain polyphosphate. The intercept of the trend lines with the specific viscosity/concentration axis yields an intrinsic viscosity value that is related to $\overline{M_w}$, based on equation 2.4. According to the viscosity measurements, NaPPs prepared by this ion exchange process were very long, many exceeding $\overline{M_w}$ of one million gram per mole. Furnace time indeed affected their $\overline{D_p}$,

with KH_2PO_4 maintained for 30 min, 2 hr and 50 hr at 775°C yielding NaPPs with $\overline{D_p}$ of 9.8±0.3 E+03 (n=3), 7.0±1.5 E+03 (n=5) and 1.9±0.2 E+04 (n=3), respectively. Based on a two-tailed student's t-test, there was no significant difference between the $\overline{D_p}$ of 30 min and 2 hr samples; however, both groups were significantly ($p < 0.05$) shorter than the 50 hr sample group.

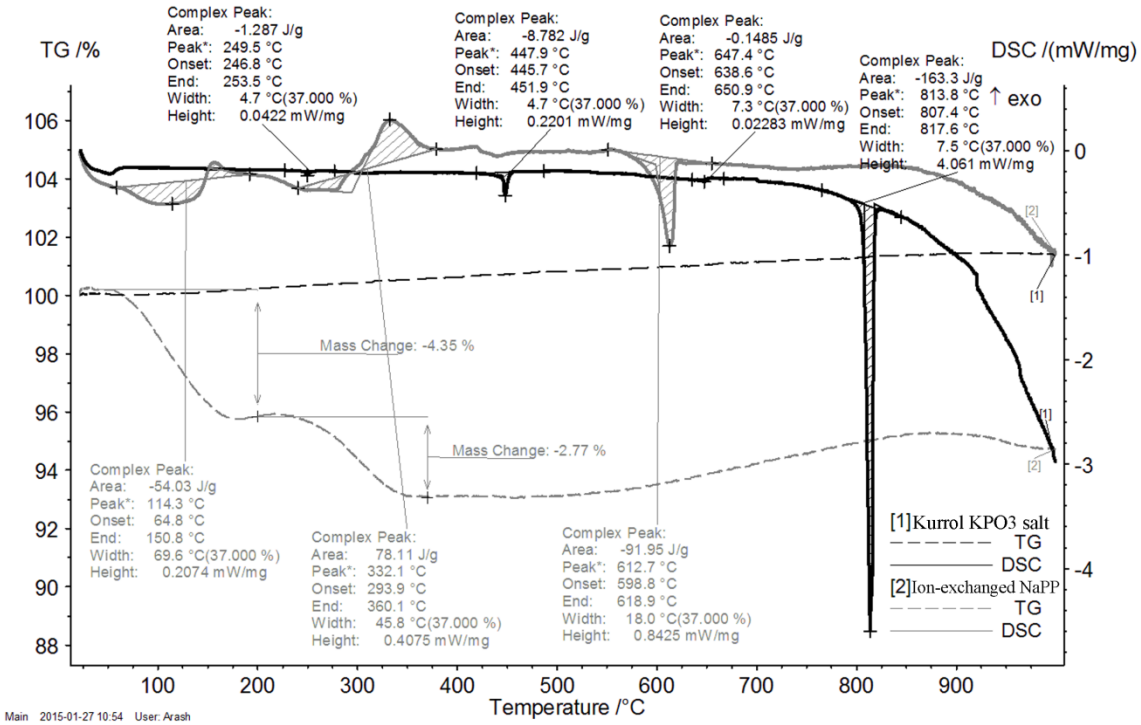

Figure 2.14 DSC/TGA graphs of Kurrol KPO_3 salt and ion-exchanged NaPP.

Figure 2.14 shows the DSC/TGA scan of NaPP obtained by ion exchange and compares it to its precursor, Kurrol salt. Kurrol salt displayed three very small endothermic peaks at 247, 446 and 639°C implying three phase transformations of KPO_3 [140, 141], followed by melting around 810°C. In contrast, ion-exchanged NaPP melts at around 600°C similar to shorter chain NaPPs. In addition, a peak around 150°C resembles a similar peak detected for the fractioned NaPP, while a peak at 330°C resembles the peak that was observed in the NaPP glass. The TGA graph also revealed a 6-9% weight loss in ion-

exchanged NaPPs after heating to 400°C. Presumably, as the ion-exchanged NaPP is heated, some of its residual water is evaporated, with the remainder reacting with the chains to yield shorter chains. The amount of residual water in long chain ion-exchanged NaPPs after freeze-drying was determined to be 8-12% based on phosphate concentration analysis.

2.5 Discussion

NaPP at a Na/P molar ratio of one is a unique glass in the sense that it is constituted of exceptionally long chain polyphosphates that, when dissolved in water, release these chains into the solution intact. The resulting inorganic polymer solution could be used for a variety of applications, though any specific application might require a specific polyphosphate $\overline{D_p}$. The preparation of polyphosphates with different $\overline{D_p}$ was the subject of several studies in the 1960's due to their applications in studying the science of polyelectrolytes. Van Wazer [134] used titration and the same fractionation method that was employed here to demonstrate that NaPP glass is indeed comprised of a distribution of polyphosphate chains, using Equation 2.5 to describe this distribution. However, we found that the random distribution equation overestimates the percentage of total number of phosphorus atoms that are in polyphosphates with large $\overline{D_p}$. The random distribution equation represents the distributions corresponding to a completely random process of chain making and scission, ignoring the increasing negative charge that is being built up as the phosphate chains grow in the melt. This growing negative charge could become an increasing repulsive force for the next phosphate anions that are seeking to bind with the chain and, as a result, a higher percentage of polyphosphate anions remain shorter than what might be expected from theoretical estimation.

We also found for NaPPs produced through melting $NaH_2PO_4.H_2O$ that $\overline{D_p}$ depends on the furnace time and temperature. Long chain phosphates are already formed when the melt is kept at 700°C for one hour, but when the furnace time is increased to three hours this $\overline{D_p}$ drops. Extending this melt period to 9 hrs or at a higher temperature of 970°C, allows the $\overline{D_p}$ to grow again, but this value never exceeds the $\overline{D_p}$ that was already obtained at the lower temperature and the shorter furnace time. In theory, the average $\overline{D_p}$ of a NaPP glass with the Na/P molar ratio of one should grow to infinity if all functional groups condense [5, 141]; in practice, however, several factors prevent chain growth. Firstly, the Na/P molar ratio of the precursor material could deviate from the stoichiometric molar ratio of one due to impurities. In addition, as the chains grow the increasing negative charge on the chains prevent further growth. The evaporation of the last traces of water from the melt also becomes extremely difficult, and these water molecules could act as chain terminators. For instance, if one water molecule remains for every 500-phosphate molecule, this will restrict growth to no higher than 500 phosphates per chain. There are two sources for water in the melt: water that is the byproduct of the condensation reaction, and water that is in the atmospheric air. With respect to the latter, Thilo [142] has shown an inverse relation between sodium polyphosphate $\overline{D_p}$ and water vapor pressure inside of the furnace. Indeed, the limited molecular weight achievable is the case for any standard polycondensation reaction, and the same limitations exist for other polymers made via polycondensation.

The NaPP glasses were fractioned to obtain a range of different $\overline{D_p}$ of polyphosphates. Their $\overline{M_n}$ was successfully determined by liquid ^{31}P NMR and titration, but the $\overline{M_w}$ as measured by viscosity appears relatively inaccurate for the shorter chain NaPP fractions. This inaccuracy could be caused by significant errors that exist in determining the accurate intrinsic viscosity value. These errors may be the result of the low sensitivity of viscometers in measuring low viscosity solutions, or may arise simply as a result of the inaccuracy of constants determined by Strauss [82, 87] for Equation 2.3 based on his light scattering results.

Even after fractionation, the longest fractioned NaPP obtained by melting sodium phosphate monobasic had a $\overline{D_p}$ of ~400. In contrast, when potassium phosphate monobasic is heated it crystalizes into potassium Kurrol salt, which is known to be comprised of polyphosphates with $\overline{D_p}$ much larger than 500 phosphorus units per chain. There are many other crystalline compounds possessing a O/P ratio of 3 that share these characteristically long polyphosphate chains [140]. Examples include Maddrell Salt, calcium polyphosphate crystalline phases, $Zn(PO_3)_2$, and $Ba_2K(PO_3)_5$; however, none are water soluble. Potassium Kurrol salt is also not water soluble but, interestingly in presence of small monovalent cations such as H^+, Na^+ or Li^+, it becomes water soluble as these cations replace some of the potassium ions, distorting the crystalline structure and releasing the chains into the solution. Based on this phenomenon very long chain NaPPs were obtained from potassium Kurrol salt. The ion exchange process was optimized to efficiently remove the maximum amount of potassium from the solutions without wasting too much resin. The resulting NaPPs were very long, as evidenced from liquid ^{31}P NMR

and viscosity measurements. Due to the high viscosity of ion-exchanged NaPP solutions, the $\overline{M_w}$ determined by viscosity measurements is reliable in contrast to short chain NaPPs.

The $\overline{M_w}$ of the ion-exchanged NaPP was directly correlated to the furnace dwell time of KH_2PO_4. Although this dependence was previously suggested by Malmgren [143, 144], his work did not include replicates to check reproducibility, lacked statistical analysis and overall was not especially convincing. Great care was taken in this current study to ensure that every step of this multi-step process was identical between replicates. In fact, our preliminary studies when such care was not considered led to non-reproducible $\overline{D_p}$.

Polyphosphates grow into extremely long chains in crystalline phases because they are not affected by the factors that prevent the chain growth in melts; in the crystalline state the charge of the chains remain neutral and also any impurity such as water or excess cation is driven to the surface of crystal as they do not fit the crystal template [145]. For instance, in potassium Kurrol salt it is known that if a slight excess of K_2O is present in the system, it won't act as the chain terminator and instead forms $K_5P_3O_{10}$, crystallizing separately from Kurrol salt [5, 135, 145]. In such a system it is expected that longer heat treatments result in longer chains since the only factor limiting the chain growth is the kinetics of the system – that is, the ability of monomers to migrate to the surface of the crystals.

Since in both the fractionation and ion-exchange methods polyphosphates are introduced to water, the resulting NaPPs will contain residual water. This residual water could only be removed by heating, but as shown in the DSC results, the heating process will also

degrade the chains. If this water is not removed, its exact amount should be determined for each NaPP sample and taken into account in experiments. Also, we have observed that over time this residual water degrades the polyphosphate chains that are kept under vacuum inside a desiccator at room temperature; it is highly recommended to preserve NaPPs inside a freezer to slow down the degradation rate.

2.6 Conclusion

NaPPs with $\overline{D_p}$ smaller than 500 phosphates per chain were successfully and reproducibly produced by fractionation of NaPP glass prepared from $NaH_2PO_4.H_2O$. NaPPs with $\overline{D_p}$ larger than 500 phosphates per chain were successfully produced by ion exchange of potassium Kurrol salt that was prepared from KH_2PO_4. The amount of remaining potassium in ion-exchanged NaPPs was reduced to K/P molar ratios lower than 5%. All prepared NaPP batches contain residual water that should be considered when using these batches. Overall, NaPPs with different $\overline{D_p}$ (50-20,000) were produced and successfully characterized. These NaPPs were routinely and reproducibly synthesized for subsequent studies of coacervation, and in the development of a hemostatic, liquid embolic system.

Chapter 3 Sodium Polyphosphate & Alkaline Earth Metal Solutions[1]

3.1 Objective

The main objectives of this chapter are *determining the amount of divalent cations required for coacervation of NaPP solutions, understanding the effect of presence of Ca, Sr and Ba in polyphosphate solution*, *determining the composition of the coacervate and investigating the process of substitution of sodium by calcium in polyphosphate coacervates*.

3.2 Introduction

Polyphosphate solutions are widely used as a water softening agent due to the very well-known ability of polyphosphate chains to chelate multivalent cations [6]. However, a very interesting phenomenon happens when an excess amount of multivalent cations are added to the polyphosphate solution: Large cations (Ba^{2+}, Sr^{2+}, Pb^{2+}, Ag^{+}, Bi^{2+}, ZrO^{2+}, UO_2^{2+}, and Hg_2^{2+}) in excess give flocculent, solid precipitates, whereas smaller cations (Ca^{2+}, Mg^{2+}, Zn^{2+}, Mn^{2+}, Ni^{2+}, Co^{2+}, Fe^{2+}, Fe^{3+}, Cr^{3+}, Hg^{2+}, and Cu^{2+}) give a highly viscous liquid or coacervate that is immiscible with water [5]. The term coacervation is used to describe a process in which aqueous colloidal solutions separate upon alteration of the thermodynamic state into two liquid phases, one rich in colloid (i.e., the coacervate) and the other containing little colloid [146]. Polyphosphate coacervates could

[1] Significant elements of the methodology and results presented in this chapter form the basis for the following publication: "*A. Momeni, M.J. Filiaggi, Comprehensive Study of the Chelation and Coacervation of Alkaline Earth Metals in the Presence of Sodium Polyphosphate Solution, Langmuir, 30 (2014) 5256-5266*". See Appendix B.

have multiple applications as a biomaterial or as a glass precursor for coating [33, 34, 37, 105, 147]. There are several basic studies on coacervates of polyphosphates with cations such as Mn^{2+} [36], Ni^{2+} [69, 100], Co^{2+} [69, 100], Fe^{3+} [31, 35], Mg^{2+} [37, 78, 102, 103], Ca^{2+} [31, 33, 34, 37, 67, 70, 78, 102-105, 147, 148], Al^{3+} [35, 102], and Zn^{2+} [38, 106].

Although several groups have reported on coacervate formation, no one has investigated or described this phenomenon in any great detail, resulting in some cases in confusing or misleading statements in the literature. For instance, it has been erroneously mentioned that acidic conditions are required for coacervation of polyphosphates [106]. In order to better understand this system and exploit its potential for different bio-application, a comprehensive study of the reactions between polyphosphate solutions and three alkaline earth metals, namely Ca, Sr and Ba, was undertaken. Ca was chosen especially since calcium polyphosphate glass has been the main focus of our group for a long time given its potential as a biomaterial. In addition, these alkaline elements represent the simplest multivalent metal group of the periodic table. From a biomaterials standpoint, evaluation of other cations such as Ag^{+}, Cu^{2+} and Zn^{2+} would also be of interest but are beyond the scope of this thesis.

First, chelation of Ca, Sr and Ba by polyphosphates and their impact on the stability of polyphosphate chains is studied by means of liquid ^{31}P-NMR, pH and viscosity measurements. Then, the exact amount of these divalent cations required for coacervation under different conditions is examined and discussed based on polyelectrolyte theories. Lastly, the composition of the resulting polyphosphate coacervates and its dependence on the coacervation process is assessed. Our observations and subsequent analyses are

valuable not only in understanding the coacervation of polyphosphates, but also in describing some of the unique properties of phosphate glasses.

3.3 Materials & Method

3.3.1 Starting Materials

NaPPs with different $\overline{D_p}$ were prepared freshly and characterized as comprehensively described in Chapter 2. Briefly, NaPPs with $\overline{D_p}$ <500 were produced by heating $NaH_2PO_4.H_2O$ (Sigma-Aldrich) at 700 °C for 1 hr to obtain an NaPP glass, followed by acetone fractionation to yield NaPPs with narrow size distribution. NaPPs with $\overline{D_p}$ >500 were produced by heating KH_2PO_4 (Sigma-Aldrich) at 775 °C for different time periods to obtain a potassium Kurrol salt, followed by an ion exchange process to replace potassium with sodium. The NaPP solutions obtained by these two processes were subsequently freeze-dried to yield NaPP powder that was subsequently stored at -20°C for later studies. A commercial NaPP with $\overline{D_p}$ of 27 (determined by NMR) was also used in these investigations (ICL Performance Products LP, Missouri, USA). Chloride salts of calcium, strontium and barium (Sigma-Aldrich) were used as the source for divalent cations in the solutions. All other materials were of reagent grade.

3.3.2 Chelation Studies

3.3.2.1 pH studies

Addition of divalent cations to NaPP solutions causes the pH of the solution to drop. To better understand this phenomenon, NaPPs with different $\overline{D_p}$ were dissolved in water at 25±0.5°C at a phosphate concentration of 0.3 M and the pH of all solutions adjusted to 7

using 1 M NaOH solution. Subsequently, 1 M Ca, Sr or Ba solutions (as the chloride salt solutions) were added dropwise using a micropipette and the pH monitored using an Accumet Basic AB15 pH meter (Fisher Scientific, Boston, MA, USA) until the solution became cloudy, indicating precipitation and subsequent coacervate formation. pH measurements were carried out in triplicate for each sample, and the average pH value and standard deviation were reported against divalent cation to phosphorus (Me^{II}/P) molar ratio (Me^{II} = divalent cation).

In addition, polyphosphate solutions at 0, 0.05, 0.10, 0.15, 0.20 and 0.25 Ca/P and 0.15 Sr/P and Ba/P molar ratios were prepared by adding the required amount of divalent cations to a 0.1 M NaCl NaPP solution having a $\overline{D_p}$ of 100±1 and phosphate concentration of 0.098 M. Subsequently, these cation-loaded polyphosphate solutions were titrated at 25°C±0.5 between a pH of 3.5 and 10 in order to determine the acid dissociation constant (pKa) of the phosphate group at the end of a polyphosphate chain. In the resulting titration curves, two inflection points were identified and then the pH at the half-way point was reported as the pKa of the hydrogen atoms at the end of the chains. For all pH studies freshly boiled water was used and pKa measurements were carried out rapidly to minimize the effect of atmospheric CO_2 on titration.

3.3.2.2 Liquid ^{31}P-NMR studies

NMR studies were conducted at three stages. First, investigations of the degradation rate of a pure NaPP solution in relation to its $\overline{D_p}$ was studied at 80°C since degradation is so slow at lower temperature. Here, NaPPs with $\overline{D_p}$ of 402±15 and 100±1 were dissolved in water in triplicate at a phosphate concentration of 0.86 M and maintained at 80±1°C for

up to ~35 hr. The pH was kept constant at 6.5, close to the pKa for NaPP, using 1 M NaOH. At predetermined time intervals the $\overline{D_p}$ was determined by a Bruker AV300MHz NMR spectrometer at 101.26 MHz, using a 15° pulse, 65536 (64 k) data points giving a 0.8 s acquisition time, a 7.0 s repetition rate and greater than 100 scans. Spectra were analyzed by Bruker TopSpin 1.3 software and reported using the d scale, with positive values downfield, and were referenced to an 85% solution of H_3PO_4 in H_2O. The peaks around 0 and -9 ppm represent the Q^0 (Orthophosphates) and Q^1 (End of chain phosphorus atoms) respectively, and the peaks around -21ppm represent $Q^{2\text{-middle}}$ (Middle of chain phosphorus atoms in polyphosphates) and $Q^{2\text{-meta}}$ (Middle of ring phosphorus atoms) [108]. Based on the area under the peaks, the $\overline{D_p}$ of NaPP was determined at different time points based on the following equation, which is similar to equation 2.1 except that here Q^3 was always equal to zero:

$$\overline{D_p} = \frac{2 \times (Q^1 + Q^{2-middle})}{Q^1} \qquad \text{Equation 3.1}$$

In the second part of the NMR experiments, the effect of type and amount of chelated cations on the degradation of polyphosphate chains in solution was investigated. For this evaluation, degradation of a 0.86 M solution of NaPP with $\overline{D_p}$ of ~86 was studied at different Me^{II}/P molar ratios. Degradation of these polyphosphate chains loaded with divalent cations was followed in triplicate for up to 14 days (37°C; pH 6) by measuring the $\overline{D_p}$ at predetermined time intervals as described above. The effect of the chelated cations on chemical shifts in the NMR spectra was also examined as was their impact on

the width at half height of the $Q^{2\text{-middle}}$ peak by fitting a Lorentzian curve to the peak using Bruker TopSpin 1.3 software.

In the third part of these NMR studies, the pKa of the phosphate group at the end of NaPP chain was determined by NMR. Here, NaPP solutions at 0 Ca/P molar ratio at different pHs between 3.5-10.25 were prepared by adding NaOH to a 0.1 M NaCl NaPP solution having a $\overline{D_p}$ of 100±1 and phosphate concentration of 0.098 M. The chemical shift of the Q^1 site highly depends on its protonation [149]. This chemical shift was plotted against pH of the solution; the pH at the inflection point in this plot is equal to the pKa [150].

3.3.2.3 Viscosity studies

The viscosity of a polyphosphate solution decreases as divalent cations are added to its solution. The objective of this study was to better understand this phenomenon. A DV3™ cone–plate rheometer (Brookfield, USA) was used to measure the viscosity of a NaPP solution with $\overline{D_p}$ of ~17,000 at a phosphate concentration of 0.171 M for divalent cation to phosphorus molar ratios of 0, 0.05, 0.10, 0.125, 0.15, 0.175 and 0.20 at temperature of 25±0.1°C and a shear rate of 750 s^{-1}. NaPP with a very large $\overline{D_p}$ was chosen in order to achieve viscosities high enough to measure this viscosity accurately. Viscosity was also measured for the same NaPP sample at different Ca/P molar ratios but at very low phosphate concentrations in order to plot specific viscosity/concentration (η_{sp}/C) against concentration (C).

3.3.3 Coacervation Studies

3.3.3.1 Turbidity studies

Turbidity studies were carried out to determine the exact amount of divalent cation required for coacervation and its relation to NaPP concentration, $\overline{D_p}$ of the NaPP, type of divalent cation, solution pH, and the presence of NaCl in the solution. NaPP solutions with phosphate concentrations ranging from 0.001 to 3 M were prepared. 1 or 0.1 M divalent chloride solutions were added dropwise using a micropipette while the temperature was kept constant at 37±0.5°C. After each drop the turbidity of the solution was measured using a Micro 100 turbidity meter (Scientific, Inc). At a certain Me^{II}/P molar ratio a sudden shift in turbidity of the solution occurs. This point is known as the cloudy point and the value of Me^{II}/P ratio at the cloudy point is known as the demixion point [97] (Me*), which is reported here. 0.05 M tris(hydroxymethyl)aminomethane (Tris) and 2-(N-morpholino)ethanesulfonic acid (MES) buffer solutions were used to stabilize the pH, respectively at 7.4 and 5.5.

3.3.3.2 Chemical composition of the coacervate

100 mg of NaPP with $\overline{D_p}$ of 402±15 was dissolved in 1 mL of water. The whole of this 1 mL solution was added at once to 4 mL of water containing 93.6, 163.8, 234, 334, 393, 468 or 936 µL of 1 M Ca, resulting in mixtures with 0.10, 0.175, 0.25, 0.357, 0.42, 0.50 and 1 Ca/P molar ratios, respectively. At Ca/P molar ratios higher or equal to 0.357, the Me* under these conditions, the coacervate formed spontaneously; at lower Ca/P molar ratios coacervate formation was subsequently induced by adding 47 mL of acetone. These mixtures were agitated for 5 min using a magnetic stirrer and the coacervate

collected and stored at -20°C until analysis. The coacervates were subsequently dissolved using 200 mM EDTA at pH of 10 to evaluate composition and $\overline{D_p}$. The volume of EDTA required for dissolution was determined based on having a minimum of 1.2 moles of EDTA for each mole of Ca; at this EDTA/Ca molar ratio and pH, polyphosphate chain degradation is kept to a minimum [151]. After dissolution, the Ca/P molar ratio of the coacervate was determined using ICP (Optima™ 7300 V ICP-OES, PerkinElmer Instruments, USA). $\overline{D_p}$ was measured using liquid ^{31}P-NMR as described above. The amount of calcium and phosphorus remaining in the supernatant solution was also determined by ICP. To assess if mixing time affected Ca/P molar ratio or the resulting $\overline{D_p}$ of the coacervate, experiments with longer mixing times (15, 30 min and 1 hr) were also conducted. All sample groups were evaluated in triplicate.

3.4 Results

3.4.1 pH results

Figure 3.1 shows the dependence of pH on Ca/P molar ratio in NaPPs having different $\overline{D_p}$. The degree of pH drop was directly related to the NaPP $\overline{D_p}$. As an example, in a NaPP fraction with $\overline{D_p}$ of 279, pH decreased from 7.10±0.00 at a Ca/P molar ratio of zero to 6.50±0.05 at its Ca*=0.293. In contrast, for a NaPP fraction with a $\overline{D_p}$ of 47, the pH decreased from 7.08±0.01 at a Ca/P molar ratio of zero to 6.08±0.05 at its Ca*=0.313.

With the exception of the commercial, unfractioned NaPP with a $\overline{D_p}$ of 27, the decrease in pH also occurred at almost a constant rate until the Ca/P molar ratio of ~0.18 was reached, at which point a gradual increase in the rate of pH drop occurs (Figure 3.1).

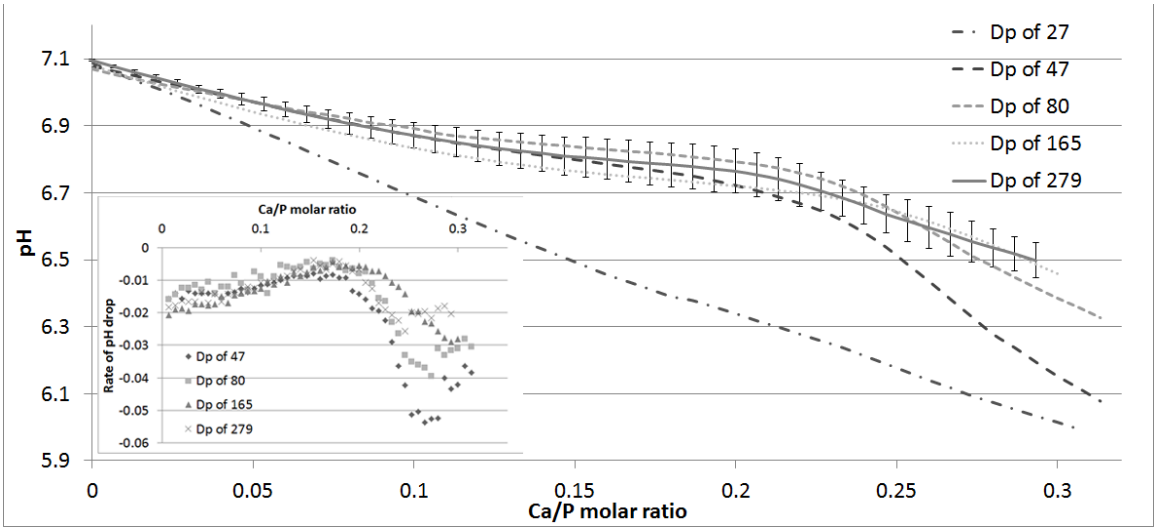

Figure 3.1 pH decrease as calcium is added to polyphosphate solutions with different $\overline{D_p}$ ([phosphate] = 0.3 M, bars of STD is shown just for one sample for clarity, large STD might be due to the presence CO_2). Inset show the rate of pH drop. Temperature in all pH studies was 25±0.5°C. The rate of pH drop refers to the slope of the titration curves.

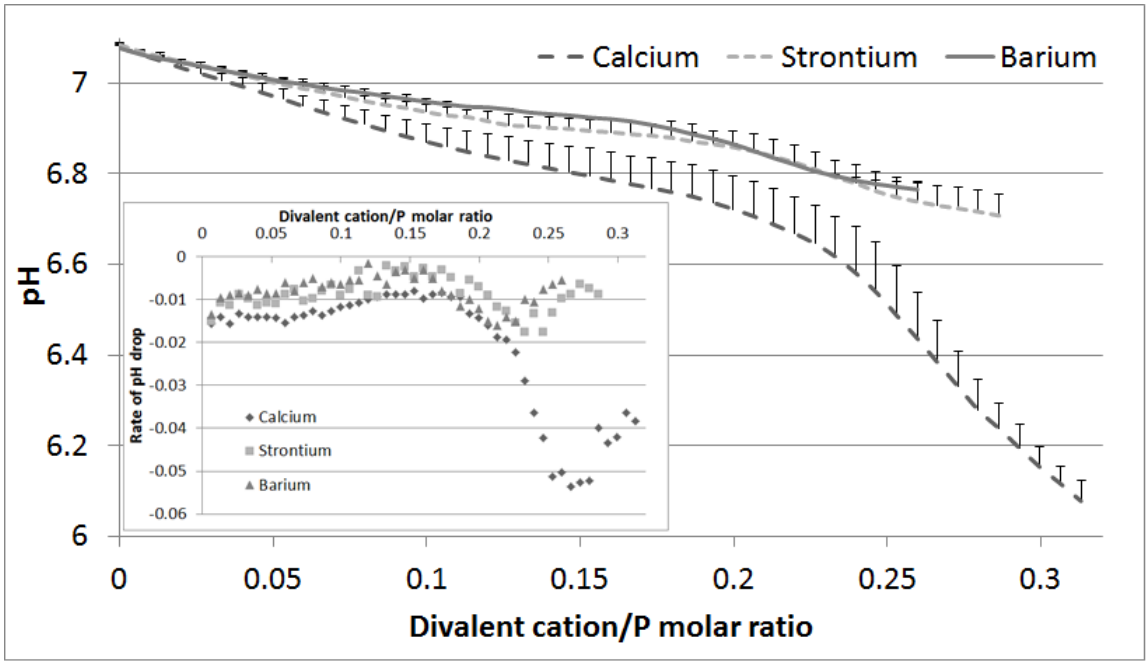

Figure 3.2 pH decrease for different divalent cations in a polyphosphate solution with $\overline{D_p}$ of 47 ([phosphate] = 0.3 M; positive STD error bars are only shown for clarity; negative error bars are equal to positive error bars). Inset show the rate of pH drop. Temperature in all pH studies was 25±0.5°C. The rate of pH drop refers to the slope of the titration curves.

The amount of pH drop in the NaPP solution was also affected by the type of divalent cation being used (Figure 3.2), with decreases in pH from 7.08±0.01 to 6.08±0.05, 7.09±0.01 to 6.71±0.05, and 7.08±0.01 to 6.77±0.01 observed for Ca, Sr and Ba addition, respectively. The shape of the pH curves were found to be similar between different divalent cations, albeit with a slight shift in the gradual increase or inflection in the rate of the pH drop to lower divalent cation/P molar ratios for cations with larger ionic radius (Figure 3.2 inset).

The most important features of the titration curves of polyphosphate solutions loaded with calcium at different Ca/P molar ratios are summarized in Table 3.1, with the corresponding titration curves provided in Figure 3.3. The values of pH at inflection points reported in Table 3.1 are not perfectly accurate due to the difficulties in determining the accurate inflection point. In contrast the pH at the half-way point, which is equal to the pKa, is more accurate (accuracy error < 0.1 pH units). Based on Table 3.1, it is clear that the pKa values for the hydrogen atom at the end of the chains decrease as the amount of calcium that is chelated by polyphosphate chains increases.

Table 3.1 also shows the results of the titration of polyphosphate solutions loaded with different divalent cations; the corresponding titration curves are provided in Figure 3.4. It seems that the pKa value is directly related to the ionic radius of the divalent cation, however further studies are required to verify this relation.

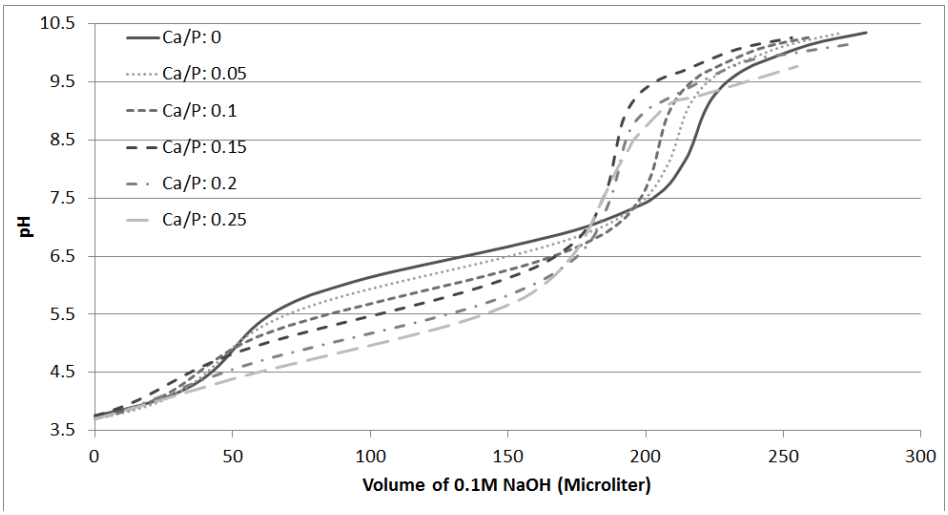

Figure 3.3 Titration of a polyphosphate solution with $\overline{D_p}$ of 100 at different Ca/P molar ratios ([phosphate]= 0.098M in 0.1M NaCl solution). Temperature in all pH studies was 25±0.5°C.

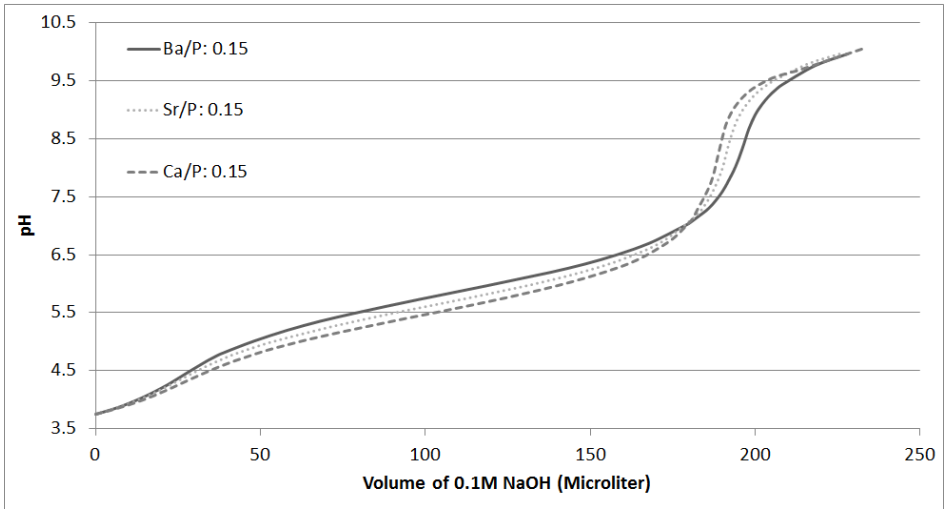

Figure 3.4 Titration of a polyphosphate solution with $\overline{D_p}$ of 100 at 0.15 (Ca, Sr or Ba)/P molar ratios ([phosphate]=0.098 in 0.1M NaCl solution). Temperature in all pH studies was 25±0.5°C.

Table 3.1 Summary of the key features from the titration curves of a polyphosphate solution with $\overline{D_p}$ of 100 at 0.15 (Sr or Ba)/P molar ratios and at different Ca/P molar ratios lower than Ca*.

Sample	pH at first inflection point	pH at second inflection point	pH at half-way = pKa	Volume of 0.1M NaOH between two inflection points (µl)
0 Ca/P	4.88	8.70	6.5	169
0.05 Ca/P	4.79	8.61	6.25	165
0.10 Ca/P	4.62	8.25	5.95	163
0.15 Ca/P	4.31	8.06	5.55	161
0.20 Ca/P	4.15	8.17	5.25	164
0.25 Ca/P	4.01	7.75	5	164
0.15 Sr/P	4.39	8.42	5.7	165
0.15 Ba/P	4.41	8.67	5.9	172

The pKa for a 0 Ca/P sample was also determined by NMR, with Figure 3.5 displaying the ^{31}P-NMR spectra of a 0 Ca/P NaPP solution at different pH values. While the $Q^{2\text{-middle}}$

peak at ~-21 to 22 ppm remained stable, a shift in the Q^1 peak downfield from around -10 ppm at low pH and to -5 ppm at high pH was observed. Figure 3.6 shows the plot of Q^1 chemical shift against solution pH; the pH at the inflection point of this plot, shown by the red line, is equal to the pKa of the phosphate group at the end of the chain. The pKa by this method was found to be 6.4, very close to that determined by titration (6.5).

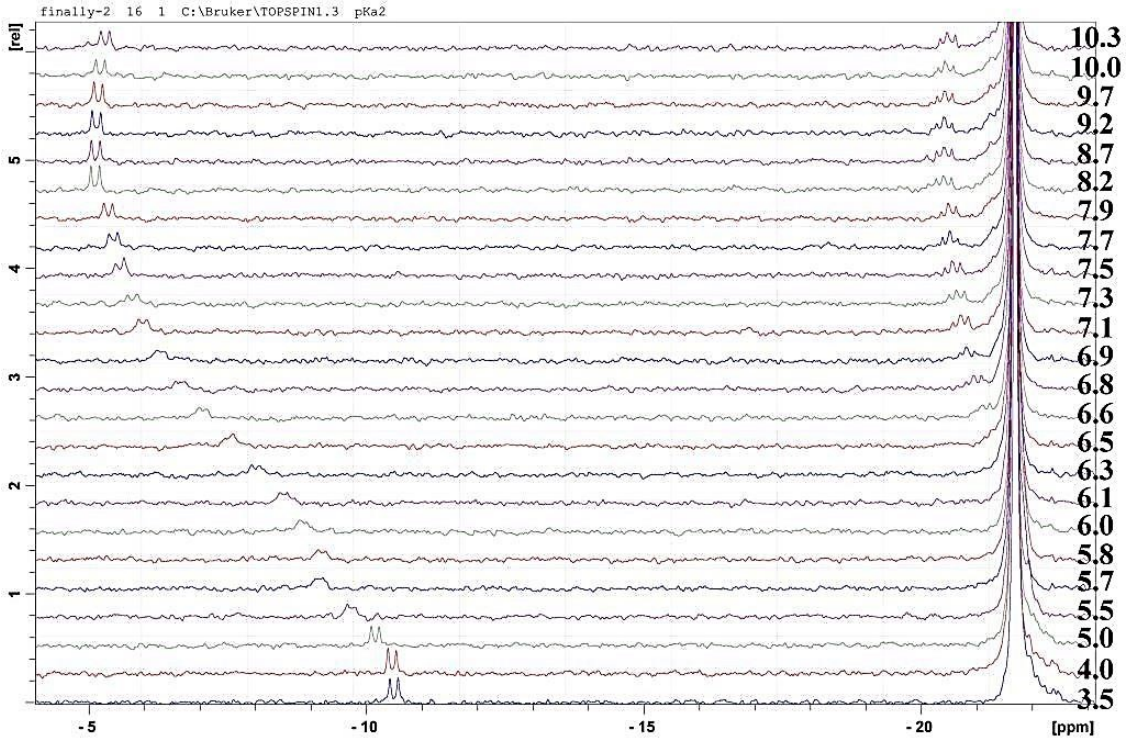

Figure 3.5 ^{31}P-NMR spectra of a NaPP solution with $\overline{D_p}$ of 100 at Ca/P molar ratio of 0, at different pH values shown on the right side of the spectra ([phosphate] = 0.098 M in 0.1 M NaCl solution).

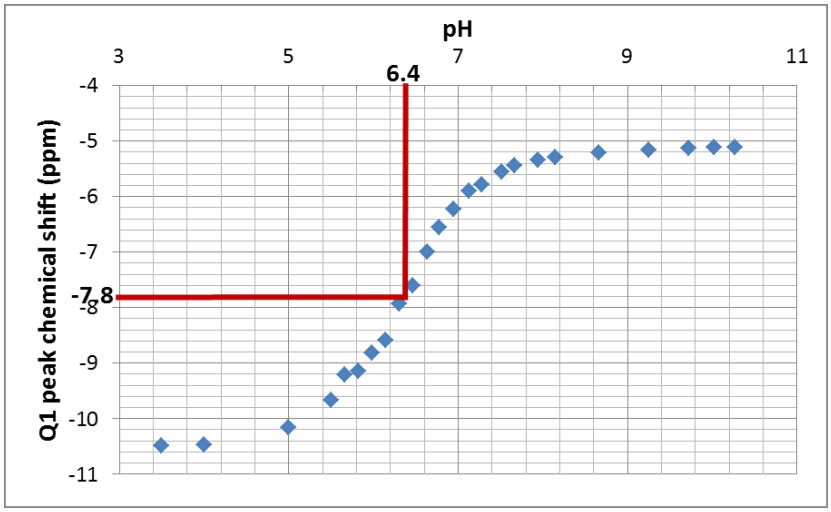

Figure 3.6 Q^1 peak chemical shift against the pH of the solution for a NaPP solution with $\overline{D_p}$ of 100 at Ca/P molar ratio of 0 ([phosphate] = 0.098 M in 0.1 M NaCl solution). pH at the inflection point is equal to the pKa of the Q^1 site. Red lines pass the inflection point.

3.4.2 Liquid ^{31}P-NMR results

The degradation rate of pure NaPP in water at 37°C and pH of 6.5 is very slow. In fact after 14 days at 37°C there is no significant drop in $\overline{D_p}$ (single factor ANOVA analysis). To accelerate NaPP degradation in order to assess the relationship between degradation rate of NaPP and its $\overline{D_p}$, subsequent studies were carried out at 80°C. The NMR spectra of NaPP fractions with $\overline{D_p}$ of 402±15 and 100±1 at different time intervals are provided in Figure 3.7. Over time, two peaks representing orthophosphate (~0.07 ppm) and trimetaphosphate (~-21.50 ppm), a ring of three phosphates, grow, with the main byproduct here being orthophosphate. The rate of formation of orthophosphates and trimetaphosphates were found to be considerably higher in the shorter NaPP fraction (Table 3.2). In contrast, the rate of formation of end groups (Q^1) were considerably higher in the longer fraction; consequently the rate of decrease in the $\overline{D_p}$ was faster for longer chains (the $\overline{D_p}$ value depends mainly on the Q^1 value, since Q^1 is the denominator in the Equation 3.1). It could be said that longer chains become shorter more quickly.

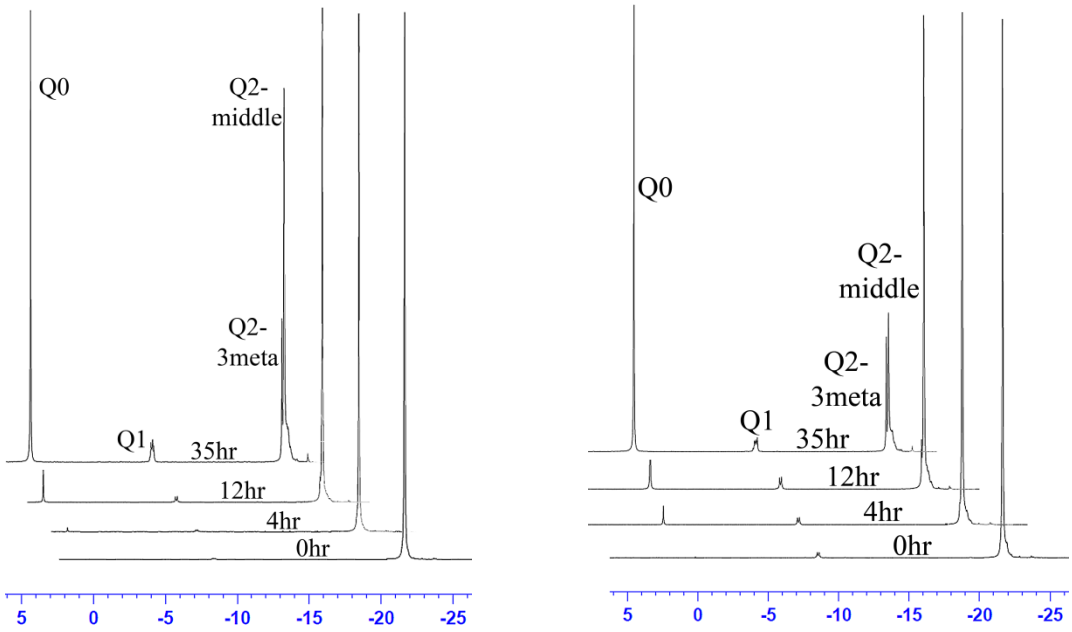

(a) **(b)**

Figure 3.7 NMR spectra of NaPP with original $\overline{D_p}$ of (a) 402±15 and (b) 100±1 being kept at 80°C at different time points. With the exception of the lowest spectra, all other spectra are shifted downfield for clarity.

Table 3.2 $\overline{D_p}$ and relative areas under NMR peaks of two NaPP fractions being kept at 80°C at different time points (Numbers show average±STD (n=3)).

	NaPP Fraction with starting $\overline{D_p}$ of 402±15					NaPP Fraction with starting $\overline{D_p}$ of 100±1				
Time (min)	Q^0 (mol%)	Q^1 (mol%)	$Q^{2\text{-meta}}$ (mol%)	$Q^{2\text{-middle}}$ (mol%)	$\overline{D_p}$	Q^0 (mol%)	Q^1 (mol%)	$Q^{2\text{-meta}}$ (mol%)	$Q^{2\text{-middle}}$ (mol%)	$\overline{D_p}$
0	0.00 ±0.01	0.49 ±0.01	0.58 ±0.1	98.95 ±0.02	402 ±15	0.04 ±0.02	2.00 ±0.01	0.77 ±0.08	97.96 ±0.03	100 ±1
240	0.61 ±0.07	0.78 ±0.01	0.59 ±0.07	98.03 ±0.02	254 ±2	2.37 ±0.15	2.28 ±0.04	0.84 ±0.11	94.05 ±0.30	85 ±2
735	4.04 ±0.20	1.87 ±0.07	1.45 ±0.10	92.65 ±0.31	101 ±4	11.21 ±0.58	3.53 ±0.02	2.84 ±0.02	81.67 ±0.64	48 ±4
2085	28.78 ±0.89	5.03 ±0.05	8.22 ±0.50	57.32 ±1.16	25 ±1	41.79 ±1.48	4.71 ±0.07	11.30 ±0.55	41.10 ±2.01	19 ±1

The NMR spectra of a polyphosphate loaded to a Ca/P molar ratio of 0.20 at different time intervals is provided in Figure 3.8. As before, the orthophosphate and trimetaphosphate peaks grow over time, though here the main byproduct is the trimetaphosphate ring. Table 3.3 summarizes the results of hydrolysis of polyphosphate at different Ca/P molar ratios. Single factor ANOVA analysis between time points for each ratio showed that, at 0.10, 0.15 and 0.20 Ca/P molar ratios, there was a significant

drop in $\overline{D_p}$ over 14 days (p value<0.05). Higher Ca/P molar ratios resulted in faster rates of formation of Q^0, $Q^{2\text{-meta}}$ and Q^1.

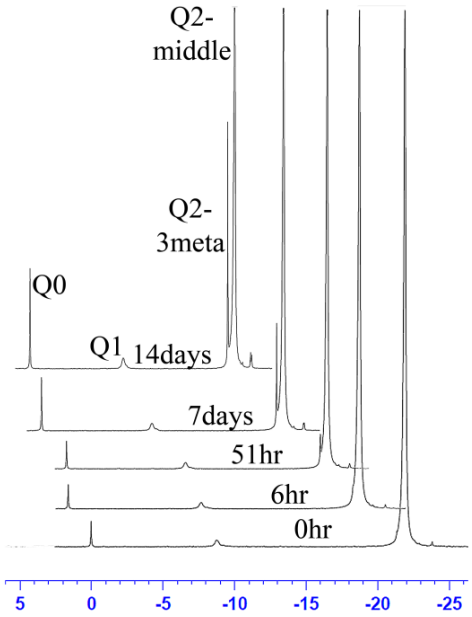

Figure 3.8 NMR spectra of NaPP with original $\overline{D_p}$ of 87±3 at Ca/P molar ratio of 0.2, kept at 37°C at different time points. With the exception of the lowest spectrum, all other spectra are shifted downfield for clarity.

Table 3.3 $\overline{D_p}$ and relative areas under NMR peaks of a NaPP with original $\overline{D_p}$ of ~86 at different Ca/P molar ratios being kept at 37°C at different time points (Numbers show average±STD (n=3)).

Time	0 Ca/P					0.10 Ca/P				
	Q^0 (mol%)	Q^1 (mol%)	$Q^{2\text{-meta}}$ (mol%)	$Q^{2\text{-middle}}$ (mol%)	$\overline{D_p}$	Q^0 (mol%)	Q^1 (mol%)	$Q^{2\text{-meta}}$ (mol%)	$Q^{2\text{-middle}}$ (mol%)	$\overline{D_p}$
0	1.32 ±0.03	2.35 ±0.06	0.91 ±0.11	95.42 ±0.10	83 ±2	1.37 ±0.03	2.28 ±0.05	0.84 ±0.06	95.51 ±0.06	86 ±2
6hr	1.48 ±0.02	2.33 ±0.05	0.88 ±0.07	95.31 ±0.05	84 ±2	1.43 ±0.04	2.28 ±0.06	0.98 ±0.15	95.31 ±0.16	86 ±2
51hr	1.52 ±0.03	2.38 ±0.06	0.93 ±0.10	95.17 ±0.08	82 ±2	1.62 ±0.04	2.36 ±0.05	0.98 ±0.07	95.04 ±0.11	83 ±2
7day	1.81 ±0.03	2.33 ±0.04	0.98 ±0.06	94.88 ±0.01	84 ±1	2.13 ±0.03	2.43 ±0.01	1.14 ±0.11	94.30 ±0.11	80 ±0
14day	2.36 ±0.08	2.42 ±0.03	0.86 ±0.06	94.36 ±0.11	80 ±1	2.99 ±0.04	2.46 ±0.04	1.25 ±0.05	93.31 ±0.03	78 ±1

Time	0.15 Ca/P					0.20 Ca/P				
	Q^0 (mol%)	Q^1 (mol%)	$Q^{2\text{-meta}}$ (mol%)	$Q^{2\text{-middle}}$ (mol%)	$\overline{D_p}$	Q^0 (mol%)	Q^1 (mol%)	$Q^{2\text{-meta}}$ (mol%)	$Q^{2\text{-middle}}$ (mol%)	$\overline{D_p}$
0	1.37 ±0.01	2.25 ±0.01	1.00 ±0.04	95.38 ±0.05	87 ±0	1.33 ±0.01	2.26 ±0.08	1.01 ±0.09	95.40 ±0.04	87 ±3
6hr	N/A	N/A	N/A	N/A	N/A	1.37 ±0.01	2.17 ±0.03	3.61 ±0.22	92.85 ±0.20	88 ±1
51hr	1.59 ±0.06	2.22 ±0.12	2.38±0.14	93.81 ±0.17	87 ±5	1.71 ±0.3	2.27 ±0.04	6.98 ±0.28	89.04 ±0.32	80 ±2
7day	2.09 ±N/A	2.35 ±N/A	6.46±N/A	89.10 ±N/A	78 ±N/A	2.71 ±0.08	2.45 ±0.13	9.71 ±0.55	85.13 ±0.45	72 ±4
14day	3.76 ±0.36	2.69 ±0.12	8.50±0.48	85.05 ±0.90	65 ±3	4.54 ±0.08	3.01 ±0.11	14.77 ±0.81	77.68 ±0.78	54 ±1

Table 3.4 summarizes the degradation results of NaPPs loaded with strontium and barium. Unlike calcium, barium and strontium generally did not induce significant formation of trimetaphosphate, with only 0.15 Ba/P at 14 days showing significant levels of trimetaphosphate that nevertheless were much lower compared to 0.15 loaded Ca/P samples. However, 0.15 loading of barium and, to a greater extent, strontium, did induce orthophosphate formation at higher rates compared to calcium.

Table 3.4 $\overline{D_p}$ and relative areas under NMR peaks of a NaPP with original $\overline{D_p}$ of ~86 at different Sr/P and Ba/P molar ratios being kept at 37°C at different time points (Numbers show average±STD (n=3)).

	0.10 Sr/P					0.15 Sr/P				
Time	**Q^0 (mol%)**	**Q^1 (mol%)**	**$Q^{2\text{-meta}}$ (mol%)**	**$Q^{2\text{-middle}}$ (mol%)**	**$\overline{D_p}$**	**Q^0 (mol%)**	**Q^1 (mol%)**	**$Q^{2\text{-meta}}$ (mol%)**	**$Q^{2\text{-middle}}$ (mol%)**	**$\overline{D_p}$**
0	**1.40 ±0.04**	**2.27 ±0.06**	**0.84 ±0.19**	**95.49 ±0.10**	**86 ±2**	**1.41 ±0.05**	**2.23 ±0.04**	**0.86 ±0.07**	**95.49 ±0.06**	**88 ±1**
51hr	**1.55 ±0.04**	**2.23 ±0.02**	**0.85 ±0.15**	**95.37 ±0.17**	**87 ±1**	**1.60 ±0.01**	**2.29 ±0.05**	**0.85 ±0.11**	**95.26 ±0.14**	**85 ±2**
7day	**1.96 ±0.06**	**2.29 ±0.05**	**0.84 ±0.19**	**94.90 ±0.17**	**85 ±2**	**2.18 ±0.03**	**2.43 ±0.07**	**0.87 ±0.09**	**94.51 ±0.09**	**80 ±2**
14day	**2.95 ±0.57**	**2.38 ±0.10**	**0.86 ±0.08**	**93.81 ±0.62**	**81 ±4**	**4.45 ±0.26**	**2.57 ±0.08**	**1.05 ±0.12**	**91.93 ±0.44**	**74 ±2**

	0.10 Ba/P					0.15 Ba/P				
Time	**Q^0 (mol%)**	**Q^1 (mol%)**	**$Q^{2\text{-meta}}$ (mol%)**	**$Q^{2\text{-middle}}$ (mol%)**	**$\overline{D_p}$**	**Q^0 (mol%)**	**Q^1 (mol%)**	**$Q^{2\text{-meta}}$ (mol%)**	**$Q^{2\text{-middle}}$ (mol%)**	**$\overline{D_p}$**
0	**1.37 ±06**	**2.28 ±0.06**	**0.93 ±0.04**	**95.42 ±0.11**	**86 ±2**	**1.42 ±0.05**	**2.26 ±0.14**	**1.19 ±0.08**	**95.13 ±0.23**	**86 ±5**
51hr	**1.63 ±0.04**	**2.24 ±0.08**	**1.03 ±0.03**	**95.10 ±0.09**	**87 ±3**	**1.65 ±0.08**	**2.30 ±0.04**	**1.00 ±0.10**	**95.05 ±0.13**	**85 ±1**
7day	**2.19 ±0.13**	**2.32 ±0.15**	**1.01 ±0.23**	**94.49 ±0.51**	**84 ±6**	**2.57 ±0.04**	**2.42 ±0.09**	**1.19 ±0.18**	**93.82 ±0.20**	**80 ±3**
14day	**3.08 ±0.24**	**2.37 ±0.03**	**1.06 ±0.09**	**93.49 ±0.29**	**81 ±1**	**3.81 ±0.09**	**2.49 ±0.09**	**4.14 ±0.80**	**89.56 ±0.80**	**74 ±2**

Similar to calcium, the rate of $\overline{D_p}$ reduction for either Ba or Sr-loaded polyphosphates was dependent on the amount of divalent cation available. Based on single factor ANOVA analysis there was no significant decrease in $\overline{D_p}$ of 0.10 Ba/P and 0.10 Sr/P samples over 14 days, but at 0.15 Ba/P and 0.15 Sr/P a significant decrease in $\overline{D_p}$ was detected. To determine which cation induces more rapid degradation of polyphosphates, 0.15 loaded samples were compared. Based on a two-tailed student t-test, no significant difference in $\overline{D_p}$ up to 7 days was found; at 14 days calcium loaded polyphosphates were

significantly shorter than barium or strontium loaded polyphosphates (p value<0.05), indicating that calcium promotes polyphosphate degradation more than barium or strontium. No significant difference between the $\overline{D_p}$ of barium loaded polyphosphate and strontium loaded samples was noted at any time point.

Unlike chelated Al^{3+}, which is reported to only bind to the Q^1 sites in polyphosphate solution [152], we observed alkaline earth metals to bind to both $Q^{2\text{-middle}}$ and Q^1 sites as evidenced by changes in the chemical shift, shape and width at half height for the $Q^{2\text{-middle}}$ and Q^1 peaks. Figure 3.9 shows the position of the $Q^{2\text{-middle}}$ peak at different Me^{II}/P molar ratios. This peak was shifted downfield (more positive values) up to 0.10 Me^{II}/P molar ratio, after which a shift upfield (more negative values) was observed. This implies that divalent cations initially chelated by the phosphate groups at the middle of the chain remove part of the electron density surrounding the phosphorus nucleus (deshielding); as the amount of divalent cations increases, they then start to contribute to the electron density around the phosphorus atom (shielding). This behavior was observed with all three divalent cations. In addition, the width at half height for the $Q^{2\text{-middle}}$ peak increases slightly as more divalent cation is being chelated, as shown in Table 3.5.

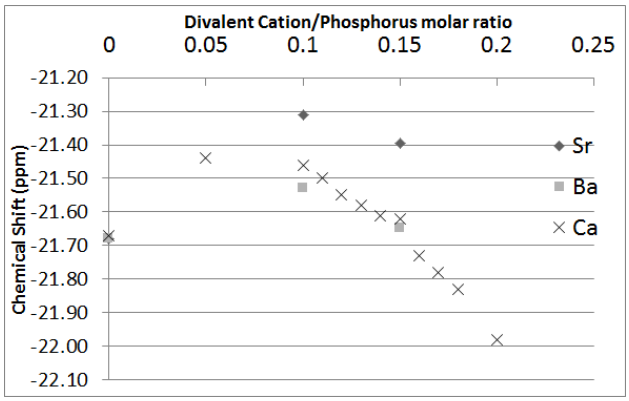

Figure 3.9 Chemical shifts of phosphate groups in the middle of the polyphosphate chains at different divalent cation/phosphorus molar ratios.

Table 3.5 The width at half height for $Q^{2\text{-middle}}$ peaks at different divalent cation to phosphorus molar ratios. NaPP with original $\overline{D_p}$ of 87±3 is used. Numbers show average±STD (n=3).

Sample	Ca/P molar ratio				Sr/P molar ratio		Ba/P molar ratio	
	0	0.1	0.15	0.2	0.1	0.15	0.1	0.15
width at half height for $Q^{2\text{-middle}}$ peak	0.087 ±0.000	0.113 ±0.001	0.129 ±0.000	0.149 ±0.002	0.114 ± 0.001	0.127 ±0.000	0.097 ±0.001	0.105 ±0.003

The intensity and resolution of the Q^1 peak was low because of a low number of scans obtained. Still, changes in the shape, chemical shift and appearance of a new peak in the upfield position suggest that alkaline earth metals also bind near the end of the chains or directly to the Q^1 site (Figure 3.10).

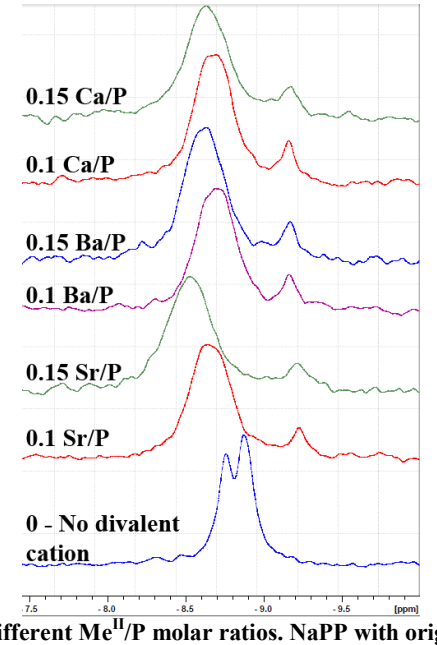

Figure 3.10 Q^1 peaks at different Me^{II}/P molar ratios. NaPP with original $\overline{D_p}$ of 87±3 was used.

3.4.3 Viscosity results

Figure 3.11 shows the effect of divalent cation addition on the viscosity of a polyphosphate solution, with viscosity decreasing with increasing molar ratio of divalent cation to phosphorus. Based on a two-tailed student t-test, barium and strontium reduced the viscosity significantly more than calcium at all Me^{II}/P molar ratios except at 0.05 (Sr vs. Ca) and 0.175 (Sr vs. Ca) (p-value<0.05). The viscosity between Ba and Sr loaded solutions was only significantly different at the 0.05 divalent cation/P molar ratio.

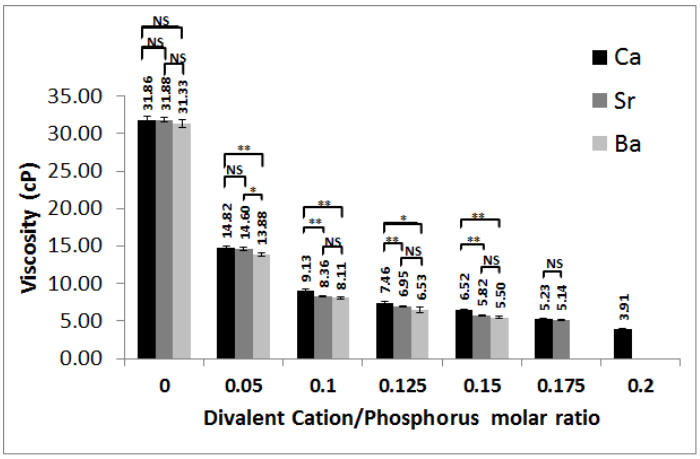

Figure 3.11 Viscosity of a NaPP with $\overline{D_p}$ of ~17,000 at phosphate concentration of 171 mM against different divalent cation/phosphorus molar ratios (two tailed student t-test: NS, * and ** stand for p-value>0.05, 0.01<p-value<0.05 and p-value<0.01, respectively) (Numbers show average and bars show STD (n=3))

Viscosity was also measured at low polyphosphate concentration for different Ca/P molar ratios. η_{sp}/C was plotted against concentration C and is shown in Figure 3.12. Plots are curved upwards as concentration decreases, a common trend in polyelectrolytes due to the un-screening of the charges on the chains at low ionic strength. As the Ca/P molar ratio increases this upward trend remains, implying that the chains are still charged in the presence of calcium. Nevertheless, it is obvious from the normalized plots (Figure 3.12 inset) that calcium affects the concavity of these curves, shifting the un-screening of the chains to lower polyphosphate concentrations.

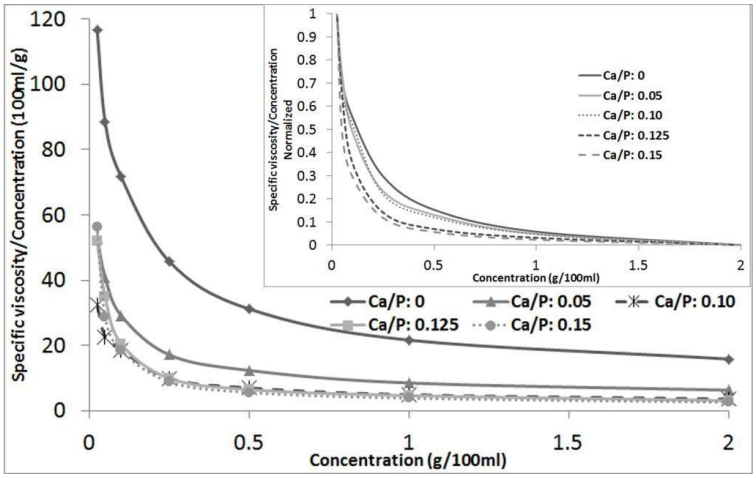

Figure 3.12 η_{sp}/C against C for a NaPP with $\overline{D_p}$ of ~17,000 at different Ca/P molar ratios (inset shows the same data after normalization).

3.4.4 Turbidity results

Figure 3.13 illustrates the method of determining the Me* by turbidity measurements using two examples. Arrows point to the amount of calcium that causes a sudden increase in the turbidity of the solution from which the Me* value could be determined. At high phosphate concentrations the cloudy point could be determined by visual inspection, but at low concentrations a turbidity meter was required.

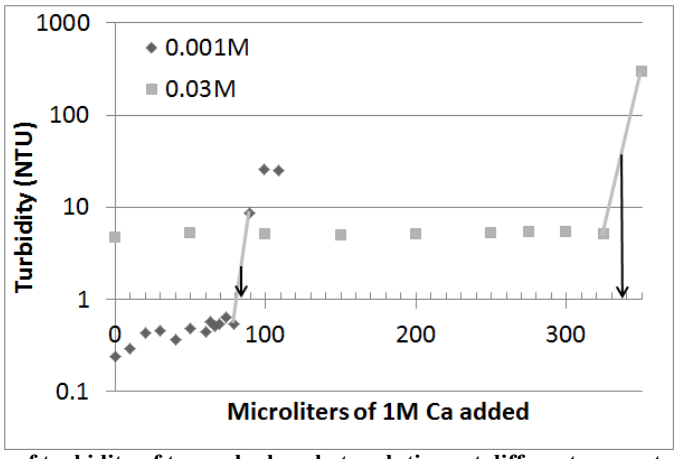

Figure 3.13 Example of turbidity of two polyphosphate solutions at different concentrations as Ca is being added, arrows point to the Ca*.

Turbidity studies demonstrated that the value of Me* continuously decreases as phosphate concentration increases (Figure 3.14a). This means that at higher NaPP concentrations, a lower amount of divalent cation per chain is required for coacervation.

The value of Ca* was also found to depend on $\overline{D_p}$ of NaPP (Figure 3.14a). For phosphate concentrations <0.6 M, Ca* was significantly lower for NaPPs with $\overline{D_p}$ of 451 and 20,000 compared to shorter chain solutions with $\overline{D_p}$ of 80; these significant differences in Ca* were not observed at higher phosphate concentrations. In addition, Ca* for NaPP with $\overline{D_p}$ of 20,000 was not significantly different from that for NaPP with $\overline{D_p}$ of 451 except at two phosphate concentrations, 0.006 and 0.03 M.

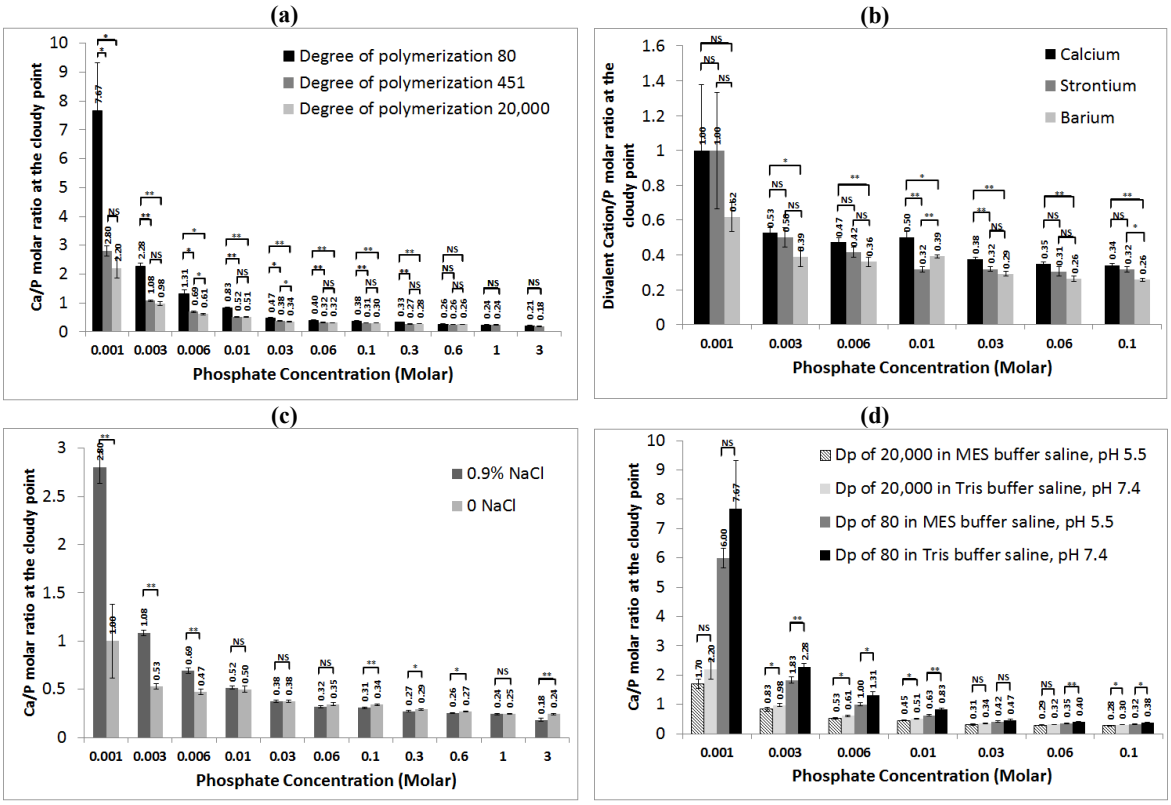

Figure 3.14 (a) Ca* for NaPPs with different $\overline{D_p}$ in 0.05 M Tris buffer saline at pH 7.4; (b) Me* for a NaPP with $\overline{D_p}$ of 451 in 0.05 M Tris buffer at pH 7.4; (c) Ca* for a NaPP with $\overline{D_p}$ of 451 in 0.05 M Tris buffer vs. 0.05 M Tris buffer saline at pH 7.4; (d) Ca* for NaPPs with different $\overline{D_p}$ in 0.05 M Tris buffer saline at pH 7.4 vs. 0.05 M MES buffer saline at pH 5.5. In all measurements temperature was 37°C±0.5. Two tailed student t-test: NS, * and ** stand for p-value>0.05, 0.01<p-value<0.05 and p-value<0.01, respectively. Numbers show average and bars show STD (n=3).

Me* also depends on the type of divalent cation as shown in Figure 3.14b. At all phosphate concentrations except the lowest concentration of 0.001 M, Ca* was significantly higher than Ba*. The differences between Ca* and Sr*, or Sr* and Ba*, were not significant for most of phosphate concentrations studied, though a general trend suggested that less of the divalent cations with the larger ionic radius was required for coacervation.

Figure 3.14c shows the effect of ionic strength on Me* using a 0.05 M Tris buffer solution and a 0.05 M Tris buffer *saline* solution. Addition of NaCl and the resulting increase in the ionic strength of the solution resulted in a decrease in Ca* at phosphate

concentrations higher than 0.03 M and an increase at phosphate concentrations lower than 0.03 M. Lastly, Figure 3.14d shows the effect of pH on Ca* for two different NaPPs ($\overline{D_p}$ of 80 and 20,000). Overall, Ca* was found to decrease in acidic pH, indicating that less calcium per chain is needed to form a coacervate under acidic conditions.

3.4.5 Chemical composition of the coacervates

Sr addition to polyphosphate solution at values higher than Sr* results in flocculation. These particles are not sticky and can only be integrated with each other when pressed by hand; even after pressing, the resulting mass easily breaks up when pulled. On the other hand, addition of Ba at values higher than Ba* results in a suspension in which particles do not flocculate. Only Ca results in a coacervate, a highly viscous mass that is characteristically very sticky. However, when long chains are used the mass develops elastic properties similar to chewing gum. Here, we focused only on the chemical composition of the calcium coacervated mass.

Figure 3.15a shows the Ca/P molar ratio of the coacervate in comparison to the original Ca/P molar ratio that was used during the coacervation process. At 0.357 and lower, the Ca/P molar ratio of the coacervate reflected the original value of Ca/P. However, at initial Ca/P ratios of 0.42, 0.50 and 1, the Ca/P molar ratios of the coacervates were lower at 0.383±0.006, 0.395±0.002, and 0.438±0.008, respectively.

As shown in Figure 3.15b, for the 0.357 coacervate almost 11% of originally available phosphates remained in the supernatant solution rather than incorporate into the coacervate, while for the 0.42, 0.50 or 1.0 samples almost all of the phosphates were incorporated into the coacervate. Nevertheless, as the amount of calcium used for

coacervation increased, the amount of free calcium remaining in the supernatant also increased profoundly.

For Ca/P > 0.357 (Ca*) it was assumed that the penetration of remaining calcium into the coacervate requires time. Figure 3.15c shows the result of these experiments for the 0.50 Ca/P ratio. Based on single factor ANOVA analysis, mixing time was found to have no significant impact on the Ca/P molar ratio of the resulting coacervate.

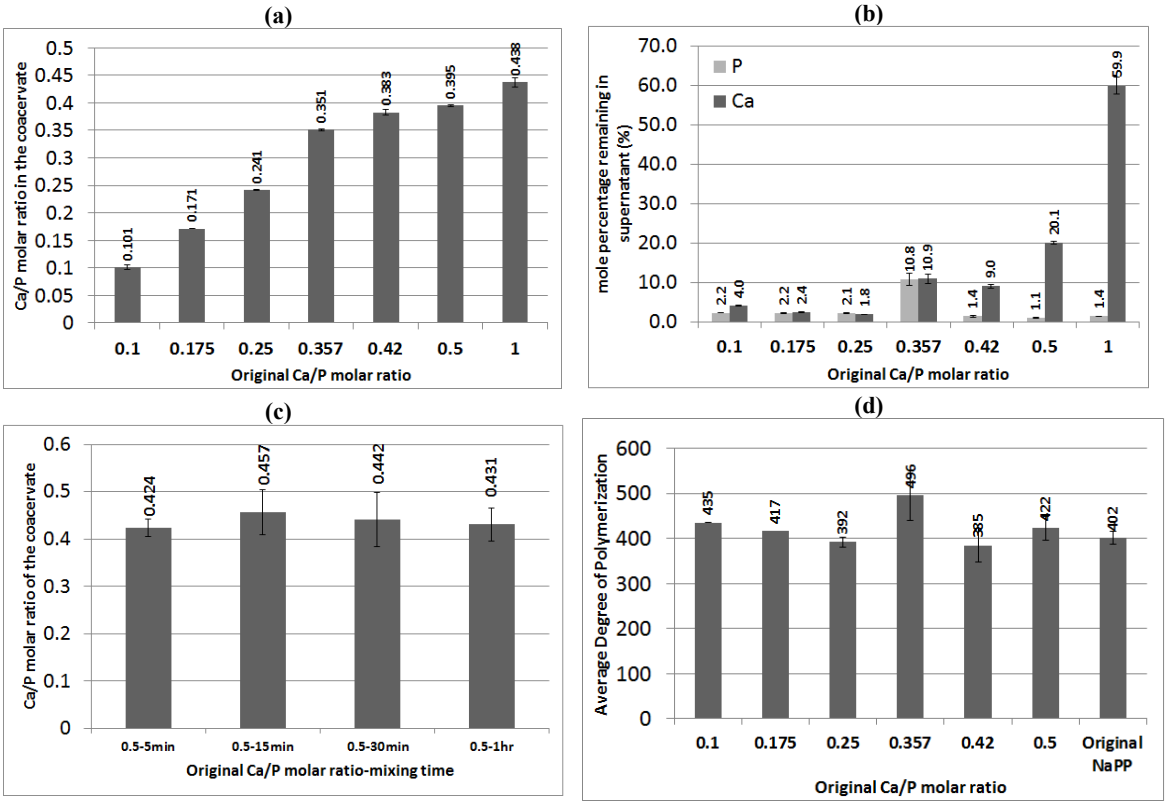

Figure 3.15 (a) Ca/P molar ratio in the coacervate in comparison to the original Ca/P molar ratio that was used during mixing; (b) mole percentage of calcium and phosphorus that is not incorporated into the coacervate; (c) Effect of mixing time on the Ca/P molar ratio of the coacervate; (d) $\overline{D_p}$ of polyphosphates inside the coacervates at different Ca/P molar ratios in comparison to the original $\overline{D_p}$ of NaPP. Numbers show average and bars show STD (n=3).

Figure 3.15d shows the $\overline{D_p}$ of polyphosphates in the coacervate in comparison to that of the original NaPP solution. Overall, no significant drop in $\overline{D_p}$ was noted. Increasing the

mixing time from 5min to 1hr also did not cause any significant drop in the $\overline{D_p}$ of the resulting coacervates (Data is not shown).

As previously mentioned, at 0.357, which is equal to Ca* at these conditions, a significant percentage of phosphates remained in the solution, which were presumably the shorter chain polyphosphates. Interestingly, only at this Ca/P molar ratio was an increase in the $\overline{D_p}$ of the coacervate observed; if some of the short chains from the original NaPP did not get incorporated into the coacervate, the $\overline{D_p}$ inside the coacervate would become higher than the original $\overline{D_p}$ of the NaPP.

3.5 Discussion

There is a relatively weak hydrogen atom at each end of a phosphate chain, but middle phosphate groups in either chains or rings do not have such weak hydrogens. Therefore, in absence of Q^0, the number of base equivalents used to titrate polyphosphate solution between the pH 4.5 and 9 is equal to moles of Q^1 sites in the solution [3, 6]. In a long polyphosphate chain where dissociation of hydrogen atom at one end does not affect hydrogen dissociation at the other end, a single acid-base equilibrium can be considered with pKa determined by titration by the following reaction:

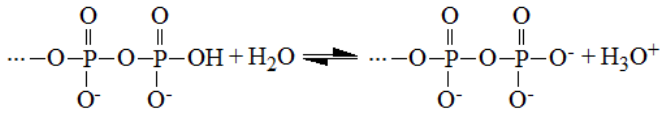

Since atmospheric CO_2 dissolution and conversion into H_2CO_3 is very slow, the effect of CO_2 on titration in this study is minimal. In addition, the pKa as determined for a 0 Ca/P sample by liquid ^{31}P-NMR was very close to the value obtained by titration, again

supporting the notion that the effect of atmospheric CO_2 on titration under the conditions of these studies is minimal.

Chelation of divalent cations by polyphosphate chains caused the pH of the solution to decrease, an effect previously reported by several researchers [38, 95, 153]. We showed that the pKa value of hydrogen atoms at the end of the chains also decreases during chelation. This pH effect can be explained, therefore, by the dissociation of hydrogen atoms at the chain ends. Since chains with larger $\overline{D_p}$ have a fewer number of end-group phosphates, they have correspondingly fewer hydrogen atoms at their ends to be released into the solution, resulting in less of a pH drop.

The extent of any decrease in the pH and pKa values of polyphosphates loaded with divalent cations seems to be directly related to the stability of the complex forming between that cation and the chain; it is known that the dissociation constant and the stability of the complexes of Ba, Sr and Ca with tripolyphosphate, tetrapolyphosphate or longer chains decrease as the ionic radius increases [154-156]. The other possible explanation for the pH decrease during chelation is hydrolysis of the chelated divalent cation, which is partially hydrated, forming hydroxyl complexes as shown in the following reaction. This uncommon reaction has been reported for alkaline earth metals that are chelated by tripolyphosphates [157].

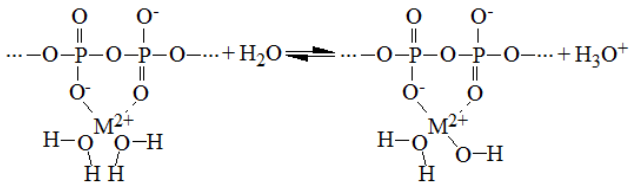

Immersion of alkaline phosphate glasses into water instantly leads to a rapid decrease in pH [148, 158]. We believe that this pH drop is fundamentally similar to the pH decrease that was observed here in polyphosphate solutions. It is expected that the extent of this drop is related to the type of the modifier cation in the glass. For instance, it has been reported that more Ca in a Na_2O-CaO-P_2O_5 glass system results in a larger pH drop [159].

pH studies also revealed a gradual increase in the rate of pH drop when the Me^{II}/P molar ratio exceeds ~0.18. This kind of anomaly has been previously reported in Raman spectroscopy and extended X-ray absorption fine structure (EXAFS) studies of polyphosphate-divalent cation systems, where shifts in behavior always occur around 0.16-0.20 Me^{II}/P [100] . It is interesting that this anomaly also happens at the same ratio in alkaline phosphate glasses [39, 43]. There are three possible explanations for this behavior. Firstly, Filho et. al [104] have shown using europium luminescence spectroscopy that at low Ca/P molar ratios, Ca^{2+} would locate in cage-like sites with a coordination number of 6 provided by phosphate units of the polyphosphate chain. However, when Ca/P ratio exceeds ~0.17, Ca^{2+} ions begin to occupy a second family of sites where they can interact with water molecules. The transition between these two sites could be the cause of the observed anomalies. A second explanation is based on the coordination number of the cation (N_{MeO}) and the number of terminal oxygen atoms (M_{TO}) on the phosphate chain [43]; Ca^{2+} has the N_{MeO} of 6 [104], and therefore at a Ca/P molar ratio of 1/6 (~0.17) all the terminal oxygen atoms are bonded and remaining Ca^{2+} ions either end up sharing the terminal oxygen atoms or satisfying their N_{MeO} with water molecules, leading to changes in behavior of the system at this ratio.

A third explanation is based on Manning theory, which states that counterions exist in three different states in a polyelectrolyte solution [89-91]: *condensed* counterions that are chemically site bonded to the polymer chain; counterions making up a *diffused layer* in close proximity to the polymer chain that are *not* chemically condensed but are able to move along the axis of the polymer chain, entrapped in the vicinity of the polyion due to electrostatic forces; and counterions that are freely scattered in the solution. In the limit of infinite dilution, the fraction of condensed counterions (θ) is given by [89]:

$$\theta = \frac{1}{Z}\left(1 - \frac{1}{Z\xi}\right) \qquad (\text{for } Z\xi > 1) \qquad \text{Equation 3.2}$$

where Z is the valence of the counterion and $\xi = \lambda_B/b$; here b is the distance between two charged groups on the polyion and λ_B is the Bjerrum length, defined as the distance at which the Coulomb interaction between two unscreened elementary charges is equal to the thermal energy – equal to 7.135Å in water at 25°C [89]. In a polyphosphate chain, (b) = 2.5Å [89], and therefore the charge density (ξ) of a polyphosphate chain in water is 2.85. From Equation 3.2, at infinite dilution, the fraction of condensed counterions (θ) for a divalent counterion is 0.41. This means that at extremely low ionic strength, in a dissolved calcium polyphosphate ($Ca(PO_3)_2$), 41% of calcium ions are chemically attached (Ca/P molar ratio~0.20). Yet, in most situations, the fraction of condensed counterions in a polyphosphate solution is lower than this theoretical value due to the presence of polyphosphate chains and other ions in the solution, which screen the charge on the chains [86]. So overall, based on the Manning theory, divalent cations are condensed on the chains up to a 0.16-0.20 Me^{II}/P molar ratio; above this threshold these

cations enter into the diffused layer leading to the anomalies in the behavior of the polyphosphate-divalent cation system.

The second part of these chelation studies focused on the relation between NaPP $\overline{D_p}$ and its degradation, and the subsequent effect of alkaline earth metals on the rate of polyphosphate degradation. Degradation of pure NaPP solutions has been well studied [160-163], proceeding through the following pathways: cleavage of orthophosphates from the chain ends; random scission in the middle of the chain; and cleavage of trimetaphosphates from the end and middle of the chains. Their reaction rates are governed by the following equations, respectively [163]:

$$\frac{d[Q^0]}{dt} = k_{E1}[Q^1] \qquad \text{Equation 3.3}$$

$$\frac{d[Q^1]}{dt} = 2k_{ME}[Q^{2-middle}] + \frac{2k_{O3}[Q^{2-meta}]}{3} \qquad \text{Equation 3.4}$$

$$\frac{d[Q^{2-meta}]}{dt} = k_{MO}\left([Q^{2-middle}] - \frac{[Q^1]}{2}\right) + k_{EO}\left([Q^1] - 2([P_2] + [P_3] + [P_4])\right) - \frac{k_{O3}[Q^{2-meta}]}{3}$$

Equation 3.5

where k_{E1} and k_{EO} are specific rates for the formation of Q^0 and trimetaphosphate from Q^1 groups, k_{ME} and k_{MO} are specific rates for the formation of Q^1 and trimetaphosphate from $Q^{2\text{-middle}}$ groups, and k_{O3} is the specific rate for the hydrolysis of trimetaphosphate to tripolyphosphate. $[P_2]$, $[P_3]$ and $[P_4]$ represent the concentrations of pyrophosphate, tripolyphosphate and tetraphosphate, respectively, which do not participate in formation of trimetaphosphate.

For pure NaPP degradation in this study, the rate of formation of ortho and trimetaphosphates was much higher in the shorter fraction. This could be explained based on the Equations 3.3 and 3.5 where the rates of formation of these two species depend mainly on [Q^1], which is higher in the shorter fraction. One should note that in Equation 3.5 the value of k_{MO} is significantly smaller than k_{EO} [163] and therefore could be neglected. On the other hand, the rate of formation of end groups was much higher in the longer fraction. This could be explained by Equation 3.4 and the higher number of Q^{2}_{middle} groups in the longer fraction. Moreover, it has been shown that k_{ME} value increases with an increase in the $\overline{D_p}$ [163], suggesting more rapid random scissions in the middle of longer chains [135].

Our results further show that the rate of degradation of polyphosphates depends on the Me^{II}/P molar ratio, in agreement with previous reports [110, 113, 164]. Trimetaphosphate was the main degradation byproduct of the polyphosphates loaded with calcium, and its formation was highly accelerated at Ca/P molar ratio ≥0.15. Presumably at low Ca/P molar ratios the chains are not coiled effectively to cleave into trimetaphosphate rings.

The viscosity of polyphosphate solutions profoundly decreases when divalent cations are chelated by the chains. Cations with a larger ionic radius possess a greater ability in coiling the polyphosphate chain on itself, reducing its viscosity in solution. A similar relationship between the viscosity of the polyphosphate solutions and ionic radii of the divalent cation has been previously reported but no explanation had been provided [93, 165, 166]. This viscosity phenomenon is common with polyelectrolytes [167], and a possible explanation could be based on the hydrated ionic radii. Unlike anhydrous ionic

radii, the hydrated ionic radii decrease from Ca^{2+} to Ba^{2+} [168]. The less hydrated the ion is, the stronger it interacts with the polyelectrolyte and the larger effect it exerts on the charge state and coiling of the chain on itself [167]. It is very interesting that the same relationship exists in phosphate glass melts; Toyoda et al. [169] have shown that the viscosity of polyphosphate glass melts is inversely related to the ionic radii of the modifier divalent cation.

Lastly we focused on the amount of alkaline earth metals required for coacervation. Precipitation of polyelectrolytes in the presence of multivalent cations has been the subject of several publications by Delsanti and colleagues [97-99]. This group realized that the nature of condensation phenomena described in the Manning theory should be differentiated into two criteria based on the functional group of the polyelectrolyte. The first criterion consists of polyelectrolytes with anionic functional groups having high dissociation constants with divalent cations, such as sulfonate on poly vinyl sulfonate (PVSF). Here, the condensation reaction is basically *electrostatic*. In contrast, if the polyelectrolyte functional group is an anion that has a low dissociation constant with a divalent cation, such as carboxylate on poly acrylic acid (PAA) or phosphates in NaPP, then the condensation reaction is *chemical*. The presence of *chemical condensation* is necessary for precipitation of polyelectrolytes by divalent counterions. As a result, divalent cations do not induce precipitation of PVSF solutions but do so for PAA [97, 98] or NaPP solutions.

A number of competing forces influence whether precipitation can occur. In a divalent cation-poly anion system, factors acting against precipitation are the entropy of the polymer, steric excluded volume and electrostatic repulsion between negatively charged

polymers. In contrast, factors acting in favor of precipitation are hydrophobicity of the chemically condensed phase and the electrostatic interaction between negatively charged free monomers and those monomers possessing an effective positive charge due to the condensation of the divalent cation [97, 98]. As calcium is being added to the NaPP solution, a $Ca(PO_4)_2$ dicomplex forms resulting in increasing hydrophobic forces and decreasing electrostatic repulsion forces until Ca* is reached; above this threshold, precipitate forms followed by aggregation to form coacervate. That Me* continuously decreases as the concentration of NaPP in the solution increases could be explained based on the increase in the shielding effect of the ions as their concentration increases and also based on the entropy of the system; soluble NaPP has higher entropy compared to NaPP trapped in a coacervate, so for a coacervate to form there is an entropy gap to be overcome. This entropy gap is overcome by other forces that are present in this system including hydrophobic and electrostatic forces. This entropy gap is larger at low NaPP concentration compared to high NaPP concentration and, as a result, at low NaPP concentrations more divalent cations are needed to overcome the entropy and formation of a coacervate.

In this study we also observed that, at the same phosphate concentration, Me* is lower for NaPPs having higher $\overline{D_p}$ and that this difference is more significant at low phosphate concentrations (≤0.3 M). This observation can also be explained based on entropy; at the same phosphate concentration, a solution of shorter chains has higher entropy compared to a solution of longer chains. Therefore, a bigger entropy gap for shorter chains must be overcome in order to form a coacervate, meaning more divalent cations are required.

Me* also depends on the type of divalent cation, or more specifically, their ionic radius. The general trend observed was that fewer divalent cations possessing larger ionic radius were required for coacervation. This originates from the ability of the divalent cation to compete with Na^+ or other monovalent cations in the solution; presumably in the presence of Na^+, Ba^{2+} and Sr^{2+} are more capable of forming hydrophobic complexes than Ca^{2+}.

The presence of Na^+ has two effects in polyphosphate solutions: it could screen the charge on a polyelectrolyte, or compete with the divalent cation forming a non-hydrophobic monovalent-polyphosphate complex. The former promotes precipitation and is effective at high phosphate concentrations, while the latter prevents precipitation and is effective at low phosphate concentrations. In contrast, rising $[H^+]$ caused Me* to decrease independent of phosphate concentration probably because H^+ only screens the charge on the chains and does not compete with Ca^{2+} as effectively as Na^+.

3.6 Conclusion

pH, viscosity and NMR studies were carried out to better understand the chelation of alkaline earth metals by polyphosphates. The pH decrease in polyphosphate solutions during the chelation is due to the decrease in the pKa value of hydrogen atoms at phosphate chain ends or possibly hydroxyl complex formation. Longer chains or larger cations cause a smaller pH drop. The gradual shift in the rate of pH drop around divalent cation/phosphorus molar ratio of 0.18 is similar to previously reported anomalies for polyphosphate solutions and glasses, and could be explained by considering Manning theory, the cation coordination number and the different sites available for the cation. The extent of viscosity decrease in polyphosphate solutions, like phosphate glass melts,

depends directly on the ionic radius of the divalent cation. Furthermore, the degradation rate of these polyphosphate chains is a function of the type and amount of divalent cation as well as the polyphosphate $\overline{D_p}$.

Coacervation of polyphosphate chains is the result of a low dissociation constant between the phosphate group and divalent cation, mimicking the precipitation of PAA under the similar conditions. The formed coacervate possesses similar $\overline{D_p}$ to that of the polyphosphate originally used for coacervation, but its Ca/P molar ratio depends largely on the amount of calcium being used and not on the mixing time. The *in vitro* degradation and rheological properties of the coacervates so formed will be the focus of Chapter 4.

Chapter 4 Polyphosphate Coacervate Degradation and Rheology

4.1 Objective

The main objective of this chapter is *understanding rheological and degradation properties of polyphosphate coacervates*.

4.2 Introduction

Hydrolysis of polyphosphate chains is a very well-known phenomenon and a primary reason for the limited industrial applications of phosphate glasses. This hydrolysis is not necessarily a disadvantage for a phosphate glass when it is being used as a biomaterial. For instance, phosphate glasses are investigated as therapeutic ion releasing agent [170] or degradable scaffold for tissue engineering [171]. Similarly, polyphosphate coacervates are expected to degrade in the presence of water. It is essential to evaluate the rate of this degradation because it determines the type of bio-applications for coacervates as a biomaterial. For instance, as an embolic agent, fast degradation would limit these coacervates to indications such as reducing blood supply to highly vascularized lesions before surgical obliteration or control of hemorrhages. Here, the degradation of polyphosphate coacervates was evaluated as a function of initial NaPP $\overline{D_p}$, type of incorporated cations and type of degradation medium by measuring the overall weight loss, decrease in $\overline{D_p}$ and divalent cation and phosphate ion release.

As shown in Chapter 3, polyphosphate solutions with Sr or Ba-chelated chains degrade slower than Ca-chelated chains. Similarly, it was hypothesized here that Sr or Ba-loaded

coacervates will degrade more slowly than Ca-only coacervate. With respect to degradation medium Tris buffer saline (TBS) and fetal bovine serum (FBS) were considered here, the latter to evaluate degradation in conditions approaching an *in vivo* environment that includes phosphatase enzymes. Faster degradation in FBS was anticipated due to the presence of these enzymes. It was also hypothesized that longer chains results in more durable coacervates as they take longer to completely hydrolyze.

Degradation aside, understanding physical properties is crucial to determining the applicability of coacervates as a biomaterial. Little is known about physical properties of these materials; only very short chain (D_p~25) Ca and Mg polyphosphate coacervates have been evaluated using a viscometer, in which it is claimed Newtonian flow properties dominated [78]. Mechanically speaking, a material can be classified as either an elastic solid, a viscous liquid or viscoelastic. Figure 4.1a shows a static test where a constant shear stress (τ) is applied. If a material behaves as an elastic solid, its shape changes the instant a force is applied, reaching a constant strain before returning back to its original shape the moment this force is removed. Figure 4.1b shows the shear strain (γ) curve for such an ideal elastic material in response to this force that is in phase with τ.

In contrast, if a material behaves as a viscous liquid its strain curve would be similar to Figure 4.1c, where the increase in strain is gradual and linear for a Newtonian liquid. In these materials there is no recovery in strain after the force is removed, and τ and γ are 90° out of phase.

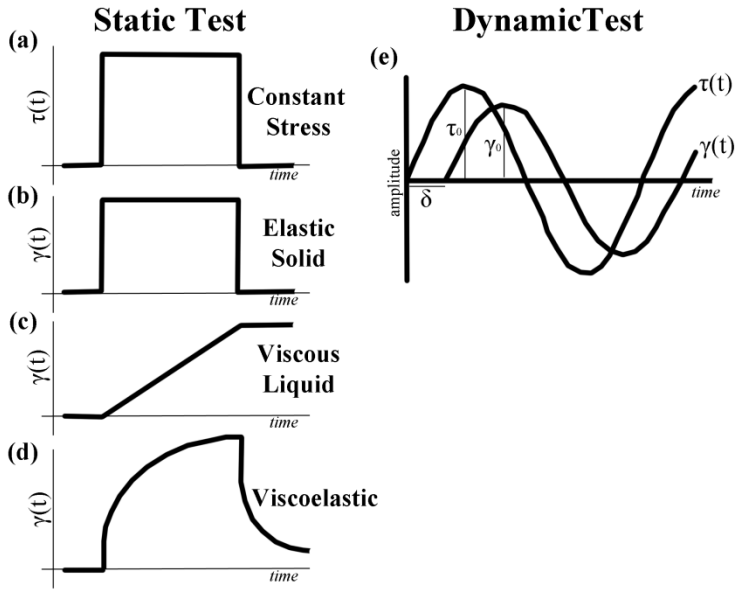

Figure 4.1 (a) Constant shear stress; Shear strain in (b) Elastic solid; (c) Viscous liquid; and (d) Viscoelastic material; (e) Dynamic test and stress-strain curves for a viscoelastic material.

Viscoelastic materials are a third class of materials exhibiting a more complicated strain curve, as shown in Figure 4.1d. Viscoelastic materials exhibit both elastic and viscous behavior, responding to a force with a delay that is not as significant as that of a completely viscous material. In order to describe these viscoelastic properties, elastic (storage) (*G'*) and viscous (loss) (*G"*) modules are defined. Determining these two modules require a rheometer and a dynamic test where a sinusoidal stress is applied to a material; the delay in response, known as the phase angle (δ), is measured as shown in Figure 4.1e. δ is related to the viscous and elastic modules according to the following equations:

$$G' = \frac{\tau_0}{\gamma_0}\cos(\delta) \qquad \text{Equation 4.1}$$

$$G'' = \frac{\tau_0}{\gamma_0}\sin(\delta) \qquad \text{Equation 4.2}$$

, where τ_0 and γ_0 are the amplitudes of the shear stress and strain, respectively. The *G'* and *G"* values are representative of the type of the material; in a liquid $G' << G''$, while in a solid $G' >> G''$. Using this rheology approach, the viscoelastic property of these

coacervates will be evaluated as a function of the type of divalent cation and the starting NaPP $\overline{D_p}$. From these rheology studies a greater understanding of the structural nature of these coacervates, including the presence or absence of cross-linking between chains, is anticipated.

4.3 Materials & Method

4.3.1 Starting Materials

All starting materials including NaPPs were freshly produced and characterized as described in section 3.3.1 of Chapter 3.

4.3.2 Degradation of polyphosphate coacervates

A cumulative type of degradation study was performed whereby, every 24 hr, almost all of the degradation medium was withdrawn and replenished with fresh medium. This type of degradation study minimizes the precipitation of degradation byproducts into the media. At selected time intervals, a sample was sacrificed to measure its weight loss, composition by ICP and $\overline{D_p}$ by NMR. The amount of released cations and phosphates was also determined.

NaPPs with $\overline{D_p}$ of 0.6±0.1 E+03 and 8.5±0.6 E+03 as determined by liquid ^{31}P-NMR and viscosity were used, representing short and long chain NaPPs, respectively. Here, 3.5 and 3.2 g of short and long chain NaPPs were dissolved in 35 and 32 mL of deionized water respectively, then enough[1] 1 M $CaCl_2$ solution added to reach a theoretical Ca/P molar

[1] For each NaPP batch, the exact mole of phosphorus per gram of NaPP is known based on ICP elemental analysis. Calculations were carried out for each individual batch of NaPP to determine the amount of 1 M Ca (or other cations) required to reach a specific theoretical divalent cation to phosphorus molar ratio.

ratio of 0.5 and volume brought up to 300 mL. In addition, two short chain sample groups were first preloaded to 0.15 Ba/P or Sr/P molar ratios (no coacervate forms at 0.15), and then enough Ca was added to reach the theoretical total divalent cation to phosphorus molar ratio of 0.5. A pure Sr-polyphosphate or Ba-polyphosphate coacervate was not tested because addition of Sr or Ba at Me^{II}/P molar ratios higher than 0.15 prevents coacervate formation, resulting instead in precipitates that flocculate rather than aggregate. Therefore, Sr or Ba was only added up to a 0.15 molar ratio, with enough calcium subsequently added for coacervate formation.All solutions were mixed for 5 min, and the resulting coacervate collected and squeezed to remove excess water. Each coacervate was divided into 48 pieces, each weighing 100±2 mg, and placed inside individual Eppendorf® tubes. To these tubes (a total of 6×8 (48) tubes for each sample group) 1 mL of 0.1 M TBS (pH 7.4 at 37°C) was added and the volume maintained at 37°C on a horizontal shaker at 100 rpm. At 24 hr intervals, 0.9 mL of the solution was collected and replaced by a fresh solution. The cumulative amount of release elements in these collected solutions was determined by ICP after correcting for 0.1 mL of the media that remained. At each time point (i.e, 0, 3, 12, 24, 48, 168, 336 and 648 hr) 6 tubes containing the coacervates were collected and washed with water twice. Three of these washed samples were dissolved by EDTA and analyzed for composition by ICP and for $\overline{D_p}$ by liquid ^{31}P-NMR using Equation 3.1. The remaining 3 coacervates were freeze-dried for at least 24 hr at -43°C in pressures lower than 133×10^{-3} mBar to remove water and then weighed to determine weight loss over time. A second long chain sample group was maintained in FBS to determine the effect of degradation medium, yielding 5 sample groups overall as shown in Table 4.1. Sodium azide was added to the FBS medium at

0.1% g/ml in order to prevent any bacterial growth. A two-tailed student t-test was used to determine statistically significant differences (*p-values*<0.05) between groups.

Table 4.1 Theoretical and experimental (*n*=3) composition of different degradation sample groups.

Group	NaPP used	Theoretical molar ratio			Degradation medium	Experimental molar ratio			Water content (weight %)
		Ca/P	Sr/P	Ba/P		Ca/P	Sr/P	Ba/P	
1	Short	0.50	N/A	N/A	TBS	0.41±0.008	N/A	N/A	39.29±0.35
2	Short	0.35	0.15	N/A	TBS	0.28±0.003	0.12±0.001	N/A	38.61±0.80
3	Short	0.35	N/A	0.15	TBS	0.25±0.003	N/A	0.13±0.002	33.11±0.25
4	Long	0.50	N/A	N/A	TBS	0.40±0.007	N/A	N/A	40.04±0.39
5	Long	0.50	N/A	N/A	FBS	0.37±0.014	N/A	N/A	41.09±0.77

4.3.3 Rheology of polyphosphate coacervates

2.3 g of NaPP with $\overline{D_p}$ between 27 and 6E+03 (determined by liquid ^{31}P-NMR and viscosity) were dissolved in 230 mL of deionized water; enough 1 M $CaCl_2$ solution was then added to reach a theoretical Ca/P molar ratio of 0.5. To evaluate the effect of different divalent cations, NaPP solutions were first preloaded to 0.15 Ba/P or Sr/P molar ratios (no coacervate forms at 0.15), and then enough 1 M $CaCl_2$ solution was added to reach the total theoretical divalent cation to phosphorus molar ratio of 0.5. All solutions were mixed for 5 min, and the resulting coacervates collected and squeezed to remove excess water.

Rheological measurements of the coacervates were performed on a controlled stress Bohlin rheometer with a 40/4 cone-plate configuration. Coacervates were loaded onto the plate to allow the stresses to relax and the samples to reach thermal equilibrium. Dynamic tests at 20°C were performed to measure storage modulus (G'), loss modulus (G'') and phase angle (δ) with frequency (ω) and stress (τ) swept between 0.1-40 rad/s and 0.1-590 Pa, respectively, depending on the sample. Static tests with stress and temperature swept between 0.1-590 Pa and 10-30°C, respectively, were performed to determine viscosity (η). Temperature was controlled by a circulating water bath connected to the plate.

Accuracy error in viscosity values is 2% based on N30000 standard oil (CANNON Instrument Company®) measurements.

Following rheology measurements, a portion of the coacervate was dissolved by EDTA and its $\overline{D_p}$ and experimental composition assessed by NMR and ICP, respectively. The remaining coacervate was weighed, freeze-dried for at least 24 hr at -43°C in pressures lower than 133×10^{-3} mBar and subsequently re-weighed to determine the % water content of the coacervate.

4.4 Results

4.4.1 Degradation results

Table 4.1 shows the composition of the coacervates. Experimental molar ratio values were consistently lower than theoretical values. As explained in Chapter 3, not all divalent cations are incorporated into the coacervates and under the conditions used here (i.e. NaPP concentration), coacervation occurs at a divalent cation to phosphorus molar ratio of roughly 0.40, with excess divalent cations used in the coacervate preparation remaining in solution. Table 4.1 also shows the weight percentage of water inside the coacervates. A significant percentage of sample weight was water, which was significantly lower in Ba-loaded samples compared to all other samples.

Figure 4.2 shows images of all coacervate sample groups over time. At t=0 all samples were cohesive, gel-like materials; sample group 1 was more transparent than sample groups 2 and 3, which contained Sr and Ba, respectively.

Visually, degradation in all sample groups was very similar. A white opaque layer formed on the surface of the coacervate that was in contact of degradation medium, and over time this white layer penetrates deeper into the coacervate, eventually transforming all of the coacervate into a white opaque powder-like material that lacked any cohesive property and could be easily broken up.

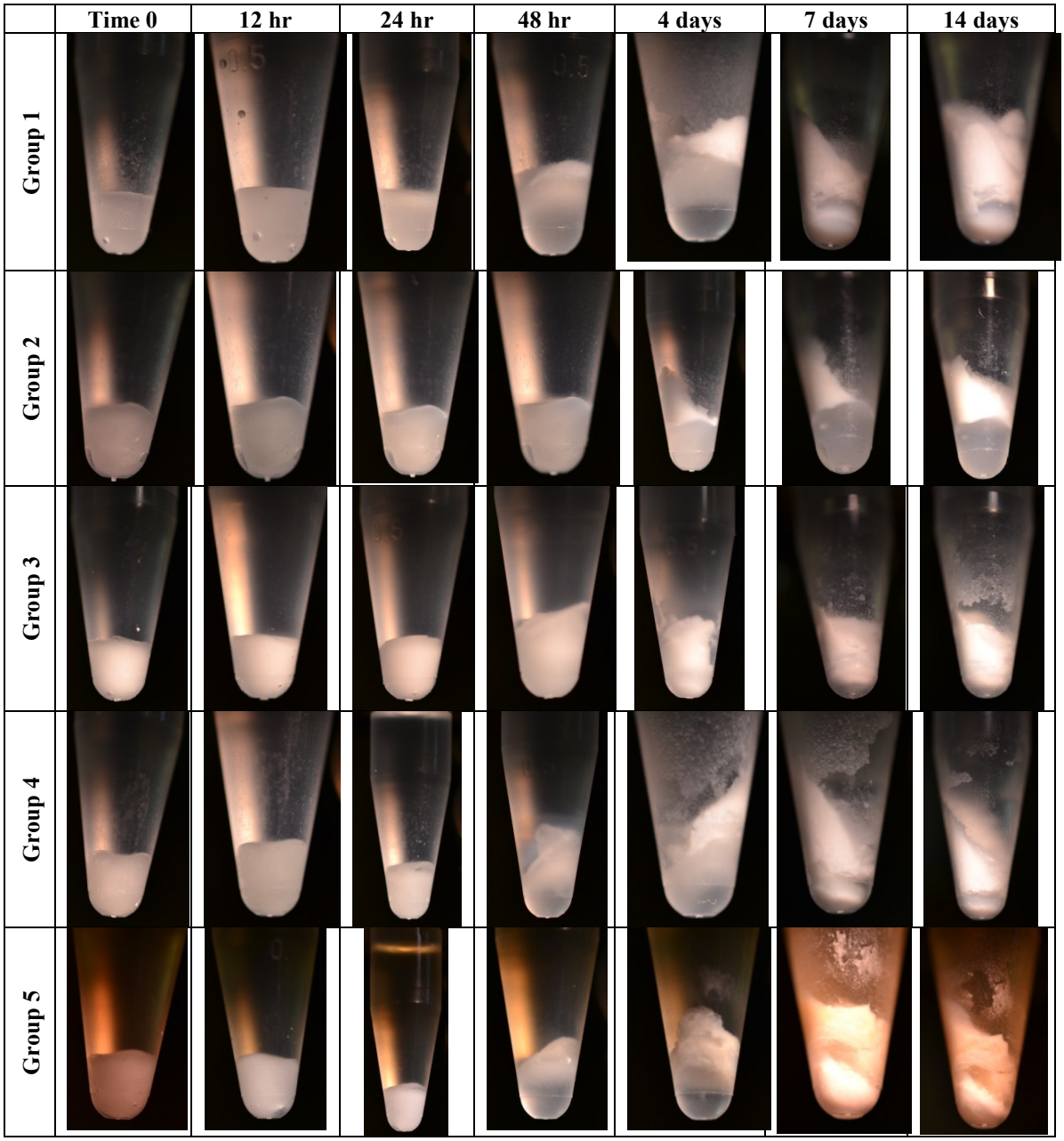

Figure 4.2 Images of the coacervates in different sample groups over a period of two weeks.

Figure 4.3 shows the weight loss of the coacervates over time. Significant weight loss was observed for all sample groups between 48 hr and 1 week, followed by a reduced rate of weight loss. Ca-only coacervates (Group 1) lost significantly more weight than 0.15 Sr or Ba loaded coacervates (Groups 2 and 3) at 7, 14 and 27 days. Although the Sr-loaded samples seemed to be more stable than corresponding Ba-loaded samples, statistically no significant differences were noted except at 48 hr.

There was also no significant weight loss difference in short vs. long chain samples (Group 1 vs. Group 4) except at 27 days. At 7, 14 and 27 days long chain samples maintained in FBS (Group 5) lost significantly less weight compared to those kept in TBS (Group 4), possibly the result of serum components accumulating inside coacervates over time or proteins binding to polyphosphates delaying degradation/dissolution.

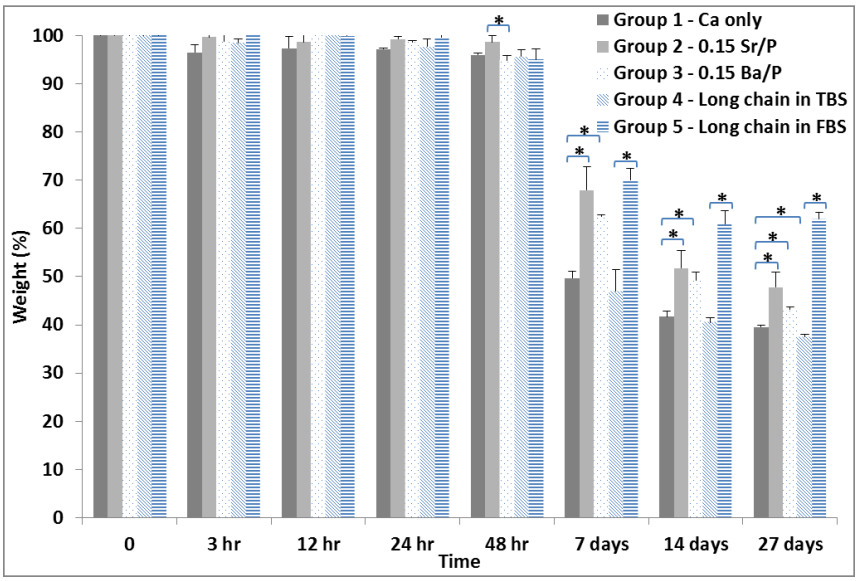

Figure 4.3 Dry weight loss of the coacervates in different sample groups over a period of 27 days (two tailed student t-test: * stand for p-value<0.05) (Bars show STD; n=3).

Figures 4.4a and b show the mole percentage of Ca, Sr, Ba and P remaining inside the coacervates over time. In accordance with weight loss results, the greatest loss of ions from the sample groups occurred between 48 hr and 1 week. The percentage of

phosphorus being lost was higher than divalent cations, indicating that higher divalent cation to phosphorus molar ratios were present in the remaining coacervates.

With respect to availability, Ba and Sr remained in the coacervates significantly more than Ca. Also the percentage of Ca and P remaining in the 0.15 Sr/P or Ba/P samples was significantly higher than for Ca-only coacervate specifically after one week. Beyond one week, the percentage of Ca and P remaining in the Sr-loaded samples was significantly higher than for corresponding Ba-loaded samples.

There was no significant difference in the percentage of Ca and P remaining in long vs. short chain samples except for the Ca at 27 days. While the percentage of Ca remaining in the long chain coacervate groups did not vary with media, the percentage of P remaining in the FBS sample group (Group 5) was significantly higher at 14 and 27 days, again presumably caused by incorporation of the serum components.

In addition to the above studies on the mole percentage of elements that remained inside the coacervates, the cumulative amount of elements released into the degradation media over the period of 27 days was also determined (Figure 4.5). The data from both of these studies corresponded perfectly, confirming the accuracy of our elemental measurements (i.e., the sum of the *moles of elements inside a coacervate at a specific time point* and the *cumulative moles of elements released into the media up to that time point* was roughly constant throughout the degradation study). Figure 4.5 shows the cumulative milli-moles of Ca, Sr, Ba and P released from the samples. The slow rate of release of Sr and Ba can clearly be seen in Figure 4.5a, and in agreement with the studies reported above, the

amount of P and Ca being released into solution was lowest for the Sr-loaded samples (Group 2).

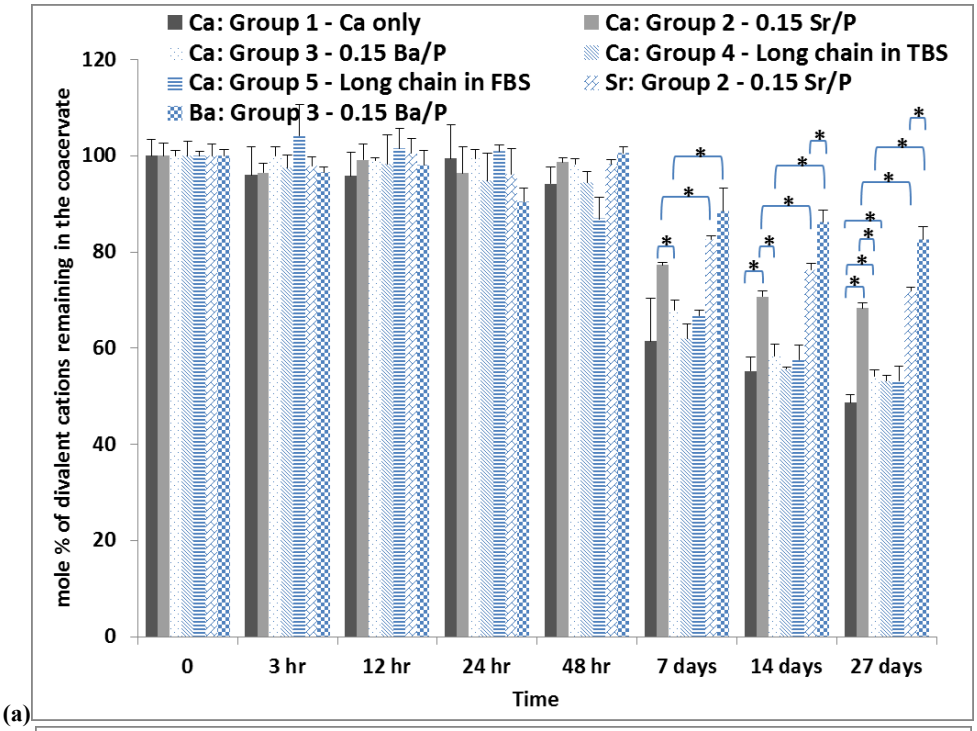

(a)

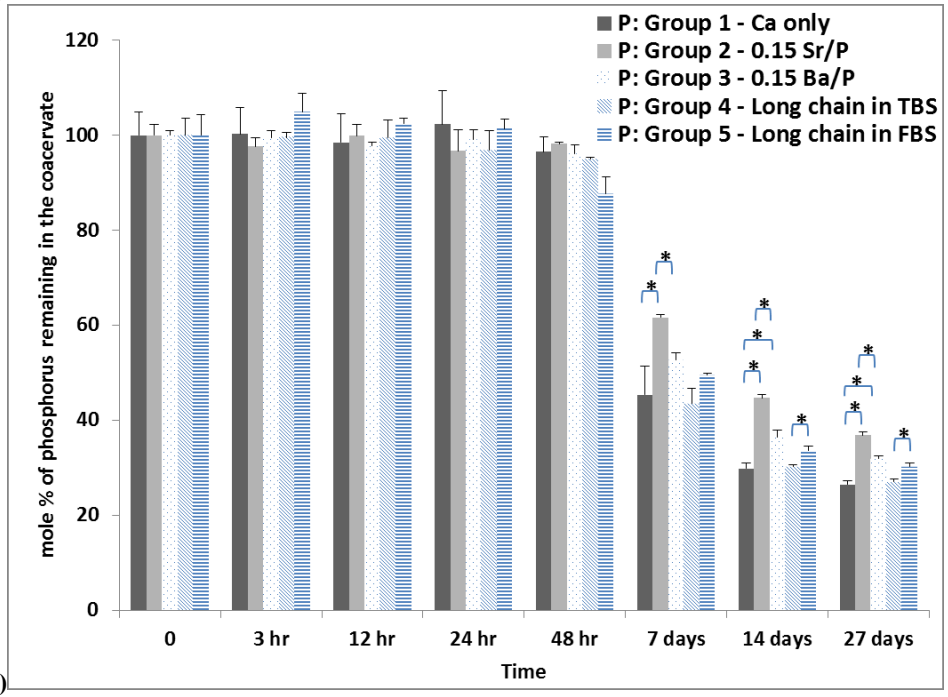

(b)

Figure 4.4 mole percentage of (a) Ca, Sr and Ba and (b) P remained inside the coacervates in different sample groups over a period of 27 days (two tailed student t-test: * stand for p-value<0.05) (Bars show STD; n=3).

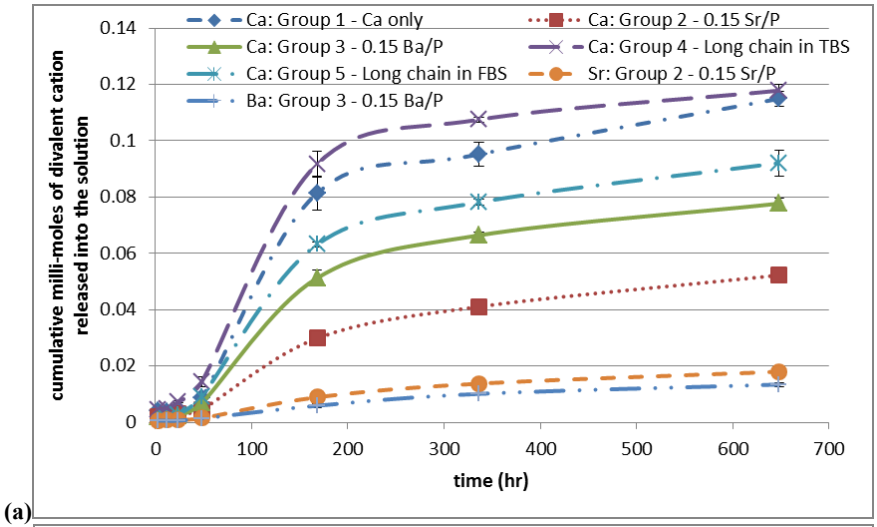

(a)

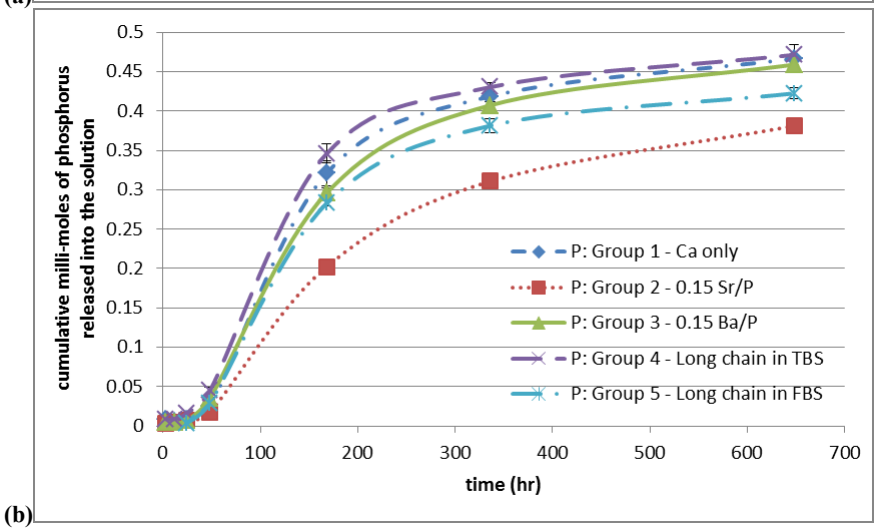

(b)

Figure 4.5 Cumulative milli-moles of (a) Ca, Sr and Ba and (b) P released into degradation media from the coacervates in different sample groups over the period of 27 days (Bars show STD; n=3).

Figure 4.6 shows the phosphorus NMR spectra of the remaining coacervates during the degradation period. In all samples it is clear that the number of $Q^{2\text{-middle}}$ phosphates (phosphates in the middle of the chains) decreases at a dramatic rate and eventually, after 27 days, they are almost all gone. The clean sharp $Q^{2\text{-middle}}$ peak at time zero also changes over time into a blend of peaks, implying formation of a mixture of short chains and rings (e.g. phosphate groups in the middle of tripolyphosphate, tetrapolyphosphate and phosphate rings).

Correspondingly, the small Q^1 peak representing phosphate groups at the end of the chains increases over time implying chain scission. The main byproduct of sample degradation at the end of the study period was pyrophosphate having two Q^1 phosphate groups. The Q^1 peak for pyrophosphates is specifically identified in Figure 4.6, as this peak is clearly separated from other Q^1 peaks representing phosphate groups at the end of longer chains. The other obvious byproduct of degradation is orthophosphate, Q^0.

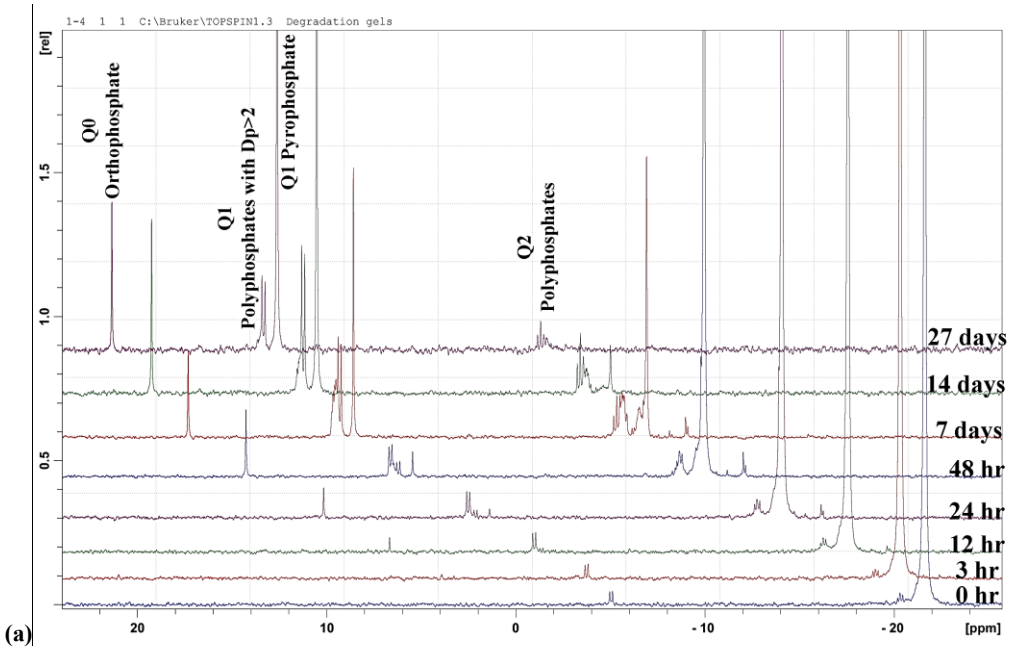

(a)

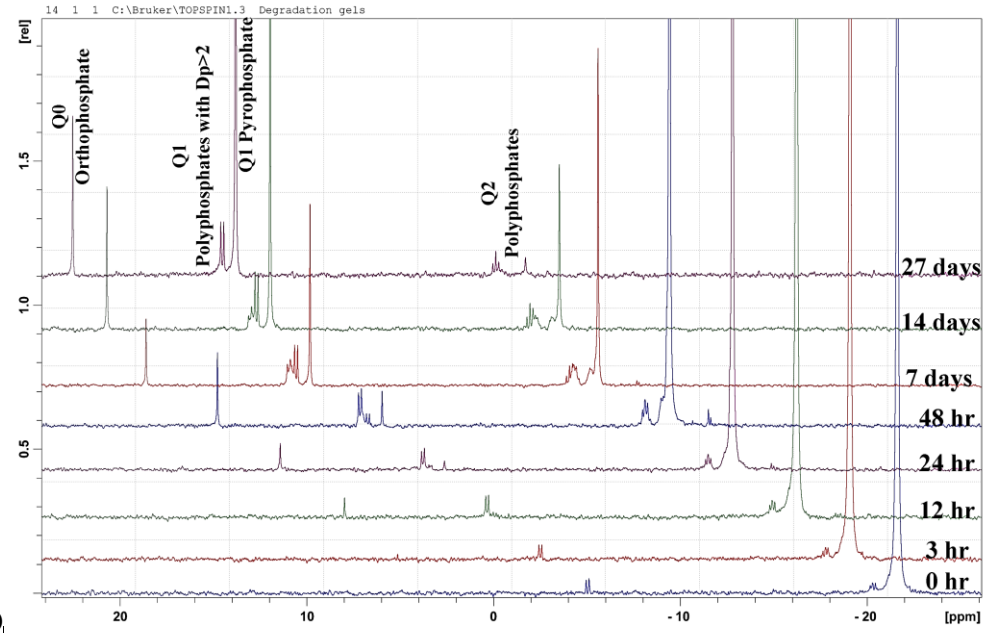

(b)

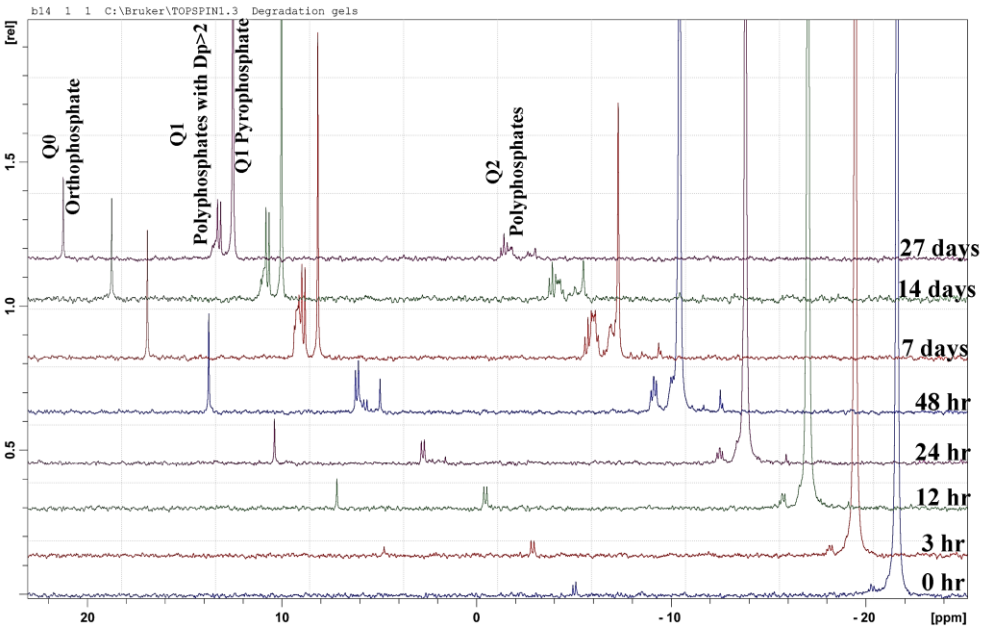
b14 1 1 C:\Bruker\TOPSPIN1.3 Degradation gels
[rel]
1.5
1.0
0.5
Q0
Orthophosphate
Q1
Polyphosphates with Dp>2
Q1 Pyrophosphate
Q2
Polyphosphates
27 days
14 days
7 days
48 hr
24 hr
12 hr
3 hr
0 hr
20
10
0
- 10
- 20
[ppm]

(c)

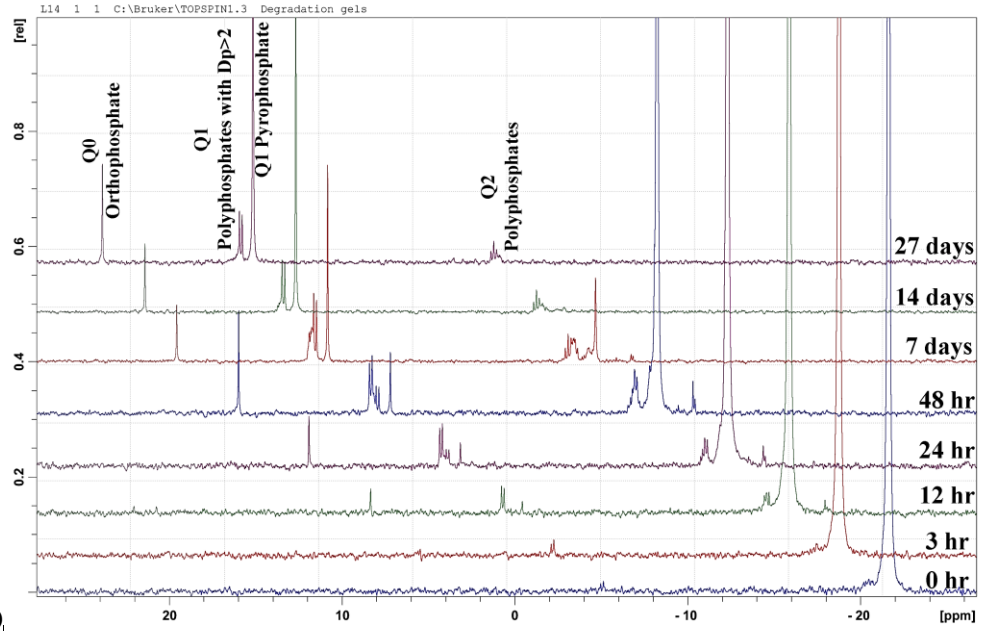
L14 1 1 C:\Bruker\TOPSPIN1.3 Degradation gels
[rel]
0.8
0.6
0.4
0.2
Q0
Orthophosphate
Q1
Polyphosphates with Dp>2
Q1 Pyrophosphate
Q2
Polyphosphates
27 days
14 days
7 days
48 hr
24 hr
12 hr
3 hr
0 hr
20
10
0
- 10
- 20
[ppm]

(d)

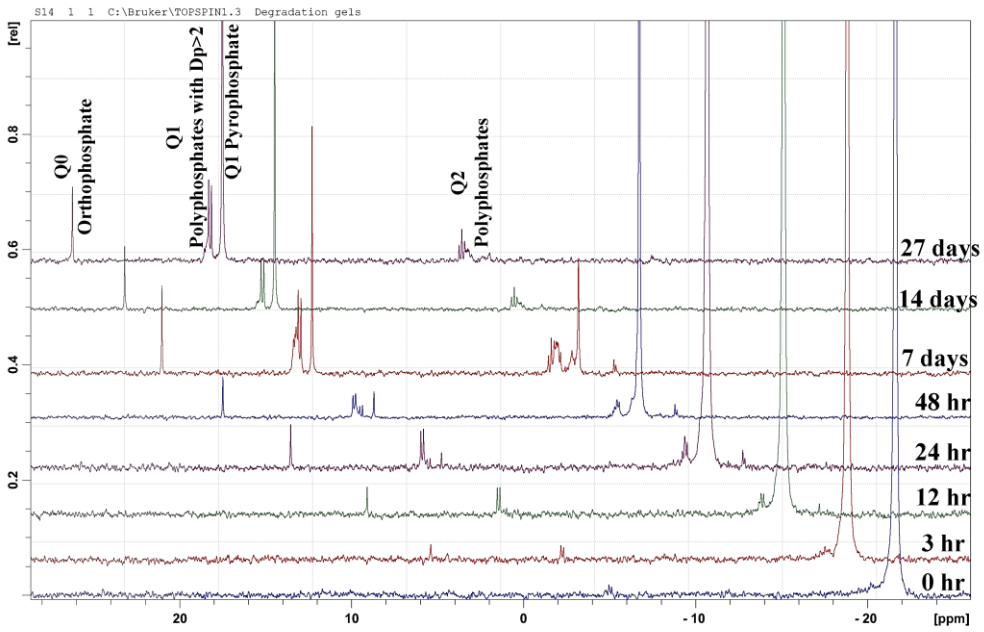

(e)

Figure 4.6 Liquid ^{31}P-NMR spectra of (a) Group 1 - Ca only; (b) Group 2 - 0.15 Sr/P; (c) Group 3 – 0.15 Ba/P; (d) Group 4 – long chain in TBS; (e) Group 5 – long chain in FBS, at different time points throughout the degradation. With the exception of the lowest spectra, all other spectra are shifted downfield for clarity.

The relative areas under the peaks in these NMR spectra were used to determine the fraction of phosphate groups in orthophosphate, pyrophosphates and in rings or chains with $\overline{D_p} > 2$; Figure 4.7 shows the results of these analysis. These plots clearly demonstrate that the polyphosphate chains within the coacervates are transforming into mainly pyrophosphate and then orthophosphate.

$\overline{D_p}$ for the remaining coacervates at the end of the study period was also determined using Equation 3.1 and is shown in Figure 4.8. Independent of the sample group type, chains rapidly shortened and, within a week, the $\overline{D_p}$ of all coacervates dropped to values lower than 10 phosphorus units per chain followed by their transformation to pyrophosphates after 27 days. Although some significant differences in $\overline{D_p}$ were noted at a few time points, overall the decrease in $\overline{D_p}$ was only marginally affected by the study variables.

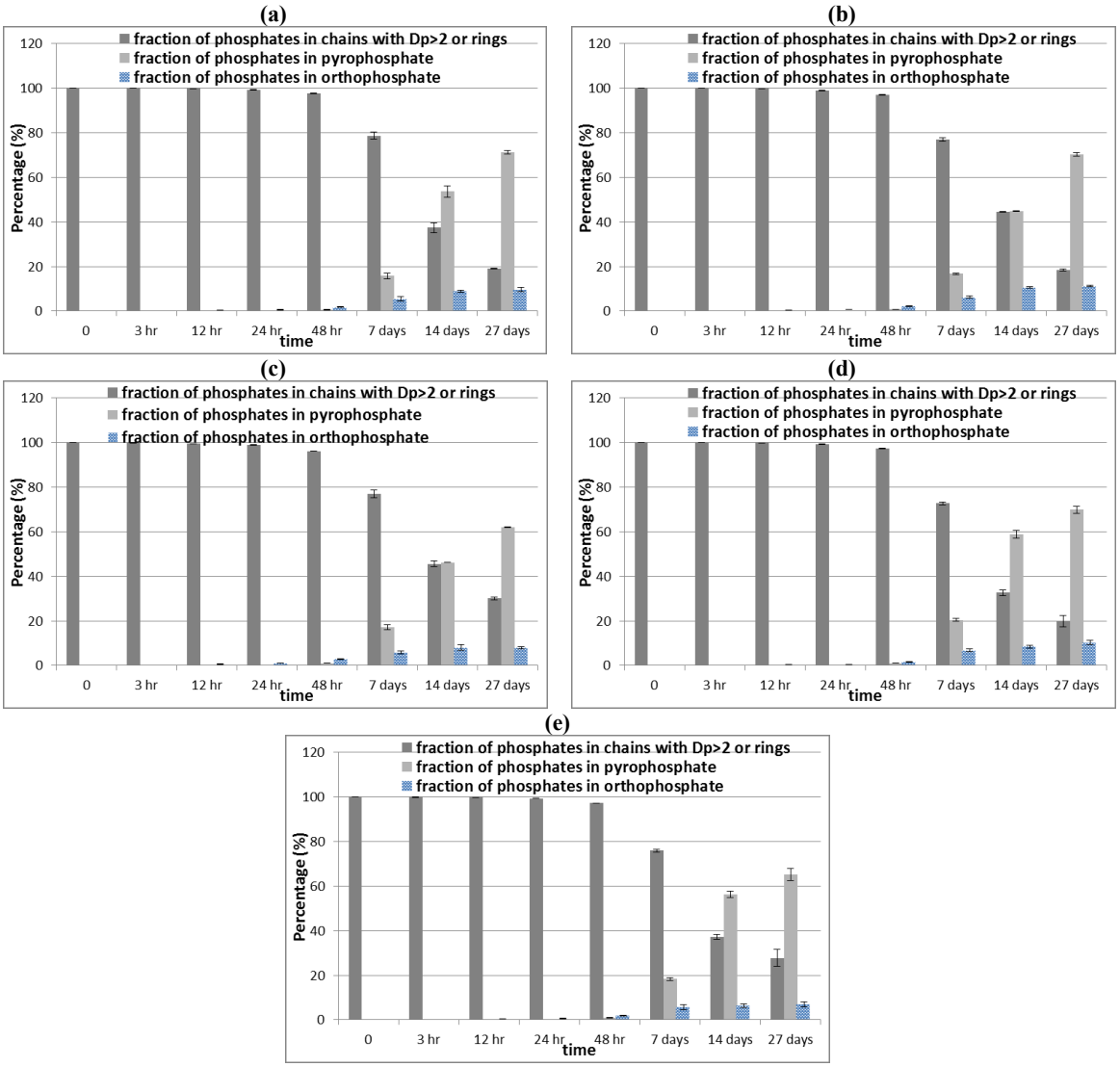

Figure 4.7 Fraction of phosphates in ortho- or pyro-phosphates or in chains with Dp>2 and rings, over the degradation period; (a) Group 1 – Ca only; (b) Group 2 - 0.15 Sr/P; (c) Group 3 – 0.15 Ba/P; (d) Group 4 – long chain in TBS; (e) Group 5 – long chain in FBS. (Bars show STD; n=3).

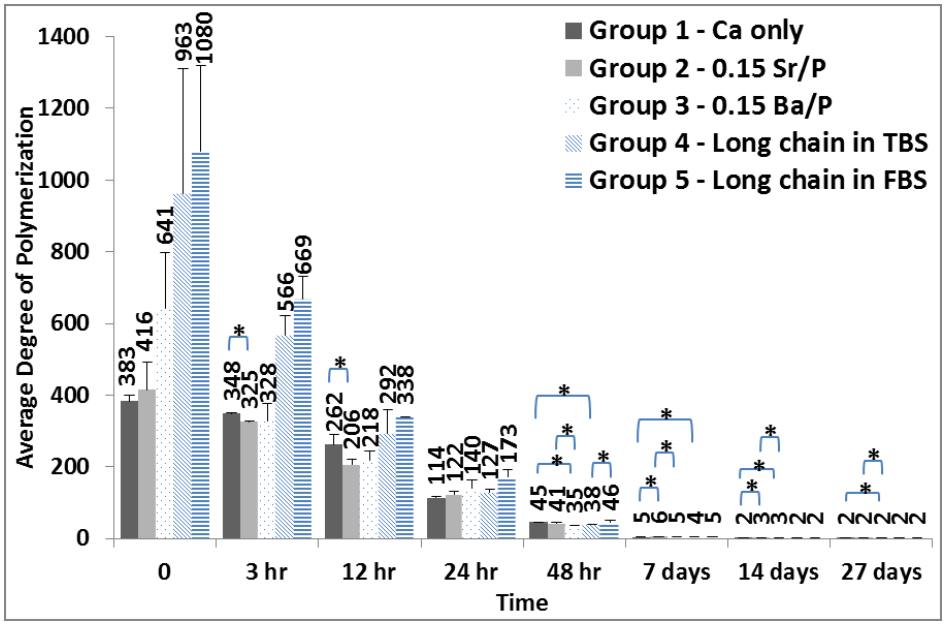

Figure 4.8 $\overline{D_p}$ of coacervates sample groups over the degradation period (two tailed student t-test: * stand for p-value<0.05) (Bars show STD; n=3).

4.4.2 Rheology results

Figure 4.9 shows images of a long chain, Ca-only coacervate along with three shorter chain coacervates (Ca-only, 0.15 Ba/P and 0.15 Sr/P). The long chain sample did not flow under its own weight when suspended; in contrast the other three shorter chain samples exhibited some flow properties. Interestingly, coacervates loaded with Sr experience a significant change in their physical characteristics over time, transforming into a brittle solid within a few hours. Here, rheology measurements were all carried out immediately after coacervate formation.

Table 4.2 shows theoretical and experimental compositions of different coacervates prepared for rheology measurements. Experimental molar ratio values were consistently lower than theoretical values similar to the coacervates prepared for degradation studies. Deviations between the $\overline{D_p}$ of the initial NaPP solution and of the resulting dissolved coacervate were also observed (Table 4.2). Increases observed for the shorter chain

groups is presumably due to the exclusion of shorter phosphate chains during coacervation, while observed decreases in coacervate $\overline{D_p}$, especially for the long-chain group, could be the result of polyphosphate degradation. As shown in Table 4.2, water content inside coacervates used for rheology was slightly lower than those used for degradation, likely due to evaporation during rheology measurements that lasted roughly 1 hr per sample.

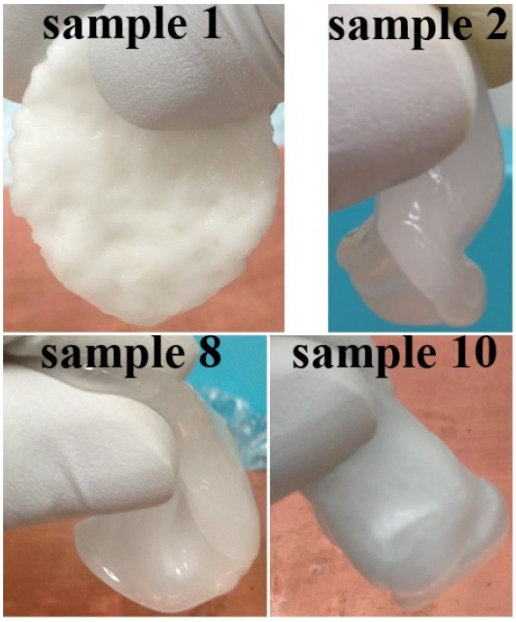

Figure 4.9 Images of polyphosphate coacervate samples (see Table 4.2 for composition of the samples).

For samples listed in Table 4.2, a dynamic test was initially performed where both shear stress (τ) and frequency (ω) were swept over a prescribed range to yield elastic modulus (G') and viscous modulus (G''), which are related to phase angle (δ), complex modulus (G^*) and complex viscosity (η^*) according to the following equations:

$$\tan(\delta) = \frac{G''}{G'} \quad \text{Equation 4.3;} \qquad G^* = \sqrt{G'^2 + G''^2} \quad \text{Equation 4.4;} \qquad \eta^* = \frac{G^*}{\omega} \quad \text{Equation 4.5}$$

Figure 4.10 shows measured *G'* and *G"* values for sample 2 at different τ and ω. Similar graphs were developed for all other samples but are not shown here. It is clear from Figure 4.10 that *G'* and *G"* values at each ω are roughly independent of shear stress, τ. This region is known as the linear viscoelastic region, i.e. the stress or strain region where *G'* and *G"* are constant. In the following studies only results from this region are reported for the samples.

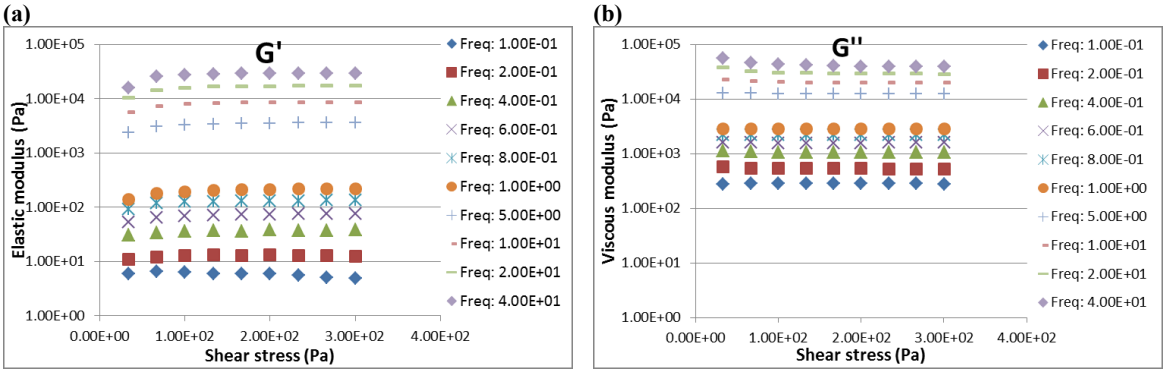

Figure 4.10 Results of dynamic test on sample 2 of table 4.2: Elastic (a) and Viscous (b) modules at different frequency and shear stress values. (Results show the average of three measurements)

The results of dynamic tests are often presented by plotting the *G'*, *G"* and η^* versus the ω, as shown in Figure 4.11. For all samples except sample 1 prepared from polyphosphate with very large $\overline{D_p}$, *G"* has much larger values than *G'*; only in sample 1 is *G'* larger than *G"*. As frequency increases, both *G'* and *G"* values increase in all samples, with *G'* values approaching those of *G"*. Both of these observations are typical viscoelastic behavior for coacervates [172], suggesting that coacervates exhibit more viscous properties at the lower frequency region and more elastic properties at the higher frequency region; at this higher frequency polymers inside the coacervate do not have the time to slip and to disengage from physical entanglements that result in elasticity.

Table 4.2 Composition of the coacervate samples and their viscoelastic properties.

Sample	Theoretical molar ratio			Experimental molar ratio			Original NaPP D_p	Dissolved coacervate D_p	Water content (weight %)	η at 10°C (Pa.s)	η at 20°C (Pa.s)	η at 30°C (Pa.s)	E_{af} (kcal /mol)	G' (Pa)[a]	G'' (Pa)[a]	δ (°)[a]
	Ca/P	Sr/P	Ba/P	Ca/P	Sr/P	Ba/P										
1	0.5	N/A	N/A	0.39± 0.005	N/A	N/A	5990[b]	1250	36.67 ±1.06	N/A	N/A	N/A	N/A	1.70E+04 ± 572	1.09E+04 ±818	32.7 ±1.1
2	0.5	N/A	N/A	0.39± 0.007	N/A	N/A	444	435	37.18 ±0.84	906.6 ±17.7	402.0 ±5.1	234.5 ±1.3	11.6	2.08E+02 ±3	2.87E+03 ±66	85.8 ±0.1
3	0.5	N/A	N/A	0.39± 0.006	N/A	N/A	320	319	34.63 ±2.08	545.1 ±18.3	255.5 ±4.6	143.8 ±1.2	11.3	4.15E+01 ±3	1.74E+03 ±93	88.6 ±0.1
4	0.5	N/A	N/A	0.41± 0.022	N/A	N/A	216	274	34.59 ±1.03	349.7 ±6.7	161.0 ±5.9	112.2 ±2.8	9.7	7.69E+00 ±0.6	1.02E+03 ±43	89.6 ±0.0
5	0.5	N/A	N/A	0.38± 0.003	N/A	N/A	170	211	37.79 ±3.07	N/A	94.5 ±1.3	N/A	N/A	4.16E+00 ±1.1	5.74E+02 ±22	89.6 ±0.1
6	0.5	N/A	N/A	0.39± 0.011	N/A	N/A	100	118	33.49 ±4.90	63.0 ±1.8	34.0 ±0.5	21.5 ±0.3	9.1	4.15E+00 ±0.6	2.10E+02 ±9	88.9 ±0.2
7	0.5	N/A	N/A	0.38± 0.004	N/A	N/A	27	38	37.94 ±0.95	23.5 ±0.3	11.7 ±0.1	7.6 ±0.4	9.6	1.38E+00 ±0.4	7.63E+01 ±4	89.0 ±0.3
8	0.35	0.15	N/A	0.26± 0.005	0.11± 0.002	N/A	444	392	35.78 ±1.33	3915.8 ±274.3	1590.8 ±224.9	N/A	14.9	N/A	N/A	N/A
9	0.35	0.15	N/A	0.26± 0.003	0.12 ±0.001	N/A	170	196	34.46 ±1.40	N/A	493.1 ±48.6	N/A	N/A	1.15E+03 ±971	4.68E+03 ±1539	78.0 ±6.6
10	0.35	N/A	0.15	0.27± 0.005	N/A	0.11± 0.001	444	488	30.56 ±1.18	29641.7 ±1847.6[c]	14222 ±62	7211.9 ±556	15.8	3.14E+04 ±1518	4.21E+04 ±1918	53.3 ±0.5
11	0.35	N/A	0.15	0.27± 0.000	N/A	0.12± 0.002	170	222	29.41 ±0.47	N/A	9768.2 ±96.1	N/A	N/A	1.32E+04 ±607	5.99E+04 ±3423	77.5 ±0.3

[a] G', G'' and δ are reported for the frequency of 1rad/s and in the stress range that materials were within their linear viscoelastic region.
[b] D_p determined by viscosity measurements.
[c] Viscosity for this specific sample is measured at 15°C.
All measurements were carried out at least in triplicate except D_p analysis. Numbers show average±STD.

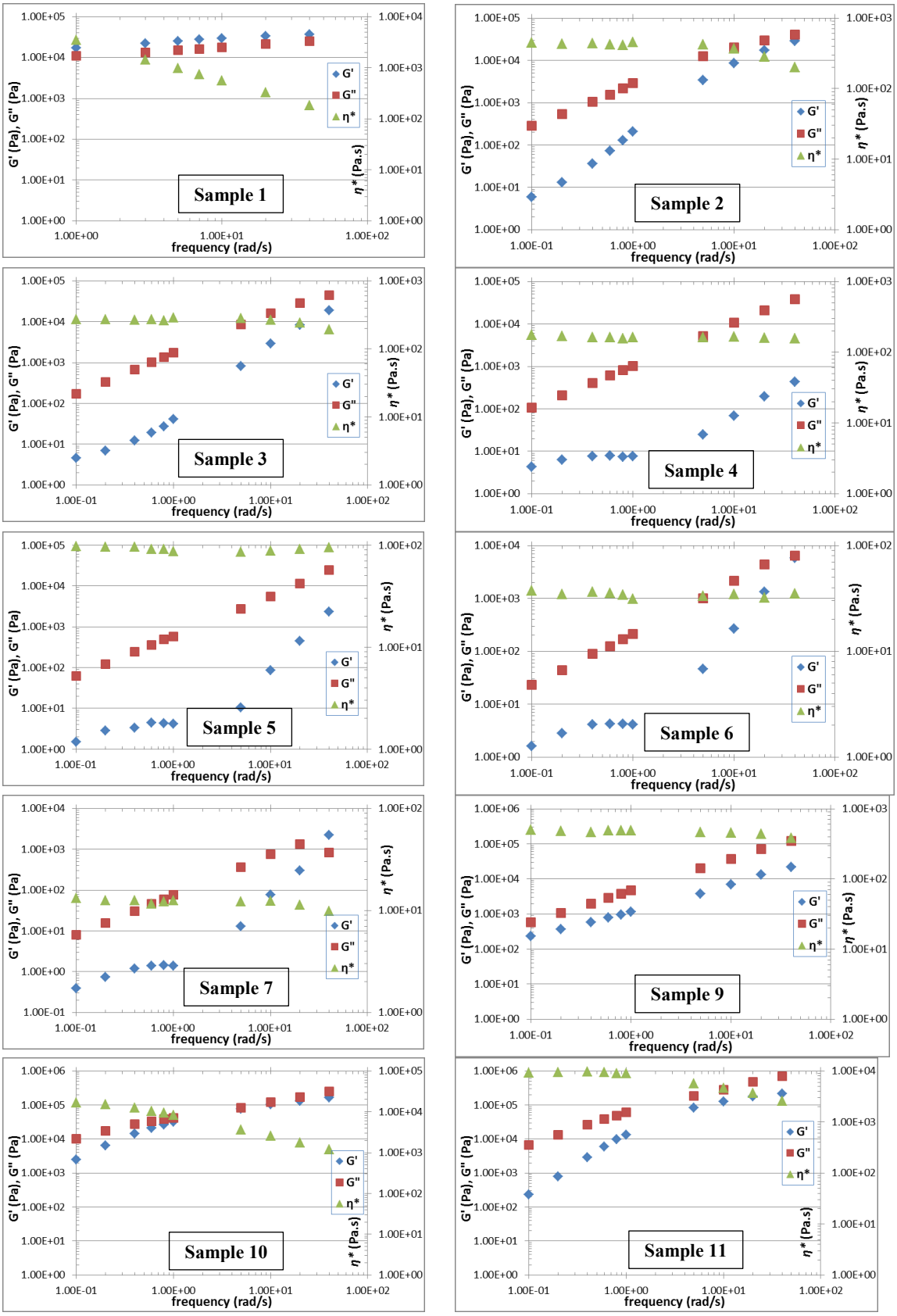

Figure 4.11 *G'*, *G"* and *η vs. *ω* for samples described in Table 4.2 (except sample 8).**

Sample 1 is the exception, as *G'* and *G"* do not increase to the same extent as seen with other samples. Figure 4.11 also shows that η^* remains roughly constant as frequency increases for all samples except sample 1 and barium-loaded sample 10. Constant η^* implies the liquid nature of these samples.

Table 4.2 summarizes these dynamic test results for all samples. Phase angle (δ), *G'* and *G"* values reported in this table are for ω = 1 rad/s. For samples 2-7, both *G'* and *G"* increased as $\overline{D_p}$ becomes larger, but δ values are all very close to 90°. The addition of Sr or Ba decreased δ but, even for sample 10, this value remains above 45°, suggesting that viscous characteristics still dominant over elastic characteristics in these samples. In contrast, in sample 1 prepared using NaPP with very large $\overline{D_p}$ without any Ba or Sr, δ was 32.7°; here, elastic behaviors dominate.

Following dynamic tests, static tests were performed on all samples except sample one, which lacked liquid qualities, in order to determine viscosity (η) values. Figure 4.12 shows an example of a shear stress - shear rate plot for only 3 of the samples. The trend line fitted to the data is perfectly linear, suggesting coacervates are Newtonian solutions with negligible shear-thinning at the shear rate range evaluated in this study. The slope of the shear stress – shear rate plot is equal to η which is related to η^* from dynamic test according to the following equation:

$$\eta = \lim_{\omega \to 0} \eta^* \quad \text{Equation 4.6}$$

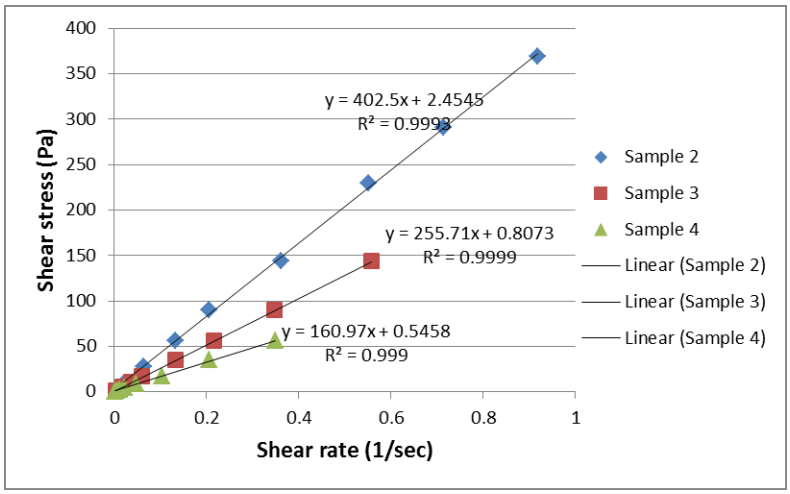

Figure 4.12 Results of static test for samples 2, 3 and 4 of table 4.2 at 20°C.

Table 4.2 shows the η values for all samples. The shortest chain, Ca-only coacervate (sample 7) had the lowest viscosity of 11.7 Pa.s at 20°C, which is still roughly more than 10,000 times that of water. The viscosity of Ca-only coacervates was found to increase for larger $\overline{D_p}$, reaching 402.5 Pa.s at 20°C for sample 2. Figure 4.13 shows the relationship between the viscosities of Ca-only coacervates and at three temperatures. Accordingly, the viscosity in Ca-only coacervates is related to the $\overline{D_p}$ based on the following equation:

$$\eta = 0.043 \times \overline{D_p}^{1.47} \quad \text{(at 20°C)} \quad \text{Equation 4.7}$$

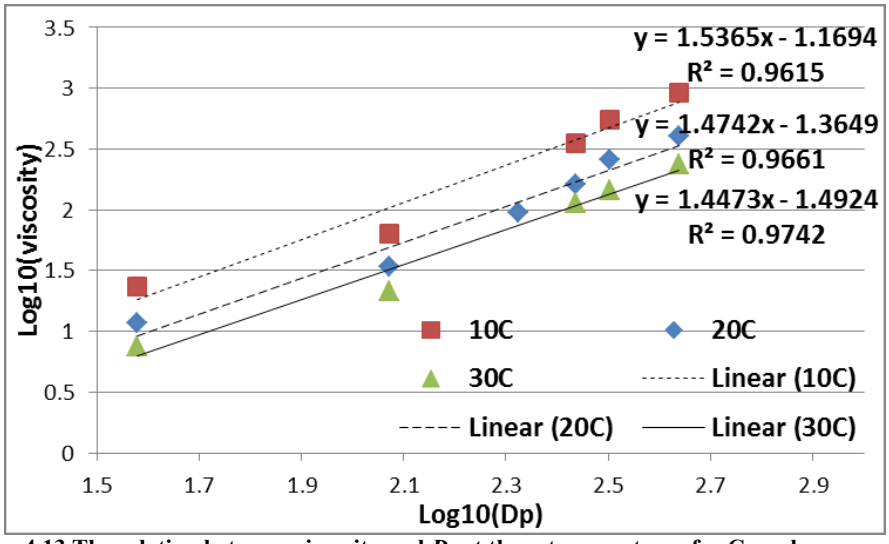

Figure 4.13 The relation between viscosity and D_p at three temperatures for Ca-only coacervates.

η was determined at 10, 20 and 30°C for samples and is shown in Table 4.2. As expected, η of the coacervates decreases as temperature increases. η values at these temperatures were used to determine the activation energy of flow (E_{af}) for the coacervates. E_{af} is the amount of energy required for the viscous flow of one mole of a material and is determined using the following equation [173]:

$$\eta = A_p \exp(\frac{E_{af}}{RT}) \qquad \text{Equation 4.8}$$

where A_p is the pre-exponential factor, T is temperature in Kelvin and R is the ideal gas constant (1.987×10^{-3} kcal/K.mol).

The E_{af} is reported for the samples in Table 4.2. E_{af} in samples 2-7 increased as $\overline{D_p}$ increased, with the exception of sample 7 – the only sample prepared using unfractioned NaPP. In polymeric melts, E_{af} values have also been reported to increase with chain length [174].

Addition of Sr or Ba increased coacervate viscosity and E_{af} profoundly, as shown in Table 4.2 for samples 2 vs. 8 and 10, or 5 vs. 9 and 11. Ba increased the viscosity far

more than Sr, with sample 10 having the highest viscosity (14E+03 Pa.s) at 20°C. In polymeric melts, the E_{af} value increases as the size of side groups increases [173].

4.5 Discussion

With respect to degradation, all coacervates were found to be relatively stable for the first 48 hr, after which rapid weight loss and ion release were observed. This rapid weight loss was concurrent with a significant decrease in polyphosphate $\overline{D_p}$ as exhibited by NMR measurements. Presumably, chains within these coacervates are continuously hydrolyzed but do not dissolve away until $\overline{D_p}$ becomes smaller than 40, which took 2 days. At this point, shorter chains lose their ability to remain as an aggregate within the coacervate such that they are easily released into solution, leading to a burst phase in degradation. Subsequently, degradation enters a lagging phase where a mixture of even shorter chains – mainly pyrophosphates – with their divalent cations are slowly dissolved into the medium, presumably because they have a higher M^{2+}/P mole ratio than the original coacervate; M^{2+}/P mole ratio is increasing over time because phosphorus is being released faster. After a week, polyphosphate chains are so short that they cannot hold on together and presumably this cause coacervates to lose their cohesive gel-like appearance as they are transformed into a powder-like material that easily disintegrates. For biomaterials applications, one would need to consider whether this powder debris could trigger a significant local inflammatory response *in vivo*.

It is generally accepted that the dissolution of polyphosphate glasses are congruent [5, 76, 77, 110, 111], i.e. the dissolved products in the solution have identical composition (same molar ratios) with that of the bulk glass at all times. However, we observed that the

release rate of phosphate from polyphosphate coacervate was faster than divalent cations, implying that degradation of polyphosphate coacervates is not congruent. This incongruent degradation over time results in a more stable coacervate with higher divalent cation/P molar ratio, as reflected in a lagging phase of degradation observed.

In contrast to Ca and P, most of the Sr and Ba remained within the coacervates, which is likely related to the lower dissolution of Sr and Ba phosphate salts compared to Ca. This observation would mitigate the risk of incorporating these cations, especially Ba, into polyphosphate coacervates, since rapid release of these cations *in vivo* could lead to systematic toxicity.

The only previous degradation study on polyphosphate coacervates was carried out for calcium and magnesium coacervates by Umegaki et al. [103]. Using paper chromatography and viscosity, they showed that calcium polyphosphate coacervates degraded into pyro and orthophosphates within 10 days, in agreement with our results. Additionally, the ^{31}P-NMR spectra of degraded coacervates in our study resembles those obtained for degradation of calcium polyphosphate glass discs [20], where similar to here after one week $Q^{2\text{-middle}}$ peak fades away and a sharp Q^1 peak representing pyrophosphate grows up.

Additional points between 48 hr and 1 week, where the greatest changes in degradation were observed, might have elucidated more differences between the coacervate groups. The current results show that using longer NaPP chains did not increase the longevity of the coacervates, likely due to the extremely fast hydrolysis rate of the P-O-P bond as evident in $\overline{D_p}$ measurements. In contrast, Ba and Sr incorporation delayed the

degradation of the coacervates significantly. It is not clear if this delay is the result of differences in the physical characteristics (e.g. water penetration) of Ba and Sr loaded samples compared to Ca-only sample, or if it is a direct result of Ba and Sr on the rate of hydrolysis of polyphosphate chains. Nevertheless, even in the presence of these two cations, coacervates degraded at a very fast rate. Hydrolysis of fine glass powders of Mg, Ca, Sr and Ba polyphosphates has been carried out previously by Akamatsu et al. [75]. They observed that Ca and Mg polyphosphate glass powders transformed to coacervates upon contact with water; interestingly, though, Mg coacervates degraded more slowly, suggesting coacervates of smaller divalent cations are more stable, contradicting our results.

The mechanism of hydrolysis of polyphosphates has been the subject of several studies [5, 42, 110, 112]. The cleaving of the P-O-P linkage happens when water or its hydronium ion or hydrated metal ion forms a bond to the

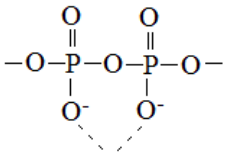

group. The formation of this complex may involve the *d*-orbitals of the phosphorus such that there would be five bonds proceeding from this atom (P) in the activated complex [5]. After formation of this complex, water cleaves the P-O-P linkage by giving its hydrogen and hydroxyl groups to each one of the phosphorus atoms of the complex. According to this mechanism, the ability of the water to hydrolyze the P-O-P linkage depends on its ability to come close to the chain to form the complex. Therefore, hydrogen or metal cations catalyze this reaction by neutralizing the charge of the chain

and allowing the water to come sufficiently close to form the complex. For a similar reason, Q^3 bonds representing phosphate branching points are so unstable because the net charge of the phosphorus atom in Q^3 is zero while it is -1 at $Q^{2\text{-middle}}$ [42].

Rheology measurements clarified the physical nature of coacervates. The tough gel-like nature of polyphosphate coacervates originates from their extremely high viscosity. For samples 2-7, *G"* has much larger values than *G'* and δ was near 90°, implying that these Ca-only coacervates lack cross-linking and possess mainly liquid-like properties rather than elastic properties. This is in agreement with the static viscosity measurements that confirmed the Newtonian response of these coacervates. This Newtonian fluid property for Ca and Mg coacervates has been previously reported but only for a polyphosphate with small $\overline{D_p}$ [78, 101, 103]. Here we showed that this is true even for Ca polyphosphate coacervates having much larger $\overline{D_p}$.

We demonstrated as well that the η for Ca polyphosphate coacervates is directly related to the $\overline{D_p}^{1.47}$ at 20°C, as shown in Equation 4.7. This relationship implies that the physical nature of these coacervates is very much similar to highly concentrated polymeric solutions or polymeric melts where the same relationship exists between η and $\overline{D_p}$ [175]:

$$\eta = K_p \times \overline{D_p}^{a} \quad \text{Equation 4.9}$$

Here, K_p is a constant depending on the polymer, $1 \leq a \leq 2.5$ for $\overline{D_p} < \overline{D_p}c$, and $a = 3.4$ for $\overline{D_p} > \overline{D_p}c$; $\overline{D_p}c$ represents a critical value for $\overline{D_p}$ above which chain entanglement

becomes important, and is in the range of 300 to 800 depending on the polymer type [175].

Based on Equation 4.7, a in our measurements is 1.47; this implies that Ca-only coacervates are not entangled at this range of $\overline{D_p}$, in agreement with our dynamic rheology measurements. However, coacervates prepared from polyphosphate with very large $\overline{D_p}$ (i.e. sample 1) showed elastic gel-like properties where $G' > G''$ and $\delta < 45°$. This elastic property is presumably caused by chain entanglement and here we are over $\overline{D_p}c$.

Replacing some of the Ca with Ba or Sr caused an increase in η and E_{af} and a decrease in δ, possibly due to the wider extension of polyphosphate chains or weak cross-linkage between chains in the presence of these cations. In the case of Ba-loaded samples, lower water content might also be related to this observation since water is acting as a plasticizer between chains in these coacervates.

4.6 Conclusion

Polyphosphate coacervates investigated here degrade at a fast rate, limiting their application only to a short-term biomaterial. Using longer polyphosphate chains does not increase the longevity of these coacervates. Incorporation of Ba or Sr does increase coacervate stability, though this effect overall is still relatively inconsequential. The key to achieving durable polyphosphate coacervates is controlling the rate of polyphosphate hydrolysis.

The viscoelastic properties of polyphosphate coacervates can be controlled by polyphosphate chain length and the type of divalent cation, allowing one to manipulate these materials for the desired biomedical application.

Chapter 5 Polyphosphate Coacervates for Hemostasis

5.1 Objective

The main objective of this chapter is *evaluating hemostasis potential of polyphosphate coacervates*.

5.2 Introduction

As shown in Chapter 4, polyphosphate coacervates investigated here degrade in the presence of water. While this would preclude their use as a permanent biomaterial, they could act, for example, as a temporary therapeutic ion releasing agent, drug delivery agent or hemostatic agent. For reasons to be elaborated below, we elected to focus on the potential of these coacervates in hemostasis.

In 2004, Ruiz et. al [127] discovered that specific platelet organelles, known as dense granules, are rich in polyphosphates, and upon thrombin stimulation platelets secrete these polyphosphates within a minute. This finding triggered several studies by other groups focusing on the role of polyphosphate in the coagulation cascade [128-130, 132, 133]. These studies concluded that polyphosphate acts at 3 different points in the blood coagulation cascade: (1) triggering the contact pathway by activating factor XII; (2) accelerating the activation of factor V by thrombin and factor Xa; and (3) increasing the stability of fibrin. In all of the experiments conducted by these researchers, soluble NaPPs was used. This approach could be debated since, *in vivo*, platelets release polyphosphates *and* calcium simultaneously resulting in the formation of polyphosphate precipitates, coacervates or particles; it is therefore essential to determine if calcium polyphosphate precipitates are equally as important as their precursor, soluble NaPP, in

hemostasis. Recently, Donovan et al. considered this postulation and showed that calcium polyphosphate nanoparticles are also a potent activator of the contact pathway [176].

In the following study, the potential of precipitated polyphosphate coacervates as bulk constructs in hemostasis is investigated. Such constructs could be used in situations where control of bleeding is ineffective or impractical by conventional procedures. Examples of current clinical hemostatic agents are Bone wax used to control bleeding from the bone surface, Hemostasyl™ used in all cases of moderate bleeding occurring in routine dental practice, or different bandages and dressings used in trauma such as HemCon® chitosan dressing. Since polyphosphate coacervate has the potential to form *in situ* by separate injection of two liquid components, NaPP and $CaCl_2$ solutions, there is also potential as an injectable liquid embolic system. This aspect is explored further in Chapter 6.

Here, we utilize conventional blood clotting tests including whole blood clotting time, prothrombin time, partial thromboplastin time and platelet adhesion to compare the hemostasis potential of coacervates prepared from different divalent cations and NaPPs with different $\overline{D_p}$.

5.3 Materials & Method

5.3.1 Starting Materials

All starting materials including NaPPs were freshly produced and characterized as described in section 3.3.1 of Chapter 3.

5.3.2 Preparing polyphosphate coacervates

To evaluate the effect of polyphosphate $\overline{D_p}$, 4 groups of coacervates loaded only with Ca were prepared using NaPPs with different $\overline{D_p}$; 0.8 g of ion-exchanged NaPPs with $\overline{D_p}$ of 1.0±0.1 E+04 (determined by viscosity; n=3) were dissolved in 80 mL of deionized water, resulting a polyphosphate solution containing 0.0069 mol phosphate based on ICP. To this solution enough 1 M Ca solution (3.45 mL, prepared from $CaCl_2$) was then added to reach a theoretical Ca/P molar ratio of 0.5, resulting in Group 1 coacervates (Table 5.1). In a similar manner, coacervates having a theoretical Ca/P molar ratio of 0.5 were prepared from NaPPs having lower $\overline{D_p}$ (as determined by liquid ^{31}P-NMR) as follows (Table 5.1): 1 g of fractioned NaPPs with $\overline{D_p}$ of 363±76 was dissolved in 100 mL of deionized water (0.0083 mol phosphate) to which 4.15 mL of 1 M Ca solution added [Group 2]; 1.2 g of fractioned NaPPs with $\overline{D_p}$ of 155±38 was dissolved in 120 mL of deionized water (0.0103 mol phosphate) to which 5.16 mL of 1 M Ca solution was added [Group 3]; and 5 g of commercial NaPP with $\overline{D_p}$ of 20±4 in 500 mL deionized water to which 24.5 mL of 1 M Ca solution was added [Group 4].

To evaluate the effect of incorporation of different divalent cations, the same NaPP solution used in Group 3 was prepared and first preloaded to 0.15 Ba/P or Sr/P molar ratios (no coacervate forms at 0.15) by addition of 1.55 mL 1 M Ba or Sr solutions (prepared from $BaCl_2$ and $SrCl_2$) prior to adding enough 1 M Ca solution (3.61 mL) to reach a total theoretical divalent cation to phosphorus molar ratio of 0.5 (Groups 5 and 6, Table 5.1).

All solutions were mixed for 5 min, and the resulting coacervates collected and squeezed to remove excess water. This coacervate was used for hemostasis tests, with a small section set aside for compositional and structural characterization. Here, the coacervate was dissolved by EDTA and the $\overline{D_p}$ of polyphosphates contained within the coacervate and its experimental composition determined by NMR and ICP, respectively, as described previously in section 3.3.3.2. Also for each group following removal of excess water with Kimwipe®, 0.25 mL of the coacervate was weighed (n=6) to determine apparent density.

Table 5.1 Theoretical and experimental composition of different coacervate groups and their density.

Group	Original NaPP D_p (n=3)	Theoretical molar ratio			Dissolved coacervate D_p (n≥5)	Experimental molar ratio (n≥5)			Density (g/ml) (n=6)
		Ca/P	Sr/P	Ba/P		Ca/P	Sr/P	Ba/P	
1	1.0±0.1E+04[a]	0.50	N/A	N/A	0.2±0.1E+03	0.40±0.016	N/A	N/A	1.65±0.15
2	363±76	0.50	N/A	N/A	441±57	0.40±0.015	N/A	N/A	1.60±0.15
3	155±38	0.50	N/A	N/A	185±26	0.40±0.009	N/A	N/A	1.65±0.07
4	20±4	0.50	N/A	N/A	44±3	0.41±0.008	N/A	N/A	1.68±0.11
5	155±38	0.35	0.15	N/A	180±32	0.26±0.009	0.12±0.005	N/A	1.78±0.10
6	155±38	0.35	N/A	0.15	173±20	0.26±0.010	N/A	0.13±0.007	1.85±0.08

[a] D_p for this sample was determined by viscosity; D_p for all other samples was determined by NMR.

5.3.3 Whole blood clotting assay

Initially the blood clotting test adapted from Shih et al. [177] and Ong et al. [178] was used to evaluate the potential of the different coacervates to form a clot. In accordance with this method, citrated sheep blood (CEDARLANE®) was added to tubes containing

coacervate. Immediately thereafter a $CaCl_2$ solution was added to initiate the coagulation cascade, with tubes incubated at 37°C to form the clot. After 10 min, water was added to lyse erythrocytes that were not trapped inside the clot and the absorbance of the resulting hemoglobin solution was measured at 540 nm. A higher absorbance value for the hemoglobin solution indicates a slower clotting rate.

Overall, this method proved to be unreliable, giving irreproducible results even for the control (empty tube), with very large standard deviations. Consequently, a simplified *in vitro* whole blood clotting time assay was improvised and found to yield reproducible results. Here, 0.25 mL of coacervate was added to Falcon® 14 mL round bottom polypropylene tube and maintained in a 37°C water bath; based on the size of the tube, each coacervate had ~115 mm^2 of surface area. 5×5×5 mm^3 pieces of commercial gelatin sponge (SURGIFOAM® from ETHICON™), giving an apparent surface area of 150 mm^2, was used as a commercial hemostat control. Empty polypropylene tubes were used as the second control. 0.1 mL of 0.2 M Ca solution (prepared from $CaCl_2$) was added to 1 mL of citrated sheep blood (CEDARLANE®), vortexed for 15 second and then 0.2 mL aliquots were dispensed to each tube containing coacervates or controls. Each tube was vortexed for 3 second then placed in a 37°C water bath. After 2 min, and every ~20 second interval thereafter, the tube was removed from the water bath and shaken to visually observe if there was blood flow. Clotting time was reported as the time when no blood flow was observed if the tube was shaken or rotated (n=6).

5.3.4 Prothrombin time and partial thromboplastin time

Prothrombin time (PT) measures how long it takes for platelet poor plasma to form fibrin gel after addition of tissue factor. It measures the state of extrinsic and common pathways

of the coagulation cascade. PT was measured in the presence of coacervates and controls. Freeze-dried normal human platelet poor plasma (PPP) from Biomedica Diagnostics Inc. (Windsor, NS) was rehydrated based on the product instructions and used immediately. PT agent from Biomedica was also rehydrated and used immediately. PT for PPP was found to be 13±1 second, in agreement with the product certificate. At such a fast rate it was not possible to distinguish between groups. Therefore, a 1/6 dilution of the PT agent was used instead of pure PT agent in all measurements in order to delay the PT. PT was subsequently measured as follows: 0.1 mL of the coacervates were added to 2 mL round bottom Eppendorf® tubes and maintained at 37°C in a water bath. 200 µL of 1/6 diluted PT agent was added to each tube, vortexed for ~1 second and incubated for a maximum of 30 second at 37°C. Subsequently, 100 µL of 37°C PPP was added to each tube, vortexed for ~ 1 second and the timer started immediately. The time required for the fibrin gel to form was reported as the PT (n=6); tubes were continuously tilted back and forth to a 45° position and the timer halted with the appearance of fibrin gel.

Activated partial thromboplastin time (aPTT) represents the time required for platelet poor plasma to form fibrin gel after addition of a contact pathway activator; it measures the state of intrinsic and common pathways of the coagulation cascade. aPTT was determined using a standard assay (Biomedica). aPTT for PPP was found to be 38±3 sec, in agreement with the product certificate. aPTT for samples was measured by addition of 100 µL of 37°C incubated aPTT agent (ellagic acid, Biomedica) to each Eppendorf® tube containing 0.1 mL of coacervates or controls, followed by immediate addition of 100 µL 37°C PPP. Each tube was vortexed for ~1 second and incubated at 37°C for 3 min. Subsequently, 100 µL 0.02 M Ca solution (prepared from $CaCl_2$) was added, vortexed

and the timer started immediately. The time for the fibrin gel to form was reported as the aPTT (n=6). Controls were empty tubes or 5×3×3 mm^3 pieces of SURGIFOAM® soaked in water prior to measurements.

5.3.5 Platelet adhesion test

A platelet adhesion test was used to quantitatively assess the number of platelets adhering to the coacervates as a function of coacervate composition and $\overline{D_p}$, complemented by SEM imaging to visualize this cell-coacervate interaction. This platelet adhesion test was adapted from Ong et al. [178] and Dai et al. [179], and platelet separated from the blood according to Cazenave et al. [180]. Rat blood was collected by a certified veterinarian according to Dalhousie's animal ethics regulations. Roughly 3.6 mL of blood was collected in sodium citrate tubes (3.8%) and centrifuged at 3600 rpm for 10 min resulting in a red layer of cells at the bottom, plasma at top and a buffy layer at the middle. The top portion of the buffy layer and plasma were collected using Pasteur pipette and centrifuged for the second time at 4400 rpm for 5 min, resulting in a pellet of platelets and supernatant platelet poor plasma that was discarded. Platelets were suspended in 10 mL of buffer without any Ca or Mg (140 mM NaCl, 3 mM KCl, 12 mM $NaHCO_3$, 0.4 mM NaH_2PO_4, 0.1% glucose, pH 7.4, adjusted with 4% HEPES) [178]. The number of platelets in this suspension was 2×10^8/mL as measured by a hemocytometer. Briefly, a small volume of the suspension was diluted by a factor of 100 in the same buffer and then 10 μL of this diluted sample was loaded onto a hemocytometer counting chamber covered by a glass. Approximately 10 min was given for the platelets to settle, and then platelets were counted in 5 of the small squares (4 squares at edges and a one in the center each has a dimension of 0.2 mm×0.2 mm) inside the large middle square using

500x magnification (Olympus BH2 microscope). The number of counted platelets in 5 squares was averaged to determine the number average of platelets per small square, which has a volume of 4×10^{-6} mL. The loading of the hemocytometer and the counting was performed in triplicate and the average number was used.

50 μL of coacervate or control (5×3×3 mm^3 pieces of SURGIFOAM®) was placed inside a 96-well microplate, with 8 replicates per group. 6 replicates were for platelet counting, with the remaining two samples reserved for SEM imaging.

10 μL of 1M Mg (prepared from $MgCl_2$) and 25 μL of 1M Ca (prepared from $CaCl_2$) were added to the platelet rich buffer suspension, and then 150 μL of the resulting solution was added immediately to each well. The microplate was maintained at 37°C for 1 hr on an orbital shaker. The supernatant was discarded and each well was washed three times with 0.01 M PBS to remove non-adhered platelets. Subsequently, 100 μL of 1% Triton X-100 in PBS was added to each well and kept at 37°C for 1 hr on an orbital shaker to lyse any adhered platelets. Lactate dehydrogenase (LDH) enzyme released upon lysing was measured using a LDH/LD kit (TOX7 SIGMA In Vitro Toxicology Assay Kit, Lactic Dehydrogenase based) according to manufacturer's instructions. Briefly, 50 μL of the platelet lysed triton solution was added to 100 μL of a LDH mixture inside a microplate. This LDH mixture was prepared by addition of equal volumes of LDH substrate, dye and cofactor. The microplate was covered to protect from light and kept at room temperature for 15 min. Background absorbance was then measured at 690 nm and subtracted this value from the primary absorbance wavelength measurement at 490 nm. Subtracting absorbance at 690 nm is for correction of nonspecific background values

caused by well plate variability, fingerprints etc. Synergy™ HT microplate reader (BioTek®) was used for spectrophotometric measurement.

A calibration curve between the number of platelets and the absorbance was developed and used to determine the number of adhered platelets. To develop this calibration curve, different volumes of the original platelet rich buffer suspension with a known number of platelets was lysed by addition of enough volume of 1% triton x-100 in PBS to reach 100 µL in total, followed by the LDH assay as described above.

Two samples from each group were used for SEM imaging. These samples were kept in presence of platelet rich suspension for 12 hr to allow platelets to fully develop and then supernatant was removed and wells washed 3 times with 0.01 M PBS. Subsequently, 250 µL of 0.1 M PBS containing 2.5% glutaraldehyde and 2.0% paraformaldehyde (pH 7.4) was added to each well containing coacervates and control and left for 2 hr at 37°C. Following this fixation step, samples were placed in 15 mL glass vials and serially dehydrated by addition of 2 mL 25, 50, 75 and 100% ethanol. From each group one sample was dried by a critical point dryer (Leica EM CPD300, Leica Microsystems) and the second sample was freeze-dried (FreeZone® 1 Liter Benchtop Freeze Dry System, Labconco Corp., USA) after replacement of ethanol with tert-butanol. Dried samples were mounted on stubs and a 10 nm gold/palladium coating was applied using a sputter coater (Leica EM ACE200, Leica Microsystems) prior to SEM imaging (Hitachi S-4700 FEG Scanning Electron Microscope).

5.4 Results

5.4.1 Composition and density of coacervates

Table 5.1 shows the experimental chemical composition of the coacervates produced. In agreement with results from Chapters 3 and 4, experimental values were consistently lower than theoretical values as presumably some of the divalent cations remained in solution.

With the exception of Group 1, a trend was also seen where the $\overline{D_p}$ of polyphosphates within the coacervate was higher than the $\overline{D_p}$ of the original NaPP. However, this increase was only significant (p value<0.01) for the very short chain group (Group 4) based on a two-tailed student t-test. As explained in Chapter 3, if some of the shorter chain polyphosphates do not get incorporated into the coacervate, the $\overline{D_p}$ of polyphosphates within the coacervate becomes higher than the original value. The large STD for dissolved coacervate $\overline{D_p}$ in Group 1 can be attributed to the lack of precision of the NMR method used for measuring the $\overline{D_p}$ in these very long chains.

The density measurements showed that Sr- and Ba-loaded Groups 5 and 6 were significantly more dense than their corresponding Ca-only Group 3 (p values<0.05 and <0.01, respectively, based on a two-tailed student t-test). Also, based on single factor ANOVA analysis, the $\overline{D_p}$ was found to have no significant effect on the density of the resulting coacervates (Groups 1-4).

5.4.2 Whole blood clotting time

Figure 5.1 shows a volume of blood that flows compared to clotted blood for which no flow is observed.

(a) 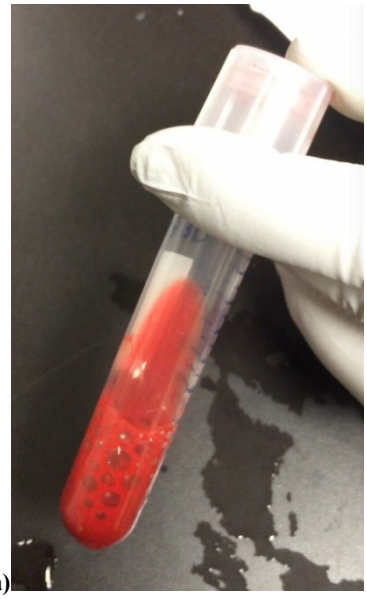 (b) 

Figure 5.1 Images of the whole blood clotting assay; (a) blood flow, (b) blood clot in the presence of a coacervate.

The time required for the blood to clot in the presence of coacervates and controls was measured and reported in Figure 5.2. All groups and the Surgifoam® were compared to an empty polypropylene tube by a two-tailed student t-test. Under the conditions used here, the blood clotted in roughly 7 minutes in the empty tube. Surgifoam® did not decrease the clotting time significantly, but all coacervates significantly decreased the clotting time except the shortest chain, Ca-only group (Group 4). The longest chain group (Group 1) consistently decreased the clotting time far more than other groups, with blood coagulating in less than 3 minutes. Based on single factor ANOVA analysis, the $\overline{D_p}$ of polyphosphate within the coacervates (Groups 1-4) was found to have a significant effect (p value < 0.01) on the clotting time. In contrast, single factor ANOVA analysis showed that divalent cation type did not have a significant effect (p value = 0.08) on the clotting

time (Groups 3, 5 and 6). The observation that Surgifoam® is not significantly affecting the clotting time is in agreement with its mode of action, which is believed to be more physical rather than altering the blood clotting mechanism [181].

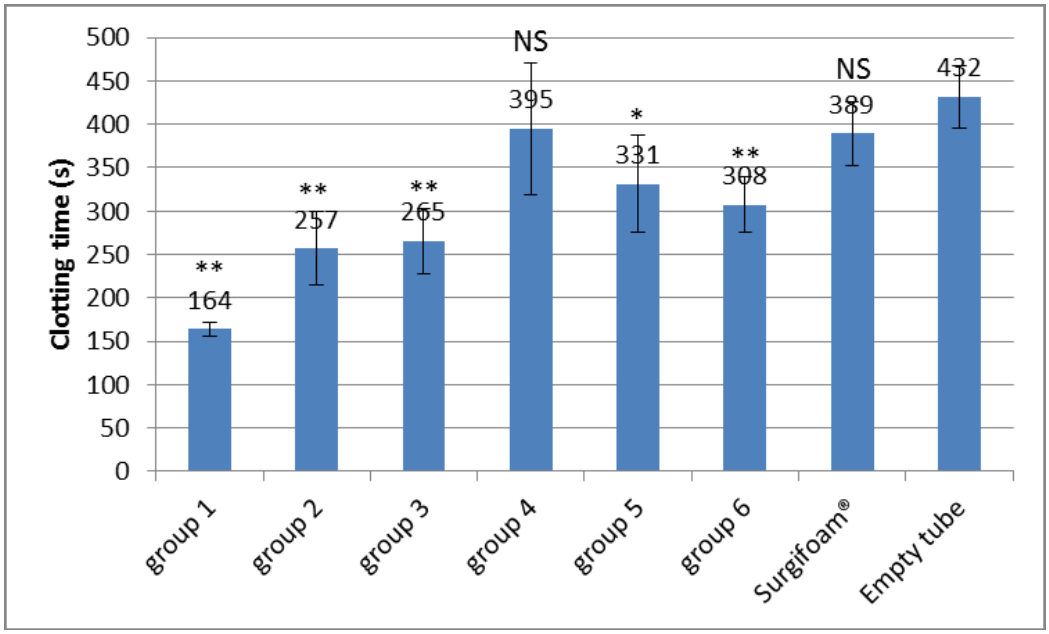

Figure 5.2 Whole blood clotting time in different coacervate groups and controls (Two tailed student t-test of each group vs. empty tube: NS, * and ** stand for p-value>0.05, 0.01<p-value<0.05 and p-value<0.01, respectively. Numbers show average and bars show STD, n=6).

5.4.3 Prothrombin time and partial thromboplastin time

As noted earlier, diluted PT agent was used rather than the undiluted PT agent due to the exceedingly short PT achieved with the latter that made distinguishing between sample groups difficult. A 1/6 dilution increased the PT to 54±12 second as shown in Figure 5.3. All coacervates except Group 2 decreased the PT significantly compared to the empty tube (Figure 5.3). Surgifoam® was found to increase the PT compared to the empty tube, though not significantly. Based on single factor ANOVA analyses, both $\overline{D_p}$ of polyphosphate within the coacervate (Groups 1-4) and divalent cation types (Groups 3, 5 and 6) were found to have a significant effect (p value < 0.01) on the PT.

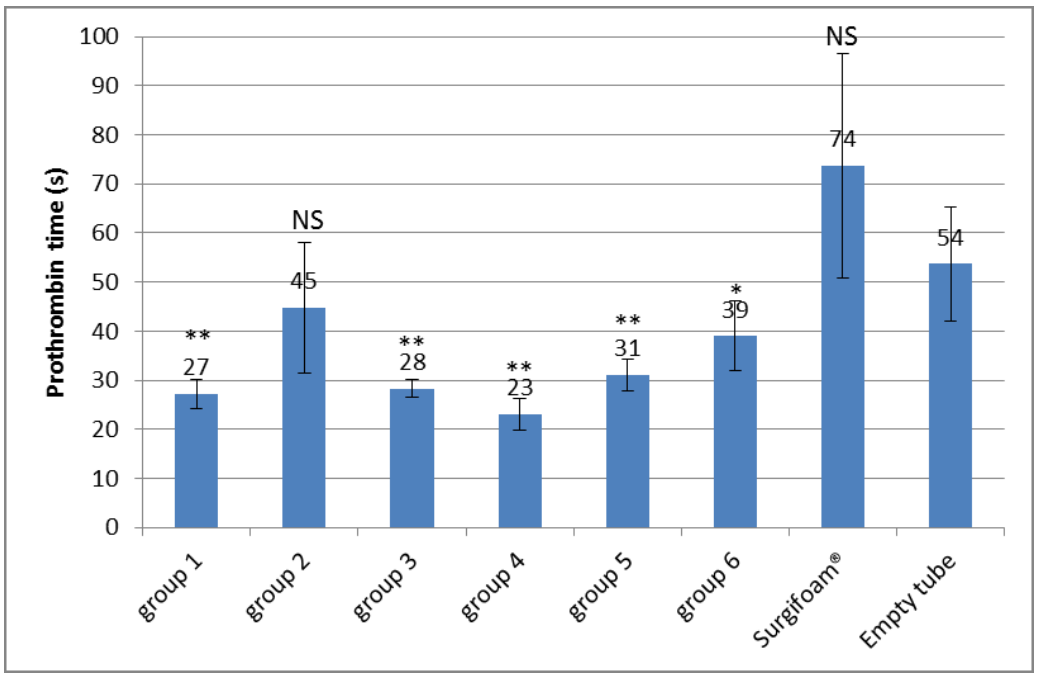

Figure 5.3 Prothrombin time for different coacervate groups and controls (Two tailed student t-test of each group vs. empty tube: NS, * and ** stand for p-value>0.05, 0.01<p-value<0.05 and p-value<0.01, respectively. Numbers show average and bars show STD, n=6).

Formation of the fibrin gel was also visually different in the control (empty) tubes compared to those with coacervate. As shown schematically in Figure 5.4a, in the absence of the coacervate a relatively transparent fibrin gel forms implying homogeneity of the gel. In contrast, in the presence of the coacervate, small discrete white particles were found to suddenly form inside the PPP (Figure 5.4b), with subsequent aggregation to yield a relatively non-transparent fibrin gel (Figure 5.4c).

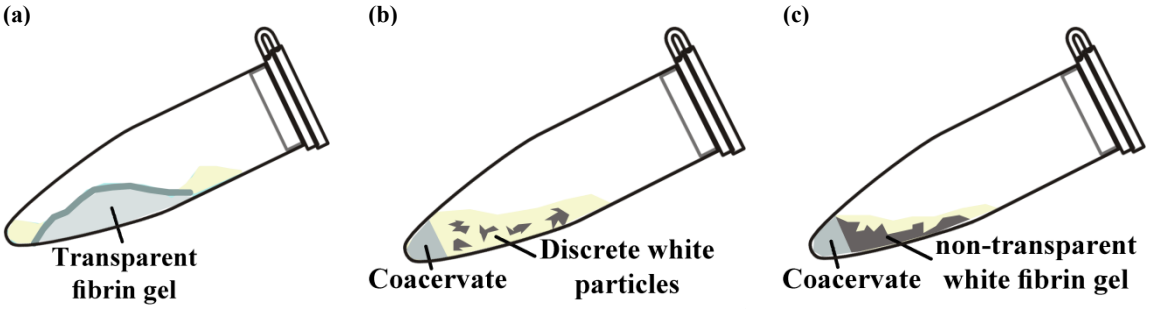

Figure 5.4 Schematic of fibrin gel formation in absence (a) and presence (b,c) of the coacervate.

Figure 5.5 shows the effect of coacervates on aPTT. Surprisingly in the presence of coacervates aPTT increased significantly compared to the control with the exception of

the short chain Ca-only group (Group 4). The aPTT for Groups 2, 3 and 5 was severely delayed for over 10 minutes. Similar to PT, based on single factor ANOVA analyses, both $\overline{D_p}$ of polyphosphate within the coacervate (Groups 1-4) and divalent cation types (Groups 3, 5 and 6) were found to have a significant effect (p value < 0.01) on the aPTT.

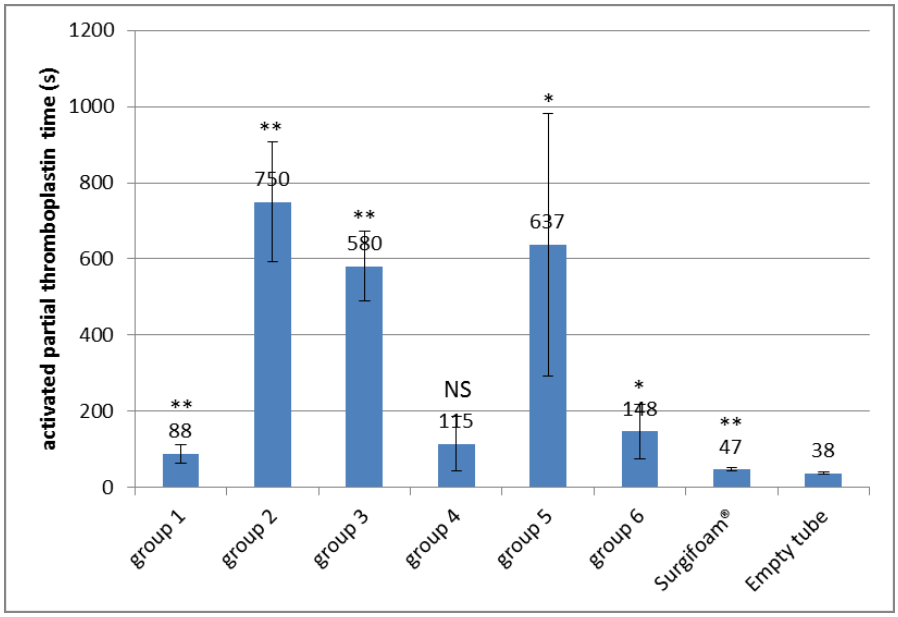

Figure 5.5 Activated partial thromboplastin time (aPTT) for different coacervate groups and controls (Two tailed student t-test of each group vs. empty tube: NS, * and ** stand for p-value>0.05, 0.01<p-value<0.05 and p-value<0.01, respectively. Numbers show average and bars show STD, n=6).

5.4.4 Platelet adhesion

Figure 5.6 shows the standard curve of absorbance vs. number of platelets. Using this calibration curve, the number of adhered platelets was determined for the different sample groups, summarized in Figure 5.7.

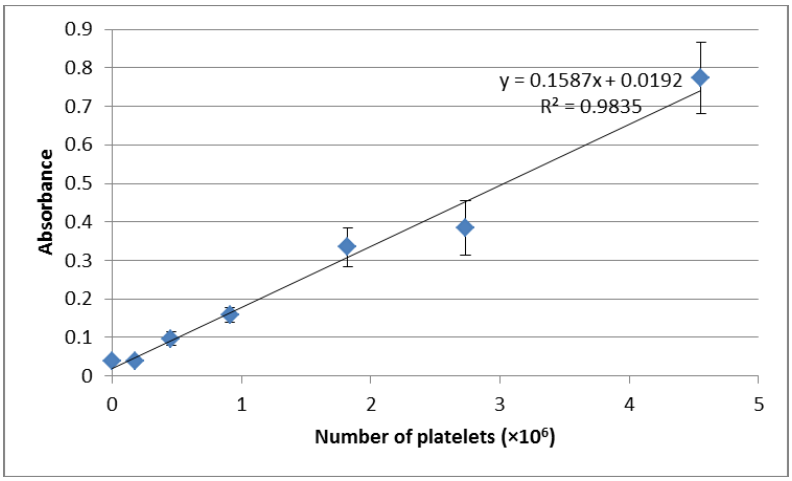

Figure 5.6 Standard curve of absorbance vs. number of platelets generated by lysing a known number of platelets and carrying out LDH assay on them (n=3).

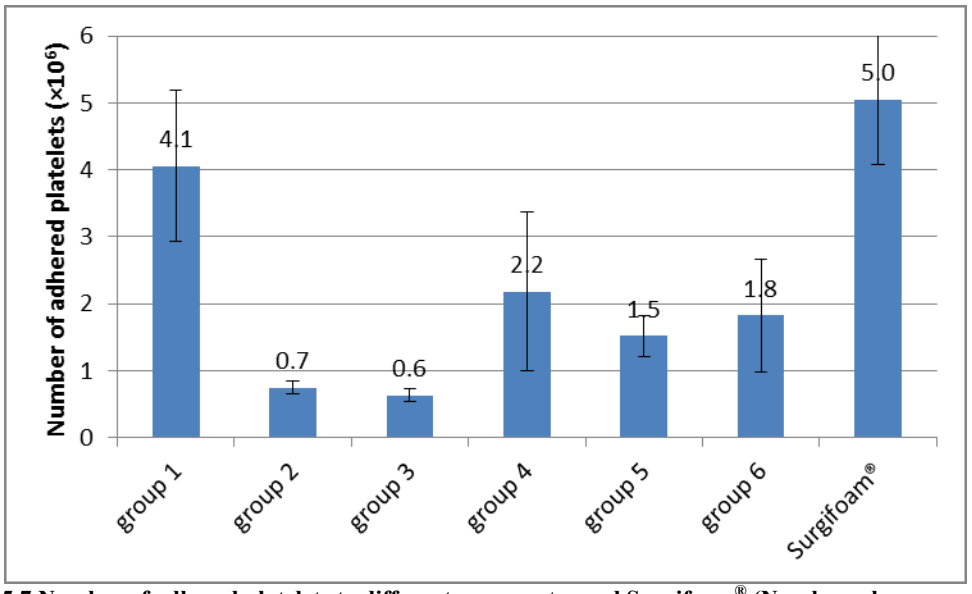

Figure 5.7 Number of adhered platelets to different coacervates and Surgifoam® (Numbers show average and bars show STD, n=6).

The greatest number of platelets adhered to long-chain, Ca-only coacervates (Group 1) and Surgifoam®. Based on single factor ANOVA analyses, both $\overline{D_p}$ of polyphosphates within the coacervate (Groups 1-4) and divalent cation types (Groups 3, 5 and 6) were found to have a significant effect (p values < 0.01 and < 0.05, respectively) on the number of adhered platelets.

Adhered platelets were imaged by SEM after several sample preparation steps that included either freeze-drying or critical point drying prior to application of a conducting layer. No visual differences were noted between samples prepared by either drying methods. Figure 5.8 shows images of platelets adhered to long-chain, Ca-only coacervates (Group 1). Overall, a very large number of platelets completely covered parts of this sample, with significant platelet aggregation; most of the platelets were small and spherical, with very few short pseudopods as shown in Figure 5.8d.

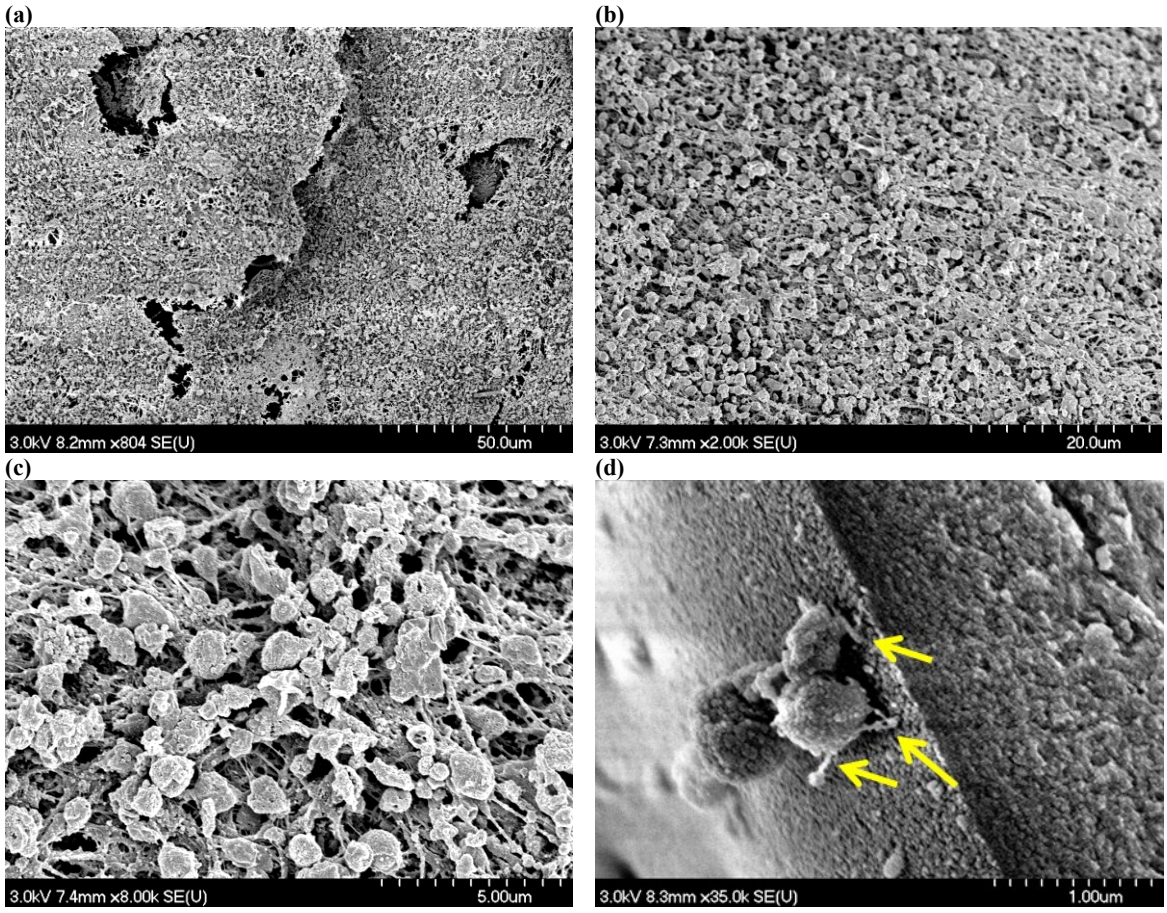

Figure 5.8 SEM images of Group 1; (a,b, c) Platelets covered the surface at three different magnifications, (d) individual platelets shape (arrows point to pseudopods).

The shape of adhered platelets with Group 1 samples is completely in contrast to that observed on Surgifoam® samples. Surgifoam® is highly porous spongy gelatin as shown in Figure 5.9a, so it was not possible to image a big surface area to get an idea on the

number of adhered platelets. Only individual platelets were observed, but all were fully shaped with a few very large pseudopods as shown in Figures 5.9b-d.

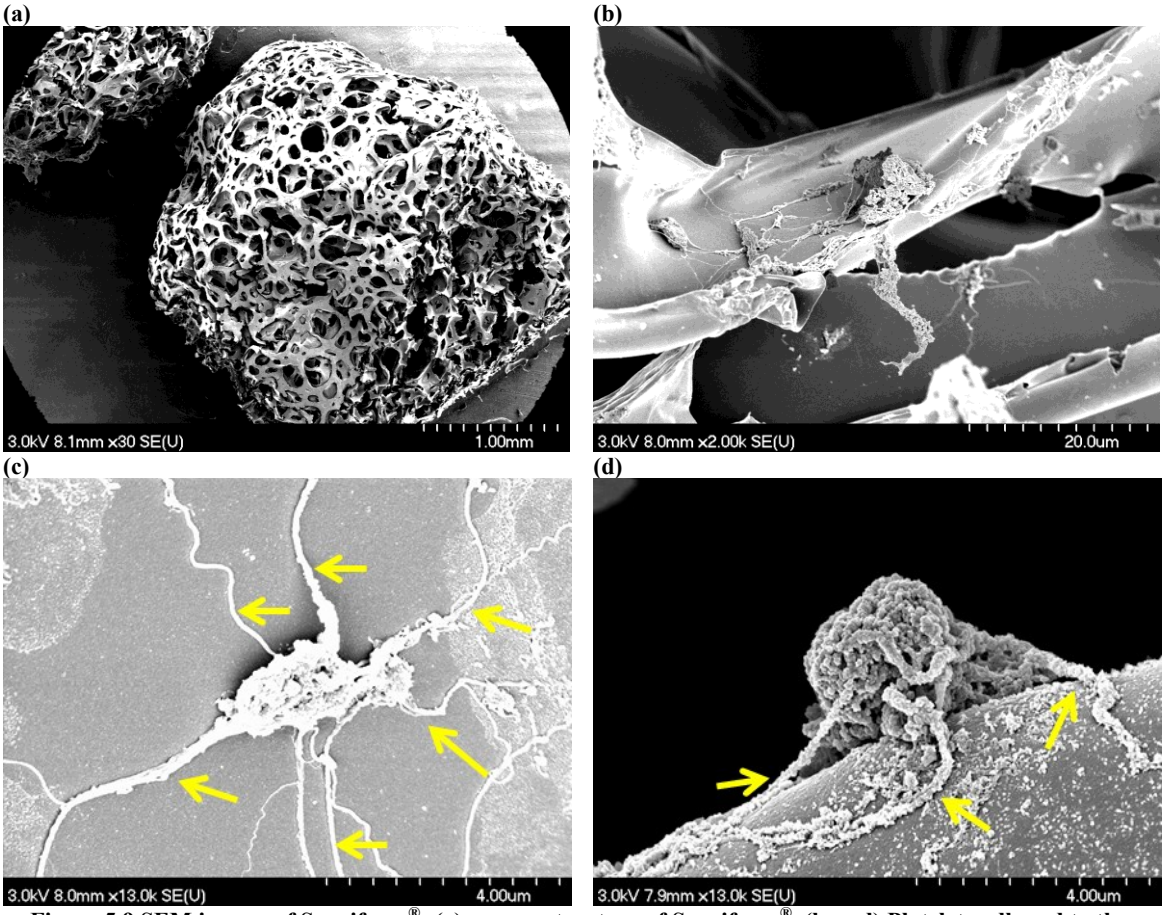

Figure 5.9 SEM images of Surgifoam®; (a) porous structure of Surgifoam®, (b, c, d) Platelets adhered to the surface (arrows point to pseudopods).

Representative SEM images of platelets adhered to the remaining coacervate groups are shown in Figure 5.10. Coacervates formed in Groups 2, 3 and 4 were very much liquid-like, resulting in the loss of the original surface during sample preparation because coacervates flow. This loss of surface could be seen in Figure 5.10a, c and e, where the new surface formed is darker and flat in contrast to the original surface that is brighter, rougher and covered with platelets. In some cases it is clear that the original surface has folded away during sample preparation, as shown by the arrows in Figure 5.10e. Images were taken from sites where minimal surface loss was observed. Qualitatively, these

images were in agreement with the platelet counts obtained; Sr- and Ba-loaded samples exhibited more platelet attachment overall compared to their Ca-only counterparts (Group 3), and the long-chain, Ca-only sample group 1 had the highest number of adhered platelets between all coacervates. Adhered platelets in all coacervates were very similar to that observed with Group 1 with platelet cohesion and focal centers and their shapes were generally spherical with few pseudopods (Figure 5.10f).

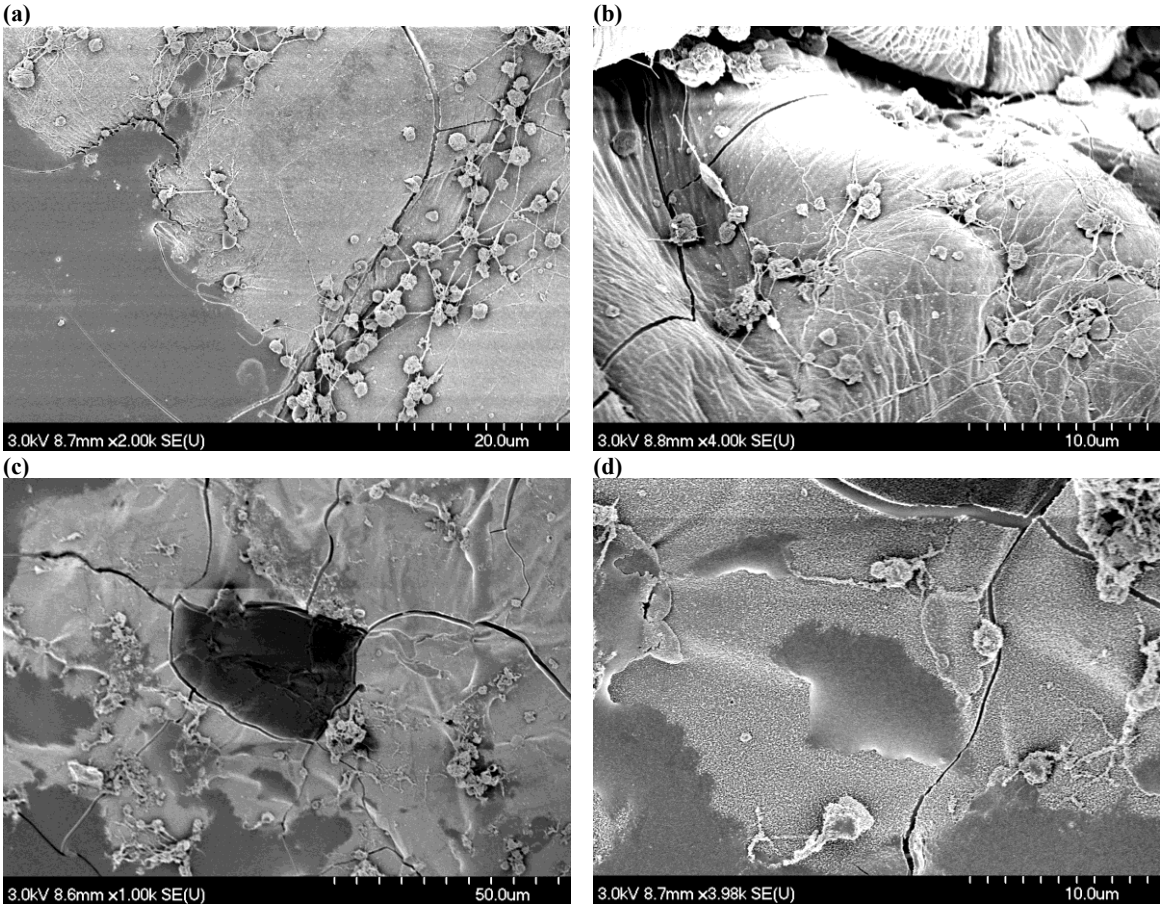

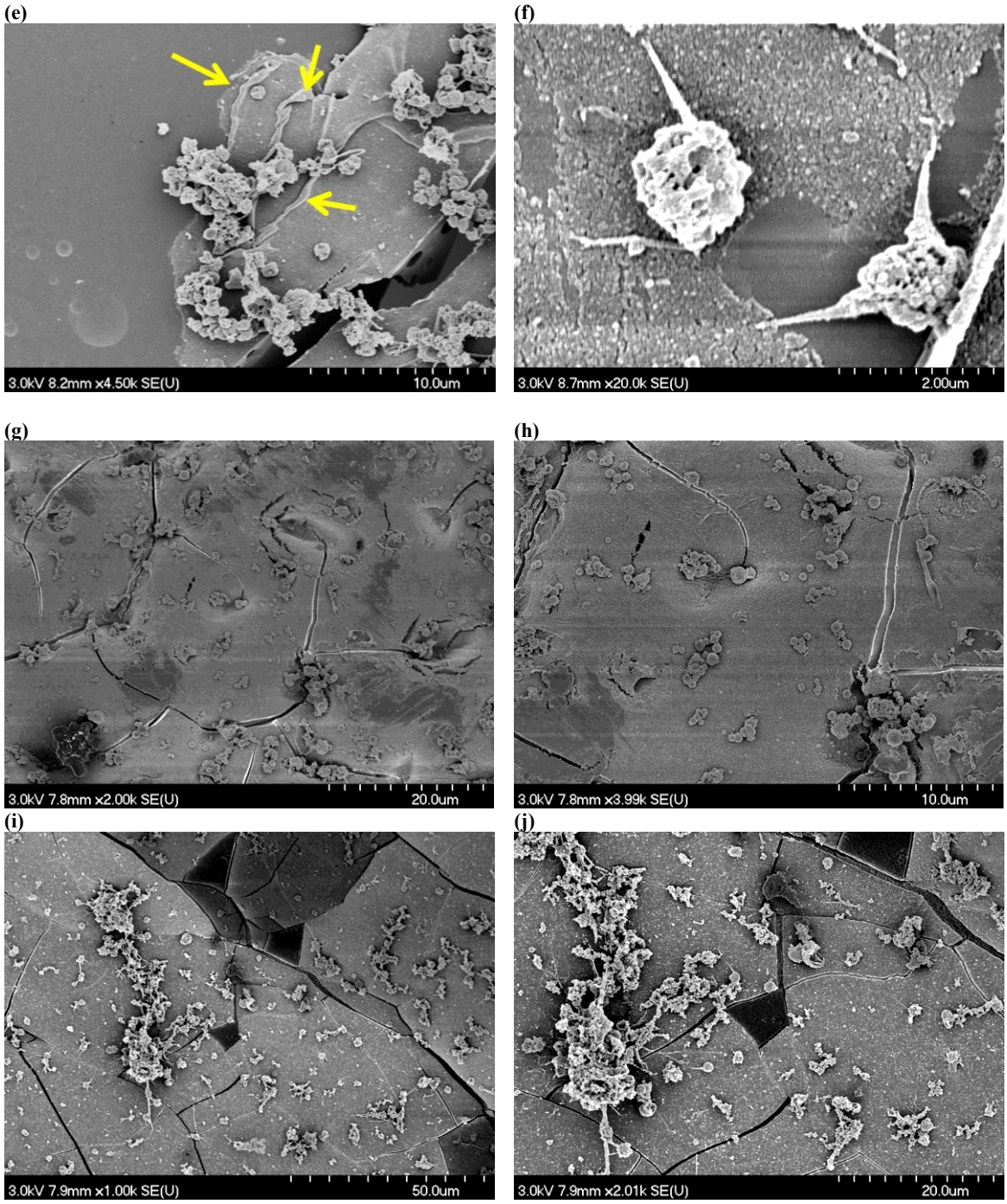

Figure 5.10 SEM images of platelet-covered coacervates; (a,b) Group 2, (c,d) Group 3, (e,f) Group 4, (g.h) Group 5, (i,j) Group 6 (arrows point to the folded surface).

5.5 Discussion

The whole blood clotting assay showed that polyphosphate coacervates hold great potential as a hemostatic agent. The dramatically shorter whole blood clotting times

observed here had been previously reported only for soluble NaPPs, with Ong et al. finding that incorporation of NaPPs with $\overline{D_p}$ of 45 and 65 at 6.7 and 10% (wt.%) into chitosan dressings accelerated blood clotting [178]. Blood clotting relies on the formation of fibrin fibers, which crosslink together forming fibrin clot. Fibrin production is highly dependent on thrombin generation, the rate of which is a function of the rates of activation of procoagulant factors and cofactors, and the inhibitory ability of anticoagulants [182]. Soluble NaPP acts at several steps that influence thrombin generation: it enhances the generation of factor Va; it serves as a contact pathway activator; and it opposes the anticoagulant activity of tissue factor pathway inhibitor [182]. These effects accelerate thrombin generation and consequently fibrin clot formation.

The precipitated polyphosphate coacervates evaluated here presumably accelerate fibrin clot formation similar to NaPPs. Either some of the precipitated polyphosphate dissolves away and induces its effect in a soluble form, or proteins from plasma directly bind to the precipitated polyphosphate and activate. In the time frame of the clotting assay used here the latter postulation is more likely, as we have previously shown (Chapter 4) that these coacervates are highly stable for 48 hr. In agreement with our results, it has recently been shown that calcium polyphosphate nanoparticles accelerate fibrin formation in citrated plasma [176].

These studies also demonstrated that clot formation is significantly faster for coacervates prepared from longer chain polyphosphates. This relationship between polyphosphate

$\overline{D_p}$ and rate of clot formation has been previously reported for soluble NaPPs; it has been shown that optimal activity of contact pathway requires very long NaPPs [130].

A change in PT shows that the surface is affecting the extrinsic and common pathways of the coagulation cascade. As observed for the Surgifoam®, PT is rarely affected by a foreign biomaterial surface which typically impacts the contact pathway only. However, PT measured for polyphosphate coacervates decreased significantly compared to the control. As previously noted, NaPPs accelerate activation of factor V and oppose the anticoagulant activity of tissue factor pathway inhibitor [182]. Both of these could directly shorten the PT. We also observed that fibrin gel formed from PPP in the presence of coacervate is different from fibrin gel that forms in its absence. This observation is in agreement with results that have suggested that the fibrin gel structures that form in the presence of NaPPs are heterogeneous and contain thicker fibrin fibers [129, 133].

Biomaterial surfaces usually decrease the aPTT since they activate the coagulation cascade through the contact pathway. Surprisingly, we found that aPTT profoundly increased for polyphosphate coacervates compared to the control. We believe this observation is an artifact caused by an interaction between the polyphosphate coacervate and phospholipids in the aPTT agent used for these experiments. Prothrombinase complex consisting of Factor Va and Factor Xa assembles on negatively charged phospholipids, and in their absence thrombin formation would be significantly hindered [176]. *In vivo* and for whole blood clotting test, phospholipids are present in large number on platelets and other blood cells, eliminating such an artifact.

Platelet adhesion test showed that platelets adhere in large numbers to polyphosphate coacervates, especially for the very long chain group where they covered the whole surface, forming large aggregates. It has been previously reported that addition of NaPP into chitosan at 10% (wt.%) enhance platelet adhesion [178].

Platelet can assume five morphological forms describing increasing activation: discoid or round; dendritic or early pseudopods; spread dendritic or intermediate pseudopods; spreading; and fully spread [183]. Based on this classification, platelets would appear to be not as fully developed on coacervates, as they did not exhibit the spread morphology with protruding pseudopods. In contrast, platelets on Surgifoam® spread with several long pseudopods. Surgifoam® is prepared from collagen, which is known to be a potent platelet activator [184]. Still, one should note that there is a possibility that the extent of platelet clustering and aggregation on coacervates, specifically the long chain samples, was so great that it obscured spread platelets underlying these aggregates.

5.6 Conclusion

Coacervates decreased the clotting time significantly especially when very long chain polyphosphates were used. Polyphosphate coacervates affected the extrinsic pathway by decreasing the PT, but they increased the aPTT presumably due to an artifact caused by phospholipid deficiency during fibrin formation. Nevertheless this result was unexpected and demands additional studies. Platelets adhered in large numbers to coacervates, especially the long chain polyphosphate coacervates, but they seemed not to be fully developed unlike gelatin foam. The longest chain polyphosphate coacervate indeed holds the greatest potential as a hemostatic agent.

Chapter 6 Polyphosphate Coacervate as an Embolic Agent

6.1 Objective

The main objectives of this chapter are *developing an in situ forming polyphosphate embolic system and investigating drug loading and release from polyphosphate coacervates*.

6.2 Introduction

Embolization is a minimally invasive interventional radiology procedure to occlude a blood vessel. This procedure is performed to infarct tumors, reduce blood supply to highly vascularized lesions before surgical obliteration, control hemorrhage, and treat arteriovenous malformations (AVM) or aneurysms. Occlusion is achieved by catheterization under fluoroscopy and injection of embolic agents. Embolic agents are categorized into coils (e.g. platinum coils), particulate (e.g. PVA particles) and liquids (e.g. Onyx® and cyanoacrylate glues) [185]. For many applications such as aneurysm [186, 187] and AVM [188, 189] liquid embolic agents that solidify *in situ* are deployed. However, available liquid embolic agents have a wide range of safety and efficacy limitations; some use cytotoxic organic solvents [190-192], they are not intrinsically radiopaque to allow for positioning and monitoring, and cases of catheter entrapment have been reported in the literature [193].

To tackle these issues with available liquid embolic agents, there are several aqueous-based liquid embolic agents under investigation utilizing alginate [194], chitosan [195], polyethylene glycol-polypropylene glycol [196] and poly vinyl acetate [197]. Still, none

of these systems are intrinsically radiopaque and thus require mixing with liquid contrast agents. These contrast agents can be carried away in the blood stream, precluding follow-up x-ray studies to evaluate the embolic mass. The study reported herein looks to develop an intrinsically radiopaque and safe liquid embolic agent.

This liquid embolic agent is comprised of aqueous solutions of sodium polyphosphate (NaPP) and divalent cations that form a coacervate on contact, as shown schematically in Figure 6.1. From a clinical standpoint, these two solutions could be separately delivered to the injection site using a dual lumen catheter as a prelude to forming the coacervate *in situ* at the targeted vascular site. As mentioned in Chapter 5, polyphosphates are found in human platelets [127] and play a significant role in the coagulation cascade [198]; polyphosphates have been added, for example, to chitosan based wound dressings to increase their hemostatic potential [178]. This superior hemostatic ability could be beneficial for an embolic agent.

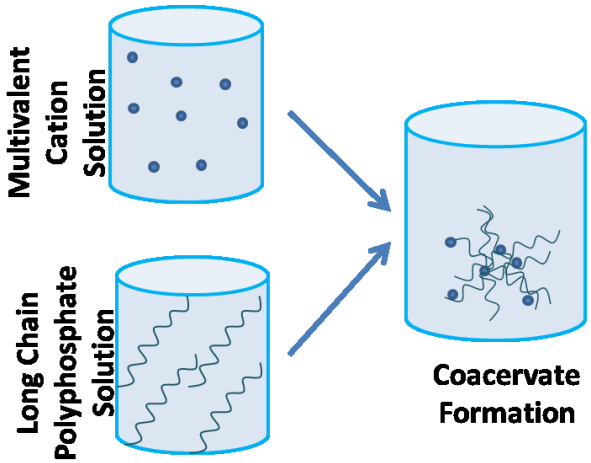

Figure 6.1 Schematic of the setting reaction in polyphosphate liquid embolic system.

In this chapter, the effect of NaPP $\overline{D_p}$, NaPP concentration, and barium and/or strontium content on the radiopacity, injectability and cytocompatibility of the resulting coacervates was evaluated and an optimum formulation selected as a precursor to an *in* vivo

biocompatibility and proof-of-principle pilot animal study performed by another member of the research group; only the key findings from this *in vivo* study will be discussed.

We believe that the liquid embolic system being developed here also has the potential to deliver and release drugs locally in procedures such as trans-arterial chemoembolization (TACE). In TACE, a biomaterial is administered directly into blood vessels feeding a tumor thereby blocking its nutrient supply and also releasing chemotherapeutics locally [199]. To this end, the capacity for loading and release of a chemotherapeutic, doxorubicin (Dox), from this polyphosphate *in situ* forming system was also evaluated. One major disadvantage of chemotherapy is the adverse side effects of anti-cancer drugs caused by widespread systemic exposure, making localized delivery a very desirable method for treating these chronic illnesses. An additional objective considered independently here, then, was to demonstrate the capability of an optimized calcium polyphosphate (CPP) coacervate to be loaded with an anti-cancer drug (Dox) that can subsequently be released in a sustained manner.

To optimize this system, experimental design methods were used. When employing such methods, theoretically all variables that can affect properties of the final product may be included in the experimental design. However, in order to limit this effort to a reasonable number of experiments, investigators must first identify the potentially dominant variables together with the key properties that they seek to optimize. Subsequently, the joint effect of these dominant variables on these key properties can be tested by a response surface method. With this method, the objective is to find a desirable location in the design space defined by the range of variables. A series of formulations are prepared within this design space and their key properties are measured. Then a surface model,

usually quadratic, is fitted by the software to these collected data. Using this fitted model, the optimum formulation that satisfies our target properties the best can be identified. There are several commercial software programs that are used to design experiments, including MODDE (Umetrics) and Design-Expert® (StatsEase); the latter is employed here for these optimization studies.

6.3 Materials & Method

6.3.1 Starting Materials

All starting materials including NaPPs were freshly produced and characterized as described in section 3.3.1 of Chapter 3.

6.3.2 Experimental Design & Optimizing Formulations

Using Design-Expert® V9 by StatsEase software, three design spaces were developed for three distinct NaPP $\overline{D_p}$ values designated as short (190±1), medium (9.6±0.4 E+03) and long (1.9±0.2 E+04). Each design space had 20 design points (15 distinctive formulations and 5 replicates) to assess the effect and significance of three variables: Ba and Sr contents and NaPP concentration on the viscosity of the NaPP solutions, the radiopacity and cytocompatibility of the resulting coacervates. These variables, their ranges and constraints are shown in Table 1. An IV-optimal design, which seeks to minimize the integral of the prediction variance across the design space, was used to determine the design points. After results were collected, Design Expert was used to determine whether a linear, two-factor-interaction or a quadratic model best fit the data. The significance of each variable was then determined by an ANOVA analysis of the model.

The optimum formulation was chosen by Design-Expert® using numerical optimization; a weight is assigned to each goal (i.e. increasing radiopacity and decreasing viscosity and cytotoxicity) to adjust the shape of its particular desirability function, and the importance of each goal is adjusted in relation to the other goals through a power function. The goals are then combined into an overall desirability function and the software numerically seeks to maximize this function to find the optimum formulation.

Table 6.1 The details of the three design spaces representing three different NaPP $\overline{D_p}$.

	Design Space 1	Design Space 2	Design Space 3
NaPP	Short	Medium	Long
NaPP $\overline{D_p}$	190±1	9.6±0.4 E+03	1.9±0.2 E+04
Variable A: NaPP concentration (g/100 mL)	3-15	3-12	3-10
Variable B: Strontium to phosphorus molar ratio (%)	0-15	0-15	0-15
Variable C: Barium to phosphorus molar ratio (%)	0-15	0-15	0-15
Constraints (mol %)	0≤B+C≤15	0≤B+C≤15	0≤B+C≤15

6.3.3 Preparing Formulations

145.1 mg of NaPP was dissolved in water and 1 M Sr, Ba and Ca solutions (prepared from their chloride salts) were added to obtain the required formulation reaching 15% (Ca+Sr+Ba)/P molar ratio. At this molar ratio the solution remains clear after mixing for 24 hr, as the NaPP chains only chelate these cations. The desired NaPP concentration was then reached by adjusting the final volume by water, resulting in the preloaded NaPP solution. To form the coacervates, 1 M Ca solution was then added to the preloaded NaPP solution, reaching a 50% divalent cation/phosphorus molar ratio that ensures coacervation.

6.3.4 Measuring the viscosity of preloaded NaPP solution

In the clinic, liquid embolic systems are injected through microcatheters; therefore the viscosity of embolic systems is extremely important. The viscosity of the NaPP solutions was determined to ensure delivery through a catheter in the clinical setting, due to the

polymeric nature of NaPP. Here, viscosity of the preloaded solutions to 15% divalent cation/phosphorus molar ratios was determined using a DV3 cone-plate rheometer (Brookfield, USA) at 25°C over a shear rate range of 30-750 s^{-1}.

6.3.5 Measuring the radiopacity of coacervate

Coacervates were packed into a 1.82 mm deep circular mould (8 mm in diameter) that was custom-produced using polysiloxane. A digital x-ray image (Belmont PHOT-XII x-ray system) was taken of the mould containing the coacervates alongside an aluminum step wedge with step sizes of 0.5 mm. Brightness of the discs and reference step wedge was measured using Image Pro®-Plus v. 6.0 software (Media Cybermetics). The average brightness of each coacervate was determined and referenced to the measured brightness of known thicknesses of aluminum. The radio-opacity of a 1.82 mm thick coacervate was reported as an equivalent thickness of aluminum.

6.3.6 Determining the composition of coacervate

Coacervates used for x-ray imaging were dissolved in 200 mM EDTA at a pH of 10. EDTA was added at 1.2 moles for each mole of divalent cation. Following dissolution, the amount of Ca, Sr, Ba and P were determined using inductively coupled plasma-optical emission spectroscopy (ICP) (Optima 7300 V ICP-OES, PerkinElmer Instruments, USA), with the ratio of divalent cation to phosphorus reported in molar ratio.

6.3.7 Measuring the cell viability of coacervate extracts

A MTT assay was performed to determine cell viability upon exposure to ions released into solution from the coacervate [200]. To prepare the ion-containing extracts, each

coacervate prepared in section 6.3.3 was placed in 2 mL Dulbecco's Modified Eagle's Medium (DMEM) supplemented with 5% calf serum for 24 h at 37°C. The pH of the extracts was then adjusted to pH 7.0 by addition of 1 M NaOH. Extracts were filter-sterilized through a 0.22 μm filter immediately before use in MTT assays. NIH/3T3 mouse embryonic fibroblasts between passages 20 and 30 were used for MTT assays. 2000 cells were plated in 200 μL of DMEM per well in 96-well plates and maintained at 37°C and 10% CO_2. After 24 h, media was removed from wells and replaced with 220 μL of extract. All samples were tested in triplicate. Dimethyl sulfoxide (DMSO) and DMEM served as negative and positive controls for the assay, respectively. After 24 h exposure to the extracts at 37°C and 10% CO_2, 22 μL of a 5 mg/mL solution of MTT in PBS was added to each well. After 3 hours incubation at 37°C and 10% CO_2, all media were removed from wells and 100 μL DMSO was added to each well. The 96-well plate was then wrapped in aluminum foil for light protection and placed on a shaker for 5-10 mins until MTT crystals had completely dissolved; absorbance was subsequently measured at 492 nm on Synergy™ HT microplate reader (BioTek®). The cytocompatibility for each extract is reported in the percent change from the positive control, DMEM without extract.

6.3.8 Evaluating doxorubicin loading and release from in situ forming calcium polyphosphate coacervates

Dox, used routinely for TACE, was chosen as the model drug for this study. Dox was added to the NaPP solution (preloaded to 20% Ca/P molar ratio) and then calcium chloride solution was mixed with this polyphosphate solution to form a coacervate instantly with some excess fluid on top. The first objective of this study was to optimize

the system by minimizing the amount of free drug in the excess fluid. Using Design-Expert® software, a surface model analysis was developed with 25 design points to assess the effect and significance of NaPP $\overline{D_p}$ (short = 272, medium = 1.0E+04, and long = 2.4E+04), NaPP concentration (3-10 g/100mL), Dox concentration (0.02-0.4 mg/mL) and overall calcium to phosphorus molar ratio (35-50%) on the ability of the coacervate to trap the highest percentage of the drug (%drug loading). Subsequently, long-chain and short-chain formulations with optimum drug loading capability were selected for use in a drug release study at 37°C in 0.05 M TRIS buffer saline (pH 7.4 at 37°C) on an orbital shaker at 100 rpm. At each time point, 4 mL of the 5 mL of buffer (added following removal of the excess fluid) was removed for analysis and replaced with 4 mL of fresh buffer. Dox cumulative release is reported after correcting for the 1 mL of the buffer that remained. Dox loading and release were determined by measuring solutions for absorbance at 480 nm using Synergy™ HT microplate reader (BioTek®). The absorbance spectrum of the released drug was also scanned using Helios-α spectrophotometer (Thermospectronic®) in the range of 350-600 nm to evaluate drug stability.

6.4 Results

6.4.1 Composition of coacervates

Coacervates were successfully formed over the entire range of compositions specified by the design space. The appearance of the coacervates varied with composition, from clear and soft, to white and tough. Representative images of two types of coacervates are shown in Figure 6.2a. Similar to results from previous studies, the experimental composition of the coacervates demonstrated consistently lower cation content than

theoretical values (Tables 6.2, 6.3 and 6.4). Coacervates form at a range of divalent cation to phosphorus molar ratios between 30-40%, depending largely on the NaPP $\overline{D_p}$ and concentration, as discussed in Chapter 3. Presumably, the excess divalent cations not incorporated into the coacervate during formation remain in the excess solution.

6.4.2 Radiopacity of coacervates

Radiopacity is a required design parameter, as embolic procedures are carried out with fluoroscopic guidance. Incorporating barium and strontium was found to increase the radiopacity of the coacervates overall (Tables 6.2, 6.3 and 6.4), with samples at higher Sr/P or Ba/P molar ratios exhibiting more radiopacity, as shown in Figure 6.2b. These results were used to create a predictive model in DesignExpert® to determine the effect of barium and strontium incorporation on radiopacity, an example of which is shown in Figure 6.3a for the medium chain design space using a two factor interaction model. Based on ANOVA, the radiopacity was only significantly affected by the Sr/P and Ba/P molar ratios for medium and long chain NaPP; with short chain systems the effect of NaPP concentration was also found to be significant. The effect of Ba/P molar ratio was more prominent than Sr/P molar ratio on radiopacity of the coacervates as shown in Figure 6.3a, an anticipated outcome given its higher atomic number.

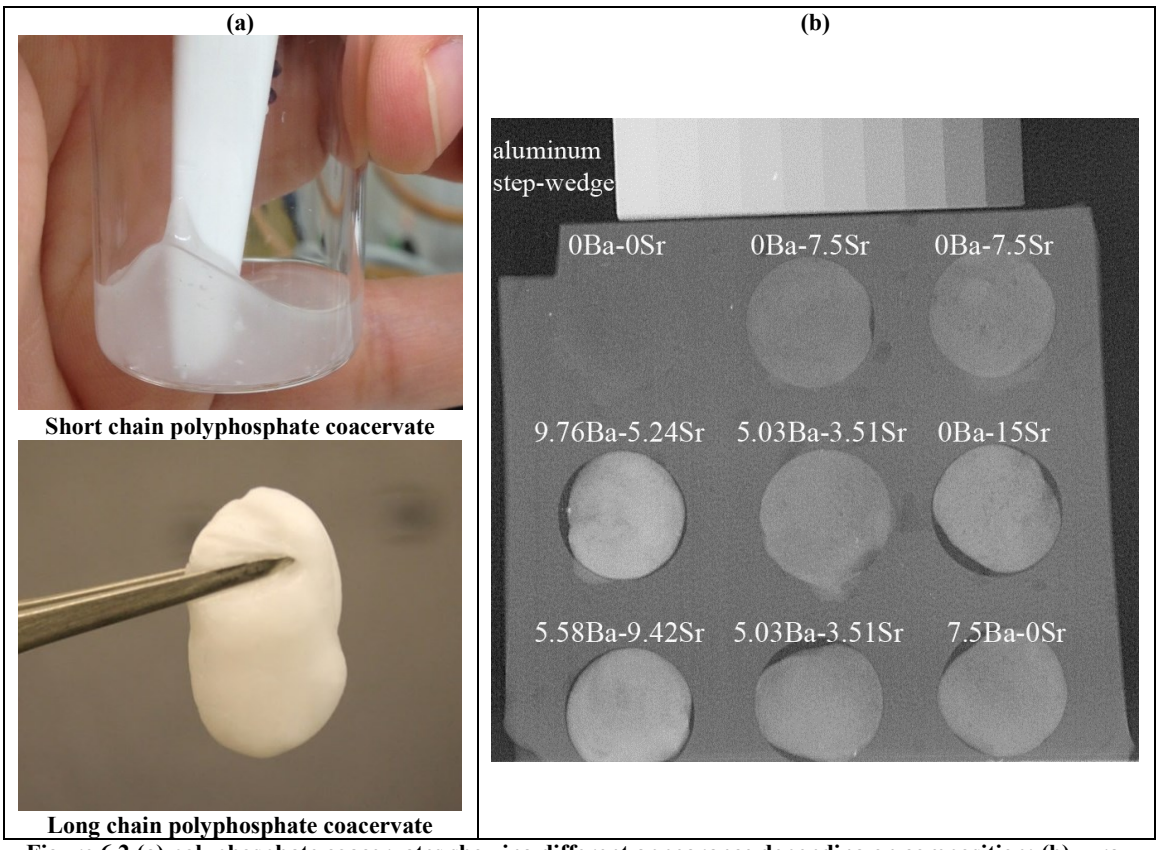

Figure 6.2 (a) polyphosphate coacervates showing different appearance depending on composition; (b) x-ray image of coacervates and dependence of radiopacity to composition (brighter samples are more radiopaque).

Table 6.2 Short chain design space 1; Theoretical and experimental composition of the samples and their viscosity, radiopacity and cell viability values.

Sample	NaPP concentration (g/100mL)	Theoretical coacervate composition			Experimental coacervate composition			Viscosity of preloaded NaPP solution (cP)	Radiopacity of coacervate (mm Al)	Cell viability (%)
		Ca/P mol%	Sr/P mol%	Ba/P mol%	Ca/P mol%	Sr/P mol%	Ba/P mol%			
S1	3.0	50.0	0	0	33.5	0	0	1.24	1.28	-19.6
S2	15.0	50.0	0	0	37.7	0	0	2.65	1.27	-26.3
S3	9.6	43.6	6.4	0	32.7	5.8	0	1.73	2.03	-30
S4	9.6	43.6	6.4	0	32.4	5.9	0	1.76	2.03	-19.2
S5	9.6	43.6	6.4	0	30.2	5.7	0	1.74	1.97	-26.5
S6	3.0	40.0	10	0	26.0	9.4	0	1.21	2.10	-6.9
S7	6.2	35.0	15.0	0	N/A	N/A	N/A	1.50	2.38	-30
S8	15.0	35.0	15.0	0	19.9	14.3	0	2.54	2.72	-9.0
S9	15.0	38.4	7.1	4.5	25.0	6.7	4.3	2.57	2.17	-13.2
S10	15.0	38.4	7.1	4.5	24.7	6.4	4.1	2.47	2.45	-7.9
S11	8.9	35.0	9.0	6.0	18.1	8.4	5.7	1.65	2.32	-5.3
S12	8.9	35.0	9.0	6.0	21.8	8.4	5.9	1.63	3.26	-11.1
S13	3.0	42.6	0	7.4	N/A	N/A	N/A	1.21	2.79	-2.4
S14	13.2	42.5	0	7.5	29.9	0	7.1	2.16	2.22	-16.0
S15	13.2	42.5	0	7.5	29.1	0	7.1	2.10	2.57	1.6
S16	3.0	35.0	7.5	7.5	25.7	7.2	7.3	1.20	3.77	5.7
S17	7.1	35.1	4.6	10.3	19.3	4.2	9.5	1.51	3.20	2.2
S18	10.1	37.2	0	12.8	N/A	N/A	N/A	1.77	3.08	-7.7
S19	3.0	35.0	0	15.0	N/A	N/A	N/A	1.21	4.12	-3.4
S20	15.0	35.0	0	15.0	N/A	N/A	N/A	2.59	3.15	-16.4

Table 6.3 Medium chain design space 2; Theoretical and experimental composition of the samples and their viscosity, radiopacity and cell viability values.

Sample	NaPP concentration (g/100mL)	Theoretical coacervate composition			Experimental coacervate composition			Viscosity of preloaded NaPP solution (cP)	Radiopacity of coacervate (mm Al)	Cell viability (%)
		Ca/P mol%	Sr/P mol%	Ba/P mol%	Ca/P mol%	Sr/P mol%	Ba/P mol%			
M1	3.0	50.0	0	0	32.2	0	0	5.79	1.49	-19.2
M2	8.0	50.0	0	0	36.4	0	0	11.55	1.67	-22.0
M3	12.0	50.0	0	0	34.4	0	0	19.62	1.56	-28.5
M4	3.0	42.5	7.5	0	29.0	7.2	0	7.05	2.27	-10.8
M5	3.0	42.5	7.5	0	30.9	6.8	0	7.29	2.08	-8.4
M6	3.0	35.0	15.0	0	24.9	13.2	0	8.40	3.24	-12.0
M7	12.0	35.0	15.0	0	19.9	12.9	0	28.29	2.88	-28.9
M8	12.0	40.2	7.5	2.3	28.3	6.0	1.6	22.13	2.56	-16.5
M9	6.1	41.5	3.5	5.0	27.6	3.0	4.1	10.24	3.06	-5.3
M10	6.1	41.5	3.5	5.0	27.4	3.0	4.5	9.99	2.63	-1.1
M11	6.1	41.5	3.5	5.0	25.6	3.2	3.6	8.37	2.29	-8.5
M12	4.2	35.0	9.4	5.6	24.7	7.9	5.0	9.69	4.05	-1.1
M13	8.0	35.0	9.4	5.6	24.8	8.0	5.2	14.86	4.39	-8.2
M14	8.0	35.0	9.4	5.6	21.3	8.1	4.9	14.22	3.92	-16.3
M15	3.0	42.5	0	7.5	31.0	0	7.2	7.17	2.78	-12.3
M16	10.2	42.5	0	7.5	22.7	0	6.1	14.80	2.80	-3.5
M17	10.2	42.5	0	7.5	25.3	0	7.2	15.72	2.70	1.6
M18	3.0	35.0	5.2	9.8	23.1	5.2	9.5	7.63	4.86	-4.6
M19	5.3	35.0	0	15.0	18.7	0	12.6	8.77	3.36	-27.1
M20	12.0	35.0	0	15.0	14.1	0	14.9	25.07	4.22	-14.0

Table 6.4 Long chain design space 3; Theoretical and experimental composition of the samples and their viscosity, radiopacity and cell viability values.

Sample	NaPP concentration (g/100mL)	Theoretical coacervate composition			Experimental coacervate composition			Viscosity of preloaded NaPP solution (cP)	Radiopacity of coacervate (mm Al)	Cell viability (%)
		Ca/P mol%	Sr/P mol%	Ba/P mol%	Ca/P mol%	Sr/P mol%	Ba/P mol%			
L1	3.0	50.0	0	0	28.6	0	0	4.37	1.49	-14.8
L2	6.5	50.0	0	0	33.7	0	0	5.21	1.51	-23.7
L3	10.0	50.0	0	0	21.2	0	0	6.27	1.68	-25.4
L4	6.5	42.5	7.5	0	27.9	6.7	0	7.28	1.92	-17.4
L5	6.5	42.5	7.5	0	27.0	6.2	0	8.12	2.20	-12.7
L6	6.5	42.5	7.5	0	30.1	6.2	0	8.05	2.17	-7.6
L7	3.0	35.0	15.0	0	15.3	12.9	0	19.77	2.64	-31.4
L8	10.0	35.0	15.0	0	18.4	12.6	0	58.54	2.64	-28.0
L9	3.4	37.8	8.4	3.8	N/A	N/A	N/A	15.40	3.03	-14.4
L10	10.0	40.0	4.9	5.1	25.4	4.5	3.9	12.72	2.64	-12.5
L11	10.0	40.0	4.9	5.1	26.2	4.2	4.2	10.65	2.10	-10.6
L12	6.5	42.5	0	7.5	27.4	0	6.2	7.74	2.41	-10.8
L13	6.5	42.5	0	7.5	29.7	0	6.1	9.42	2.42	3.6
L14	6.5	35.0	7.4	7.6	N/A	N/A	N/A	36.47	3.36	-17.2
L15	6.5	35.0	7.4	7.6	18.8	6.7	6.4	36.24	3.44	-15.0
L16	3.0	40.6	1.8	7.6	28.2	1.8	6.3	11.26	2.70	-5.3
L17	8.9	38.0	2.1	9.9	21.0	2.2	8.1	18.31	2.97	-8.1
L18	5.6	35.0	1.9	13.1	27.0	1.6	13.3	32.11	3.66	-22.7
L19	3.0	35.0	0	15.0	20.8	0	14.7	23.37	3.55	-27.5
L20	10.0	35.0	0	15.0	17.6	0	13.2	67.05	3.40	-31.6

6.4.3 Viscosity of preloaded NaPP solution

The viscosities of 15% preloaded NaPP solutions were determined (Tables 6.2, 6.3 and 6.4) and the results modeled in DesignExpert®. Based on ANOVA, viscosity was significantly impacted by all three design variables (Ba/P, Sr/P and NaPP concentration). However, as could be seen in Figure 6.3b, NaPP concentration had a greater impact on viscosity than the type of divalent cation. The viscosity was also found to be highly dependent upon the NaPP $\overline{D_p}$; the highest viscosity for short, medium and long chain samples were 2.65, 28.29 and 67.05 cP, respectively. Nevertheless, all of the solutions tested in this study are easily injectable through available commercial catheters, which are able to inject solutions with viscosities up to 120 cP at an acceptable flow rate [201]. One should note that the viscosity of a NaPP solution that has not been preloaded with divalent cations is much higher; for instance, the viscosity of the longest chain NaPP (design space 3) at a concentration of 10% g/mL is over 2000 cP when it is not preloaded with divalent cations.

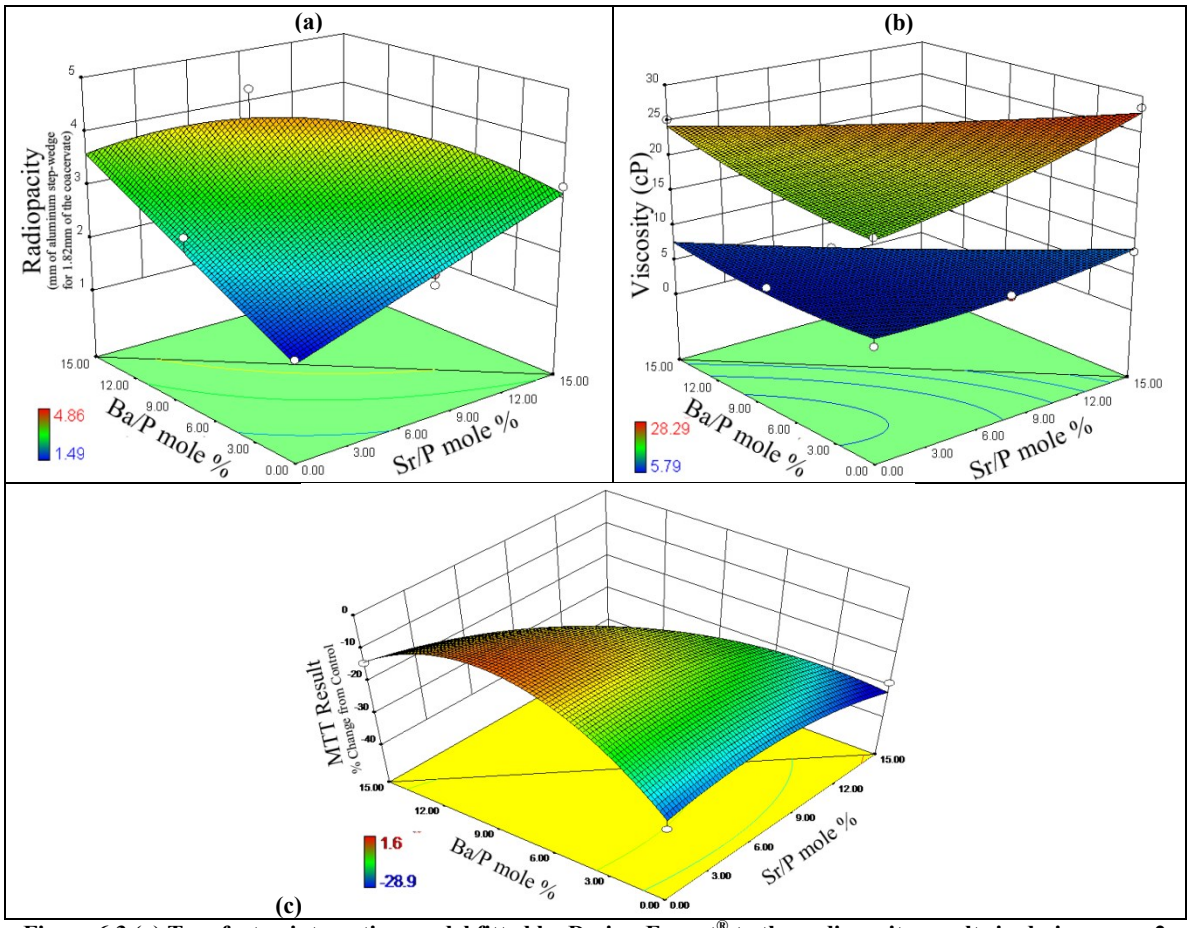

Figure 6.3 (a) Two-factor-interaction model fitted by Design-Expert® to the radiopacity results in design space 2 (Medium chain) at a fixed [NaPP] of 3% g/mL; (b) Quadratic models fitted by Design-Expert® to the viscosity results in design space 2 at a fixed [NaPP] of 3% and 12% g/mL, lower and upper 3D surfaces, respectively; (c) Quadratic model fitted by Design-Expert® to the MTT results in design space 2 at a fixed [NaPP] of 12% g/mL.

6.4.4 Cell viability in presence of coacervate extracts

Cell viability in the presence of coacervate extracts was measured as a percentage change from the positive control, DMEM, and is reported in Tables 6.2, 6.3 and 6.4. Most of the 24 hr extracts were not cytotoxic, as defined by ISO 10993-5 where an extract is deemed to be cytotoxic if the viability is reduced to < 70% of the control [200]. For all three design spaces, MTT results showed that increasing the Ba/P molar ratio significantly increased the cell viability of coacervates, an example of which is shown in Figure 6.3c for the medium chain coacervates (design space 2). In contrast, the Sr/P molar ratio did not have a significant effect except in the long chain samples where cytocompatibility

decreased in higher Sr content samples. The effect of NaPP concentration on cell viability was not significant for any of design spaces. The highest cytocompatibility was achieved around 9% Ba/P for medium and long chain coacervates and at the highest Ba/P of 15% for the short chain coacervates.

6.4.5 Optimized liquid embolic formulation

The optimal liquid embolic formulation must be safe for patients, easy for clinicians to deliver and visible during fluoroscopic procedures. To achieve this, our polyphosphate embolic agent must have maximum radiopacity and minimum cytotoxicity. Viscosity was found not to restrict the polyphosphate embolic design as all preloaded NaPP solutions had viscosities suitable for use in commercial microcatheters. In addition, a high NaPP concentration is preferred because the resulting coacervate *in situ* is more cohesive and resistant to disintegration in high flow environment such as inside of arteries. Consequently, the goals chosen in DesignExpert® to maximize radiopacity and cell viability were both set to an importance power of 5 and the goal to maximize NaPP concentration was set to a lower importance power of 3. The optimum formulations for each of the long, medium and short design space determined by the software from these set goals are reported in Table 6.5 with their predicted viscosity, radiopacity and cell viability values. The optimal long chain formulation was chosen for animal studies as preliminary tests *in vitro* showed they had higher cohesiveness after forming *in situ* when delivered by a dual-lumen syringe. This optimum long chain formulation was prepared and its radiopacity, viscosity and cell viability were measured. Experimental results corresponded strongly with predicted values (Table 6.5), lending support to the effectiveness and accuracy of the fitted models for navigation through the design space.

Table 6.5 Optimized formulations of the three design spaces; Experimental composition, viscosity, radiopacity and cell viability values were only tested for the Long chain optimized formulation.

NaPP D_p	NaPP concentration (g/100mL)	Theoretical coacervate composition			Experimental coacervate composition (n=3)			Viscosity of preloaded NaPP solution (cP)		Radiopacity of coacervate (mm Al)		Cell viability (%)	
		Ca/P mole%	Sr/P mole%	Ba/P mole%	Ca/P mole%	Sr/P mole%	Ba/P mole%	Predicted	Experimental (n=3)	Predicted	Experimental (n=3)	Predicted	Experimental (n=5)
Long	9.5	38.8	2.2	9.0	20.2 ±2.1	1.9 ±0.4	8.4 ±1.1	25.24	31.33 ±6.72	2.86	2.95 ±0.18	-11.1	-12.7 ±4.3
Med.	12.0	35.0	5.2	9.8	N/A	N/A	N/A	24.93	N/A	4.47	N/A	-6.2	N/A
Short	15.0	35.0	0.0	15.0	N/A	N/A	N/A	2.56	N/A	3.39	N/A	-3.7	N/A

6.4.6 Doxorubicin loading and release from in situ forming calcium polyphosphate coacervates

Table 6.6 shows the drug loading results obtained with the prepared samples. The weight percentage of Dox trapped inside the coacervates varied from 0 to near 100% depending on the formulation. These results were used to create a predictive model in DesignExpert® to determine the effect of NaPP $\overline{D_p}$, [NaPP], [Dox] and overall calcium to phosphorus molar ratio on the %drug loading of the resulting coacervates. Based on ANOVA, all four variables were found to significantly affect the %drug loading (p value < 0.003), with NaPP $\overline{D_p}$ and [Dox] being the most significant variables (p value < 0.0001). Figure 6.4 shows the quadratic model that was fitted to the experimental data representing the %drug loading against these two variables. Increasing the NaPP $\overline{D_p}$ and decreasing the [Dox] both lead to decreased %drug loading.

Table 6.6 Different *in situ* forming CPP samples that were prepared by changing 4 variables and weight percentage of Dox that is trapped inside the coacervate.

Sample	Variables				Response
	NaPP Dp	[NaPP] (g/100mL)	[Dox] (mg/mL)	Ca/P mol%	%drug loading
1	23500	6.25	0.02	36.8	0
2	272	3	0.02	35	71.4
3	23500	3	0.4	35	49.4
4	272	3	0.21	42.5	93.1
5	272	6.85	0.4	35	94.9
6	10000	6.43	0.2	35	17.9
7	10000	6.43	0.2	35	28.4
8	10000	8.95	0.14	50	47.4
9	23500	10	0.02	50	0
10	272	3	0.4	50	93.5
11	272	3	0.21	42.5	90.6
12	272	10	0.31	50	77.5
13	23500	3	0.02	50	0
14	23500	10	0.4	35	49.3
15	23500	6.5	0.4	50	47.7
16	23500	6.5	0.4	50	48.3
17	272	6.42	0.02	50	0
18	10000	4.26	0.19	50	12.7
19	10000	5	0.4	42.58	40.3
20	272	9.79	0.24	39.11	86.5
21	10000	10	0.4	43.25	46.2
22	23500	6.25	0.02	36.8	0
23	10000	5	0.4	42.58	42.9
24	272	10	0.02	35	29.5
25	272	10	0.04	44.46	7.9

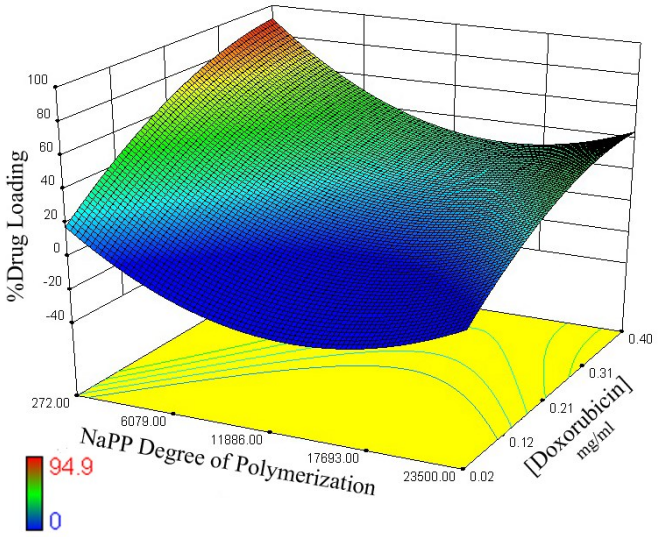

Figure 6.4 %Drug loading model produced by Design-Expert® for fixed [NaPP] of 6.5 g/100mL and Ca/P molar ratio of 42.5%.

A short-chain ($\overline{D_p}$ of 272) and a long-chain ($\overline{D_p}$ of 2.4E+04) NaPP sample was subsequently used to observe how different molecular weights impact the drug release profile. The software generated the highest %drug loading conditions for each of these

chain lengths based on the fitted model (Table 6.7). For short-chain coacervates the model predicted 100% drug-loading and, when tested, 97±0.2% drug retention was observed (n=3). Similarly, for long-chain coacervates, excellent agreement was found between the predicted drug loading (53%), and the value of 53±2% obtained (n=3).

Table 6.7 Optimized samples and their predicted and experimental %drug loading.

NaPP D_p	[NaPP] (g/100mL)	[Dox] (mg/mL)	Ca/P mol%	Predicted theoretical drug loading (%)	Actual experimental drug loading (%) (n=3)
Long chain-23500	3	0.34	42.17	53	53±2
Short chain-272	3	0.4	35	100	97±0.2

The release behaviors of these two sample groups were studied in triplicate in TRIS buffer saline at 37°C. Figure 6.5 describes the release profile of the long chain and short chain samples. Over a period of roughly 220 hr, long chain coacervates released 81% of their drug depot, while for short chain samples approximately 74% was released after 145 hours. In both formulations release reached a plateau at around 80%; the remaining drug% was found to be inside the aged coacervates when they were subsequently dissolved by EDTA. Overall, drug release was more variable for the long chain samples compared to the short chain coacervates.

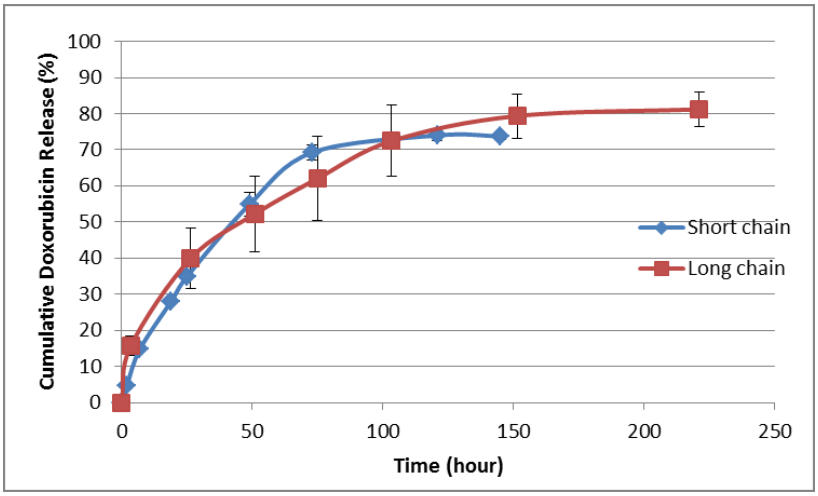

Figure 6.5 Cumulative Dox release from samples optimized for drug loading (n=3).

Figure 6.6 chronicles physical changes in a long chain sample at different time intervals. Over time, the sample gradually lost its red colour indicative of Dox loading as the drug was being released.

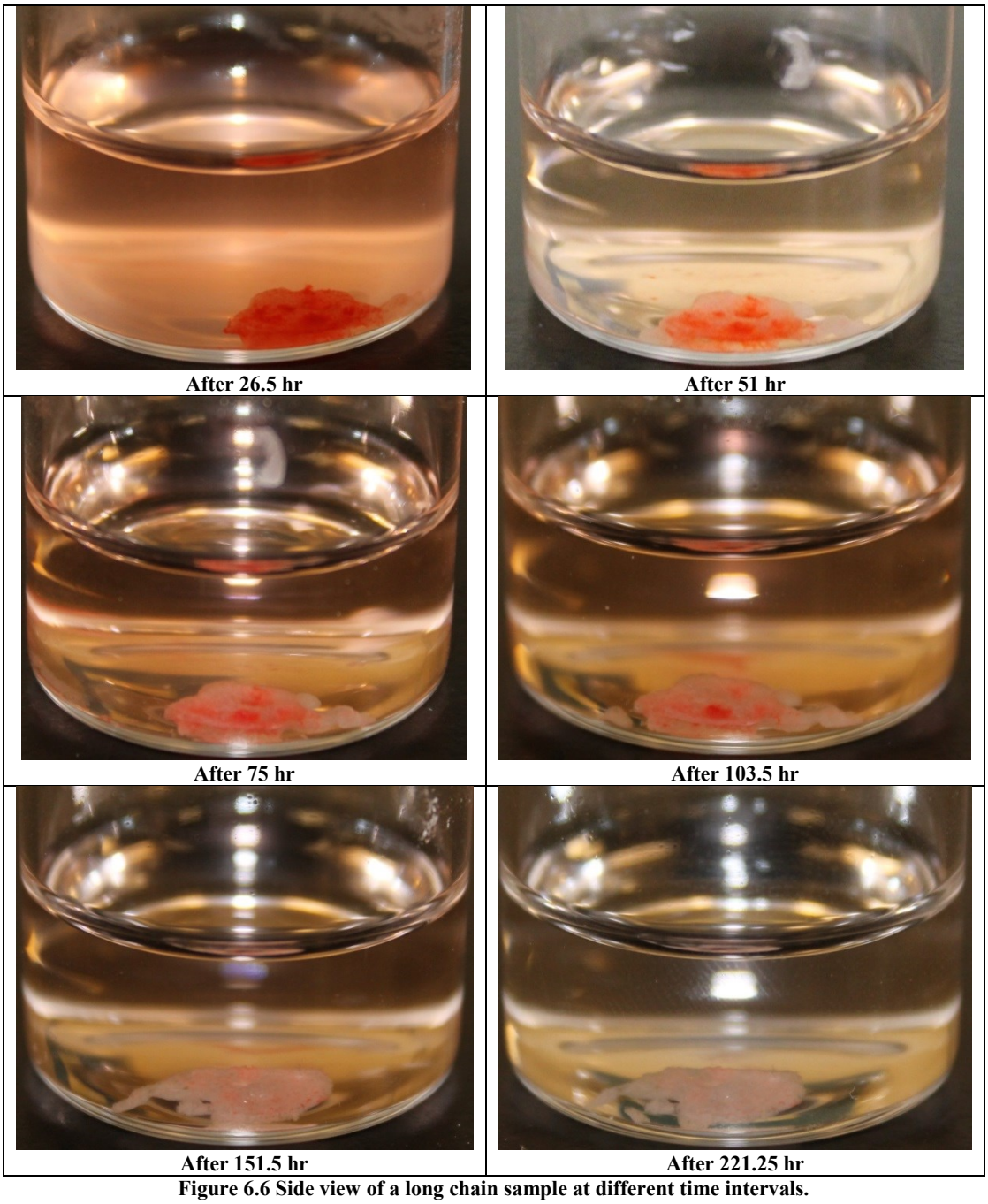

Figure 6.6 Side view of a long chain sample at different time intervals.

Dox is reported to degrade slowly, with the rate of degradation dependent on pH and temperature [202]. Generally speaking, the recommended shelf life of Dox solution for

chemotherapy is just 48 hr [202]. In our experiments the eluted Dox was rather stable based on comparable absorbance spectra of the eluted drug samples compared to a 20 ppm as-prepared Dox solution maintained in TRIS buffer saline under identical conditions (Figure 6.7). For both eluted and as-prepared Dox, a peak at around 575 nm can be seen to grow larger over time, indicative potentially of inevitable slow degradation of Dox that is not directly related to the drug loading process or coacervate interaction.

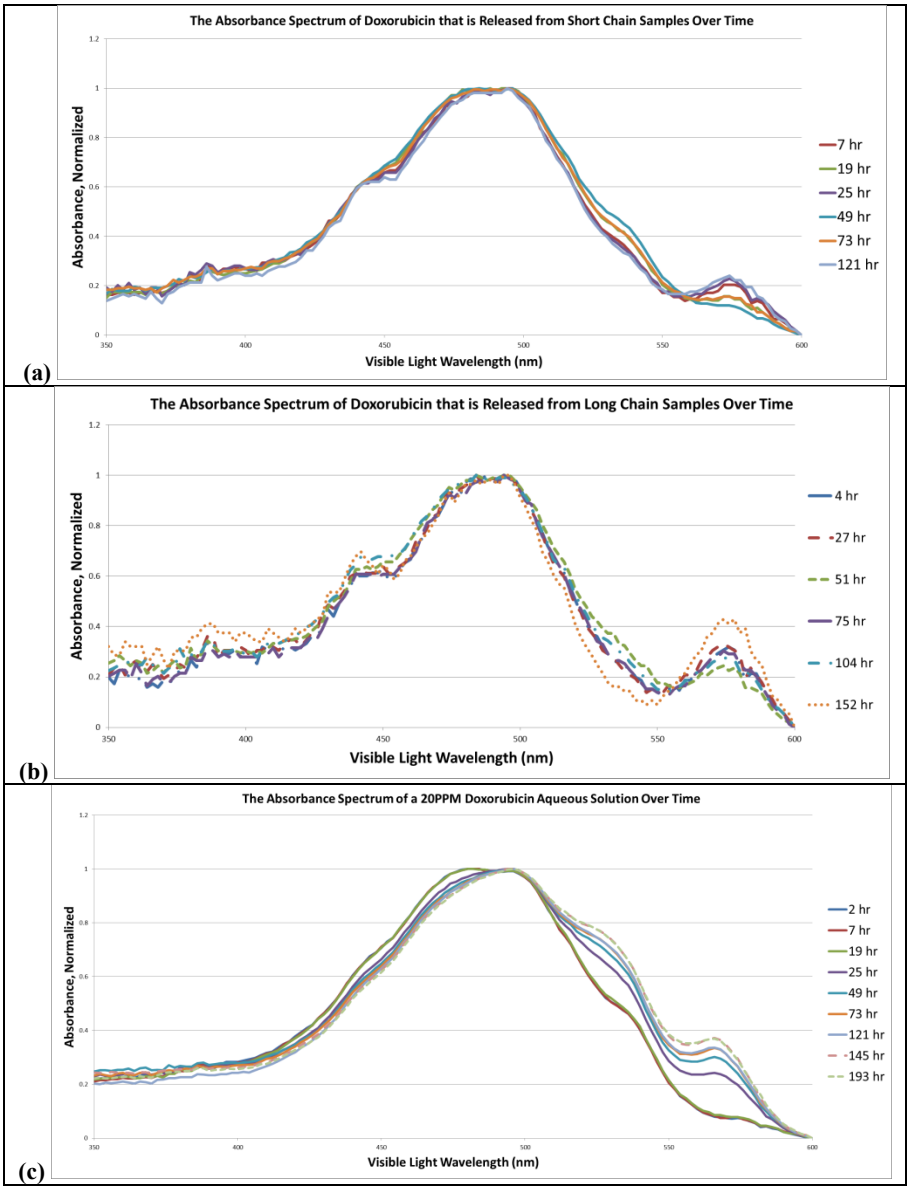

Figure 6.7 Normalized absorbance spectra of Dox at different time intervals: (a) Dox that is released from short chain samples; (b) Dox that is released from long chain samples; (c) an as-prepared 20 ppm Dox solution maintained under identical conditions.

6.5 Discussion

The first objective in this chapter was to optimize an intrinsically radiopaque liquid embolic system based on NaPP and divalent cation solutions. Key to this optimization was the introduction of Ba and Sr to the system to enhance radiopacity as Ca-only coacervates do not have sufficient radiopacity. The role of NaPP concentration and NaPP $\overline{D_p}$ in optimizing key physical properties such as viscosity which directly affect injectability was also assessed.

Since liquid embolic agents are injected through very thin catheters, low viscosity is critical. Here, NaPP solution was intentionally preloaded with divalent cations. Divalent cation chelation by polyphosphates reduces the viscosity of NaPP solutions significantly (see Chapter 3, section 3.4.3). This reduction in viscosity is basically the result of a decrease in polyphosphate negative charge as it chelates cations. Viscosity measurements confirmed that all preloaded polyphosphate solutions prepared here are injectable through available catheters, which are able to inject solutions with viscosities up to 120 cP [201].

Addition of Sr and Ba to this CPP liquid embolic agent significantly improves its radiopacity, distinguishing this system from other available embolic agents that require contrast agents. Nevertheless, there was some concern with the level of cytotoxicity that might be induced by virtue of having Ba and Sr in the system. Paradoxically, MTT results showed that replacing Ca with Ba or Sr improved the cytocompatibility of the coacervates. This observation is likely attributed to the higher stability of Ba or Sr loaded coacervates, as has already been noted in other degradation rate studies (Chapter 4).

After evaluating 60 different formulations and fitting models to the obtained data within the three design spaces, the software suggested the best formulations for each of the design spaces. A focus was placed especially on an optimal *long chain* formulation from Table 6.5, owing not only to its high radiopacity, acceptable viscosity and cytocompatibility, but also to an ability to produce a more cohesive coacervate from these long-chain PPs, particularly at high [NaPP]; a cohesive coacervate would be expected to be advantageous under a high flow environment such as that experienced inside arteries.

This optimal formulation was evaluated in a proof-of-principle embolization of the central artery of the rabbit ear by another member of our group. Embolization of the central artery was achieved by insertion of a lab-made dual lumen syringe into the auricular artery and injection of both solutions of the two-part embolic agent (preloaded NaPP and $CaCl_2$ solutions). The central artery became white distal from the tip of the needle, and the tissue became blanched for at least 1 cm on either side of the vessel (Figure 6.8a), with the vessel itself becoming firm to the touch. This visually confirmed the successful occlusion of the artery with the embolic agent. Later, the location of the coacervate was confirmed by x-ray imaging (Figure 6.8b). Due to the good radio-opacity of the coacervate, the auricular artery is clearly visible as was distal penetration of the embolic agent into small, contiguous arteries.

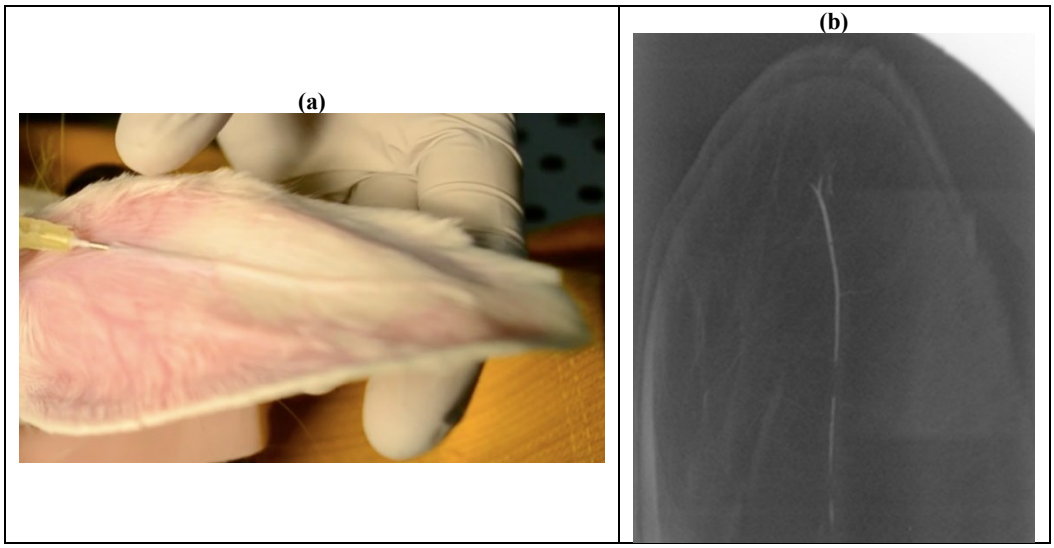

Figure 6.8 (a) Injection of embolic material into the auricular artery with polyphosphate embolic agent; (b) x-ray image of rabbit ear after the embolization showing the location of the embolic agent within the vessel (Images are courtesy of Esther Valliant).

Overall the liquid embolic system developed here is injectable, radiopaque and cyto-compatible, with further *in vivo* studies showing the potential of this system to effectively embolize blood vessels. However, there are several key problems that should be addressed if this system is to be developed into a viable commercial product. As discussed in Chapter 4, there is no cross-linking in divalent cation-polyphosphate coacervates; only in the long chain coacervates does physical chain entanglement exist, accounting for their more cohesive properties and resistance to disintegration under the high flow environment inside arteries. Still, physical entanglement alone is likely not enough to achieve complete control on embolization; as one can see in Figure 6.8b, there are several gaps in the coacervated mass that has filled the artery. An ideal liquid embolic should be a uniform mass without any detachment. One suggestion here would be to use other multivalent cations with valency higher than 2, as they have been shown to chemically crosslink polyphosphates forming hydrogels [35, 79]. An alternative would be addition of other polymers such as chitosan to the polyphosphate system, which might change its physical characteristics, resulting in a more cohesive gel. The second issue to

address with this liquid embolic system is the rapid degradation of coacervates, as described more fully in Chapter 4. This rapid degradation limits this system to only those applications where temporary embolization is required, such as reducing blood supply to highly vascularized lesions before surgical obliteration, controlling a hemorrhage during a traumatic injury or in TACE. A third limitation to this system is the delivery device; this liquid embolic is comprised of two liquid components that should be delivered separately. Therefore, a dual lumen catheter is required which may prove difficult to handle during practice. Although an alginate-based liquid embolic agent has been developed based on a dual lumen device [194, 203], these types of devices have generally not gained much traction in the clinical community.

The second objective in this chapter was to demonstrate the capability of CPP coacervate to be loaded with Dox and to release it in a sustained manner. The results of this experiment were very positive. It was demonstrated that a CPP matrix can be loaded with Dox and this matrix broke down at a slow rate alongside the drug. These two properties may allow this material to be used to treat hepatocellular carcinoma more effectively than current approaches that rely on non-degradable drug delivery microspheres [204]. Dox solutions used for intravenous injection usually have a concentration of 2 mg/mL [202]. While the CPP system developed here has a lower [Dox] of ~0.5 mg/mL, it would deliver its entire contents locally unlike intravenous injection of Dox solution. It was evident that both chain lengths tested had their own strengths. Short chains can be loaded with a much higher percent of drug. On the other hand, long chains were more cohesive and provided longer release. The high drug loading ability of polyphosphate coacervates is probably related to an interaction between negatively charged polyphosphate and positively

charged Dox. Dox has an amine group with pKa of 8.2 [205], causing it to be positively charged under the conditions used in this study. This positive charge might have also affected the release profiles observed. The shape of release curves suggest that Dox release is probably diffusion-controlled.

In theory, a dual lumen device could be used to administer the drug loaded CPP into a tumor's blood supply. As the two components mix together, and enter smaller and smaller blood vessels, they will embolize the vessel. The drug that is not fully incorporated into the CPP matrix could provide an initial bolus of drug to the tumor. Future work should include testing the cytotoxic properties of the released drug to confirm its stability within a CPP matrix. Also, testing the loading and release process in an environment that simulates a human blood vessel would give a better feel for the practicality of this entire process. It would be also useful to consider chemotherapeutic delivery together with other properties such as radiopacity in an overall design approach moving forward.

6.6 Conclusion

Viscosity results confirm that polyphosphate solutions are injectable through available catheters. Addition of Sr and Ba to the CPP liquid embolic improved its radiopacity, and MTT results showed that these cations do not compromise the cytocompatibility of the coacervates. The optimum long chain embolic formulation was found to effectively block a rabbit auricular artery *in vivo*. Overall, a liquid embolic system based on NaPP and divalent cations does have potential but also it has its own limitations. Further studies should be carried out to address these limitations.

It was further demonstrated that an *in situ* forming CPP system can be predictably and efficiently loaded with Dox with a subsequent slow rate of release. This study established the potential of CPP coacervates as a drug delivery agent, inviting further future studies.

Chapter 7 Conclusion

7.1 Summary and conclusions

Using a variety of NaPPs and alkaline earth metal solutions, a series of polyphosphate coacervates with very interesting and unique characteristics were developed. The main objective of this thesis project was to contribute substantially to existing knowledge on how to prepare these coacervates, and to evaluate some of the key chemical and physical properties that are key to their application as a biomaterial and more specifically in hemostasis.

A comprehensive description of methods to synthesize NaPPs with different $\overline{D_p}$ from very basic ingredient was initially provided. These NaPP batches were used throughout this project to prepare polyphosphate coacervates in the presence of divalent cations. Prior to focusing on the bio-potential of these coacervates, it was deemed necessary to better understand this coacervation mechanism by carrying out some basic science studies of their formation and subsequent properties. The reactions between these polyphosphate solutions and three alkaline earth metals, namely Ca, Sr and Ba, were comprehensively studied by means of liquid ^{31}P-NMR, pH and viscosity measurements. The effect of cation chelation on polyphosphate chains in solution was evaluated and the exact amount of these cations to cause phase separation and coacervate formation was determined under different conditions. This knowledge was crucial to exacting control over coacervate formation.

The focus was then switched to the coacervate itself by characterizing some of the key physical properties, particularly those potentially critical to their use in clinical

applications. Degradation studies of polyphosphate coacervates prepared from different NaPPs and cations showed that they degrade at a fast rate, limiting them to short-term biomedical applications. Rheological studies further revealed that they possess very distinctive physical characteristics depending on the cation type and NaPP $\overline{D_p}$, allowing one to tweak their composition to achieve a desired physical property.

Due to the current interest on the role of polyphosphates in hemostasis, this project explicitly focused on the potential of these coacervates as a hemostatic agent. Polyphosphate coacervates were found to be an excellent candidate for hemostasis applications, decreasing clotting time significantly especially when very long chain polyphosphates were used. These coacervates could be used in situations where control of bleeding is ineffective or impractical by conventional procedures.

Lastly as a clinical application piece to this work, the potential of an *in situ* forming polyphosphate system as a liquid embolic agent and a drug delivery agent was investigated. A polyphosphate liquid embolic system with optimum radiopacity, injectability and cyto-compatibility was developed and tested *in vivo* with promising results. The ability of a polyphosphate coacervate to be loaded with an anticancer drug, with a subsequent slow rate of release, was also demonstrated. These studies established the potential of a polyphosphate *in situ* forming system and polyphosphate coacervates in general as a unique and interesting platform for bio-applications.

7.2 Study limitations

There were a number of limitations with respect to the synthesized NaPPs. Dispersity, a measure of the distribution of molecular mass in a given polymer sample, was only

determined for the un-fractioned NaPP glass melts based on their fractionation data (see Table 2.1). For all other NaPPs including fractions themselves and long chain ion-exchanged samples, dispersity was not determined. Chromatographic methods such as gel permeation chromatography might be useful for determining dispersity in NaPPs. The second limitation to NaPP synthesis was the lack of control over humidity in the furnace during melting. A controlled atmosphere furnace would likely provide better control over chain growth by removing humidity from the chamber.

In Chapter 3 pH studies were carried out in water in the presence of atmospheric CO_2, the dissolution of which could lead to carbonic acid formation that could affect both titration and pH results. While it would be ideal to carry out these experiments in a CO_2-free atmosphere, using freshly boiled water and carrying out experiments immediately mitigated any CO_2 effects. Due to time limitations, small angle X-ray scattering (SAXS) studies originally planned were not undertaken. SAXS is an extremely useful technique for probing the overall structure of amorphous samples in solutions, and because of this ability, SAXS has been utilized for studying the shape of polyelectrolytes in presence of counterions [206, 207]. SAXS of polyphosphate solutions in the presence of divalent cations could potentially yield some valuable information on the structural shape of the chains in the solution, such as the radius of gyration (R_g) and its dependence on the divalent cation/phosphorus molar ratio.

In Chapter 4, the water content of coacervates was determined by weighing the coacervate, freeze-drying, and then re-weighing. This method neglects the amount of water that remains inside the coacervate even after freeze drying. In the same chapter, there were limitations to the degradation studies carried out on these coacervates. TRIS

buffered saline, which is not very physiologically relevant, was primarily used as a degradation medium to avoid the possibility of having compounds from the media interfering with the degradation. Coacervates may behave differently in phosphate buffered saline or other physiological solution like Hank's solution. Nevertheless, degradation of one of the coacervates carried out in Fetal Bovine Serum did not have any significant effect on degradation compared to TRIS. In order to resemble *in vivo* conditions, degradation studies were carried out in highly dynamic environment where almost all of the media was replenished every 24 hr; one might anticipate that the behavior of these coacervates will be different in a static environment where degradation media is untouched. Lastly, carrying out degradation studies on coacervates is challenging because of flow arising from their liquid-like nature. Eppendorf® tubes were used to contain coacervates at the bottom of the tube, and only their top surface was in direct contact with degradation media. In a more ideal degradation study, media has access to all surfaces of the sample and also the exact surface area is known, allowing degradation to be reported more precisely in terms of mg of weight lost per mm^2 of surface area per hr.

Dynamic viscoelastic measurements were all performed at 20°C and static viscoelastic measurements were carried out at a maximum of 30°C. From a biological perspective it would make sense to also measure rheology at 37°C, however this higher temperature was avoided in order to minimize any water evaporation from coacervates that could significantly affect their rheology. The relationship between viscosity and temperature was determined for the coacervates by carrying out static viscoelastic experiments at

three temperatures (10, 20 and 30°C); using this relationship one could predict the viscosity at 37°C.

Limitations were also noted for hemostasis investigations. For the whole blood clotting assay, citrated sheep blood from CEDARLANE® was used and experiments were carried out immediately after the blood was received; ideally, fresh blood would have been collected and used for these experiments as blood components degrade slowly with time. For the activated partial thromboplastic time (aPTT) assay, an expected decrease in aPTT was not realized; rather, an increase was observed instead. An assumption here was that a reaction occurred between the polyphosphate coacervate and phospholipids inside the commercial aPTT agent used in this study. It would be ideal to carry out similar experiments using other commercial aPTT agents or the aPTT agent used here but after addition of excess phospholipid vesicles. Additionally for these blood studies, imaging of platelet covered coacervates using electron microscopy proved challenging because of the liquid-like nature of coacervates that resulted in the loss of the surfaces covered with these platelets. Specimen cracking during freeze-drying or critical point drying also impacted these surfaces. As a consequence of these artifacts, most of surface of the shortest chain Ca-only coacervates were found to be flat without any platelets, contrary to platelet attachment assays.

Cell viability studies carried out in Chapter 6 were used only to compare the biological safety of different coacervate formulations; cell viability was measured by carrying out MTT assay on cells that were in contact with coacervate extracts. Although this method is based on ISO 10993-5 [200], it is a very basic assay, as only one specific cell line (in our case NIH/3T3 mouse embryonic fibroblasts) was used. In addition, an MTT assay is

not a direct measure of number of viable cells but instead measures cellular metabolic activity. Therefore MTT results collected here might not reflect the dynamic *in vivo* response to these coacervates.

7.3 Future directions

It would be very interesting to evaluate incorporation of other cations into polyphosphate coacervates. Here, only Ca, Sr and Ba coacervates were investigated. It was shown that replacing some of the Ca with Sr or Ba profoundly changes the physical and chemical properties of the coacervates. Similar observations should be expected if coacervates are loaded with other cations. Evaluating incorporation of cations such as Al^{3+}, Ga^{3+} and cations in the lanthanide group of elements is especially intriguing, as their higher valency should result in a completely different physical (e.g. rheology) and, perhaps, chemical (e.g. degradation) properties. For example, it is known that Al^{3+} ions form hydrogels [35, 79] or nanoparticles [208] in the presence of polyphosphates. One should be aware that the behavior of polyphosphates in the presence of these multivalent cations might be more complicated; for instance it has been shown that gel formation in the Al^{3+}-polyphosphate system is temperature-dependent [79]. If more durable polyphosphate coacervates are required, incorporation of cerium might prove beneficial because it has been reported that cerium phosphate glasses are highly water resistant, a response attributed to the much stronger P-O-P bond in the presence of cerium [209].

Specific cations could also be loaded into coacervates to achieve a therapeutic benefit. In this manner coacervates would act as an ion releasing agent. Examples include cobalt, which has been shown to promote angiogenesis [210]; copper and silver, noted for their antibacterial effects [211, 212]; cerium, which supports differentiation and proliferation

of osteoblast cells [213]; and zinc and gallium, which have been found to be antibacterial and also stimulate bone formation [214, 215]. An overview of therapeutic metallic ions is provided by Mourino et al. [216]. Calcium polyphosphate coacervates loaded with silver has been recently developed and shown to possess significant antibacterial activity against the bacterium *Psuedomonas aeruginosa* [147].

Metallic cations aside, organic cations could also be added to a NaPP solution resulting in interesting materials that might find to be useful for specific bio-applications. Examples of organic cations are polycations such as chitosan, or long chain quaternary ammonium salts such as cetyltrimethylammonium. It has been shown that NaPP solutions precipitate in the presence of cetyltrimethylammonium, lauryl pyridinium, dimethyl dioctadecyl ammonium and N-octadecyl dimethyl benzyl, forming a gummy or waxy hydrophobic solid [217, 218]. A recent review on interactions of NaPPs and a variety of polycations and biological macromolecules is given by Cini and Ball [219].

Polyphosphate coacervates of metallic cations could also be used to prepare phosphate glasses. The potential of such coacervates as glass precursors has been evaluated previously by Iost et al. [37]; in their approach, however, the coacervate is heated, melted and cooled to form the glass. It would be very interesting to investigate formation of phosphate glasses directly from the coacervate without the use of elevated temperatures. The coacervate transforms to glass when it loses its water. Heating removes water, but inevitably it would also degrade the polyphosphate chains. Simple drying methods such as maintaining the coacervate at room temperature also result in a glass, probably with minimum chain degradation, but these glasses are of no use because they are highly brittle and full of cracks. Dipping coacervates in water-miscible organic solvents (e.g.

acetone, ethanol, glycerin, etc.), or in highly ionic aqueous solution (e.g. 300 mg/mL NaCl in deionized water) are example of methods of solidifying coacervates which might result in crack-free solid glasses. Furthermore, dipping the coacervate in a highly ionic solution might also alter key phys-chem properties of the coacervate such as durability.

Taking advantage of the liquid nature of coacervates, phosphate glass *microspheres* could also be prepared from polyphosphate coacervates using common emulsion methods. Such microspheres could be loaded with active radioisotopes for a variety of biomedical applications. Glass microspheres containing yttrium^{90}, a beta emitter, are used for radio-embolization of liver cancer [220]. These glass microspheres are silicate-based and non-degradable [221]. However, biodegradability of the glass microsphere is advantageous in order to remove the radionuclide particles after the radioactive treatment [222]. Developing degradable phosphate glass microsphere loaded with active radioisotopes through the coacervation method could meet this requirement; however, one should note that absolutely no degradation is wanted until complete decay of the radioisotope [223]. Other radioisotopes such as rhenium$^{186/188}$ [224], holmium^{166} [225], samarium^{153} and dysprosium^{165} [226] have also been loaded into glass microspheres for radiotherapy. Gamma emitting radioisotopes such as technetium^{99} or gallium^{67} could also be loaded into microspheres for Single-photon emission computed tomography. A comprehensive review of the application of radioactive microspheres for medical purposes is provided by Hafeli [223].

Polyphosphate coacervates also showed potential as a drug delivery agent in this thesis. The drug delivery potential of these coacervates should be more systematically investigated. These coacervates are an excellent candidate for drug delivery because of

the ease of drug incorporation into the coacervates and mild processing conditions that prevent destruction of the therapeutic agents. The drug could be added to the polyphosphate solution and then the coacervate formed by addition of a cation to trap the drug, as was demonstrated in studies involving doxorubicin, or the drug could be added directly as a powder to a previously formed coacervate and then mixed until it is homogenously dispersed or dissolved inside the coacervate.

For further consideration of these polyphosphate coacervates – especially the longest chain polyphosphate coacervates – as a hemostatic agent, the next step would be to evaluate their ability to stop bleeding *in vivo*. In order to transform this polyphosphate *in situ* forming system into a viable liquid embolic agent, one should focus on the limitations discussed in Chapter 6 that is improving physical cohesiveness of the formed coacervates and designing a delivery device for the two phase liquid system.

Lastly, for some biomedical applications more durable polyphosphate systems might be required. One finding from Chapter 3 was that polyphosphate chains within a pure NaPP solution are highly stable; it is assumed here that the high negative charge on the chains prevents hydrolysis. Therefore, it could be suggested that a polyphosphate hydrogel system where chains are crosslinked together by covalent bonds should be very durable. In such a hydrogel the chains are still negatively charged but they are held together by the covalent bonding. To prepare such a hydrogel, phosphate groups at the end of the polyphosphate chains could be covalently crosslinked to each other. It is known that phosphate groups can be covalently attached to primary amine-containing molecules using EDAC (1-ethyl-3-[3-(dimethylamino)propyl]carbodiimide) [227, 228]. Using EDAC, polyphosphate has been bonded to dendrimers, amino bound polystyrene beads

and gold nanoparticles [229]. Similarly, polyphosphate hydrogels could be prepared using EDAC and a compound with multiple primary amine moieties.

Overall the uniqueness of polyphosphate arises from its simple chemistry, hydrolysis into simple byproducts, ability to bind with different cations and to be loaded with drugs. These unique properties guarantee a bright future for this polymer in general as a biomaterial.

Bibliography

1. Berzelius, J., *Untersuchungen über die Zusammensetzung der Phosphorsäure, der phosphorigen Säure und ihrer Salze.* Annalen der Physik, 1816. **53**(8): p. 393-446.
2. Graham, T., *Researches on the Arseniates, Phosphates, and Modifications of Phosphoric Acid.* Philosophical Transactions of the Royal Society of London, 1833. **123**: p. 253-284.
3. Callis, C.F., J.R. Van Wazer, and P.G. Arvan, *The Inorganic Phosphates as Polyelectrolytes.* Chemical Reviews, 1954. **54**(5): p. 777-796.
4. Laubengayer, A.W. and R.D. Rosenstein, *Condensation in the boric acids and borates*, in *Symposium on complex ions in polyelectrolytes*1951: New York.
5. Van Wazer, J.R., *Phosphorus and its compounds*. Vol. 1. 1958: Interscience Publishers, Inc.
6. Van Wazer, J.R. and C.F. Callis, *Metal Complexing By Phosphates.* Chemical Reviews, 1958. **58**(6): p. 1011-1046.
7. Hall, R.E., *Water softening and washing*, 1934, Hall Laboratories, Inc.: USA.
8. Ilardi, V., *Renaissance Vision from Spectacles to Telescopes*. 1 ed2007: Amer Philosophical Society.
9. Davidson, C.L. and I.A. Mjor, *Advances in Glass-Ionomer Cements*. 1 ed1999: Quintessence Pub Co.
10. Hench, L., *The story of Bioglass®.* Journal of Materials Science: Materials in Medicine, 2006. **17**(11): p. 967-978.
11. Hench, L.L., *Bioceramics: From Concept to Clinic.* Journal of the American Ceramic Society, 1991. **74**(7): p. 1487-1510.
12. Filiaggi, M. and G. Hall, *A Compaction Route for Low Temperature Processing of Porous Calcium Polyphosphate Matrices.* Key Engineering Materials, 2001. **218-220**: p. 43-46.
13. Filiaggi, M.J., N. Djogbenou, and G. Hall, *A Processing Approach to Tuning the Drug Delivery Characteristics of Calcium Polyphosphate Matrices.* Bioceramics Development and Applications, 2011. **1**.
14. Dion, A., et al., *Vancomycin release behaviour from amorphous calcium polyphosphate matrices intended for osteomyelitis treatment.* Biomaterials, 2005. **26**(35): p. 7276-7285.
15. Wheland, G.W., *Advanced organic chemistry*1949: J. Wiley.
16. Chow, L.C. and E.D. Eanes, *Octacalcium Phosphate*. 1 ed2001: S. Karger AG.
17. Hench, L.L., *Physical chemistry of glass surfaces.* Journal of Non-Crystalline Solids, 1977. **25**(1-3): p. 343-369.
18. Ding, Y., et al., *Immersion behaviour of calcium polyphosphate in simulated body fluid.* Applied Surface Science, 2008. **255**(2): p. 534-537.
19. Dion, A., et al., *The effect of processing on the structural characteristics of vancomycin-loaded amorphous calcium phosphate matrices.* Biomaterials, 2005. **26**(21): p. 4486-4494.
20. Schofield, S.C., et al., *Gelled Calcium Polyphosphate Matrices Delay Antibiotic Release.* Journal of Dental Research, 2006. **85**(7): p. 643-647.
21. Petrone, C., et al., *Compaction strategies for modifying the drug delivery capabilities of gelled calcium polyphosphate matrices.* Acta Biomaterialia, 2008. **4**(2): p. 403-413.
22. Bray, J.M., et al., *Measurement of fluid ingress into calcium polyphosphate bioceramics using nuclear magnetic resonance microscopy.* Solid State Nuclear Magnetic Resonance, 2007. **32**(4): p. 118-128.

23. Saltzman, W.M., *Drug Delivery: Engineering Principles for Drug Therapy*. 1 ed2001: Oxford University Press.
24. Draoui, M., G. Palavit, and P. Vast, Rev. Chim. Min., 1985. **22**.
25. Omelon, S., *Polyphosphate ceramic and method of making same*, 2007: USA.
26. Krausher, J.L., *Investigating calcium polyphosphate addition to a conventional calcium phosphate cement for bone-interfacing applications*, in *School of Biomedical Engineering*2010, DALHOUSIE UNIVERSITY: Halifax. p. 129 pages.
27. Matsuya, Y., et al., *Polymeric calcium phosphate cements derived from poly(methyl vinyl ether-maleic acid).* Dental Materials, 1996. **12**(1): p. 2-7.
28. Miyazaki, K., et al., *Polymeric calcium phosphate cements: analysis of reaction products and properties.* Dental Materials, 1993. **9**(1): p. 41-45.
29. Thilo, E., G. Schulz, and E.-M. Wichmann, *Zur Chemie der kondensierten Phosphate und Arsenate. IX. Die Konstitution des GRAHAMschen und KURROLschen Salzes (NaPO3)x.* Zeitschrift für anorganische und allgemeine Chemie, 1953. **272**(1-4): p. 182-200.
30. Pleith, K. and C. Wurstner, Zeitschrift für anorganische und allgemeine Chemie, 1951. **267**.
31. Masson, N.C., E.F. de Souza, and F. Galembeck, *Calcium and iron(III) polyphosphate gel formation and aging.* Colloids and Surfaces A: Physicochemical and Engineering Aspects, 1997. **121**(2-3): p. 247-255.
32. Pereira de Abreu Filho, P., et al., *Genesis of a solid foam: iron(III) metaphosphate transformation in sol-gel crystallization processes.* Langmuir, 1990. **6**(5): p. 1013-1016.
33. de Oliveira, C.I.R., et al., *Spectroscopic investigation of a new hybrid glass formed by the interaction between croconate ion and calcium polyphosphate.* Spectrochimica Acta Part A: Molecular and Biomolecular Spectroscopy, 2005. **61**(9): p. 2023-2028.
34. da Silva, R.V., et al., *Repair of Cranial Bone Defects With Calcium Phosphate Ceramic Implant or Autogenous Bone Graft.* Journal of Craniofacial Surgery, 2007. **18**(2): p. 281-286 10.1097/scs.0b013e31802d8ac4.
35. Fatima de Souza, E., C.C. Bezerra, and F. Galembeck, *Bicontinuous networks made of polyphosphates and of thermoplastic polymers.* Polymer, 1997. **38**(26): p. 6285-6293.
36. de Oliveira, L., et al., *Amorphous manganese polyphosphates: preparation, characterization and incorporation of azo dyes.* Journal of Sol-Gel Science and Technology, 2009. **50**(2): p. 158-163.
37. Iost, A., et al., *Mechanical behavior of metaphosphate glasses used as coating on metals in relation to their structure and preparation method.* Journal of Materials Science, 1999. **34**(16): p. 3991-3996.
38. Willot, G., et al., *Preparation of zinc sodium polyphosphates glasses from coacervates precursors. Characterisation of the obtained glasses, and their applications.* Comptes Rendus Chimie, 2002. **5**(12): p. 899-906.
39. Brow, R.K., *Review: the structure of simple phosphate glasses.* Journal of Non-Crystalline Solids, 2000. **263-264**: p. 1-28.
40. Kirk-Othmer, *Kirk-Othmer Encyclopedia of Chemical Technology*. 5 ed2004: Wiley-Interscience.
41. Strauss, U.P. and T.L. Treitler, *Chain Branching in Glassy Polyphosphates: Dependence on the Na/P Ratio and Rate of Degradation at 25°1.* Journal of the American Chemical Society, 1955. **77**(6): p. 1473-1476.
42. Strauss, U.P. and T.L. Treitler, *Degradation of Polyphosphates in Solution. I. Kinetics and Mechanism of the Hydrolysis at Branching Points in Polyphosphate Chains1.* Journal of the American Chemical Society, 1956. **78**(15): p. 3553-3557.

43. Hoppe, U., *A structural model for phosphate glasses.* Journal of Non-Crystalline Solids, 1996. **195**(1-2): p. 138-147.
44. Wetherall, K.M. and et al., *The structure of calcium metaphosphate glass obtained from x-ray and neutron diffraction and reverse Monte Carlo modelling.* Journal of Physics: Condensed Matter, 2009. **21**(3): p. 035109.
45. HOPPE, et al., *The short range order of metaphosphate glasses investigated by x-ray diffraction*. Vol. 33. 1992, Sheffield, ROYAUME-UNI: Society of Glass Technology.
46. Jost, K., *Die Struktur des Kurrol'schen Na-Salzes (NaPO3)x Typ A.* Acta Crystallographica, 1961. **14**(8): p. 844-847.
47. McAdam, A., K.H. Jost, and B. Beagley, *Refinement of the structure of sodium Kurrol salt (NaPO3)x, type A.* Acta Crystallographica Section B, 1968. **24**(12): p. 1621-1622.
48. Jost, K., *Die Struktur des Kurrol'schen Na-Salzes (NaPO3)x, Typ B.* Acta Crystallographica, 1963. **16**(7): p. 640-642.
49. Jost, K., *Zur Struktur des Maddrellschen Salzes.* Acta Crystallographica, 1963. **16**(5): p. 428.
50. Dornberger-Schiff, K., F. Liebau, and E. Thilo, *Zur Struktur des [beta]-Wollastonits des Maddrellschen Salzes und des Natriumpolyarsenats.* Acta Crystallographica, 1955. **8**(12): p. 752-754.
51. Hoppe, U., et al., *Structure of rare-earth phosphate glasses by X-ray and neutron diffraction.* Journal of Non-Crystalline Solids, 2005. **351**(40-42): p. 3179-3190.
52. Weil, M., et al., *Synthesis, Crystal Structure, and Characterization (Vibrational and Solid-State 31P MAS NMR Spectroscopy) of the High-Temperature Modification of Calcium catena-Polyphosphate(V).* Chemistry of Materials, 2007. **19**(21): p. 5067-5073.
53. Hoppe, U., et al., *Structural specifics of phosphate glasses probed by diffraction methods: a review.* Journal of Non-Crystalline Solids, 2000. **263-264**: p. 29-47.
54. Speghini, A., et al., *Structural investigation of NaPO3 glass using molecular dynamics simulation.* Physical Chemistry Chemical Physics, 1999. **1**(1): p. 173-177.
55. Uo, M., et al., *Properties and cytotoxicity of water soluble Na2O-CaO-P2O5 glasses.* Biomaterials, 1998. **19**(24): p. 2277-2284.
56. Ahmed, I., et al., *Phosphate glasses for tissue engineering: Part 1. Processing and characterisation of a ternary-based P2O5-CaO-Na2O glass system.* Biomaterials, 2004. **25**(3): p. 491-499.
57. Franks, K., et al., *Investigation of thermal parameters and crytallisation in a ternary CaO-Na2O-P2O5-based glass system.* Biomaterials, 2001. **22**(5): p. 497-501.
58. Griffith, E.J., *The Structure of the Salt Sodium Calcium Metaphosphate (Na4CaP6O18).* Inorganic Chemistry, 1962. **1**(4): p. 962-962.
59. Abrahams, I., et al., *Structures of the chain metaphosphates NaM(PO3)3 (M = Ca or Sr).* Magnetic Resonance in Chemistry, 2008. **46**(4): p. 316-322.
60. Knowles, J.C., K. Franks, and I. Abrahams, *Investigation of the solubility and ion release in the glass system K2O-Na2O-CaO-P2O5.* Biomaterials, 2001. **22**(23): p. 3091-3096.
61. Erragh, F., et al., *Sodium Nickel Polyphosphate.* Acta Crystallographica Section C, 1998. **54**(12): p. 1746-1747.
62. Sandstrom, M. and D. Bostrom, *Calcium potassium cyclo-triphosphate.* Acta Crystallographica Section E, 2004. **60**(2): p. i15-i17.
63. Durif, A., et al., Bull. Soc. Fr. Mineral. Crystallogr., 1966. **89**.
64. Jong, H.G.B.d. and H.R. Kruyt, Proc. Kon. Ned. Akad. Wetensch., 1929. **32**.

65. Catti, M., G. Ferraris, and M. Franchini-Angela, *The crystal structure of Na2HPO4.2H2O. Competition between coordination and hydrogen bonds.* Acta Crystallographica Section B, 1977. **33**(11): p. 3449-3452.
66. Walter, G., G. Goerigk, and C. Rüssel, *The structure of phosphate glass evidenced by small angle X-ray scattering.* Journal of Non-Crystalline Solids, 2006. **352**(38-39): p. 4051-4061.
67. Sinyaev, V.A., et al., *Synthesis and Dehydration of Amorphous Calcium Phosphate.* Inorganic Materials, 2001. **37**(6): p. 619-622.
68. McElroy, S.M.K., J.F. Hazel, and W.M. McNabb, *Adsorption of ferripolyphosphate.* Journal of Chemical & Engineering Data, 1968. **13**(3): p. 364-366.
69. Silva, M.A.P., et al., *Spectroscopic studies on glassy Ni(II) and Co(II) polyphosphate coacervates.* Materials Chemistry and Physics, 2010. **124**(1): p. 547-551.
70. Gomez, F., et al., *Dehydroxylation mechanisms of polyphosphate glasses in relation to temperature and pressure.* Journal of Non-Crystalline Solids, 1997. **222**: p. 415-421.
71. Umegaki, T., Y. Nakayama, and T. Kanazawa, *Thermal change of magnesium highpolyphosphate coacervates.* Bulletin of the chemical society of Japan, 1976. **49**(8): p. 2105-2107.
72. Pfanstiel, R. and R.K. Iler, *Magnesium Polymetaphosphate.* Journal of the American Chemical Society, 1956. **78**(21): p. 5510-5511.
73. Brown, E.H. and J.R. Lehr, *Fertilizer Materials, Vitreous Calcium Metaphosphate-Some Properties of Its Aqueous Systems.* Journal of Agricultural and Food Chemistry, 1964. **12**(3): p. 201-204.
74. Kasuga, T., et al., *Hydrogelation of Calcium Metaphosphate Glass.* Chemistry letters, 2001. **30**(8): p. 820-821.
75. Akamatsu, T., T. Kasuga, and M. Nogami, *Formation of metaphosphate hydrogels and their proton conductivities.* Journal of Non-Crystalline Solids, 2005. **351**(8-9): p. 691-696.
76. Delahaye, F., et al., *Acid dissolution of sodium-calcium metaphosphate glasses.* Journal of Non-Crystalline Solids, 1998. **242**(1): p. 25-32.
77. Bunker, B.C., G.W. Arnold, and J.A. Wilder, *Phosphate glass dissolution in aqueous solutions.* Journal of Non-Crystalline Solids, 1984. **64**(3): p. 291-316.
78. Umegaki, T. and T. Kanazawa, *Viscosity behavior of coacervates of magnesium and calcium highpolyphosphates.* Bulletin of the chemical society of Japan, 1975. **48**(5): p. 1452-1454.
79. de Oliveira Lima, E.C. and F. Galembeck, *Thermoreversible Gel Formation from Aqueous Aluminum Polyphosphate Solutions.* Journal of Colloid and Interface Science, 1994. **166**(2): p. 309-315.
80. Koetz, J. and S. Kosmella, *Polyelectrolytes and nanoparticles*2007, Berlin: Springer.
81. Miyajima, T., S. Ohashi, and J.C.T. Kwak, *A Two Phase Model for the Binding of Cations To Long-Chain Polyphosphate Anions.* Phosphorous and Sulfur and the Related Elements, 1987. **30**(3-4): p. 581-584.
82. Strauss, U.P., E.H. Smith, and P.L. Wineman, *Polyphosphates as Polyelectrolytes. I. Light Scattering and Viscosity of Sodium Polyphosphates in Electrolyte Solutions1.* Journal of the American Chemical Society, 1953. **75**(16): p. 3935-3940.
83. Strauss, U.P. and E.H. Smith, *Polyphosphates as Polyelectrolytes. II. Viscosity of Aqueous Solutions of Graham's Salts1.* Journal of the American Chemical Society, 1953. **75**(24): p. 6186-6188.
84. Strauss, U.P. and S. Bluestone, *Counterion Binding by Polyelectrolytes. II. The Determination of the Binding of Univalent Cations by Long-chain Polyphosphates from*

Conductivity and Electrophoresis Data1. Journal of the American Chemical Society, 1959. **81**(20): p. 5292-5295.

85. Strauss, U.P. and P.D. Ross, *Counterion Binding by Polyelectrolytes. III. Stability Constants for the Binding of Univalent Cations by PO3--Groups of Polyphosphates from Electrophoresis Measurements1.* Journal of the American Chemical Society, 1959. **81**(20): p. 5295-5298.
86. Strauss, U.P. and P.D. Ross, *Counterion Binding by Polyelectrolytes. IV. Membrane Equilibrium Studies of the Binding of Univalent Cations by Long-chain Polyphosphates1.* Journal of the American Chemical Society, 1959. **81**(20): p. 5299-5302.
87. Strauss, U.P. and P.L. Wineman, *Molecular Dimensions and Interactions of Long-chain Polyphosphates in Sodium Bromide Solutions1.* Journal of the American Chemical Society, 1958. **80**(10): p. 2366-2371.
88. Lifson, S. and A. Katchalsky, *The electrostatic free energy of polyelectrolyte solution. II. Fully stretched macromolecules.* J Polym Sci, 1954. **13**: p. 43–56.
89. Manning, G.S., *Limiting Laws and Counterion Condensation in Polyelectrolyte Solutions I. Colligative Properties.* JOURNAL OF CHEMICAL PHYSICS, 1969. **51**(3): p. 924-933.
90. Manning, G.S., *Limiting Laws and Counterion Condensation in Polyelectrolyte Solutions II. Self-Diffusion of the Small Ions.* Journal of Chemical Physics, 1969. **51**(3): p. 934-938.
91. Manning, G.S., *Limiting Laws and Counterion Condensation in Polyelectrolyte Solutions III. An Analysis Based on the Mayer Ionic Solution Theory.* JOURNAL OF CHEMICAL PHYSICS, 1969. **51**(8): p. 3249-3252.
92. Hao, M.H. and S.C. Harvey, *A lattice theory for counterion binding on polyelectrolytes.* Macromolecules, 1992. **25**: p. 2200–2208.
93. Mehrotra, R.C., *Synthesis and properties of simple and complex polymetaphosphate glasses of alkali metals.* Pure and Applied Chemistry, 1975. **44**(2): p. 201-220.
94. Campbell, J.A. and C. Schenker, *A Polarographic Study of Barium Ion Removal by Complex Phosphates1.* Journal of the American Chemical Society, 1945. **67**(5): p. 767-769.
95. Wazer, J.R.V. and D.A. Campanella, *Structure and Properties of the Condensed Phosphates. IV. Complex Ion Formation in Polyphosphate Solutions.* Journal of the American Chemical Society, 1950. **72**(2): p. 655-663.
96. Irani, R.R. and C.F. Callis, *METAL COMPLEXING BY PHOSPHORUS COMPOUNDS. I. THE THERMODYNAMICS OF ASSOCIATION OF LINEAR POLYPHOSPHATES WITH CALCIUM1.* The Journal of Physical Chemistry, 1960. **64**(10): p. 1398-1407.
97. Sabbagh, I. and M. Delsanti, *Solubility of highly charged anionic polyelectrolytes in presence of multivalent cations: Specific interaction effect.* Eur. Phys. J. E, 2000. **1**(1): p. 75-86.
98. Radeva, T., *Physical chemistry of polyelectrolytes*. Surfactant science, ed. T. Radeva2001, New York: CRC Press.
99. Sabbagh, I., M. Delsanti, and P. Lesieur, *Ionic distribution and polymer conformation, near phase separation, in sodium polyacrylate/divalent cations mixtures: small angle X-ray and neutron scattering.* Eur. Phys. J. B, 1999. **12**(2): p. 253-260.
100. Silva, M.c.A.P., D.F. Franco, and L.F. C. de Oliveira, *New Insight on the Structural Trends of Polyphosphate Coacervation Processes.* The Journal of Physical Chemistry A, 2008. **112**(24): p. 5385-5389.
101. Umegaki, T. and T. Kanazawa, *Torsional braid analysis of magnesium highpolyphosphate coacervates.* Bulletin of the chemical society of Japan, 1973. **46**: p. 3587-3588.

102. Kanazawa, T., et al., *A solubility study of coacervate of magnesium, calcium and aluminum highpolyphosphates in acid solutions.* Bulletin of the chemical society of Japan, 1974. **47**(6): p. 1419-1421.
103. Umegaki, T. and T. Kanazawa, *Degradation of Magnesium and Calcium Highpolyphosphate Coacervates.* Bulletin of the chemical society of Japan, 1979. **52**(7): p. 2124-2126.
104. Dias Filho, F.A., et al., *Spectroscopic Study and Local Coordination of Polyphosphate Colloidal Systems.* Langmuir, 2005. **21**(5): p. 1776-1783.
105. Bigerelle, M., et al., *Fracture toughness of polyphosphate glasses in relation with chemical composition and curing process.* Journal of Materials Science Letters, 2001. **20**(11): p. 1037-1039.
106. Palavit, G., L. Montagne, and R. Delaval, *Preparation of zinc---sodium phosphate glass precursors by coacervation.* Journal of Non-Crystalline Solids, 1995. **189**(3): p. 277-282.
107. Van Wazer, J.R., C.F. Callis, and J.N. Shoolery, *NUCLEAR MAGNETIC RESONANCE SPECTRA OF THE CONDENSED PHOSPHATES.* Journal of the American Chemical Society, 1955. **77**(18): p. 4945-4946.
108. Van Wazer, J.R., et al., *Principles of Phosphorus Chemistry. II. Nuclear Magnetic Resonance Measurements1.* Journal of the American Chemical Society, 1956. **78**(22): p. 5715-5726.
109. Crutchfield, M.M. and R.R. Irani, *A P31 Nuclear Magnetic Resonance Study of Complexing between Li+, Ca, and Mg2+ Ions and the Lower Condensed Phosphate Polyanions1.* Journal of the American Chemical Society, 1965. **87**(13): p. 2815-2820.
110. Huffman, E.O. and J.D. Fleming, *CALCIUM POLYPHOSPHATE—RATE AND MECHANISM OF ITS HYDROLYTIC DEGRADATION.* The Journal of Physical Chemistry, 1960. **64**(2): p. 240-244.
111. Ahmed, A.A., et al., *Preparation and characterization of antibacterial P2O5–CaO–Na2O–Ag2O glasses.* Journal of Biomedical Materials Research Part A, 2011. **98A**(1): p. 132-142.
112. Bhargava, H.N. and D.C. Srivastava, *Degradation of Graham's salt in presence of water-miscible organic solvents.* The Journal of Physical Chemistry, 1970. **74**(1): p. 36-39.
113. Miller, D.L., G.J. Krol, and U.P. Strauss, *Degradation of polyphosphates in solution. IV. Catalytic effects of divalent metal ions on trimetaphosphate formation.* Journal of the American Chemical Society, 1969. **91**(24): p. 6882-6883.
114. Bell, R.N., *Hydrolysis of dehydrated Sodium Phosphates.* Industrial & Engineering Chemistry, 1947. **39**(2): p. 136-140.
115. Kulaev, I.S., et al., *The biochemistry of inorganic polyphosphates*. 2 ed2004: Wiley.
116. Brown, M.R.W. and A. Kornberg, *Inorganic polyphosphate in the origin and survival of species.* Proceedings of the National Academy of Sciences of the United States of America, 2004. **101**(46): p. 16085-16087.
117. Kornberg, A., N.N. Rao, and D. Ault-Riché, *INORGANIC POLYPHOSPHATE: A Molecule of Many Functions.* Annual Review of Biochemistry, 1999. **68**(1): p. 89-125.
118. Kornberg, A., *Inorganic polyphosphate: toward making a forgotten polymer unforgettable.* J. Bacteriol., 1995. **177**(3): p. 491-496.
119. Kulaev, I. and T. Kulakovskaya, *POLYPHOSPHATE AND PHOSPHATE PUMP.* Annual Review of Microbiology, 2000. **54**(1): p. 709-734.
120. Kulaev, I.S., *Inorganic polyphosphate functions at various stages of cell evolution.* Journal of Biological Physics, 1995. **20**(1): p. 255-273.

121. Gabel, N.W. and V. Thomas, *EVIDENCE FOR THE OCCURRENCE AND DISTRIBUTION OF INORGANIC POLYPHOSPHATES IN VERTEBRATE TISSUES.* Journal of Neurochemistry, 1971. **18**(7): p. 1229-1242.
122. Hacchou, Y., et al., *Inorganic Polyphosphate: a Possible Stimulant of Bone Formation.* Journal of Dental Research, 2007. **86**(9): p. 893-897.
123. Leyhausen, G., et al., *Inorganic Polyphosphate in Human Osteoblast-like Cells.* Journal of Bone and Mineral Research, 1998. **13**(5): p. 803-812.
124. Usui, Y., et al., *Inorganic Polyphosphate Induces Osteoblastic Differentiation.* Journal of Dental Research, 2010. **89**(5): p. 504-509.
125. Schröder, H.C., et al., *Polyphosphate in Bone.* Biochemistry (Moscow), 2000. **65**(3): p. 296-303.
126. Omelon, S.J. and M.D. Grynpas, *Relationships between Polyphosphate Chemistry, Biochemistry and Apatite Biomineralization.* Chemical Reviews, 2008. **108**(11): p. 4694-4715.
127. Ruiz, F.A., et al., *Human Platelet Dense Granules Contain Polyphosphate and Are Similar to Acidocalcisomes of Bacteria and Unicellular Eukaryotes.* Journal of Biological Chemistry, 2004. **279**(43): p. 44250-44257.
128. Smith, S.A., et al., *Polyphosphate modulates blood coagulation and fibrinolysis.* Proceedings of the National Academy of Sciences of the United States of America, 2006. **103**(4): p. 903-908.
129. Smith, S.A. and J.H. Morrissey, *Polyphosphate enhances fibrin clot structure.* Blood, 2008. **112**(7): p. 2810-2816.
130. Smith, S.A., et al., *Polyphosphate exerts differential effects on blood clotting, depending on polymer size.* Blood, 2010. **116**(20): p. 4353-4359.
131. Morrissey, J.H., et al., *COAGULATION AND FIBRINOLYTIC CASCADES MODULATOR*, 2010, The Board of Trustees of the University of Illinois: USA.
132. Pendurthi, U.R., *Size matters for polyP to clot.* Blood, 2010. **116**(20): p. 4042-4043.
133. Mutch, N.J., et al., *Polyphosphate modifies the fibrin network and down-regulates fibrinolysis by attenuating binding of tPA and plasminogen to fibrin.* Blood, 2010. **115**(19): p. 3980-3988.
134. Wazer, J.R.V., *Structure and Properties of the Condensed Phosphates. III. Solubility Fractionation and Other Solubility Studies.* Journal of the American Chemical Society, 1950. **72**(2): p. 647-655.
135. Pfanstiel, R. and R.K. Iler, *Potassium Metaphosphate: Molecular Weight, Viscosity Behavior and Rate of Hydrolysis of Non-cross-linked Polymer.* Journal of the American Chemical Society, 1952. **74**(23): p. 6059-6064.
136. Stover, F.S., J.A. Bulmahn, and J.K. Gard, *Polyphosphate separations and chain length characterization using minibore ion chromatography with conductivity detection.* Journal of Chromatography A, 1994. **688**(1–2): p. 89-95.
137. Janice, K.G., R.G. David, and F.C. Clayton, *Quantitative Analysis of Inorganic Phosphates Using ³¹P NMR Spectroscopy*, in *Phosphorus Chemistry*1992, American Chemical Society. p. 41-55.
138. Gard, J., et al., *Automated 31p NMR: A complete assay of oligophosphates and their mixtures using a robotic sample manager.* Spectroscopy, 1992. **7**(6): p. 28-31.
139. Wazer, J.R.V., *Structure and Properties of the Condensed Phosphates. II. A Theory of the Molecular Structure of Sodium Phosphate Glasses1.* Journal of the American Chemical Society, 1950. **72**(2): p. 644-647.
140. Durif, A., *Crystal chemistry of condensed phosphates*1995: Plenum Press.

141. Corbridge, D.E.C., *The structural chemistry of phosphorus*1974: Elsevier Scientific Pub. Co.
142. Thilo, V.E. *Poly-phosphate und -arsenate*. in *International Symposium on Inorganic Polymers*. 1961. University of Nottingham, Great Britain: Chemical Society.
143. Malmgren, H., *A contribution to the physical chemistry of colloidal metaphosphates.* Acta Chemica Scandinavica, 1948. **2**: p. 147-165.
144. Malmgren, H., *A contribution to the physical chemistry of colloid metaphosphates II.* Acta Chemica Scandinavica, 1952. **6**: p. 1-15.
145. Griffith Edward, J., *Factors Influencing the Chain Lengths of Inorganic Polyphosphates*, in *Phosphorus Chemistry*1992, American Chemical Society. p. 86-101.
146. Gander, B., et al., *Coacervation and Phase Separation*, in *Encyclopedia of Pharmaceutical Technology, Third Edition*. p. 600-614.
147. Pickup, D.M., et al., *Characterisation of phosphate coacervates for potential biomedical applications.* Journal of Biomaterials Applications, 2013.
148. Lee, I.-H., et al., *Effects of magnesium content on the physical, chemical and degradation properties in a MgO–CaO–Na2O–P2O5 glass system.* Journal of Non-Crystalline Solids, 2013. **363**(0): p. 57-63.
149. Yoza, N., N. Ueda, and S. Nakashima, *pH-dependence of 31P-NMR spectroscopic parameters of monofluorophosphate, phosphate, hypophosphate, phosphonate, phosphinate and their dimers and trimers.* Fresenius' Journal of Analytical Chemistry, 1994. **348**(10): p. 633-638.
150. Handloser, C.S., M.R. Chakrabarty, and M.W. Mosher, *Experimental determination of pKa values by use of NMR chemical shift.* Journal of Chemical Education, 1973. **50**(7): p. 510.
151. Tischendorf, B., et al., *A study of short and intermediate range order in zinc phosphate glasses.* Journal of Non-Crystalline Solids, 2001. **282**(2–3): p. 147-158.
152. de Oliveira Lima, E.C., et al., *Aluminum Polyphosphate Thermoreversible Gels: A Study by31P and27Al NMR Spectroscopy.* Journal of Colloid and Interface Science, 1995. **176**(2): p. 388-396.
153. Frankenthal, L., *Interaction between Sodium Triphosphate and Salts of Polyvalent Cations as Shown by pH Measurements.* Journal of the American Chemical Society, 1944. **66**(12): p. 2124-2126.
154. Thilo, E., *Condensed Phosphates and Arsenates*, in *Advances in Inorganic Chemistry and Radiochemistry*, H.J. Emeléus and A.G. Sharpe, Editors. 1962, Academic Press. p. 1-75.
155. Sillen, L.G., *Stability constants of metal-ion complexes*1964, London: Chemical Society.
156. Martell, A.E. and R.M. Smith, *Critical Stability Constants*. Vol. 1-6. 1974, New York: Plenum Press.
157. Wolhoff, J.A. and J.T.G. Overbeek, *Determination of equilibrium constants for a number of metal-phosphate complexes.* Recueil des Travaux Chimiques des Pays-Bas, 1959. **78**(10): p. 759-782.
158. Salih, V., A. Patel, and J.C. Knowles, *Zinc-containing phosphate-based glasses for tissue engineering.* Biomedical Materials, 2007. **2**(1): p. 11.
159. Ahmed, I., et al., *Quantification of Anion and Cation Release from a Range of Ternary Phosphate-based Glasses with Fixed 45 mol% P2O5.* Journal of Biomaterials Applications, 2005. **20**(1): p. 65-80.
160. Gill, J.B. and S.A. Riaz, *Kinetics of degradation of long chain polyphosphates.* Journal of the Chemical Society A: Inorganic, Physical, Theoretical, 1969(0): p. 183-187.

161. GRIFFITH, E.J., *THE CHEMICAL AND PHYSICAL PROPERTIES OF CONDENSED PHOSPHATES*, in *Second Symposium on Inorganic Phosphorus Compounds*1975: Prague.
162. McCullough, J.F., J.R. Van Wazer, and E.J. Griffith, *Structure and Properties of the Condensed Phosphates. XI. Hydrolytic Degradation of Graham's Salt.* Journal of the American Chemical Society, 1956. **78**(18): p. 4528-4533.
163. Strauss, U.P. and G.J. Krol, *Degradation of polyphosphates in solution. III. Hydrolysis of linear long-chain sodium polyphosphate.* Journal of Polymer Science Part C: Polymer Symposia, 1967. **16**(4): p. 2171-2179.
164. van Steveninck, J., *The Influence of Metal Ions on the Hydrolysis of Polyphosphates*.* Biochemistry, 1966. **5**(6): p. 1998-2002.
165. Mehrotra, R.C. and V.S. Gupta, *Studies in condensed phosphates. Part II. Viscosities of simple and complex sodium metaphosphate solutions.* Journal of Polymer Science, 1961. **55**(161): p. 81-88.
166. Das, S.S., et al., *Viscosity behaviour of salt free aqueous solutions of sodium nickel and sodium copper copolyphosphate glasses.* Physics and Chemistry of Glasses, 2001. **42**(1): p. 74-77.
167. Jia, P. and J. Zhao, *Single chain contraction and re-expansion of polystyrene sulfonate: A study on its re-entrant condensation at single molecular level.* JOURNAL OF CHEMICAL PHYSICS, 2009. **131**(23): p. 2311031-2311034.
168. Conway, B.E., *Ionic Hydration in Chemistry and Biophysics*1981: Elsevier Sci.
169. Toyoda, S., S. Fujino, and K. Morinaga, *Density, viscosity and surface tension of 50RO–50P2O5 (R: Mg, Ca, Sr, Ba, and Zn) glass melts.* Journal of Non-Crystalline Solids, 2003. **321**(3): p. 169-174.
170. Abou Neel, E.A., et al., *Characterisation of antibacterial copper releasing degradable phosphate glass fibres.* Biomaterials, 2005. **26**(15): p. 2247-2254.
171. Ahmed, I., et al., *Processing, characterisation and biocompatibility of iron-phosphate glass fibres for tissue engineering.* Biomaterials, 2004. **25**(16): p. 3223-3232.
172. Priftis, D., et al., *Complex coacervation of poly(ethylene-imine)/polypeptide aqueous solutions: Thermodynamic and rheological characterization.* Journal of Colloid and Interface Science, 2013. **398**(0): p. 39-50.
173. Schott, H., *Dependence of activation energy for viscous flow of polyhydrocarbons on bulk of substituents.* Journal of Applied Polymer Science, 1962. **6**(23): p. S29-S30.
174. Pearson, D.S., et al., *Viscosity and self-diffusion coefficient of linear polyethylene.* Macromolecules, 1987. **20**(5): p. 1133-1141.
175. Berry, G.C. and T.G. Fox, *The viscosity of polymers and their concentrated solutions*, in *Fortschritte der Hochpolymeren-Forschung*1968, Springer Berlin Heidelberg. p. 261-357.
176. Donovan, A.J., et al., *Size-Controlled Synthesis of Granular Polyphosphate Nanoparticles at Physiologic Salt Concentrations for Blood Clotting.* Biomacromolecules, 2014. **15**(11): p. 3976-3984.
177. Shih, M.-F., et al., *Platelet adsorption and hemolytic properties of liquid crystal/composite polymers.* International Journal of Pharmaceutics, 2006. **327**(1-2): p. 117-125.
178. Ong, S.-Y., et al., *Development of a chitosan-based wound dressing with improved hemostatic and antimicrobial properties.* Biomaterials, 2008. **29**(32): p. 4323-4332.
179. Dai, C., et al., *Degradable, antibacterial silver exchanged mesoporous silica spheres for hemorrhage control.* Biomaterials, 2009. **30**(29): p. 5364-5375.

180. Cazenave, J.-P., et al., *Preparation of Washed Platelet Suspensions From Human and Rodent Blood*, in *Platelets and Megakaryocytes*, J. Gibbins and M. Mahaut-Smith, Editors. 2004, Humana Press. p. 13-28.
181. Jenkins, H., et al., *Present status of gelatin sponge for the control of hemorrhage: With experimental data on its use for wounds of the great vessels and the heart.* Journal of the American Medical Association, 1946. **132**(11): p. 614-619.
182. Smith, S.A. and J.H. Morrissey, *Polyphosphate: a new player in the field of hemostasis.* Current Opinion in Hematology, 2014. **21**(5): p. 388-394.
183. Goodman, S.L., *Sheep, pig, and human platelet–material interactions with model cardiovascular biomaterials.* Journal of Biomedical Materials Research, 1999. **45**(3): p. 240-250.
184. Gorbet, M.B. and M.V. Sefton, *Biomaterial-associated thrombosis: roles of coagulation factors, complement, platelets and leukocytes.* Biomaterials, 2004. **25**(26): p. 5681-5703.
185. Krysl, J. and D.A. Kumpe, *Embolization agents: A review.* Techniques in Vascular and Interventional Radiology, 2000. **3**(3): p. 158-161.
186. Dalyai, R.T., et al., *Redefining Onyx HD 500 in the Flow Diversion Era.* International Journal of Vascular Medicine, 2011. **2012**: p. 9 pages.
187. Raymond, J., et al., *Cyanoacrylate Embolization of Experimental Aneurysms.* American Journal of Neuroradiology, 2002. **23**(1): p. 129-138.
188. van Rooij, W.J., M. Sluzewski, and G.N. Beute, *Brain AVM Embolization with Onyx.* American Journal of Neuroradiology, 2007. **28**(1): p. 172-177.
189. Pelz, D.M., et al., *Preoperative embolization of brain AVMs with isobutyl-2 cyanoacrylate.* American Journal of Neuroradiology, 1988. **9**(4): p. 757-64.
190. Chaloupka, J.C., et al., *A Reexamination of the Angiotoxicity of Superselective Injection of DMSO in the Swine Rete Embolization Model.* American Journal of Neuroradiology, 1999. **20**(3): p. 401-410.
191. Chaloupka, J.C., et al., *Technical feasibility and histopathologic studies of ethylene vinyl copolymer (EVAL) using a swine endovascular embolization model.* American Journal of Neuroradiology, 1994. **15**(6): p. 1107-15.
192. Dudeck, O., et al., *Organic Solvents as Vehicles for Precipitating Liquid Embolics: A Comparative Angiotoxicity Study with Superselective Injections of Swine Rete Mirabile.* American Journal of Neuroradiology, 2006. **27**(9): p. 1900-1906.
193. Murayama, Y., et al., *Nonadhesive Liquid Embolic Agent for Cerebral Arteriovenous Malformations: Preliminary Histopathological Studies in Swine Rete Mirabile.* Neurosurgery, 1998. **43**(5): p. 1164-1172.
194. Becker, T.A., D.R. Kipke, and T. Brandon, *Calcium alginate gel: A biocompatible and mechanically stable polymer for endovascular embolization.* Journal of Biomedical Materials Research, 2001. **54**(1): p. 76-86.
195. P, C., et al., *Embolization and endothelial ablation with chitosan and sodium sotradecol sulfate: preliminary results in an animal model.* Journal of Endovascular Therapy, 2012. **19**(3): p. 439-449.
196. McLemore, R., M.C. Preul, and B.L. Vernon, *Controlling delivery properties of a waterborne, in-situ-forming biomaterial.* Journal of Biomedical Materials Research Part B: Applied Biomaterials, 2006. **79B**(2): p. 398-410.
197. Sadato, A., et al., *Experimental study and clinical use of poly(vinyl acetate) emulsion as liquid embolisation material.* Neuroradiology, 1994. **36**(8): p. 634-641.
198. Morrissey, J.H., S.H. Choi, and S.A. Smith, *Polyphosphate: an ancient molecule that links platelets, coagulation, and inflammation.* Blood, 2012. **119**(25): p. 5972-5979.

199. Georgiades, C. and J.-F. Geschwind, *Transarterial Chemoembolization*, in *Hepatocellular Carcinoma:*, K.M. McMasters, Editor 2011, Springer New York. p. 287-297.
200. ISO, *10993: Biological evaluation of medical devices*, in *Part 5: Tests for in vitro cytotoxicity*2009.
201. Becker, T.A. and D.R. Kipke, *Flow properties of liquid calcium alginate polymer injected through medical microcatheters for endovascular embolization.* Journal of Biomedical Materials Research, 2002. **61**(4): p. 533-540.
202. Allwood, M., A. Stanley, and P. Wright, *The Cytotoxics Handbook*2002: Radcliffe Medical Press.
203. Barnett, B.P. and P. Gailloud, *Assessment of EmboGel—A Selectively Dissolvable Radiopaque Hydrogel for Embolic Applications.* Journal of Vascular and Interventional Radiology. **22**(2): p. 203-211.
204. Tam, K.Y., K.C.-F. Leung, and Y.-X.J. Wang, *Chemoembolization agents for cancer treatment.* European Journal of Pharmaceutical Sciences, 2011. **44**(1–2): p. 1-10.
205. Yang, S.C., et al., *Doxorubicin-loaded poly(butylcyanoacrylate) nanoparticles produced by emulsifier-free emulsion polymerization.* Journal of Applied Polymer Science, 2000. **78**(3): p. 517-526.
206. Ise, N., et al., *Ordered structure in dilute solutions of ionic biopolymers. 1. Preliminary small-angle x-ray scattering study of aqueous solutions of sodium polyacrylate.* Journal of the American Chemical Society, 1979. **101**(19): p. 5836-5837.
207. Ise, N., et al., *Ordered structure in dilute solutions of ionic biopolymers. 2. Small-angle x-ray scattering study of sodium polyacrylate solution.* Journal of the American Chemical Society, 1980. **102**(27): p. 7901-7906.
208. do Rego Monteiro, V.A., et al., *Aluminum Polyphosphate Nanoparticles: Preparation, Particle Size Determination, and Microchemistry.* Journal of Colloid and Interface Science, 1999. **217**(2): p. 237-248.
209. Shinozaki, H., et al., *Water resistance of cerium phosphate glasses as studied by in situ high temperature IR microspectroscopy.* Journal of Non-Crystalline Solids, 2013. **378**(0): p. 55-60.
210. Tanaka, T., et al., *Cobalt promotes angiogenesis via hypoxia-inducible factor and protects tubulointerstitium in the remnant kidney model.* Laboratory Investigation, 2005. **85**(10): p. 1292-1307.
211. Ruparelia, J.P., et al., *Strain specificity in antimicrobial activity of silver and copper nanoparticles.* Acta Biomaterialia, 2008. **4**(3): p. 707-716.
212. Atiyeh, B.S., et al., *Effect of silver on burn wound infection control and healing: Review of the literature.* Burns. **33**(2): p. 139-148.
213. Zhang, J., et al., *Effect of cerium ion on the proliferation, differentiation and mineralization function of primary mouse osteoblasts in vitro.* Journal of Rare Earths, 2010. **28**(1): p. 138-142.
214. Habibovic, P. and J.E. Barralet, *Bioinorganics and biomaterials: Bone repair.* Acta Biomaterialia, 2011. **7**(8): p. 3013-3026.
215. Hoppe, A., V. Mourino, and A.R. Boccaccini, *Therapeutic inorganic ions in bioactive glasses to enhance bone formation and beyond.* Biomaterials Science, 2013. **1**(3): p. 254-256.
216. Mouriño, V., J.P. Cattalini, and A.R. Boccaccini, *Metallic ions as therapeutic agents in tissue engineering scaffolds: an overview of their biological applications and strategies for new developments*2011.

217. Her, R.K., *Linear Polymetaphosphates—Quaternary Ammonium Salts.* The Journal of Physical Chemistry, 1952. **56**(9): p. 1086-1089.
218. Goebel, M.T. and R.K. Iler, *Quaternary ammonium salts of high molecular weight polymetaphosphoric acid*, 1952, Google Patents.
219. Cini, N. and V. Ball, *Polyphosphates as inorganic polyelectrolytes interacting with oppositely charged ions, polymers and deposited on surfaces: fundamentals and applications.* Advances in Colloid and Interface Science, 2014. **209**(0): p. 84-97.
220. Murthy, R., P. Mutha, and S. Gupta, *Yttrium-90 Radioembolotherapy for Hepatocellular Cancer*, in *Hepatocellular Carcinoma:*, K.M. McMasters, Editor 2011, Springer New York. p. 319-335.
221. Day, D.E. and G.J. Ehrhardt, *Glass microspheres*, 1992, Google Patents.
222. Cacaina, D., et al., *The behaviour of selected yttrium containing bioactive glass microspheres in simulated body environments.* Journal of Materials Science: Materials in Medicine, 2008. **19**(3): p. 1225-1233.
223. Häfeli, U., *Radioactive Microspheres for Medical Applications*, in *Physics and Chemistry Basis of Biotechnology*, M. De Cuyper and J.M. Bulte, Editors. 2002, Springer Netherlands. p. 213-248.
224. Conzone, S.D., et al., *Preparation and properties of radioactive rhenium glass microspheres intended for in vivo radioembolization therapy.* Journal of Biomedical Materials Research, 1998. **42**(4): p. 617-625.
225. Brown, R.F., L.C. Lindesmith, and D.E. Day, *166Holmium-containing glass for internal radiotherapy of tumors.* International Journal of Radiation Applications and Instrumentation. Part B. Nuclear Medicine and Biology, 1991. **18**(7): p. 783-790.
226. Day, D.E. and G.J. Ehrhardt, *Composition and method for radiation synovectomy of arthritic joints*, 1991, Google Patents.
227. Chu, B.C.F., F.R. Kramer, and L.E. Orgel, *Synthesis of an amplifiable reporter RNA for bioassays.* Nucleic Acids Research, 1986. **14**(14): p. 5591-5603.
228. Wan, A.C.A., et al., *Poly(phosphoester) ionomers as tissue-engineering scaffolds.* Journal of Biomedical Materials Research Part B: Applied Biomaterials, 2004. **70B**(1): p. 91-102.
229. Kudela, D., et al., *Polyphosphate-functionalized inorganic nanoparticles as hemostatic compositions and methods of use*, 2014, Google Patents.

Appendix A Elsevier Copyright Permission Letter

ELSEVIER LICENSE
TERMS AND CONDITIONS

Mar 16, 2015

This is a License Agreement between Arash Momeni ("You") and Elsevier ("Elsevier") provided by Copyright Clearance Center ("CCC"). The license consists of your order details, the terms and conditions provided by Elsevier, and the payment terms and conditions.

All payments must be made in full to CCC. For payment instructions, please see information listed at the bottom of this form.

Supplier	Elsevier Limited The Boulevard,Langford Lane Kidlington,Oxford,OX5 1GB,UK
Registered Company Number	1982084
Customer name	Arash Momeni
Customer address	Apt 1201, 5264 Morris street
	Halifax, NS B3J1B5
License number	3590830368235
License date	Mar 16, 2015
Licensed content publisher	Elsevier
Licensed content publication	Journal of Non-Crystalline Solids
Licensed content title	Synthesis and characterization of different chain length sodium polyphosphates
Licensed content author	None
Licensed content date	15 December 2013
Licensed content volume number	382
Licensed content issue number	n/a
Number of pages	7
Start Page	11
End Page	17
Type of Use	reuse in a thesis/dissertation
Portion	full article
Format	both print and electronic
Are you the author of this Elsevier article?	Yes
Will you be translating?	No
Title of your thesis/dissertation	DEVELOPING AN INJECTABLE IN-SITU-FORMING CALCIUM POLYPHOSPHATE SYSTEM AS A HEMOSTATIC AGENT

Expected completion date	Mar 2015
Estimated size (number of pages)	250
Elsevier VAT number	GB 494 6272 12
Permissions price	0.00 CAD
VAT/Local Sales Tax	0.00 CAD / 0.00 GBP
Total	0.00 CAD

Terms and Conditions

INTRODUCTION

1. The publisher for this copyrighted material is Elsevier. By clicking "accept" in connection with completing this licensing transaction, you agree that the following terms and conditions apply to this transaction (along with the Billing and Payment terms and conditions established by Copyright Clearance Center, Inc. ("CCC"), at the time that you opened your Rightslink account and that are available at any time at http://myaccount.copyright.com).

GENERAL TERMS

2. Elsevier hereby grants you permission to reproduce the aforementioned material subject to the terms and conditions indicated.

3. Acknowledgement: If any part of the material to be used (for example, figures) has appeared in our publication with credit or acknowledgement to another source, permission must also be sought from that source. If such permission is not obtained then that material may not be included in your publication/copies. Suitable acknowledgement to the source must be made, either as a footnote or in a reference list at the end of your publication, as follows:

"Reprinted from Publication title, Vol /edition number, Author(s), Title of article / title of chapter, Pages No., Copyright (Year), with permission from Elsevier [OR APPLICABLE SOCIETY COPYRIGHT OWNER]." Also Lancet special credit - "Reprinted from The Lancet, Vol. number, Author(s), Title of article, Pages No., Copyright (Year), with permission from Elsevier."

4. Reproduction of this material is confined to the purpose and/or media for which permission is hereby given.

5. Altering/Modifying Material: Not Permitted. However figures and illustrations may be altered/adapted minimally to serve your work. Any other abbreviations, additions, deletions and/or any other alterations shall be made only with prior written authorization of Elsevier Ltd. (Please contact Elsevier at permissions@elsevier.com)

6. If the permission fee for the requested use of our material is waived in this instance, please be advised that your future requests for Elsevier materials may attract a fee.

7. Reservation of Rights: Publisher reserves all rights not specifically granted in the combination of (i) the license details provided by you and accepted in the course of this licensing transaction, (ii) these terms and conditions and (iii) CCC's Billing and Payment

terms and conditions.

8. License Contingent Upon Payment: While you may exercise the rights licensed immediately upon issuance of the license at the end of the licensing process for the transaction, provided that you have disclosed complete and accurate details of your proposed use, no license is finally effective unless and until full payment is received from you (either by publisher or by CCC) as provided in CCC's Billing and Payment terms and conditions. If full payment is not received on a timely basis, then any license preliminarily granted shall be deemed automatically revoked and shall be void as if never granted. Further, in the event that you breach any of these terms and conditions or any of CCC's Billing and Payment terms and conditions, the license is automatically revoked and shall be void as if never granted. Use of materials as described in a revoked license, as well as any use of the materials beyond the scope of an unrevoked license, may constitute copyright infringement and publisher reserves the right to take any and all action to protect its copyright in the materials.

9. Warranties: Publisher makes no representations or warranties with respect to the licensed material.

10. Indemnity: You hereby indemnify and agree to hold harmless publisher and CCC, and their respective officers, directors, employees and agents, from and against any and all claims arising out of your use of the licensed material other than as specifically authorized pursuant to this license.

11. No Transfer of License: This license is personal to you and may not be sublicensed, assigned, or transferred by you to any other person without publisher's written permission.

12. No Amendment Except in Writing: This license may not be amended except in a writing signed by both parties (or, in the case of publisher, by CCC on publisher's behalf).

13. Objection to Contrary Terms: Publisher hereby objects to any terms contained in any purchase order, acknowledgment, check endorsement or other writing prepared by you, which terms are inconsistent with these terms and conditions or CCC's Billing and Payment terms and conditions. These terms and conditions, together with CCC's Billing and Payment terms and conditions (which are incorporated herein), comprise the entire agreement between you and publisher (and CCC) concerning this licensing transaction. In the event of any conflict between your obligations established by these terms and conditions and those established by CCC's Billing and Payment terms and conditions, these terms and conditions shall control.

14. Revocation: Elsevier or Copyright Clearance Center may deny the permissions described in this License at their sole discretion, for any reason or no reason, with a full refund payable to you. Notice of such denial will be made using the contact information provided by you. Failure to receive such notice will not alter or invalidate the denial. In no event will Elsevier or Copyright Clearance Center be responsible or liable for any costs, expenses or damage incurred by you as a result of a denial of your permission request, other than a refund of the amount(s) paid by you to Elsevier and/or Copyright Clearance Center for denied permissions.

LIMITED LICENSE

The following terms and conditions apply only to specific license types:

15. **Translation**: This permission is granted for non-exclusive world **English** rights only unless your license was granted for translation rights. If you licensed translation rights you may only translate this content into the languages you requested. A professional translator must perform all translations and reproduce the content word for word preserving the integrity of the article. If this license is to re-use 1 or 2 figures then permission is granted for non-exclusive world rights in all languages.

16. **Posting licensed content on any Website**: The following terms and conditions apply as follows: Licensing material from an Elsevier journal: All content posted to the web site must maintain the copyright information line on the bottom of each image; A hyper-text must be included to the Homepage of the journal from which you are licensing at http://www.sciencedirect.com/science/journal/xxxxx or the Elsevier homepage for books at http://www.elsevier.com; Central Storage: This license does not include permission for a scanned version of the material to be stored in a central repository such as that provided by Heron/XanEdu.

Licensing material from an Elsevier book: A hyper-text link must be included to the Elsevier homepage at http://www.elsevier.com . All content posted to the web site must maintain the copyright information line on the bottom of each image.

Posting licensed content on Electronic reserve: In addition to the above the following clauses are applicable: The web site must be password-protected and made available only to bona fide students registered on a relevant course. This permission is granted for 1 year only. You may obtain a new license for future website posting.

17. **For journal authors:** the following clauses are applicable in addition to the above:

Preprints:

A preprint is an author's own write-up of research results and analysis, it has not been peer-reviewed, nor has it had any other value added to it by a publisher (such as formatting, copyright, technical enhancement etc.).

Authors can share their preprints anywhere at any time. Preprints should not be added to or enhanced in any way in order to appear more like, or to substitute for, the final versions of articles however authors can update their preprints on arXiv or RePEc with their Accepted Author Manuscript (see below).

If accepted for publication, we encourage authors to link from the preprint to their formal publication via its DOI. Millions of researchers have access to the formal publications on ScienceDirect, and so links will help users to find, access, cite and use the best available version. Please note that Cell Press, The Lancet and some society-owned have different preprint policies. Information on these policies is available on the journal homepage.

Accepted Author Manuscripts: An accepted author manuscript is the manuscript of an article that has been accepted for publication and which typically includes author-incorporated changes suggested during submission, peer review and editor-author communications.

Authors can share their accepted author manuscript:

- immediately
  - via their non-commercial person homepage or blog
  - by updating a preprint in arXiv or RePEc with the accepted manuscript
  - via their research institute or institutional repository for internal institutional uses or as part of an invitation-only research collaboration work-group
  - directly by providing copies to their students or to research collaborators for their personal use
  - for private scholarly sharing as part of an invitation-only work group on commercial sites with which Elsevier has an agreement
- after the embargo period
  - via non-commercial hosting platforms such as their institutional repository
  - via commercial sites with which Elsevier has an agreement

In all cases accepted manuscripts should:

- link to the formal publication via its DOI
- bear a CC-BY-NC-ND license - this is easy to do
- if aggregated with other manuscripts, for example in a repository or other site, be shared in alignment with our hosting policy not be added to or enhanced in any way to appear more like, or to substitute for, the published journal article.

Published journal article (JPA): A published journal article (PJA) is the definitive final record of published research that appears or will appear in the journal and embodies all value-adding publishing activities including peer review co-ordination, copy-editing, formatting, (if relevant) pagination and online enrichment.

Policies for sharing publishing journal articles differ for subscription and gold open access articles:

Subscription Articles: If you are an author, please share a link to your article rather than the full-text. Millions of researchers have access to the formal publications on ScienceDirect, and so links will help your users to find, access, cite, and use the best available version.

Theses and dissertations which contain embedded PJAs as part of the formal submission can be posted publicly by the awarding institution with DOI links back to the formal publications on ScienceDirect.

If you are affiliated with a library that subscribes to ScienceDirect you have additional private sharing rights for others' research accessed under that agreement. This includes use for classroom teaching and internal training at the institution (including use in course packs

and courseware programs), and inclusion of the article for grant funding purposes.

Gold Open Access Articles: May be shared according to the author-selected end-user license and should contain a CrossMark logo, the end user license, and a DOI link to the formal publication on ScienceDirect.

Please refer to Elsevier's posting policy for further information.

18. **For book authors** the following clauses are applicable in addition to the above: Authors are permitted to place a brief summary of their work online only. You are not allowed to download and post the published electronic version of your chapter, nor may you scan the printed edition to create an electronic version. **Posting to a repository:** Authors are permitted to post a summary of their chapter only in their institution's repository.

19. **Thesis/Dissertation**: If your license is for use in a thesis/dissertation your thesis may be submitted to your institution in either print or electronic form. Should your thesis be published commercially, please reapply for permission. These requirements include permission for the Library and Archives of Canada to supply single copies, on demand, of the complete thesis and include permission for Proquest/UMI to supply single copies, on demand, of the complete thesis. Should your thesis be published commercially, please reapply for permission. Theses and dissertations which contain embedded PJAs as part of the formal submission can be posted publicly by the awarding institution with DOI links back to the formal publications on ScienceDirect.

Elsevier Open Access Terms and Conditions

You can publish open access with Elsevier in hundreds of open access journals or in nearly 2000 established subscription journals that support open access publishing. Permitted third party re-use of these open access articles is defined by the author's choice of Creative Commons user license. See our open access license policy for more information.

Terms & Conditions applicable to all Open Access articles published with Elsevier:

Any reuse of the article must not represent the author as endorsing the adaptation of the article nor should the article be modified in such a way as to damage the author's honour or reputation. If any changes have been made, such changes must be clearly indicated.

The author(s) must be appropriately credited and we ask that you include the end user license and a DOI link to the formal publication on ScienceDirect.

If any part of the material to be used (for example, figures) has appeared in our publication with credit or acknowledgement to another source it is the responsibility of the user to ensure their reuse complies with the terms and conditions determined by the rights holder.

Additional Terms & Conditions applicable to each Creative Commons user license:

CC BY: The CC-BY license allows users to copy, to create extracts, abstracts and new works from the Article, to alter and revise the Article and to make commercial use of the Article (including reuse and/or resale of the Article by commercial entities), provided the user gives appropriate credit (with a link to the formal publication through the relevant

DOI), provides a link to the license, indicates if changes were made and the licensor is not represented as endorsing the use made of the work. The full details of the license are available at http://creativecommons.org/licenses/by/4.0.

CC BY NC SA: The CC BY-NC-SA license allows users to copy, to create extracts, abstracts and new works from the Article, to alter and revise the Article, provided this is not done for commercial purposes, and that the user gives appropriate credit (with a link to the formal publication through the relevant DOI), provides a link to the license, indicates if changes were made and the licensor is not represented as endorsing the use made of the work. Further, any new works must be made available on the same conditions. The full details of the license are available at http://creativecommons.org/licenses/by-nc-sa/4.0.

CC BY NC ND: The CC BY-NC-ND license allows users to copy and distribute the Article, provided this is not done for commercial purposes and further does not permit distribution of the Article if it is changed or edited in any way, and provided the user gives appropriate credit (with a link to the formal publication through the relevant DOI), provides a link to the license, and that the licensor is not represented as endorsing the use made of the work. The full details of the license are available at http://creativecommons.org/licenses/by-nc-nd/4.0. Any commercial reuse of Open Access articles published with a CC BY NC SA or CC BY NC ND license requires permission from Elsevier and will be subject to a fee.

Commercial reuse includes:

- Associating advertising with the full text of the Article
- Charging fees for document delivery or access
- Article aggregation
- Systematic distribution via e-mail lists or share buttons

Posting or linking by commercial companies for use by customers of those companies.

20. **Other Conditions**:

Questions? customercare@copyright.com or +1-855-239-3415 (toll free in the US) or +1-978-646-2777.

Gratis licenses (referencing $0 in the Total field) are free. Please retain this printable license for your reference. No payment is required.

Appendix B ACS Copyright Permission Letter

RightsLink®

Home | Account Info | Help | Live Chat

Title:	Comprehensive Study of the Chelation and Coacervation of Alkaline Earth Metals in the Presence of Sodium Polyphosphate Solution
Author:	Arash Momeni, Mark Joseph Filiaggi
Publication:	Langmuir
Publisher:	American Chemical Society
Date:	May 1, 2014

Logged in as:
Arash Momeni
LOGOUT

PERMISSION/LICENSE IS GRANTED FOR YOUR ORDER AT NO CHARGE

This type of permission/license, instead of the standard Terms & Conditions, is sent to you because no fee is being charged for your order. Please note the following:

- Permission is granted for your request in both print and electronic formats, and translations.
- If figures and/or tables were requested, they may be adapted or used in part.
- Please print this page for your records and send a copy of it to your publisher/graduate school.
- Appropriate credit for the requested material should be given as follows: "Reprinted (adapted) with permission from (COMPLETE REFERENCE CITATION). Copyright (YEAR) American Chemical Society." Insert appropriate information in place of the capitalized words.
- One-time permission is granted only for the use specified in your request. No additional uses are granted (such as derivative works or other editions). For any other uses, please submit a new request.

BACK | CLOSE WINDOW